الجمهورية الجزائرية الديمقراطية الشعبية

République Algérienne Démocratique et Populaire

Ministère de L'Enseignement Supérieur et de la Recherche Scientifique

UNIVERSITÉ FERHAT ABBAS - SETIF1

FACULTÉ DE TECHNOLOGIE

THÈSE

Présentée au Département de génie des procédés

Pour l’obtention du diplôme de

DOCTORAT

Domaine : Sciences et Technologie

Filière : Génie des procédés **Option : Génie des Polymères**

Par

BOUBLIA Abir

THÈME

Modeling and elaboration of multifunctional and eco-friendly nanocomposite materials based on polyaniline and functionalized graphene

Soutenue le 30 / 05 / 2024 devant le Jury:

BENACHOUR Djaafer	**Professeur**	**Univ. Ferhat Abbas Sétif 1**	**Président**
GUEZZOUT Zahir	**M.C.A**	**Univ. Ferhat Abbas Sétif 1**	**Directeur de thèse**
HADDAOUI Nacerddine	**Professeur**	**Univ. Ferhat Abbas Sétif 1**	**Co-Directeur**
HELLATI Abdelhak	**Professeur**	**Univ. BBA**	**Examinateur**
DADACHE Derradji	**M.C.A.**	**Univ. BBA**	**Examinateur**
BENGUERBA Yacine	**Professeur**	**Univ. Ferhat Abbas Sétif 1**	**Membre invité**

Année universitaire : 2023/2024

الجمهورية الجزائرية الديمقراطية الشعبية
République Algérienne Démocratique et Populaire
Ministère de L'Enseignement Supérieur et de la Recherche Scientifique

FERHAT ABBAS UNIVERSITY ABBAS - SETIF1

FACULTY OF TECHNOLOGY

THESIS

Presented at Department of Process Engineering

For obtaining the degree of

PhD

Domaine : Sciences et Technologie

Process Engineering **Polymer Engineering**

Presented by

BOUBLIA Abir

THEME

Modeling and elaboration of multifunctional and eco-friendly nanocomposite materials based on polyaniline and functionalized graphene

Presented publicly on 30 / 05 / 2024 to **the jury committee of:**

BENACHOUR Djaafer	Professor	Univ. Ferhat Abbas Sétif 1	President
GUEZZOUT Zahir	M.C.A	Univ. Ferhat Abbas Sétif 1	Supervisor
HADDAOUI Nacerddine	Professor	Univ. Ferhat Abbas Sétif 1	Co-Supervisor
HELLATI Abdelhak	Professor	Univ. BBA	External Examiner
DADACHE Derradji	M.C.A.	Univ. BBA	External Examiner
BENGUERBA Yacine	Professor	Univ. Ferhat Abbas Sétif 1	Invited member

Academic Year : 2023/2024

Abstract

This PhD thesis presents a comprehensive exploration of the development and optimization of polyaniline (PANI) and functionalized graphene nanocomposites, a pivotal advancement in materials science and engineering. Emphasizing a multidisciplinary approach, this work integrates innovative experimental strategies, computational modeling, and advanced machine learning techniques to refine the properties of these nanocomposites. The research encapsulates innovative synthesis methods and employs groundbreaking machine learning models for predictive analysis, significantly enhancing the accuracy in forecasting electrical conductivity and gas-sensing responses of PANI/graphene nanocomposites. These models, a first in the field, set new standards in sustainable material science. Furthermore, the thesis introduces an eco-friendly synthesis pathway for PANI/reduced graphene oxide nanocomposites using deep eutectic solvents, marking a leap towards environmental sustainability. This integrative research not only enriches the understanding of PANI/graphene nanocomposites but also makes substantial contributions to developing sustainable materials. The findings and methodologies presented in this thesis are anticipated to have far-reaching impacts, opening new avenues in technology and environmental conservation, particularly in areas like supercapacitors, gas detection devices, and energy storage systems.

Keywords: Polyaniline (PANI); Graphene Nanocomposites; Machine Learning in Material Science; Experimental Design Optimization; Computational Modeling; Density Functional Theory (DFT); Electrical Conductivity; Gas Sensing; Environmental Sustainability.

Résumé

Cette thèse de doctorat offre une exploration complète du développement et de l'optimisation de nanocomposites de polyaniline (PANI) et de graphène fonctionnalisé, une avancée cruciale en science et ingénierie des matériaux. Mettant l'accent sur une approche multidisciplinaire, ce travail intègre des stratégies expérimentales innovantes, la modélisation informatique et des techniques avancées d'apprentissage automatique pour affiner les propriétés de ces nanocomposites. La recherche englobe des méthodes de synthèse novatrices et utilise des modèles révolutionnaires d'apprentissage automatique pour l'analyse prédictive, améliorant significativement la précision dans la prévision de la conductivité électrique et des réponses des capteurs de gaz des nanocomposites PANI/graphène. Ces modèles, une première dans le domaine, établissent de nouvelles normes en science des matériaux durables. De plus, la thèse présente un chemin de synthèse respectueux de l'environnement pour les nanocomposites PANI/oxide de graphène réduit en utilisant des solvants eutectiques profonds, marquant un pas vers la durabilité environnementale. Cette recherche intégrative enrichit non seulement la compréhension des nanocomposites PANI/graphène, mais contribue également de manière substantielle au développement de matériaux durables. Les découvertes et méthodologies présentées dans cette thèse devraient avoir un impact considérable, ouvrant de nouvelles voies dans la technologie et la conservation de l'environnement, notamment dans des domaines tels que les supercondensateurs, les capteurs de gaz et les solutions de stockage d'énergie.

Mots-clés : Polyaniline (PANI) ; Nanocomposites de Graphène ; Machine Learning en Science des Matériaux ; Optimisation du Plan d'expérience ; Modélisation Moléculaire ; Théorie Fonctionnelle de la Densité (DFT) ; Conductivité Électrique ; Détection de Gaz ; Durabilité Environnementale.

المُلخص

تقدم هذه الأطروحة استكشافًا شاملًا لتطوير وتحسين نانومركبات البولي أنيلين والغرافين المُعدّل، وهو تقدم محوري في علم وهندسة المواد. مع التركيز على المنهج الشمولي المتعدد التخصصات، يدمج هذا العمل استراتيجيات تجريبية مبتكرة ونمذجة حسابية وتقنيات تعلم الآلة المتقدمة لتحسين خصائص هذه النانومركبات. تتضمن البحوث طرق تصنيع مبتكرة وتستخدم نماذج التعلم الآلي الرائدة للتحليل التنبؤي، مما يعزز بشكل كبير الدقة في التنبؤ بالتوصيل الكهربائي واستجابات الكشف عن الغاز لنانومركبات بولي أنيلين/غرافين. تُعد هذه النماذج الأولى من نوعها في هذا المجال، تضع معايير جديدة في علم المواد المستدامة. علاوة على ذلك، تقدم الأطروحة طريقة تصنيع صديقة للبيئة لنانومركبات بولي أنيلين/أكسيد الجرافين المخفض باستخدام المذيبات المنصهرة بعمق، مما يمثل تطوراً مهماً نحو الاستدامة البيئية. هذا البحث المتكامل لا يثري فقط على إثراء فهم نانومركبات البولي أنيلين/الجرافين فحسب، بل يقدم أيضًا مساهمات جوهرية في تطوير المواد المستدامة. من المتوقع أن تكون النتائج والمنهجيات المقدمة في هذه الأطروحة ذات تأثيرات بعيدة المدى، فتفتح آفاقًا جديدة في التكنولوجيا والحفاظ على البيئة، خاصة في مجالات مثل المكثفات الفائقة وأجهزة استشعار الغازات وحلول تخزين الطاقة.

الكلمات المفتاحية: البولي أنيلين؛ نانومركبات الجرافين؛ التعلم الآلي في علم المواد؛ تحسين تصميم التجارب ؛ النمذجة الحسابية؛ نظرية الكثافة الوظيفية ؛ التوصيل الكهربائي؛ الاستشعار للغاز؛ الاستدامة البيئية.

Dedication

This thesis is dedicated to the loving memory of **my dearest mother**, whose guidance and love have shaped me in lasting ways. Though she is no longer with us, her spirit continues to inspire and drive me forward. Her unwavering support and belief in my abilities carried me through the challenges of this academic journey. It is with deep gratitude and love that I dedicate this achievement to **her** – a proof to her lasting impact on my life.

To **my beloved father**, who has always been a source of unwavering strength and profound wisdom. His enduring support and belief in me have been the bedrock of my perseverance and the compass in my academic voyage. His presence is a constant reminder of the power of encouragement and the fortitude that comes from knowing you are never alone in your endeavors. His guidance has shaped not just this thesis, but the very person I strive to be. **Thank you, PAPA**!

To my dear brothers, **Massinissa**, **Mohamed**, and **Mounder Ghassan** - my comrades in arms through life's journey. Your brotherly love, endless encouragement, and shared moments of joy and challenge have been the tapestry of my personal growth.

To the entire **BOUBLIA** and **AGOUNI** families, and especially to my precious **Grandmother**, for your unwavering support and love.

To **Prof. Yacine BENGUERBA**, a mentor whose wisdom illuminates the dark waters of research with the clarity of a lighthouse, whose support has been nothing short of familial!

To my dear friends, **Imane**, **Saousen**, **Aicha**, **Amel**, and my cousin **Nora** for the shared laughter and unwavering camaraderie.

Finally,

And to all who have contributed to this journey, near and far, who have invested their time and efforts in me, I extend my deepest appreciation:

I'm deeply grateful, from the core of my heart.

Acknowledgement

I extend my deepest gratitude to **Allah**, **the Almighty**, for the strength and perseverance granted to me throughout this research journey.

Throughout my PhD I have had the privilege to work with many incredible people and academics who provided me with help and advice. Without them, these three and a half years would have been extremely difficult to handle.

Foremost, my profound gratitude extends to my supervisors, **Prof. Zahir GUEZZOUT** and **Prof. Nacerddine HADDAOUI**. Their guidance has been an inspiration throughout my academic voyage, offering not just direction but also immense patience, encouragement, and academic knowledge. Their passion for research and solid support have profoundly influenced both my research trajectory and professional development. Their mentorship has not only illuminated my path in academia but also introduced in me a deep appreciation for the rigor and beauty of scientific inquiry.

Special appreciation goes to **Prof. Yacine BENGUERBA**, and **Prof. Michael BADAOUI** for their remarkable collaborative spirit and indispensable contributions to my research. Their unwavering support, encouragement, and trust in my decisions have been a source of great inspiration and confidence throughout this journey. Their invaluable input and guidance have not only enriched my research but also greatly supported my personal and professional growth.

My sincere thanks to the PhD thesis Committee members, **Prof. BENACHOUR Djafer**, **Prof. HELLATI Abdelhak**, and **Prof. DADACHE Derradji**, whose insightful feedback and suggestions during my defense were immensely beneficial.

Gratitude is also due to Ferhat Abbas Setif University 1, the Laboratoire de Physico-Chimie des Hauts Polymères (LPCHP), Laboratoire de Biopharmacie Et Pharmacotechnie (LPBT), and the Laboratory of Electrochemistry-Corrosion, Metallurgy and Inorganic Chemistry (USTHB El-Alia, Algiers) for their unwavering support throughout my PhD journey.

A heartfelt thank you to **the exceptional research group** for their hard work, cooperation, and the familial bond we shared. I am proud to be part of this team and look forward to future collaborations.

My deepest gratitude to **my dear family** and **friends**, thank you for your unwavering support and patience during these demanding years of my academic pursuit. Your belief in me has been the cornerstone of my success.

Finally, a special acknowledgment to the memory of **my beloved mother**. Her love and blessings have been a guiding light in my life, specially throughout this PhD journey, and her memory continues to inspire me every day. May her soul rest in peace.

Thank you all for being part of my academic adventure!

Abir Boublia

List of Abbreviations

PANI	Polyaniline
CPs	Conducting polymers
Ppy	Polypyrrole
PTh	Polythiophene
PPy	Polypyrrole
PTh	Polythiophene
PA	Polyacetylene
PPP	Poly-*para*-Phenylene
PPV	Poly-*para*-Phenylene-Vinylene
PEDOT	Poly-3,4-ethylene-dioxythiophene
PF	Polyfluorene
PET	Polyethylene terephthalate
Gr	Graphene
GO	Graphene oxide
rGO	Reduced graphene oxide
CrGO	Chemically reduced graphene oxide
SN-rGO	Sulfur and nitrogen doped rGO
SN-GO	Sulfur and nitrogen doped GO
GQDs	Graphene quantum dots
N-GQDs	Nitrogen doped GQDs
S-GQDs	Sulfur doped GQDs
Gr@Ag	Graphene decorated with silver
Gr@Ni	Graphene decorated with nickel
Gr@Au	Graphene decorated with gold
GCs	Quasi-graphite capsules
VPP	Vapor-phase polymerization
CVD	Chemical vapor deposition
GICs	Graphite intercalation compounds
SiC	Silicon carbide
APS	Ammonium peroxydisulfate
ANI	Aniline
HCl	Hydrochloric acid
CNTs	Carbon nanotubes
MWCNTs	Multiwall carbon nanotubes
CTAB	Cetyltrimethylammonium bromide
DBSA	Dodecylbenzene sulfonic acid
LCNF	Lignocellulosic cellulose nanofibrils
PANIHs	Rambutan-like PANI hollow nanosphere
2D	Two-Dimensional
3D	Three-Dimensional
ppm	Parts Per Million
ppb	Parts Per Billion
$\mathbf{NH_3}$	Ammonia
$\mathbf{C_6H_6}$	Benzene
$\mathbf{CO_2}$	Carbon dioxide
CO	Carbon monoxide
$\mathbf{H_2}$	Hydrogen
$\mathbf{H_2S}$	Hydrogen sulfide
$\mathbf{H_2O_2}$	Hydrogen peroxide
$\mathbf{CH_4}$	Methane
$\mathbf{N_2}$	Nitrogen
$\mathbf{NO_2}$	Nitrogen dioxide
NO	Nitrogen monoxide
$\mathbf{C_3H_8}$	Propane
$\mathbf{C_7H_8}$	Toluene
HCOOH	Formic acid
$\mathbf{HClO_4}$	Perchloric acid
$\mathbf{H_2SeO_3}$	Selenous acid
$\mathbf{H_2SO_4}$	Sulfuric acid
$\mathbf{H_2O}$	Water
$\mathbf{CH_2O}$	Formaldehyde
$\mathbf{CHCl_3}$	Chloroform
$\mathbf{CH_3OH}$	Methanol
$\mathbf{C_2H_5OH}$	Ethanol
$\mathbf{(C_2H_5)_2O}$	Ethyl ether
$\mathbf{C_2H_6O_2}$	Ethylene glycol
$\mathbf{C_3H_8O}$	Propanol
$\mathbf{CH_3COCH_3}$	Acetone
$\mathbf{C_3H_8O_3}$	Glycerol
$\mathbf{(CH_3)_2CHOH}$	Isopropyl alcohol
$\mathbf{C_3H_7NO}$	Dimethylformamide
$\mathbf{C_5H_9NO}$	N-Methyl-2-pyrrolidone
$\mathbf{C_6H_{14}}$	Hexane
$\mathbf{C_6H_{12}N_2O}$	Dimethyl propylene urea
$\mathbf{C_7H_8O}$	M-cresol
$\mathbf{C_7H_8O_3S}$	P-toluenesulfonic acid
$\mathbf{C_8H_{10}}$	Xylene
$\mathbf{C_{10}H_{16}O_4S}$	Camphorsulfonic acid
$\mathbf{CCl_4}$	Tetrachloromethane
APTES	3-aminopropyltriethoxysilane
$\mathbf{NH_4OH}$	Ammonia solution
$\mathbf{CeO_2}$	Cerium dioxide
ChCl	Choline chloride
DESs	Deep eutectic solvents

List of Abbreviations

RT	Room temperature
DC	Direct Current
E_v	Valence band
E_c	Conduction band
E_f	Fermi level
E_g	Band/Energy gap
DOS	Density of States
T_g	Glass transition temperature
T_d	Degradation temperature
T_m	Melting temperature
UV-Vis	UV-Visible Spectroscopy
PL	Photoluminescence Spectroscopy
FT-IR	Fourier Transform Infrared Spectroscopy
XRD	X-ray Diffraction
XPS	X-ray Photoelectron Spectroscopy
CV	Cyclic Voltammetry
AFM	Atomic Force Microscopy
SEM	Scanning Electron Microscopy
TEM	Transmission Electron Microscopy
TGA	Thermogravimetric Analysis
C_p	Specific capacitances
DFT	Density Functional Theory
MDs	Molecular Dynamics
GGA	Generalized Gradient Approximation
DNP	Dynamic Nuclear Polarization
NVT	Constant temperature, constant volume
TZVP	Valence triple-zeta polarization
HBA	Hydrogen Bond Acceptor
HBD	Hydrogen Bond Donnor
COSMO-RS	COnductor like Screening MOdel for Real Solvents
FMO	Frontier Molecular Orbital
HOMO	Highest Occupied Molecular Orbitals
LUMO	Lowest Unoccupied Molecular Orbitals
NCI	Non-Covalent Interaction
RDG	Reduced Density Gradient
VDW	van der Waals
VMD	Visual Molecular Dynamics
QTAIM	Quantum Theory of Atoms in Molecules
BCP	Bond Critical Points
$N_2H_4.H_2O$	Hydrazine monohydrate
I_2	Iodine
MnO_2	Manganese dioxide
KPS	Potassium persulfate
SDBS	Sodium 4-dodecyl benzene sulfonic acid
SDS	Sodium dodecylsulfate
NaOH	Sodium hydroxide
$NaNO_3$	Sodium nitrate
SMO	Sorbitan monooleate
TEG	Tetraethylene glycol
SnO_2	Tin (IV) oxide
TiO_2	Titanium dioxide
V_2O_5	Vanadium pentoxide
ZnO	Zinc oxide
In_2O_3	Indium oxide
RSM	Response Surface Methodology
BBD	Box-Behnken Design
CCD	Central Composite Design
DM	Doehlert Matrix
ML	Machine Learing
ANNs	Artificial Neural Networks
MLNR	Multiple Non-Linear Regression
DT	Decision Tree
RF	Random Forest
MLR	Multi Linear Regression
GBM	Gradient Boosting Machine
***k*-NN**	*k*-Nearest Neighbors
SVR	Support Vector Regression
AD	Applicability Domain
BFGS	Broyden-Fletcher-Goldfarb-Shanno algorithm
RMSE	Root Mean Square Error
R^2	Coefficient of Determination
ASD	Average Standard Deviation
AARD	Average Absolute Relative Deviation
MAE	Mean Absolute Error
MSE	Mean Squared Error
RSE	Residual Errors
RD	Relative Deviation
SDR	Standardized Residual

List of Tables

Chapter I

Chapter II

Chapter III

Chapter IV

List of Figures

Chapter I

Chapter II

Chapter III

Chapter IV

Appendix

Table of Contents

General Introduction

General Introduction

The aim of the present section is to provide an introductory material on the research conducted in this PhD thesis, outlining its motivation, objectives, and organization. It delves into the rationale behind the study, the aims driving the research, and the outcomes achieved. Furthermore, it provides a structured overview of the thesis, guiding readers through the journey of the investigation from its inception to its conclusion. This introductory section sets the stage for a detailed exploration of the innovative work undertaken in the field of polyaniline and graphene-based nanocomposites, highlighting their multifunctional applications and contributions to materials science.

The quest for designing high-performance, conducting, and multifunctional nanocomposites has rapidly gained momentum in recent years, marking a significant stride in advanced material science (Raza et al. 2021). This field is particularly vibrant in the context of conducting polymers and graphene-based materials, which are being explored for their unique and tunable attributes. These properties include enhanced electrical conductivity, mechanical strength, and advanced sensing capabilities, making these nanocomposites highly sought-after in various industrial applications (Chee et al. 2015; Fu et al. 2019; Guezzout et al. 2023). Polyaniline (PANI), known for its easy synthesis and exceptional gas-sensing properties, emerges as a key player when integrated with nanoparticles like carbon-based materials, enhancing its intrinsic qualities and broadening its application spectrum (Tanguy et al. 2018; Singh and Shukla 2020; Kausar 2021; Kazemi et al. 2021). Simultaneously, graphene's extensive surface area and remarkable physicochemical properties revolutionize gas sensor technologies, offering highly sensitive detection capabilities. The fusion of graphene with PANI-based systems results in cost-effective, high-performance nanocomposites, leveraging both materials' strengths (Bogue 2014; Vikrant et al. 2018; Zamiri and Haseeb 2020; Kazemi et al. 2021; Yap et al. 2021).

However, the development of PANI/graphene nanocomposites faces significant challenges, primarily due to the complexity of optimizing their properties. Achieving a deep understanding of their intricate molecular interactions is crucial for enhancing their functional performance. Traditional methods, involving exhaustive experimental testing to explore every possible material combination, are not only impractical but also resource-intensive. In this context, predictive modeling emerges as a crucial strategy. Innovative techniques like machine learning (ML) and molecular modeling offer a promising pathway to overcome these challenges. They facilitate efficient, cost-effective predictions of the nanocomposites' properties, thereby reducing the dependency on extensive laboratory work. This approach not only paves the way for precise customization of nanocomposites for specific industrial applications but also marks a significant advancement towards the development of sustainable and high-performance material technologies. The integration of computational and experimental methodologies is vital in addressing the complexity of material interactions, ensuring the progression of nanocomposite development towards a more sustainable and application-specific future.

Within the framework of this PhD project, focused on the development and optimization of PANI and functionalized graphene nanocomposites. This endeavor aims to address the critical need for advanced materials that exhibit both enhanced performance and eco-friendliness. The specific objectives include:

- **Innovative Synthesis:** To design and develop PANI/graphene nanocomposites through innovative synthesis methods, enhancing their functional properties and eco-friendliness.
- **Computational Modeling:** Utilizing computational techniques such as density functional theory (DFT) and molecular dynamics (MD) to accurately model the electronic and molecular behavior within the nanocomposites.
- **Machine Learning Integration:** Implementing machine learning, particularly Artificial Neural Networks (ANNs), for predicting and enhancing the nanocomposites' electrical conductivity and gas sensing properties.
- **Experimental Validation:** Conducting comprehensive experimental studies to corroborate the predictions of computational models, aiming to understand the nanocomposites' real-world applicability.
- **Application Exploration:** Investigating the practical uses of these nanocomposites in supercapacitors, gas sensors, and energy storage devices, showcasing their potential for diverse industrial applications.
- **Future Material Innovations:** Focusing on future material developments, particularly in sustainable advancements, by experimenting with novel functionalization techniques and broadening the application spectrum of these nanocomposites.
- **Sustainable Material Science Contributions:** Striving to contribute significantly to the field of sustainable material science by developing eco-friendly solutions to address global environmental and technological challenges.

Therefore, the construction of this PhD thesis is meticulously organized to provide a comprehensive understanding of the development and applications of polyaniline and graphene-based nanocomposites. The structure of this thesis is as follows:

- **General Introduction -** Establishes the research context, detailing the general overview, problem statement, and research aims. It also outlines the thesis structure, setting the foundation for the ensuing chapters.
- **Chapter I: Literature Review -** Presents a comprehensive literature review on the development and applications of polyaniline and graphene-based nanocomposites, particularly focusing on their roles in electrical conductivity and gas sensing. This chapter offers an in-depth examination of the evolution, methodologies, and properties of these innovative materials, setting the stage for subsequent experimental and computational analysis.
- **Chapter II: Theoretical and Methodological Framework -** Details the theoretical and methodological framework employed in the research. This chapter explains the computational methods, materials characterization techniques, and experimental procedures utilized in the study, offering a foundational understanding of the mechanisms and operations involved in the development and application of PANI/graphene nanocomposites.
- **Chapter III: Machine Learning in Nanocomposite Research -** Delves into the groundbreaking application of advanced machine learning methodologies for predicting the electrical and gas sensing properties of PANI/graphene nanocomposites. This chapter covers an extensive dataset analysis from over 100 references, with a focus on the accuracy and robustness of ANNs in predictions. It includes a detailed examination of the applicability domain (AD) for model evaluation and the influence of molecular inputs on the performance of PANI/graphene nanocomposites. This chapter will contribute significantly to the development of high-performance nanocomposites, underlining the potential of machine learning in material science and its applicability in areas like supercapacitors, gas sensors, and energy storage devices.
- **Chapter IV: Synthesis and Characterization of PANI/rGO Nanocomposites -** Presents an extensive investigation into the synthesis, modeling, and characterization of polyaniline/reduced graphene oxide (PANI/rGO) nanocomposites, highlighting the innovative use of deep eutectic solvents (DES) in their synthesis. This chapter explores the successful synthesis of PANI/rGO nanocomposites via in-situ chemical polymerization,

employing DES as an electrolyte—a novel approach in nanocomposite fabrication. It details the application of Response Surface Methodology (RSM), ANNs, and molecular simulation techniques for a holistic modeling and optimization process. The chapter provides critical insights into the electrical conductivity, structural changes, and thermal stability of PANI/rGO nanocomposites, positioning them as promising materials for supercapacitors and gas sensors and underscoring their potential in eco-friendly innovations.

- **Conclusion and Future Directions -** Concludes the thesis by summarizing key findings, particularly in gas sensor applications. It opens a window into prospective research avenues, particularly focusing on the enhancement of gas detection methodologies for environmental monitoring. This concluding chapter not only summarizes the significant strides made in the field but also sketches a roadmap for future explorations that promise to elevate the practical efficacy of gas sensing technologies in tackling environmental challenges.

Chapter I

Chapter I: Literature Review

This chapter affords an insightful overview of the developments in the modeling and elaboration of polyaniline (PANI) and graphene nanocomposites, focusing on their application in electrical conductivity and gas sensing. It elucidates the pivotal role these nanocomposites play as materials for detecting a variety of gases, exploring the mechanisms behind their sensing abilities. Highlighting the timeliness of this review, it draws predominantly from studies published in the last decade, showcasing the field's progression towards contemporary and innovative research.

I.1. Introduction

The survey of polyaniline (PANI) and graphene nanocomposites represents a significant stride in the advancement of materials science, especially in developing high-end applications, like sensitive and efficient electrical and gas sensors or energy storage materials. This chapter delves deeply into the synergistic integration of PANI and graphene, underscoring the significant strides made in enhancing the performance and applicability of these nanocomposites for cutting-edge engineering solutions. Through a comprehensive literature review, this chapter purposes to map out the up-to-date landscape of PANI/graphene nanocomposites, elucidating the potential that lies in their unique combination for technological innovation.

Drawing from a wealth of scientific research published over the last decade, meticulously curated to capture the essence of innovation in PANI/graphene nanocomposites over the recent decade. This exploration is meticulously illustrated in Figure I.1, which serves as a visual gateway to understanding the structural and compositional nuances that make these materials stand out in the field of gas sensing technologies. The figure is a proof to the architectural elegance of PANI/graphene nanocomposites, shedding light on the molecular interactions and structural configurations that underpin their exceptional properties.

In parallel, Table I.1 offers an organized summary of seminal research findings and pivotal developments in the field, spanning from 2010 to 2024. This table summarize the essence of scholarly discourse on PANI/graphene nanocomposites, presenting a curated overview of the evolutionary trajectory of research within this function. It provides a snapshot of the progress and challenges encountered in the synthesis, electrical, and sensing performances of these materials, particularly in the context of gas sensor applications. Notably, our analysis identifies a research gap in the synthesis, electrical, and sensing performances of

PANI and graphene materials, highlighting the need for further exploration in gas sensor systems. For readers seeking foundational insights and background information, a selection of comprehensive reviews is provided, including works by (Chauhan et al. 2016; Sen et al. 2016; Pandey 2016; Huang et al. 2018; Tanguy et al. 2018; Shoaie et al. 2019; Al-Haidary et al. 2021). These reviews, cataloged in Table I.1, offer a broad spectrum of knowledge, setting the stage for the subsequent discussions in this chapter.

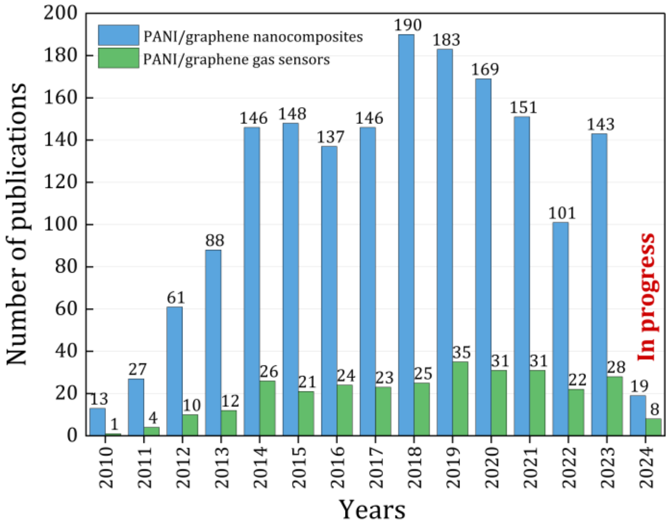

Figure I.1. Research trends and millstones in terms of “PANI/graphene nanocomposites”, and “PANI/graphene gas sensors”: A Scopus database analysis.

Upon reviewing Table I.1, it becomes evident that existing literature primarily delves into the foundational theories and synthesis methodologies concerning either PANI or graphene independently. Notably, discussions on PANI/graphene nanocomposites with a specific focus on supercapacitors have been observed (Huang et al. 2018), yet comprehensive analyses emphasizing the latest breakthroughs in PANI/graphene composites, particularly in gas sensing applications, remain uncommon. The inception of scholarly discourse on PANI/graphene nanocomposites in the context of gas sensing was marked by a pivotal study in 2010 (Al-Mashat et al. 2010), underscoring the novelty and increasing interest in this research domain. Despite this growing fascination, a thorough review that solely concentrates on the gas sensing capabilities of PANI/graphene composites is yet to be found.

Hence, this chapter inventors in offering an exhaustive overview of PANI/graphene-based nanocomposites, spotlighting their utility as conductive mediums across various domains, notably in gas sensors. This discourse begins by laying down the foundational principles of PANI and graphene, subsequently navigating through the latest advancements and applications of these materials, spanning the years 2010 to 2024, as depicted in Figure I.1. This endeavor aims to bridge the existing knowledge gap and furnish a holistic perspective on the potential of PANI and graphene composites in the evolving landscape of material science.

Table I.1. Selected key review articles in the literature on PANI, Graphene, and PANI/graphene nanocomposite gas sensors.

Review title	**Main Focus**	**Reference**
Synthesis and sensing applications of polyaniline nanocomposites: a review	PANI nanocomposites	(Sen et al. 2016)
Highly Sensitive and Selective Chemiresistor Gas/Vapor Sensors based on Polyaniline Nanocomposite: A comprehensive review	PANI-based sensors	(Pandey 2016)
High-performance supercapacitors based on polyaniline - graphene nanocomposites: Some approaches, challenges and opportunities	Developmental stage of different PANI/graphene nanocomposites	(Chauhan et al. 2016)
Polyaniline/graphene nanocomposites towards high - performance supercapacitors: A review	PANI/graphene nanocomposites for supercapacitors	(Huang et al. 2018)
A review on advances in application of polyaniline for ammonia detection	PANI based ammonia detection sensors	(Tanguy et al. 2018)
Electrochemical sensors and biosensors based on the use of polyaniline and its nanocomposites: a review on recent advances	PANI-based biosensors	(Shoaie et al. 2019)
Development of polyaniline for sensor applications: A review	PANI as conductive sensors	(Al-Haidary et al. 2021)
A Review on Polyaniline: Synthesis, Properties, Nanocomposites, and Electrochemical Applications	PANI-based nanocomposites and its applications	(Majeed et al. 2022)

I.2. Background on Conducting Polymers

Conducting polymers (CPs), such as polypyrrole (PPy), polythiophene (PTh), and PANI, have emerged as materials of significant interest due to their remarkable electrical and mechanical properties. These polymers have found extensive applications across various domains owing to their unique combination of conductivity and flexibility (Gerard et al. 2002; Yan et al. 2020). The exploration of CPs began in earnest in 1963 when Bolto et al. discovered the conductor properties of PPy derivatives, achieving impressively low resistivity levels of 1 Ωcm (Bolto et al. 1963). The field was further revolutionized in 1977 with Shirakawa, MacDiarmid, and Heeger's synthesis of doped polyacetylene (PA), a breakthrough that led to their Nobel Prize in Chemistry in 2000 for pioneering work on conducting polymers (Chiang et al. 1977; Heeger et al. 2000).

The conductivity in CPs arises from their extended π conjugated systems, which facilitate the delocalization of π electrons across the polymer chain, imparting them with semiconductor-like properties (MacDiarmid 2001). Doping processes are employed to enhance the conductivity of these materials, making them suitable for an extensive array of applications, such as energy storage, electronics, and sensors (Gubler et al. 2002; Harun et al. 2007). The conductivity spectrum of these materials is depicted in Figure I.2.

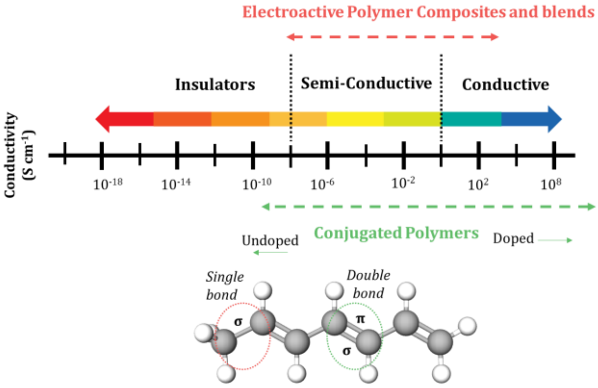

Figure I.2. Conductivity range of conducting polymers and polymer composites (Kaur et al. 2015; Ahmadi et al. 2019).

Following the initial discoveries, the development of various CPs such as PPy, PTh, PANI, and others continued to expand. Figure I.3 showcases the molecular structures of these pivotal conducting polymers, while Table I.2 summarizes the properties and electrical conductivities of several well-studied CPs, indicating the scope for enhancing these materials through advanced synthesis techniques and doping strategies (Pionteck et al. 2007; Kar et al. 2015; Idumah 2021). Despite their promising applications, the use of some CPs in biomedical fields is limited due to potential air oxidation and hazardous by-products (Mozafari et al. 2012; Yi and Abidian 2016). Nonetheless, the electrical and electrochemical properties of CPs are significantly enhanced through doping or by incorporating additional components, such as inorganic oxides or other organic compounds (Zhang et al. 2018).

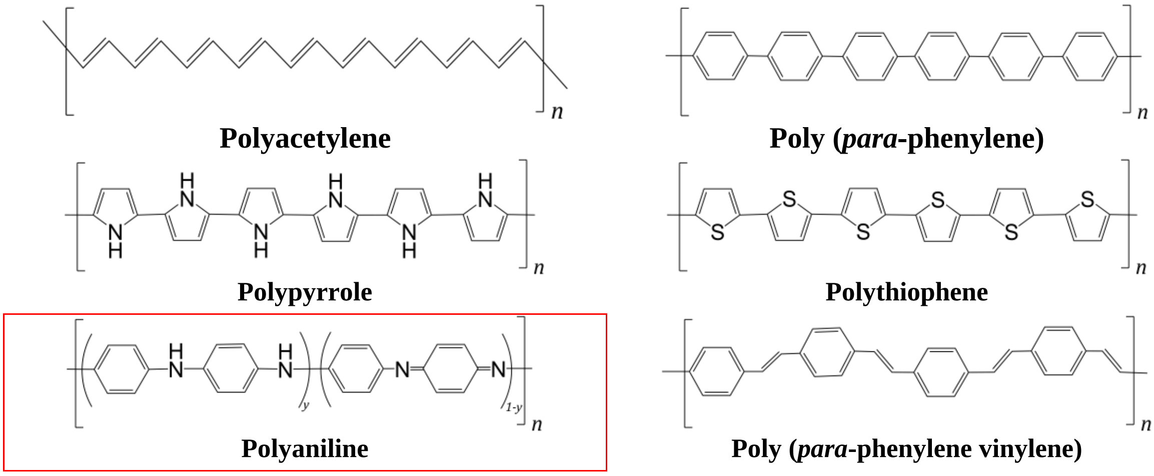

Figure I.3. Chemical structures of common conducting polymers (Ramakrishnan 2011).

Table I.2. Conductivity and other properties of some commonly available CPs (Pionteck et al. 2007; Kar et al. 2015; Idumah 2021).

Conducting polymer	**Chemical structure**	**Conductivity (S cm^{-1})**	**Doping type**	**Properties**
Polyacetylene (PA)	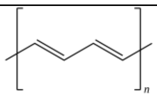	200 – 1000	*n, p*	High electrical conductivity
Polyaniline (PANI)	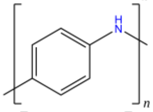	30 – 200	*n, p*	Various structural configurations, environmentally durable, cost-effective
Polypyrrole (PPy)	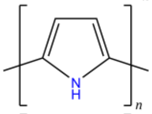	10 – 700	*p*	Excellent electrical conductivity, Simplicity in synthesis, and ease of surface modification
Polythiophene (PTh)	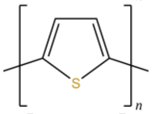	10 – 1000	*p*	Ease of synthesis and favorable optical characteristics
Poly(*para*-phenylene) (PPP)		10^{-7} – 100	*n, p*	Environmentally stable
Poly (3, 4-ethylenedioxy thiophene) (PEDOT)	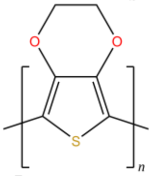	0.4 – 400	*n, p*	Transparent conductor that exhibits both environmental and electrochemical stability
Poly (*para*-phenylene vinylene) (PPV)	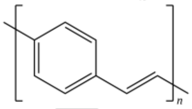	1 – 1000	*p*	Transformed into a thin film with a highly organized crystalline structure
Poly(*iso*-thionaphthene) (PITN)	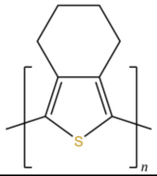	1 – 50	*p*	Colorless and transparent conductor

Despite their advantages, CPs face challenges such as reduced electrical conductivity, low surface area due to agglomeration, varied polymerization methods leading to uncontrolled morphologies, and instability of nanostructured CPs. To address these limitations, graphene's incorporation into CP matrices is explored to enhance the electroactivity of resulting nanocomposites. This strategic direction is underscored by ongoing studies dedicated to understanding the interplay between CPs and graphene-based nanocomposites, aiming to unlock new potentials for CP applications (Roth and Graupner 1993; Skotheim 1997; Partridge et al. 2000; Mishra 2018).

Ongoing research focuses on improving existing CPs for broader applications, leveraging techniques like doping and the creation of nanocomposites to enhance their properties. CPs-based sensors, in particular, benefit from their lightweight, corrosion resistance, low cost, and environmental stability. The inclusion of materials including metal oxides, carbon nanotubes, and graphene derivatives into CPs has been explored to improve their reversibility, sensitivity, and response times.

A key focus of recent investigations has been the integration of graphene into CP frameworks to develop nanocomposites with significantly improved electroactivity. This approach seeks to leverage the synergistic interactions between CPs and graphene derivatives, aiming to transcend the traditional limitations of CPs by exploiting graphene's remarkable properties. Among the spectrum of CPs, PANI emerges as a particularly notable material due to its superior electrical conductivity, stability under environmental conditions, and straightforward synthetic route. PANI's versatile doping/dedoping chemistry facilitates a modifiable conductivity spectrum, positioning it as a prime candidate for diverse applications, including but not limited to sensors, supercapacitors, and anti-corrosion coatings. Furthermore, the compatibility of PANI with various doping agents and its adaptability to different forms—ranging from fibers and films to complex nanocomposites—significantly broadens its practical and research-based applications. These distinguishing features highlight the central role of PANI in the ongoing evolution of conducting polymers and prelude a more detailed examination of its essential properties in the following section.

I.2. Basic of Polyaniline

PANI has been a subject of extensive investigation due to its noteworthy characteristics, drawing significant interest for possible use in electronic devices such as batteries, capacitors, and sensor materials. Its outstanding conductivity and adaptable features position it as a compelling choice for advancing modern electronic technologies (Sen et al. 2016; Boublia et al. 2023a; Kyomuhimbo and Feleni 2023). Notably, the combination of PANI with carbonaceous elements in nanocomposites has surfaced as an attractive tactic for crafting sophisticated materials, capitalizing on their mutually beneficial attributes.

PANI is distinguished by its outstanding electrical conductivity, elevated pseudocapacitance, and robust resilience against environmental degradation (Hong et al. 2019; Heme et al. 2021). Simultaneously, carbonaceous materials, encompassing graphene, carbon nanotubes, and carbon black, are recognized for their remarkable mechanical strength, extensive surface area, and excellent electrical conductivity. Researchers have significantly enhanced electrochemical performance through this combination, making these materials well-suited for diverse applications (Chen et al. 2023a; Zhang et al. 2023).

I.2.1. History of Polyaniline Research

PANI stands as a keystone within the domain of conducting polymers, with its inception tracing over a century and a half ago, marking it as one of the most venerable materials in this field. The early 1980s witnessed a resurgence of academic interest in PANI, sparked by its unique conductive properties and versatile applications (Huang et al. 1986; Rasmussen 2017). Originally referred to as "black aniline" for its dark green hue, a consequence of the bulk polymerization of aniline monomers, its initial misidentification as aniline black underscores the early complexity of its chemistry (Travis 1994). The historical trajectory of PANI began in 1862 with Henry Letheby's pioneering work, which laid the foundational understanding of aniline's transformative chemistry through oxidation processes. Letheby's experiments, particularly the oxidation of aniline monomer in sulfuric acid solutions using a platinum electrode, yielded a spectrum of colors from blue to purple, eventually leading to the synthesis of a pigment adhering to the electrode in shades ranging from dark blue to bluish green (Letheby 1862). By the 1890s, PANI's application extended to the textile industry as a pigment, a period that also saw the material's conductive properties being enhanced through acid doping, thus modulating its conductivity based on the pH environment. The seminal work of Alan MacDiarmid in the late 20th century introduced a paradigm shift in the understanding of PANI by identifying its variable oxidation forms - leucoemeraldine (fully reduced), emeraldine (partially oxidized), and pernigraniline (fully oxidized) states (Macdiarmid et al. 1987). This breakthrough provided insights into the tunability of PANI's electrical and electrochemical properties through doping and dedoping processes, employing a range of dopants including carbon-based materials and metal oxides. Such advancements not only expanded the functional versatility of PANI but also its morphological diversity, paving the way for its application across various technological and industrial sectors. This era of research opened new avenues for innovation, leveraging the inherent variability of conducting polymers to develop materials with tailored electrical properties and structural configurations (Sengupta et al. 2006; Visakh et al. 2017).

I.2.2. Structural Insights and Properties of Polyaniline

Subsequent research has elucidated the structural intricacies and diverse physical forms of PANI, underscoring its versatility and adaptability as a conducting polymer. PANI can be synthesized into various morphologies, including globular structures, nanotubes, and fibrils, each exhibiting distinct properties that contribute to its superiority over other conducting polymers (Zare et al. 2020). This versatility is not just a testament to PANI's morphological diversity but also to its multifaceted applications in various fields. Central to PANI's exceptional performance is its reversible redox property, a characteristic intimately linked to its unique molecular structure, which comprises alternating reduced and oxidized repeated units – specifically, benzene diamine and quinone diamine functional groups. This duality is beautifully illustrated in Figure I.4, which depicts the chemical structure of PANI.

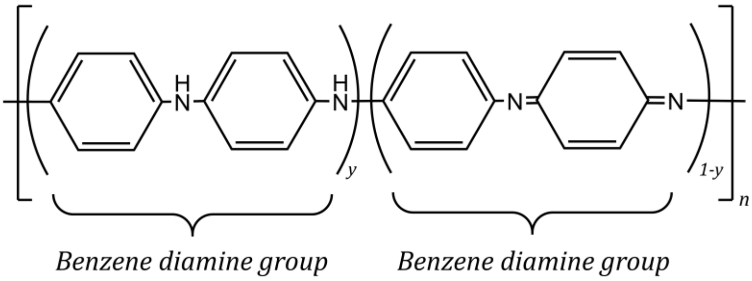

Figure I.4. Structural composition of PANI, illustrating benzene diamine and quinone diamine repeated units (Luo and Wang 2018).

The seminal insights by MacDiarmid shed light on the diverse nature of PANI, famously summarized in his quote: "*There are as many different types of PANI as there are people who synthesize it*" (MacDiarmid et al. 2001; Company and Laureates 2003). This diversity is largely a function of the synthesis method, choice of chemical or electrochemical doping agents, and the accompanying electrolytes, leading to PANI's varied oxidation states. For instance, a y-value of 1 corresponding to the fully reduced leucoemeraldine base state, whereas y = 0 denotes the fully oxidized pernigraniline base form. The most stable form, the emeraldine base, manifests at a semi-oxidized form when y = 0.5 (Macdiarmid et al. 1987). This variability is further illustrated in Figure I.5, which provides a comprehensive overview of PANI's redox and protonation states. PANI's color spectrum, ranging from transparent yellow color to green, blue, and violet, is a direct reflection of its oxidation states (Gupta and Miura 2006). Typically synthesized in acidic conditions, the protonated form of PANI, known as emeraldine salt, exhibits electrical conductivity in the range of $1 - 10\ S\ cm^{-1}$. In contrast, its base form has significantly lower conductivity, around $10^{-10}\ S\ cm^{-1}$ (Kulkarni 1993). This conductivity is modifiable through alterations in pH, dopant concentration, exposure to ambient oxygen or nitrogen, and variations in the electrochemical process parameters. On the other hand, the leucoemeraldine and pernigraniline forms of PANI are generally non-conductive, corresponding to their respective reduced, semi-oxidized, and fully oxidized forms. The synthetic versatility of PANI allows for its transformation from one form to another, such as the conversion of Emeraldine salt to either leucoemeraldine salt or pernigraniline salt, through oxidative or reductive processes (Huang et al. 1986; Wnek 1986; Li et al. 2009). Moreover, modifying the oxidation state of emeraldine salt through the introduction of diverse dopants and adjusting the doping level can significantly augment its conductivity. This highlights the tunability of PANI for a wide range of applications (Bhadra et al. 2009; Fratoddi et al. 2015a).

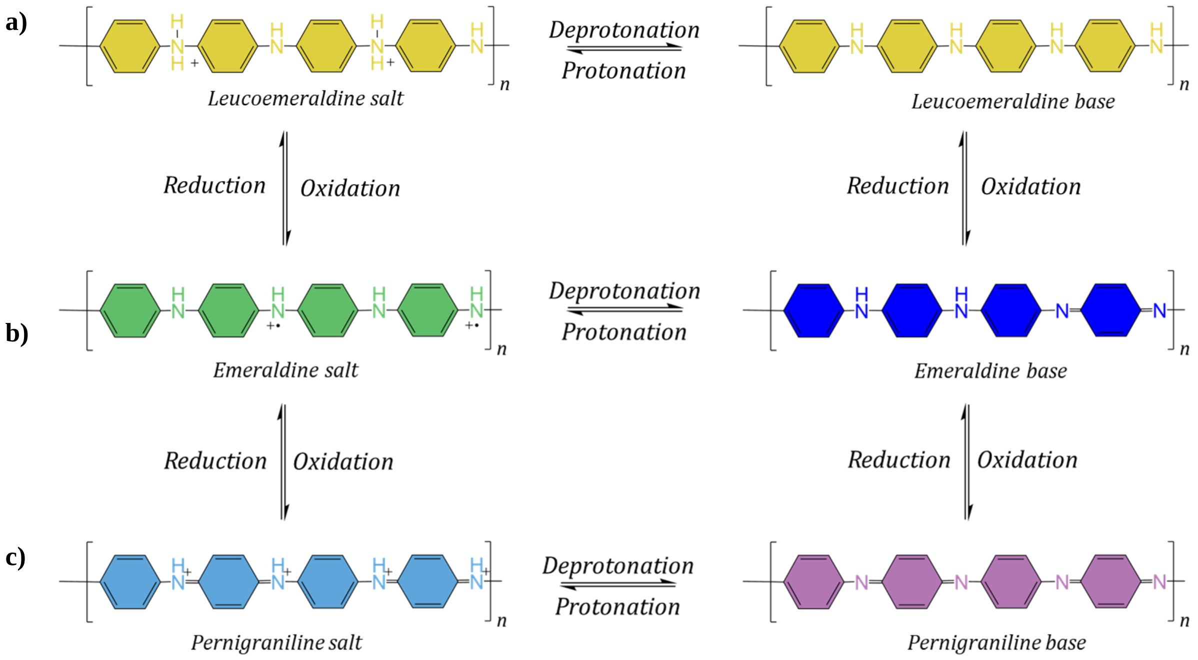

Figure I.5. Redox/Protonation forms and color variations of polyaniline (Zhang 2007).

I.2.3. Polyaniline Synthesis

The synthesis of PANI has evolved markedly, benefiting from a suite of innovative methodologies that span electrochemical polymerization, chemical polymerization, vapor-phase polymerization (VPP), photochemically initiated polymerization, enzyme-catalyzed polymerization, and polymerization employing electron acceptors. These varied approaches signify the breadth of ongoing research and development in PANI synthesis, underscoring a commitment to enhancing the polymer's properties and morphologies for bespoke applications and material specifications (Majeed et al. 2022).

A paradigmatic synthesis procedure commonly cited in literature involves oxidatively polymerizing aniline with ammonium peroxydisulfate (APS) under acidic medium, predominantly hydrochloric acid (HCl). This process results in the production of significant amounts of conductive PANI granules (Figure I.6). For example, detailed procedural documentation includes preparing a solution of APS (4.564 g) in 200 mL of HCl (2.5 M), followed by the gradual addition of 2 mL aniline under vigorous stirring at temperatures maintained below or equal to 5°C. This addition phase, lasting approximately 30 minutes, precedes a further 2 hours of stirring at near-freezing conditions, after which the reaction mixture is permitted to stand at room temperature (~28 °C) for 10–15 hours, leading to the formation of a dark green precipitate. This precipitate is then filtered, thoroughly washed until nearly colorless, and subsequently dried at 80 °C for 12 hours, culminating in the production of powdered PANI (Yang et al. 2010; Kumar et al. 2016; Kebiche et al. 2020).

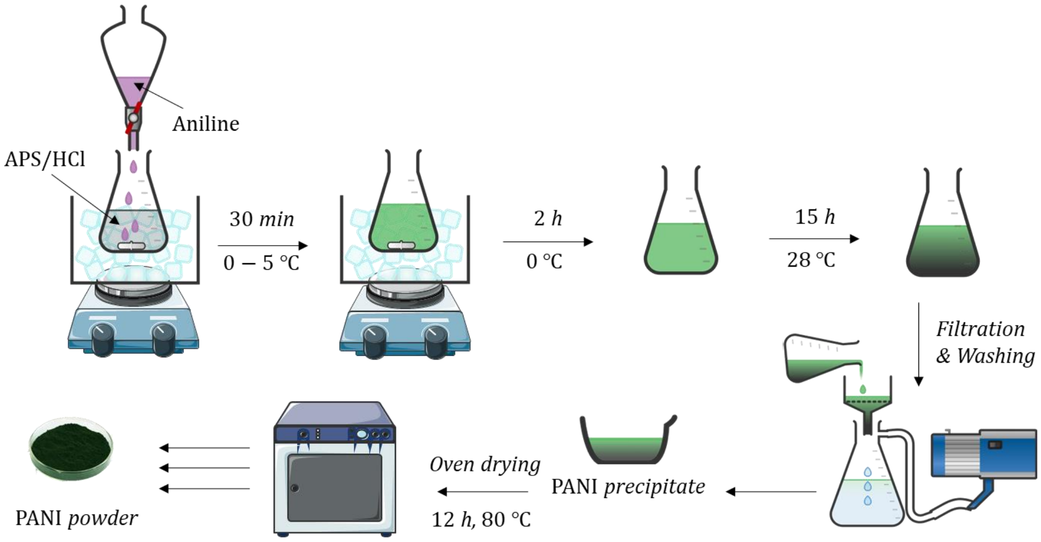

Figure I.6. Schematic illustration of PANI synthesis *via* oxidative polymerization (Rangel-Olivares et al. 2021).

The inherent electrical conductivity of PANI is closely tied to the uniform distribution of dopant sites across the surface of the polymer. These sites play a crucial role in adsorbing species that influence and regulate conductivity. PANI's synthesis yields elongated chains comprised of alternating structural units: the reduction unit $[B\text{-}NH\text{-}B\text{-}NH]_n$ and the oxidation unit $[B\text{-}N{=}Q{=}N]_n$ (Figure I.4 and Figure I.7). This *redox* dynamic facilitates the transition between benzenoid and quinoid structures, imbuing PANI with a distinct conjugated symmetry and resulting in pronounced asymmetry within its conducting and valence bands (Bhadra et al. 2009).

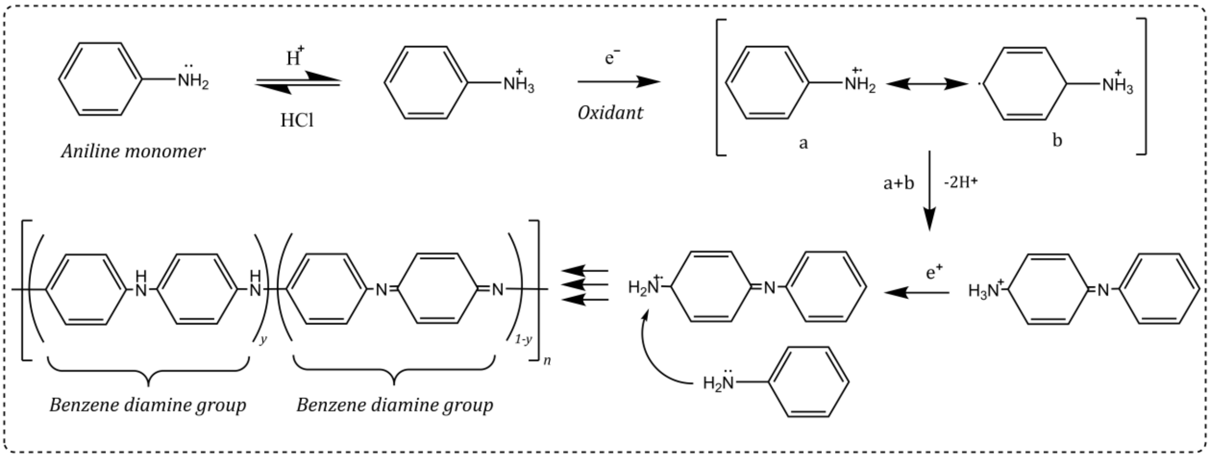

Figure I.7. Mechanism of PANI synthesis highlighting the structural units (Zhang et al. 2019c).

I.2.4. Polyaniline Applications

The exploration of conducting PANI nanostructures has become a focal point in contemporary materials science research, attributed to their versatile applicability across a spectrum of industrial domains. This interest is propelled by PANI's distinctive attributes, including its variable conductivity through doping and dedoping processes, remarkable chemical stability, cost-efficiency, ease of fabrication, and processability (Kulkarni et al. 1989; Stockton and Rubner 1997; Huang et al. 2003; Li et al. 2009). As a quintessential conducting polymer, PANI's adoption in the realms of electrical, optoelectrical, electrochemical, and gas sensing applications underscores its unparalleled utility (Sengupta et al. 2006; Kumar et al. 2020). PANI emerges as a superior alternative to traditional sensor materials, boasting fast response and recovery times, exceptional selectivity at room temperature, and obviating the need for the high operational temperatures—up to 300 °C—typically required by conventional sensors (Chakraborty et al. 2020). Pioneering developments by Hirata et al. (Hirata and Sun 1994) and Kukla et al. (Kukla et al. 1996) introduced the initial PANI-based material used as a sensors capable of detecting NH_3 gas, demonstrating response rates of 27% and 135% for concentrations of 10 and 100 ppm, respectively. These findings not only attest to PANI's environmental robustness and operability at ambient temperatures but also its repeatability in measurement accuracy. Despite these advances, challenges persist in fabricating PANI-based gas sensor devices that combine rapidity, full reversibility, heightened sensitivity, and functionality at ambient conditions (Li et al. 2018b; Zhang et al. 2019a). The seminal work of Hirata et al. has catalyzed a burgeoning interest in multifunctional PANI-based sensors, positioning them at the forefront of sensor technology research. Notably, the integration of PANI with graphene to form nanocomposites enriches the material's architecture with expansive surface areas attributed to well-defined two-dimensional (2D) nanostructures, enhancing its efficacy in gas detection applications. This evolving landscape of PANI applications, particularly in sensor technology, signifies a paradigm shift towards the development of highly efficient, cost-effective, and environmentally stable sensing materials. The subsequent section will delve into the foundational aspects of graphene and its derivatives, further elucidating their synergistic role in complementing PANI's functional versatility.

I.3. Brief introduction of Graphene and its derivatives

I.3.1. Fundamentals of Graphene

Graphene, a 2D monolayer of sp^2-bonded carbon atoms arranged in a hexagonal honeycomb lattice, stands as a revolutionary material within the realm of nanotechnology and materials science. This zero-band-gap semiconductor, characterized by its remarkable electrical, mechanical, and thermal properties, has catalyzed a paradigm shift in various research domains, including photovoltaics, biomedicine, and environmental engineering (Malik et al. 2019). The unique electronic structure of graphene, resulting from its sp^2 hybridization, endows it with extraordinary conductivity and optical transparency. Figure I.8 delineates the diverse allotropes of carbon, positioning graphene within the wider context of carbon nanostructures (Clemons et al. 2010).

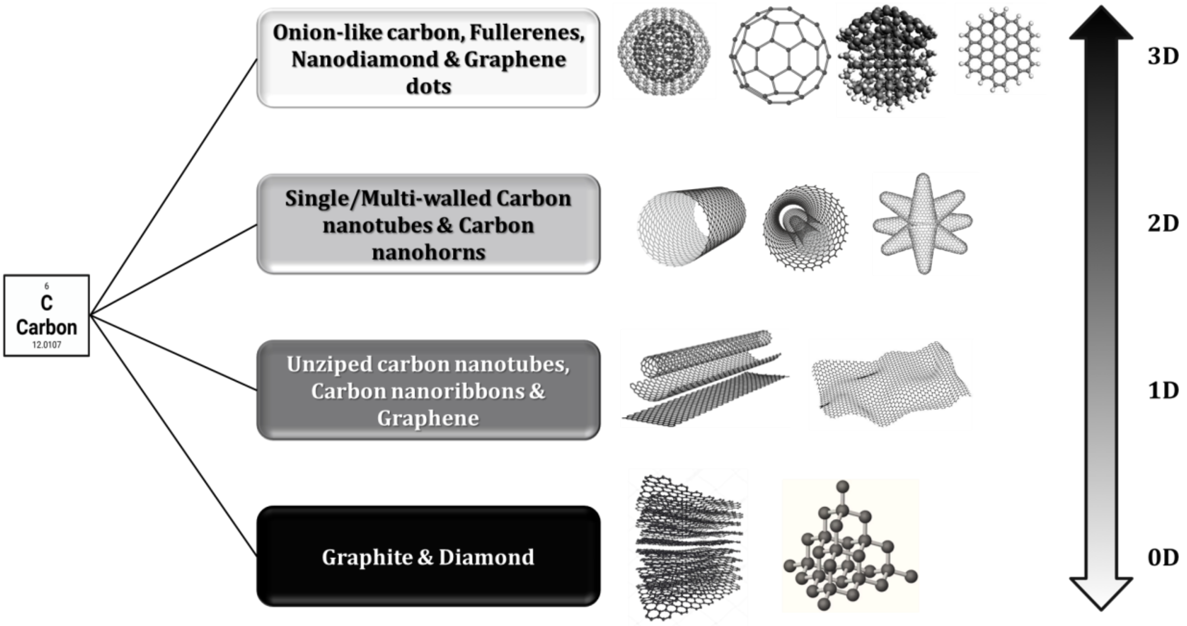

Figure I.8. Spectrum of carbon nanoallotropes: positioning graphene within the family of carbon materials (Jindal et al. 2022).

Since its isolation in 2004 by Andre Geim and Konstantin Novoselov, graphene has consistently occupied a prominent position in scientific inquiry. This recognition reached its pinnacle with the Nobel Prize in Physics awarded in 2010 for their groundbreaking research on this 2D material (Novoselov et al. 2004; Geim and Novoselov 2010; Bogue 2014).

I.3.2. Structural Characteristics and Synthesis

Graphene is not just a singular entity but extends to multilayer configurations, with up to ten layers being considered multilayer graphene (Waite and Nazarpour 2016). The interlayer van der Waals forces and the covalent bonding within the layers give rise to graphene's distinctive physical and chemical properties. The carbon-carbon bond length within the lattice is a mere 0.142 nm, contributing to the strength and flexibility of graphene sheets (D Ghuge et al. 2017). Figure I.9 offers an insight into the bonding configuration of graphene, highlighting its hybridized orbitals and the distribution of free electrons that facilitate its conductivity.

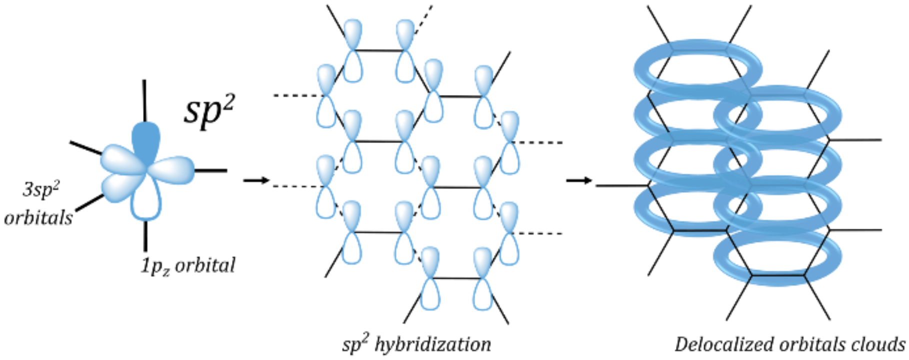

Figure I.9. Bonding configuration in graphene (Tiwari et al. 2020).

Graphene synthesis relies on two primary strategies: top-down and bottom-up methods, as depicted in Figure I.10. The top-down approach begins with graphite, with the goal of separating it into graphene layers using methods such as solid, liquid, or electrochemical exfoliation. A variation within this category involves transforming graphite oxide into graphene oxide (GO), then reducing it chemically or thermally. Conversely, the bottom-up technique constructs graphene by assembling molecular precursors through processes like chemical vapor deposition (CVD) or epitaxial growth. The resulting graphene's characteristics, including its layer count, defect levels, and its electrical and thermal conductivities, as well as its solubility and affinity towards water, vary significantly based on the chosen production method (Bhuyan et al. 2016; Lee et al. 2019; Zhang et al. 2019d, 2022b; Saeed et al. 2020; Wu et al. 2020).

The top-down approach commences with graphite as the starting material. It involves mechanical exfoliation techniques, such as the use of adhesive tape or atomic force microscopy (AFM) tips, to peel off graphene layers. This method also includes liquid-phase exfoliation, where graphite intercalation compounds (GICs) are expanded and then exfoliated to graphene, and subsequent steps where GO is chemically or thermally reduced to graphene. This procedure is noted for its economic efficiency and ability to produce graphene with minimal defects, and it can yield sheets of varying sizes, from nanometers to micrometers (Chen et al. 2010; Huh 2011; Park et al. 2011).

On the other hand, the bottom-up approach synthesizes graphene from smaller molecular precursors. This is achieved through processes such as the epitaxial growth on silicon carbide (SiC) substrates or by CVD, where hydrocarbons such as methane are decomposed on catalytic surfaces of metals like nickel or copper. The CVD process is particularly advantageous for producing large-area graphene films with properties such as high transparency and flexibility, suitable for various applications (Kumar et al. 2011; Brownson and Banks 2012; Mahmoudi et al. 2018; Plutnar et al. 2018).

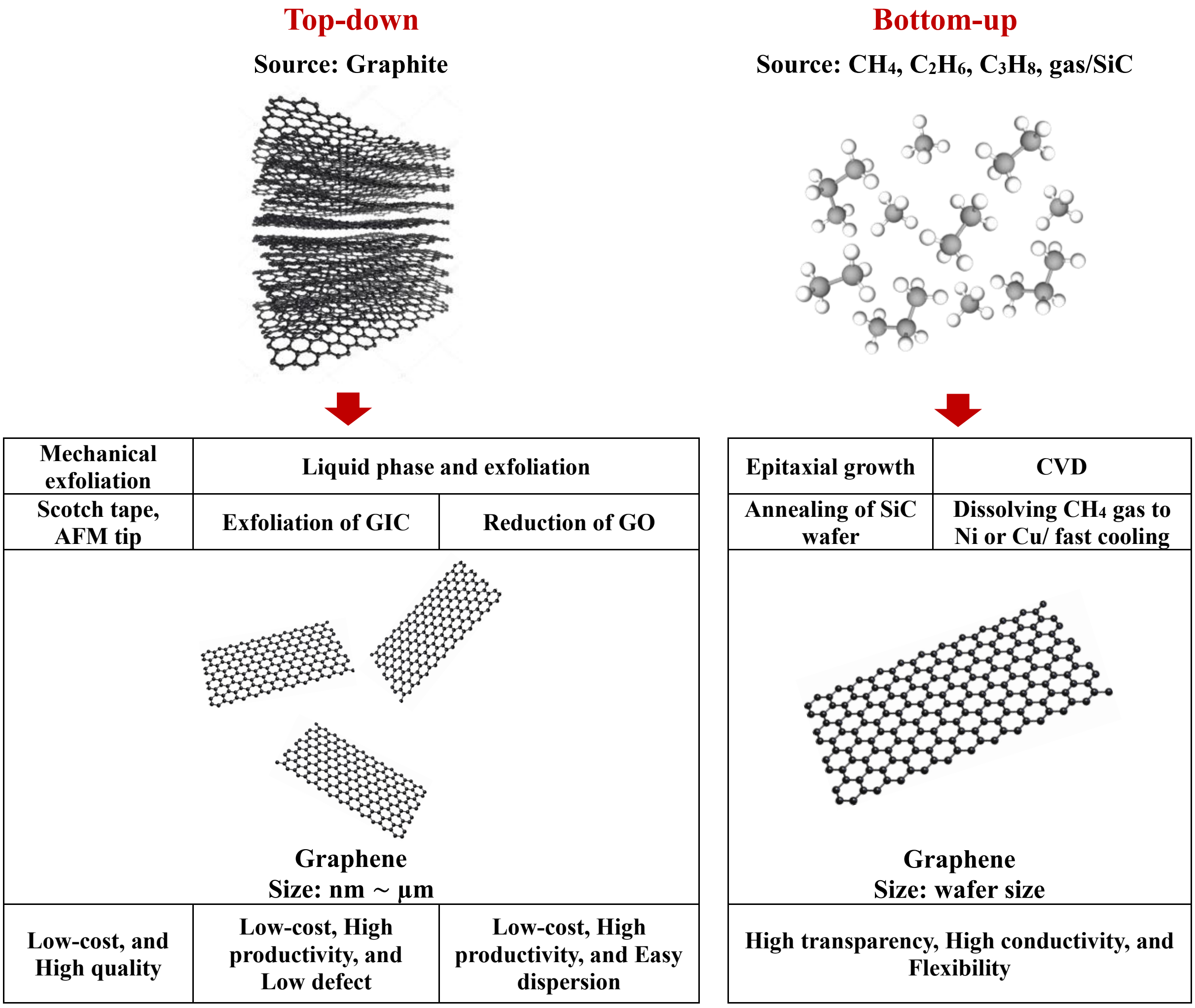

Figure I.10. Diagram illustrating the methods for synthesizing graphene, categorized into top-down and bottom-up strategies (adapted from reference (Mahmoudi et al. 2018)).

I.3.3. Functionalization of Graphene

The modification of graphene's functional forms, encompassing GO, rGO, graphene quantum dots (GQDs), as well as functionalized graphene, has propelled graphene's application spectrum forward, particularly by ameliorating its solubility and processability. Such derivatives have become critical in the innovation of applications ranging from advanced energy storage systems to sophisticated sensing technologies. Figure I.11 presents the distinct chemical structures of these graphene derivatives, highlighting the strategic chemical modifications designed to customize their attributes for specific applications (Young et al. 2012; James and Tour 2013).

For example, the functional groups present on GO, including carboxylic, hydroxyl, and epoxy, as depicted in Figure I.11, not only improve its aqueous dispersion but also prevent re-stacking of individual layers, thus maintaining its exfoliated state. This functionality is leveraged to attain superior dispersion of graphene derivatives in various solvents. Efforts to enhance the compatibility of GO and rGO within polymer matrices have focused on functionalizing these derivatives with organic molecules that fortify the interfacial interaction with the matrix (Guezzout et al. 2023).

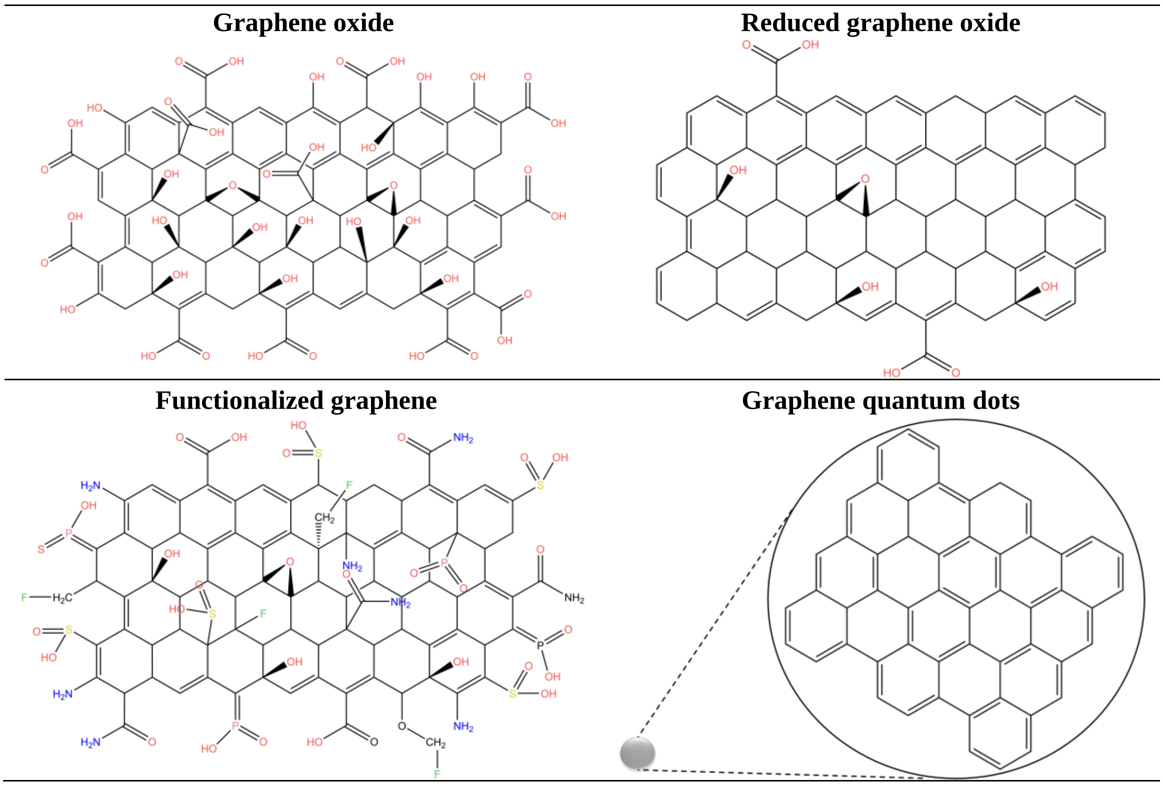

Figure I.11. Chemical structures of graphene derivatives (Tiwari et al. 2020; Díez-Pascual and Luceño-Sánchez 2021).

Table I.3. Overview of the physicochemical properties of graphene, GO, rGO and GQD.

Property	Graphene	GO	rGO	GQD	Reference
Electrical conductivity (S m^{-1})	~10^4	~0.50	2.00×10^2 – 3.50×10^5	-	(Gao et al. 2009; Park et al. 2009; Goenka et al. 2014)
Surface area (m^2 g^{-1})	2.63×10^4	~2.39×10^4	~2.73×10^4	18.41×10^4	(Stoller et al. 2008; Zhang et al. 2020b; Tang et al. 2022)
Electron mobility (cm^{2}V^{-1}s^{-1})	2.00×10^5 – 2.50×10^5	0.10–10.00	3.00×10^3 – 1.00×10^4	-	(Gómez-Navarro et al. 2007; Bolotin et al. 2008)
Energy gap (eV)	~0.27	~2.20	~1.00 – 1.69	2.20 – 3.10	(Zhan et al. 2012; Liang 2014; Mattson et al. 2014; Tian et al. 2014a; Yan et al. 2018)

The physicochemical properties of graphene and its derivatives, as presented in Table I.3, offer a comparative perspective on their respective electrical conductivities, surface areas, and additional essential properties. This table emphasizes the superior performance enhancements achievable when graphene is integrated into polymer matrices, even at minimal filler concentrations. Notably, graphene's vast surface-to-volume ratio presents a significant advantage over conventional fillers like carbon nanotubes (CNTs), further promoting its utilization for the reinforcement of polymer matrices.

I.3.4. Emerging Trends in Graphene Research

The advent of graphene-based nanocomposites marks a significant milestone in the realm of material science, heralding a new era of technological advancements and sustainable solutions. Figure I.12 serves as a testament to the wide array of applications stemming from graphene derivatives in nanocomposite materials, showcasing the material's exceptional adaptability and its substantial influence on enhancing polymer matrix performance (Madurani et al. 2020). The strategic incorporation of graphene into conducting polymers transcends mere property enhancement, paving the way for groundbreaking applications across a spectrum of sectors. This pivotal integration highlights the revolutionary capacity of graphene-based nanocomposites to redefine the landscape of modern industries. The synergy between graphene and polymers, particularly conducting polymers, not only augments the intrinsic properties of the composites but also fosters the emergence of cutting-edge applications, from revamping electronics to pioneering eco-friendly materials.

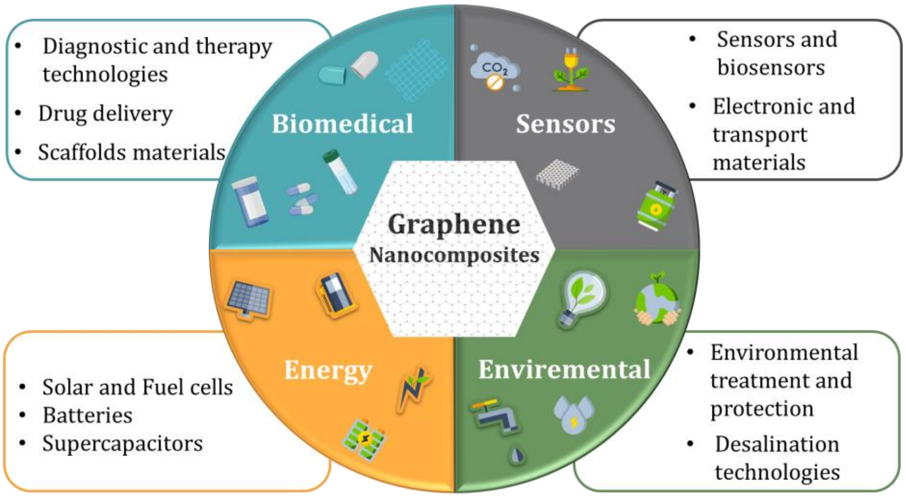

Figure I.12. Graphene-based nanocomposites applications in research and industry. Reproduced from (Madurani et al. 2020).

This collaboration underlines the transformative essence of graphene-based nanocomposites, positioning them as key players in the evolution of industry practices and the pursuit of sustainability. For instance, the intrinsic sensitivity of graphene to gas molecule adsorption renders it an extraordinary candidate for semiconductor gas sensors. Such sensors benefit from graphene's eminent sensitivity, a characteristic so pronounced that Geim and Novoselov have deemed it to possess "ultimate sensitivity" for detecting molecular interactions (Novoselov et al. 2004). Thus, ongoing research and development efforts are poised to further unlock the potential of graphene-polymer nanocomposites, tailoring their attributes to meet specific technological and scientific demands. The future of graphene nanocomposite research promises a trajectory of continual innovation, offering bespoke solutions to the intricate challenges of contemporary engineering and material science. This forward momentum is anticipated to catalyze a wave of technological breakthroughs, cementing the role of graphene-based materials in shaping the next frontier of scientific exploration and industrial application.

I.4. Polyaniline/graphene-based nanocomposites

The combination of PANI with graphene represents a frontier in the development of nanocomposites, merging the electrical prowess of conducting polymers with the mechanical robustness and sensory acuity of carbon-based materials. This synergistic combination has sparked considerable interest, thanks to its potential to revolutionize fields ranging from energy storage to environmental sensing (Meer et al. 2016; Hong et al. 2019; Zhao et al. 2022). Figure I.13 offers an illustrative summary of the multifaceted properties, synthesis methodologies, and the expansive application spectrum of graphene-PANI nanocomposites, underlining the substantial enhancements these composites introduce to polymer matrices.

I.4.1. Synthesis and Morphological Control

Recent advancements in the field of material science have led to the development of graphene/PANI nanocomposites, showcasing a notable synergy between the electrical and mechanical properties of conducting polymers and carbon-based materials (Wang et al. 2014a; Kazemi et al. 2021).

This section delves into the diverse synthesis techniques and the controlled morphological characteristics of these innovative materials, highlighting their significant impact on enhancing composite properties and broadening application horizons. Moreover, a variety of synthesis methods have been explored to fabricate PANI/graphene nanocomposites, each contributing to the unique textural, electrical, and mechanical properties of the final product. These include:

- ***In-situ* electropolymerization:** These methods involve direct polymerization of aniline in the company of either graphene or its derivatives. The process facilitates fine integration of graphene into the PANI matrix, enhancing electrical conductivity and thermal stability through π-π interactions (Ansari et al. 2014a; Zhang et al. 2019a).
- **Interfacial polymerization:** Leveraging the interface between two immiscible phases, this technique allows for the precise control over the polymerization process, leading to nanocomposites with distinct interfacial properties.
- ***In-situ* oxidative polymerization:** Commonly used for PANI, this approach introduces graphene or its derivatives into the polymerization medium, enhancing the interaction between PANI and graphene (Yang et al. 2014; Raji et al. 2019). Although *in-situ* polymerization offers numerous advantages for promoting the effective dispersion of nanofillers within PANI matrix, it is not without drawbacks. These includes complicated methods and processing stages and the use of costly reactants (Verdejo et al. 2009).
- **Solution mixing:** This approach, often used for its simplicity and effectiveness in achieving even distribution of graphene, involves the blending of graphene with PANI in a suitable solvent. Despite its advantages, challenges arise in completely removing solvents post-processing (He et al. 2014).
- **Self-Assembly:** Leveraging molecular interactions to create ordered structures, this method faces challenges in scalability and purification but offers precise control over composite architecture (Gao et al. 2006; Smith et al. 2011; Wu et al. 2018b).
- **Electropolymerization:** An innovative method characterized by its rapid process and environmental friendliness, electropolymerization utilizes a three-electrode system to

polymerize aniline on the electrode surface, efficiently integrating graphene into the PANI structure (Zhang et al. 2015; Tomczykowa and Plonska-Brzezinska 2019).

Each method impacts the composite's morphology, influencing properties such as conductivity, mechanical strength, and surface area. Figure I.13 illustrates the synthesis, structural characteristics, and multifunctional applications of these nanocomposites, providing a visual comprehension of their role in advancing material science and engineering solutions.

Consequently, Table I.4 and Figure I.13 collectively provide an in-depth analysis of various synthesis strategies employed for crafting graphene/PANI nanocomposites, showcasing the breadth of their applications across multiple technological fields. This detailed compilation underscores the adaptability and efficacy of these nanocomposites in addressing contemporary technological challenges. Table I.4 further elucidates the diverse synthetic pathways leveraged to integrate graphene derivatives with polyaniline, tailoring the nanocomposite's properties for specific functionalities. From enhancing the sensitivity of gas sensors to improving the energy storage capacity of supercapacitors, these methodologies reflect the transformative impact of PANI/ graphene nanocomposites across a spectrum of applications.

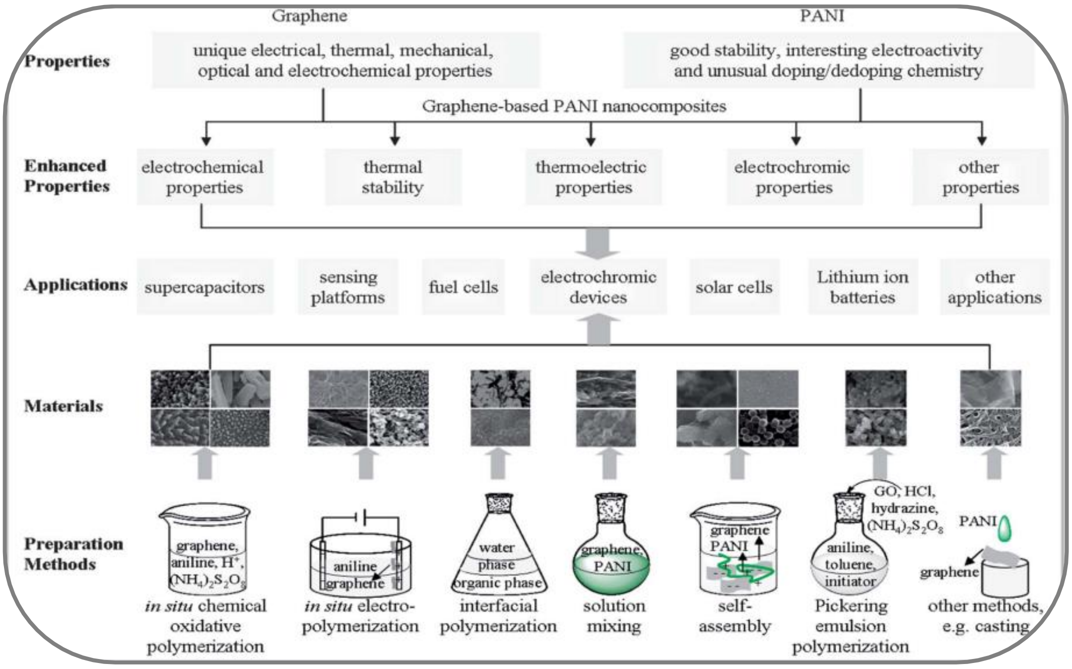

Figure I.13. Diagrammatic summary of characteristics, synthesis approaches, and utilizations of nanocomposites comprising PANI and graphene (Wang et al. 2014a).

Table I.4. Selected preparation methods for nanocomposites of polyaniline with graphene and their applications.

Conducting Polymer	Nanofiller	Synthesis method	Application	Reference
PANI	rGO	Chemical oxidative polymerization *(In-situ)*	NH_3 Sensors	(Huang et al. 2012)
		Microwave irradiation and *in-situ* chemical polymerization	Active electrode material for supercapacitors	(Nguyen and Shim 2015)
		Reduction, doping, and *in-situ* chemical polymerization	High-performance supercapacitors	(Wang et al. 2014b)
PANI	Graphene	*In situ* chemical oxidatively polymerization	Electrodes and hydrophobicity	(Parveen et al. 2016)
		Single-step electrochemical co-layering	Flexible supercapacitors	(Wen et al. 2017)
		Chemical decreasing and electro-polymerization	High-efficiency supercapacitor	(Cong et al. 2013)
PANI	GO	Modified Hummers method and layer-by-layer assembly	Lithium-sulfur batterie	(Moon et al. 2015)
		In situ chemical oxidatively polymerization	NH_3 and CH_3OH detection	(Konwer et al. 2013; Li et al. 2018c)

I.4.2. Synergistic Material Properties of Polyaniline/Graphene Nanocomposites

As aforementioned, the integration of PANI with graphene and its derivatives has heralded a new era in the development of nanocomposites, characterized by a harmonious blend of properties that significantly exceed those of their individual components. The exceptional electrical conductivity, environmental robustness, and pseudocapacitive nature of PANI synergize with the mechanical resilience, vast surface area, and electrical conductivity inherent to graphene. This symbiotic relationship fosters marked enhancements in electrochemical performance, rendering these nanocomposites highly suitable for a broad array of applications spanning electronic devices to energy storage systems (Chen et al. 2023a; Zhang et al. 2023).

The interplay between PANI and graphene leads to pronounced improvements across several metrics, including thermal behavior, electrical conductivity, mechanical strength, optical properties, and electrochemical performance. These advancements position the nanocomposites as superior alternatives to their pristine counterparts (Kumar and Baek 2014; Wang et al. 2014a). However, challenges associated with graphene's insolubility in water and its tendency to agglomerate, a consequence of van der Waals interactions, have necessitated the exploration of graphene derivatives. Thus, GO, and rGO as well as functionalized graphene have thus emerged as viable nanofillers, addressing these limitations and enhancing the compatibility of graphene within polymer matrices (Díez-Pascual and Luceño-Sánchez 2021; Chen et al. 2023b).

Incorporating graphene into PANI leads to the formation of a donor-acceptor complex, where graphene acts as the electron acceptor and aniline, the monomer of PANI, as the electron donor. This interaction, facilitated by their conjugated π electrons, results in the formation of PANI fibers on the surface of graphene, establishing a *π*-*π** conjugation arrangement that significantly augments the doping level of PANI. Figure II.14 illustrates the stages of this interaction, from the initial adsorption of aniline onto graphene to the polymerization of PANI and the resultant effects of the *π*-*π** conjugation arrangement on the performance of the nanocomposite (Zengin et al. 2002; Zhou et al. 2010; Terrones et al. 2011).

This conjugation system not only enhances the electrical conductivity of the nanocomposites but also improves their electrochemical performance, making them particularly attractive for applications requiring high conductivity and stability (Wu et al. 2013a). The graphene-PANI interaction, especially the creation of the *π*-*π** conjugation arrangement, enriches the nanocomposites with a greater electron cloud area, facilitating improved charge interaction among gas particles and the *π* electrons of the system (Yan et al. 2010; Zhou et al. 2010).

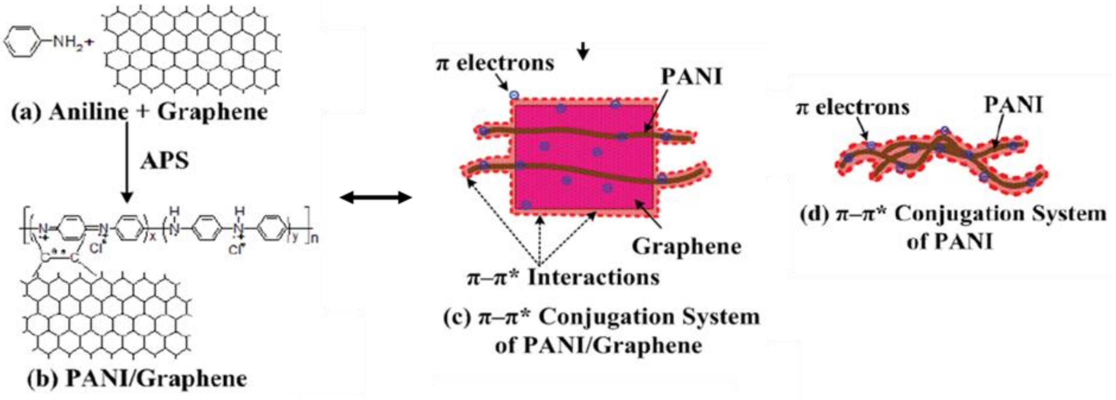

Figure I.14. Illustrative representation of the *π*-*π** conjugated network: (a) Interaction of aniline with graphene, (b) synthesis of the graphene/PANI composite, (c) Influence of the *π*-*π** conjugated structure in graphene/PANI, and (d) Influence of the π-π* conjugated structure in PANI.

The advancement of polyaniline/graphene nanocomposites, underpinned by the strategic control of their synthesis and the in-depth understanding of their synergistic material properties, underscores the potential of these materials in pushing the boundaries of current technologies. As research progresses, these materials are predictable to performance a pivotal role in the development of next-generation electronic and energy storage solutions, among other applications.

I.4.3. Prospects and Innovations in Polyaniline/Graphene Nanocomposites

The journey to enhance the electrical characteristics of graphene-based PANI nanocomposites has been marked by significant scholarly attention, resulting in notable improvements in electrical conductivity and supercapacitance. These advancements have broadened the spectrum of applications for these materials, spanning electronic devices (Mitra et al. 2015), high-performance supercapacitors (Ladrón-de-Guevara et al. 2019), advanced energy storage systems (Martins et al. 2021), sensitive sensing arrays (Huang et al. 2012; Chang et al. 2021) and innovative fuel-cell technologies (Zhao et al. 2018), among others. This multifaceted exploration underscores a transformative phase in materials science, where PANI/graphene nanocomposites are at the forefront of pioneering new realms of possibilities within various technological sectors.

Looking ahead, the trajectory for PANI/graphene nanocomposites is rich with potential. The ongoing advancements are not just enhancing the physical and chemical properties of these materials but are also paving the way for their integration into next-generation technological solutions. The focus on optimizing their electrical characteristics is expected to yield even more sophisticated applications, thereby expanding the role of conducting polymers in addressing complex engineering and environmental challenges.

Key future directions include:

- **Enhanced Performance:** Continuous efforts to refine the synthesis processes and post-treatment techniques aim to further elevate the intrinsic qualities of PANI/graphene nanocomposites, particularly targeting higher conductivity and energy density for supercapacitors and batteries.
- **Sustainability and Environmental Applications:** Leveraging the eco-friendly nature of PANI and the mechanical robustness of graphene, future research will likely explore sustainable applications, such as biodegradable electronics and green energy solutions.
- **Biomedical Innovations:** The biocompatibility and flexible characteristics of these nanocomposites open new avenues in medical technology, including wearable health monitors and implantable devices for drug delivery and diagnostics.
- **Advanced Sensing Platforms:** With their enhanced sensitivity and selectivity, PANI/graphene sensors are set to revolutionize environmental monitoring, healthcare

diagnostics, and security systems through the detection of a wider variety of chemical and biological analytes.

As a results, the exploration and development of PANI/graphene nanocomposites are carving out a niche in the landscape of materials science, championing the evolution of conducting polymers into a cornerstone of modern technological and environmental solutions. As this field continues to mature, it promises to deliver groundbreaking innovations that will redefine the capabilities of smart materials in the 21st century and beyond.

I.5. Literature survey: Insights for improving polyaniline/graphene performance

A comprehensive survey of the literature reveals extensive research aimed at optimizing the electrical properties of PANI/graphene nanocomposites under ambient conditions. These studies identify several critical factors influencing performance, including synthesis methods, morphologies, component ratios, doping types, protonation degrees, redox states, and temperature (Tian et al. 2014b). For example, doped PANI/GO composites have demonstrated an electrical conductivity (σ) of $10\, S\, cm^{-1}$ and a specific capacitance of $531\, F\, g^{-1}$, significantly surpassing the performance of pristine PANI, which shows values of 2 $2\, S\, cm^{-1}$and $216\, F\, g^{-1}$, respectively (Wang et al. 2009). These enhancements underscore the potential of PANI/graphene nanocomposites for broad application in electronics, supercapacitors, sensors, fuel cells, and more (Kazemi et al. 2021).

Nanocomposite materials comprising PANI and graphene have demonstrated enhanced electrical properties when compared to their individual constituents. The conductivity and dielectric constants of these nanocomposites are influenced by the graphene loading in PANI, suggesting a diverse array of potential applications in the electrical sector. Research findings indicate that the conductive PANI forms selectively ordered deposits on the surfaces of GO due to the influence of electrostatic forces, hydrogen bonding, and π-π interactions, thus facilitating carrier mobility (Zhou et al. 2010; Tung et al. 2017; Kulkarni et al. 2018). For example, the electrical conductivity of PANI/GO nanocomposites increased from 0.71 to 4.71 S cm^{-1} as the GO loading was raised from 0 to 20 wt.% (Yin et al. 2016). In another research work, the reported conductivity of PANI/rGO with 50 wt.% rGO loading was 18.078 S cm^{-1}, demonstrating a substantial increase compared to the conductivity of pure PANI (Mitra et al. 2015). Graphene's exceptional properties, such as direct current (DC) conductivity, high carrier mobility, and robust mechanical attributes, contribute to its outstanding electrical, mechanical, and morphological characteristics. Enhanced conductivity rGO synthesized through microwave-assisted reduction highlights these capabilities (Iskandar et al. 2017). Research studies by Chen et al. (Chen et al. 2013) and Lin et al. (Lin et al. 2014) reported PANI/GO nanocomposites achieving higher electrical conductivities than pure PANI, attributed to improved charge transfer mechanisms facilitated by graphene integration. Similarly, Ansari et al. (Ansari et al. 2014b) found that sulfonated PANI/graphene nanocomposites exhibited significantly higher electrical conductivity. Table I.5 compiles electrical conductivities from various PANI and PANI/graphene nanocomposites, elucidating the significant role of synthesis methodologies and graphene modifications in tuning electrical properties. This comprehensive overview showcases the promising capabilities of PANI/graphene nanocomposites as high-performance materials for a myriad of technological implementations. In Table I.5, the conjunction with the insights from the literature, underscores the significant advancements in synthesizing PANI/graphene nanocomposites with tailored electrical properties. As the field progresses, these findings are poised to spur further innovations in material science, opening avenues for new applications in electronics, energy storage, and sensing technologies. The ongoing exploration and refinement of these composites promise to yield even more sophisticated materials, harnessing the unique synergies between PANI and graphene to meet the evolving demands of modern engineering and technology.

Table I.5. Conductivity properties of nanocomposites based on PANI, graphene, and their derivatives.

PANI-based nanocomposite	Synthesis method	Temperature (℃)	Electrical Conductivity (S cm^{-1})	References
PANI	Electro-chemical method	RT	6.30×10^{-4}	(Bhadra et al. 2007)
PANI	*In-situ* oxidative method	-	10^{-4}	(Kar and Choudhury 2013)
PANI	*In-situ* self-organization method	RT	3.50×10^{-3}	(Reddy et al. 2009)
PANI/Carbon black			1.38	
PANI	*In-situ* oxidative method	30 ℃	6.02	(Li et al. 2010)
PANI		10 ℃	1.88	
PANI/ZnO	*In-situ* oxidative method	RT	1.93	(Khan and Khalid 2010)
PANI	*In-situ* oxidative method	RT	3.26×10^{-4}	(Umare et al. 2010)
PANI	*In-situ* polymerization	RT	3.18×10^{-4}	(Chen et al. 2013)
PANI/Gr			2.53	
PANI/Gr@Ag			20.32	
PANI/Gr@Ni			6.28	
PANI	*In-situ* oxidative method	RT	15.40	(Du et al. 2013)
PANI/Gr			120.10	
PANI/GO	Emulsion polymerization	RT	4.74	(Imran et al. 2014)
PANI/GO	*In-situ* polymerization	RT	1.23×10^{-2}	(Lin et al. 2014)
PANI/rGO	*In-situ* polymerization	RT	18.08	(Mitra et al. 2015)
PANI	*In-situ* oxidative method	RT	4.40	(Islam et al. 2016)
PANI/Gr			5.20	
PANI/Gr@Au			7.00	
PANI	Chemical polymerization	90 ℃	7.5×10^{-4}	(Konwer 2016)
PANI/GO		30 ℃	0.47	
PANI/GO		110 ℃	0.84	
PANI	*In-situ* polymerization	RT	1.25	(Ismail et al. 2019)
PANI/MoO_2			2.37	
PANI/Gr			5.58	
PANI/Gr/MoO_2			9.87	
PANI	*Interfacial* polymerization method	RT	4.12×10^{-2}	(Adrian et al. 2019)
PANI-DBSA			5.56×10^{-2}	
PANI/Gr-DBSA			7.31×10^{-2}	
PANI	*In-situ* oxidative method	RT	2.05×10^{-2}	(Usman et al. 2019)
PANI/rGO			6.74×10^{-2}	
PANI/rGO/Chitosan			5.28×10^{-2}	
PANI	*In-situ* polymerization	RT	1.79×10^{-2}	(Firdaus et al. 2020)
PANI/Gr			7.28×10^{-2}	
PANI/Gr-DBSA			8.07×10^{-2}	
PANI/Gr	Solvent blending method		8.62×10^{-3}	
PANI/Gr-DBSA			1.20×10^{-2}	
PANI	*In-situ* oxidative method	RT	1.27×10^{-2}	(Ali et al. 2021)
PANI/N-GO			0.75	
PANI/rGO/LCNF	*In-situ* oxidative method	RT	0.96	(Tanguy et al. 2022)
PANI/GO/APTES	Chemical polymerization	RT	7.32×10^{-2}	(Alruwais et al. 2021)

I.4. Gas sensor properties of PANI/graphene-based nanocomposites

Recent advancements in the field of PANI/graphene-based gas sensors have garnered significant attention due to their unique structural characteristics, superior sensing performance, room temperature operational ability, and broad application spectrum (Wang et al. 2016; Hosseingholipourasl et al. 2020). These developments mark a notable progression in enhancing the functionality of graphene-centric gas detection technologies. Hadano et al.

(Hadano et al. 2021) described the gas detection mechanism within PANI/rGO composites, noting the strategic positioning of rGO clusters among PANI molecular chains, as depicted in Figure I.15. The use of N-methyl-2 pyrrolidone as a softening agent during the composite synthesis encourages cluster formation. This composite is then applied as a slender film over an interdigital electrode array, serving as the sensor for NH_3, showing a 250% sensitivity at 100 ppm within 97 s and detecting levels as low as 5 ppm.

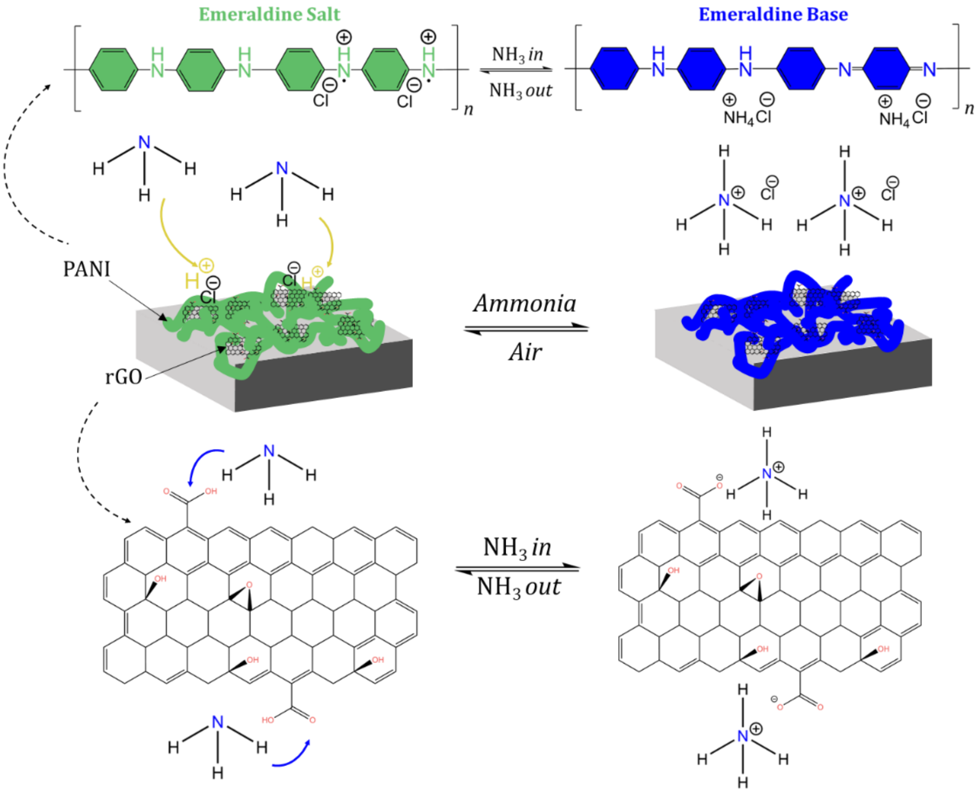

Figure I.15. The proposed NH_3 sensing mechanism of PANI/rGO nanocomposites (adapted from reference (Hadano et al. 2021)).

As illustrated in Figure I.15, NH_3's interaction with PANI/rGO leads to a phase shift in PANI from its emeraldine salt form to the emeraldine base state, diminishing the availability of charge carriers and, consequently, the mobility of charge transfer, thereby elevating the composite's resistance (Javadian-Saraf et al. 2021; Gautam et al. 2022). This deprotonation process impacts the conductivity of both PANI as well as PANI/rGO (Timmer et al. 2005). Furthermore, the role of rGO in the sensing mechanism is emphasized, where its resistance spikes upon NH_3 contact, primarily due to the interaction between NH_3's nucleophilic hydrogen and the electrophilic carboxyl (-COOH) groups on rGO's surface, alongside its extensive surface area (Hu et al. 2013; Samaddar et al. 2018; Zhang et al. 2019b).

The performance of gas sensors is gauged by several parameters including response, sensitivity, selectivity, stability, response and recovery times, detection limits, and operational temperatures (Yang et al. 2013). The gas sensor's response is determined by the redox properties of the analyzed gas and the type of majority carrier in the sensing material, causing shifts in the sensor's resistance (Zhang et al. 2022a). Sensitivity is closely associated with the resistance change of the sensing material when exposed to gas. The sensitivity (S) of a gas sensor can be quantified through different equations (Mirzaei et al. 2016):

$$S = \frac{R_a}{R_g} \tag*{Eq. (1)}$$

$$S = \frac{R_g}{R_a} \tag*{Eq. (2)}$$

$$S = \frac{R_a - R_g}{R_g} \tag*{Eq. (3)}$$

$$S = \frac{R_a - R_g}{R_a} \tag*{Eq. (4)}$$

where R_a is the resistance in clean air and R_g is the resistance in the presence of the target gas. The sensor's response is presented as a percentage, calculated as $S \times 100\%$. This mechanism affects electron mobility and thus alters the material's conductivity, inversely related to resistivity. The electrical conductivity (σ) is defined by Eq. (5) (Chen et al. 2013):

$$\sigma = \frac{1}{q} \tag*{Eq. (5)}$$

where q represents electrical resistivity, further detailed as (Chen et al. 2013):

$$q = R_s \times t \tag*{Eq. (6)}$$

Here, R_s stands for the sheet resistance and t denotes the thickness of the sample. Therefore, integrating Eq. (5) and Eq. (6) (Chen et al. 2013), gives us:

$$\sigma = \frac{1}{R_s \times t} \tag*{Eq. (7)}$$

The variations in resistance observed in PANI/graphene nanocomposite materials are explicated through a recognized gas sensing mechanism. Figure I.16 presents a diagrammatic portrayal of the custom-built apparatus for testing gas sensor functionality. The process operates on the principle that when gas molecules adhere to the sensor material's surface, it results in a concomitant increase in the Schottky barrier height (Skucha et al. 2010).

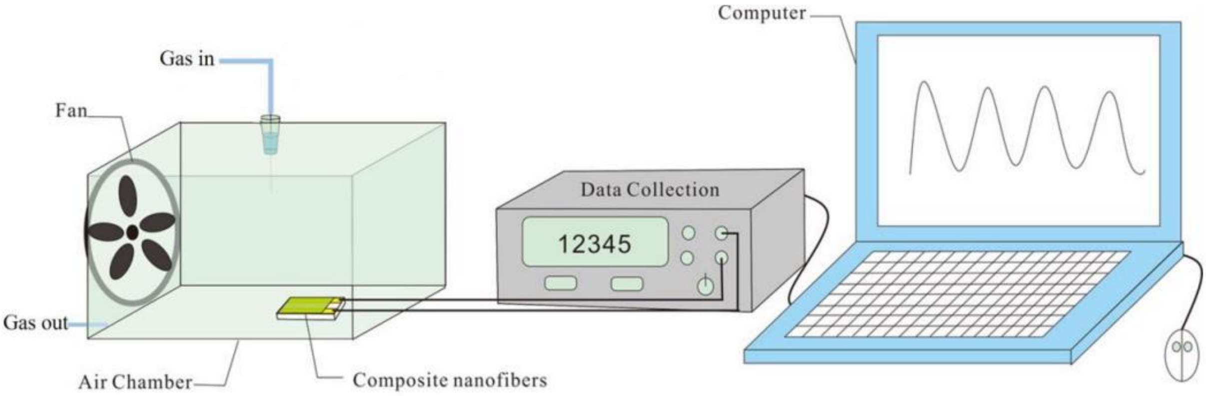

Figure I.16. Diagrammatic representation of the custom-designed gas sensing evaluation setup (Pang et al. 2021b).

Identifying the mechanism of charge transfer, the spatial distribution of surface electron charge, and the electrostatic potential shift upon gas exposure is pivotal (Wang et al. 2020). Illustrative in Figure II.17 are the energy differentials between the conduction band (E_c) and the valence band (E_v) in N-QGD, as well as the delineation of the highest occupied (HOMO) and lowest unoccupied (LUMO) molecular orbitals in PANI, alongside the Fermi level (E_f) alignments relative to the vacuum across the energy band structure of PANI/N-GQD nanocomposites. A synergistic p-n junction is formed where the *p*-type PANI robustly interfaces with the *n*-type N-GQD (Hong et al. 2021), depicted in Figure I.18. Within this intersection's depletion zone, a unique electronic environment is established. The resistive properties of the PANI/N-GQD nanocomposites are subject to change upon NH_3 gas exposure, due to the migration of electrons from PANI's depletion layer and the counter-movement of holes in N-GQD. In ambient air, surface-bound oxygen molecules siphon electrons from the nanocomposites' conduction and valence bands, heightening resistivity. These oxygen molecules, once engaged with NH_3, can alleviate electron concentration within the conductive band, diminishing the depletion region. The surface interactions with gas profoundly influence the semiconductor's conductive traits, consequently altering the resistance and heightening the material's gas detection response (Meng et al. 2015; Zhang et al. 2018). Subsequently, the conductive and resistive features of the sensor material are interdependent, shifting with the nature of the material and the gas concentration encountered.

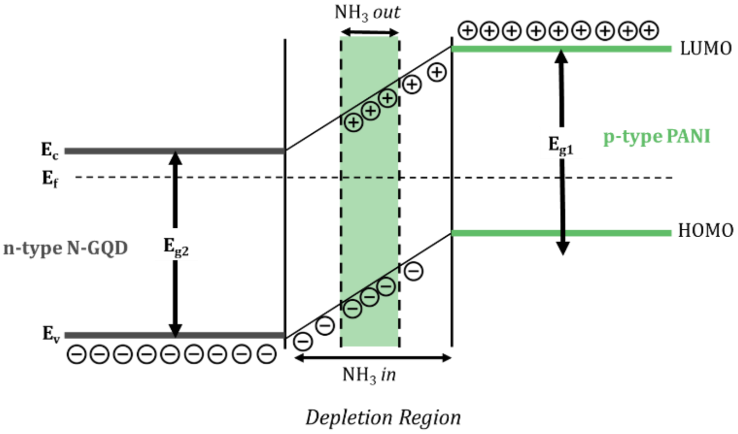

Figure I.17. Diagrammatic representation of the p-n heterojunction and energy band gap structure of PANI/N-GQD (Produced from (Hong et al. 2021)).

PANI, while utilized in gas sensor materials, faces limitations such as sensor variability over time, low temperature stability, minimal responsiveness, and sensitivity to moisture. Notably, its reaction to NH_3 gas is non-reversible, and its stability decreases with extended exposure to the gas, although reversibility can be achieved if exposure is under 10 minutes (Nicolas-Debarnot and Poncin-Epaillard 2003). To overcome these challenges, PANI has been combined with nanoscale graphene-based materials to create composites. (Pandey 2016; Hakimi et al. 2018). These composites benefit from the interaction between PANI and carbon nanoparticle materials, which includes sp^2 bonds, through robust π-π stacking interactions (Cho et al. 2014). This interaction enhances electron movement, thus improving charge carrier delocalization and consequently boosting the performance of the electrical sensing layer (Hu et al. 2013; Christopholi et al. 2020). Additionally, extensive research efforts have been dedicated to advancing the sensor systems of PANI-based nanocomposites by integrating graphene and its derivatives.

The first reported effort to combine PANI and graphene was by Al-Mashat et al. in 2010 (Al-Mashat et al. 2010). They developed a hydrogen gas sensor using a PANI/graphene nanocomposite as the sensitive layer through chemical synthesis. The process involved coating graphene with PANI via ultrasonication, using a mix of aniline monomer and ammonium persulfate. The resulting PANI/graphene nanocomposite sensor exhibited a 16.57% sensitivity to 1% H_2 gas, a significant improvement over sensors made solely of graphene sheets or PANI. Following this pioneering work, PANI/graphene-based nanocomposites have been widely adopted in various sensing applications (Tanguy et al. 2018). For instance, chemical oxidation-synthesized PANI/graphene nanocomposites have been employed to detect NH_3 in concentrations ranging from 1 to 6400 ppm (Wu et al. 2013b). PANI/graphene nanocomposites have also been developed using solution mixing techniques (Parmar et al. 2013) and *in-situ* polymerization (Al-Hartomy et al. 2019b), specifically for toluene detection. These composites demonstrated a response of 11.6% at 100 ppm and a significant 90.0% at 5000 ppm. Additionally, Javadian-Saraf and team (Javadian-Saraf et al. 2021) made a PANI/GO nanocomposite with exceptional NH_3 gas sensing capabilities, owing to the interplay between p-n heterojunctions and the synergistic effect of GO sheets, translating NH_3 concentrations into chemoresistive changes. In another development, (Bai et al. 2015) fabricated an NH_3 sensor from a PANI/rGO hybrid using the chemical oxidative method. This sensor was then coated onto a flexible polyethylene terephthalate (PET) film, exhibiting rapid response at room temperature, high sensitivity, and remarkable selectivity. The enhanced performance of the NH_3 sensor based on the PANI/rGO hybrid is likely due to the acidic/basic de-doping mechanism and the interactions between PANI and rGO (Virji et al. 2004).Wu and colleagues (Wu et al. 2013b) discovered that PANI/GO sensors possess a lower NH_3 detection threshold compared to those based solely on PANI, detecting concentrations as low as 1 ppm, which is significantly lower than the 10 ppm limit of PANI sensors, albeit with a modest sensitivity of about 3%. Li et al. (Li et al. 2018c) developed a unique PANI hollow nanosphere GO-hybrid (PANIHs/GO), resembling rambutan, using in-situ chemical oxidation polymerization. This hybrid was then integrated into flexible devices on PET substrates for NH3 gas detection. The resulting PANIHs/GO-based sensor exhibited a 31.80% response to 100 ppm of NH_3, with response and recovery times of 102 and 186 seconds, respectively, and a detection limit as low as 50 ppb.

Furthermore, while metal oxides are deemed highly promising for gas sensing due to their advantageous characteristics, they are not without limitations. These sensors often show reduced sensitivity at room temperature and typically function effectively only at high temperatures. The necessity for elevated operational temperatures, usually in the range of 150°C to 500°C, presents issues related to stability and energy consumption (Mirzaei et al. 2015). The complexity of the heating systems required for traditional metal oxide sensors poses a challenge. To mitigate these issues, an effective strategy is to develop innovative gas-sensing materials using hybrid nanocomposites of conducting polymers and metal oxides. These nanocomposites, which merge the distinct properties of both constituents, demonstrate enhanced performance over their individual components in sensor applications (Zegebreal et al. 2023). Specifically, the integration of metal oxides like zinc oxide (ZnO), manganese dioxide (MnO_2), tin (IV) oxide (SnO_2), vanadium (V) oxide (V_2O_5), indium (III) oxide (In_2O_3), and nickel cobaltite ($NiCo_2O_4$) into PANI and PANI/graphene-based sensors can significantly increase the contact points. This integration not only addresses the limitations of pure metal oxide sensors but also augments the sensitivity, stability, and energy efficiency of the resulting nanocomposite sensors, offering considerable advantages for gas detection technologies. Xu et el. (Xu and Wu 2020), developed a novel ternary nanocomposite, PANI/Gr/In_2O_3, through in-situ chemical oxidative polymerization. They explored its NH_3 sensing response and compared it with that of pure PANI and PANI/Graphene nanocomposites. Figure I.18 displays the sensor response to varying NH_3 concentrations, revealing a distinct linear relationship between response and NH_3 levels. Notably, the PANI/Gr/In_2O_3 sensor outperformed both PANI and PANI/GNR in sensitivity, evidenced by a steeper response curve. This enhanced performance is credited to the combined effects of graphene and In_2O_3, improving gas adsorption and electrical conductivity. Consequently, this sensor shows heightened sensitivity and a broader detection range, enabling detection of lower gas concentrations, potentially down to the ppb level. The exceptional efficacy of the PANI/Gr/In_2O_3 sensor stems from the synergistic interaction between graphene and In_2O_3, enhancing its gas sensing abilities (Andre et al. 2019; Amu-Darko et al. 2023).

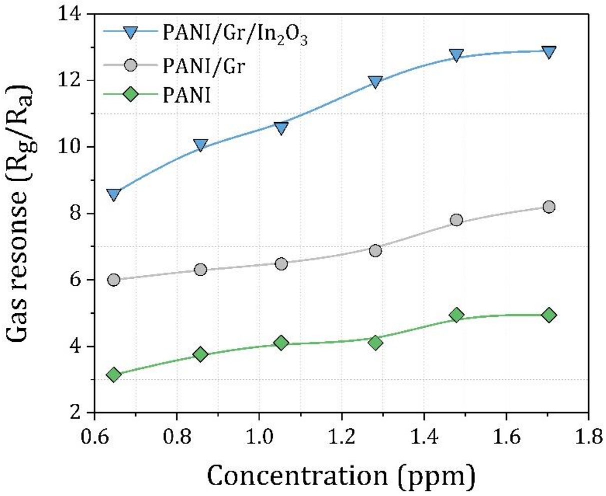

Figure I.18. Response concentration fitting curves of the PANI/Gr/In_2O_3-based sensor (Xu and Wu 2020).

Likewise, Gaikwad and colleagues (Gaikwad et al. 2017) conducted a study on the sensing capabilities of PANI nanofibers, PANI/GO, and PANI/GO/ZnO nanocomposites, synthesized via a nano-emulsion technique. The PANI/GO/ZnO composite showed a 5.71% response to 1000 ppm of NH_3 at 80°C, which was 10.3 times higher than that of the PANI sensor, with a recovery time of 90 seconds. In a related study, Huang et al. (Huang et al. 2012) utilized aniline monomer with rGO-MnO_2 as both a template and oxidant, leading to the creation of PANI nanoparticles adhered to rGO sheets. This composite exhibited a 45% sensitivity to NH_3 gas.

Moreover, PANI/rGO/SnO_2 nanocomposites, synthesized using in-situ chemical oxide polymerization, were tested for detecting various gases including NH_3 (Kebiche et al. 2013; Ye et al. 2015; Kwak et al. 2019), H_2S (Zhang et al. 2019a), and CH_4 (Navazani et al. 2018), all at room temperature. The outcomes revealed that the PANI/rGO/SnO_2 sensor had a 160% response to an NH_3 concentration of 20 ppm, a 9.10% response to 100 ppb of H_2S, and a 26.10% response to 100 ppm of CH_4. Xu and Wu (Xu and Wu 2020) recently developed a PANI/graphene nanoribbon/In_2O_3 nanocomposite, demonstrating notable improvements in gas sensing at room temperature over pure graphene nanoribbons (GNR) or In_2O_3 porous spheres. This enhanced sensing ability is attributed to the formation of a p-n junction between the p-type PANI and n-type In_2O_3, leading to an increased electron depletion layer. Consequently, the PANI/Gr-based sensor, enriched with metal oxides, showcases exceptional performance with heightened sensitivity and the ability to detect low gas concentrations, paving the way for advancements in gas sensing technologies. The remarkable sensitivity of this composite sensor makes it highly efficient in detecting even minute amounts of gases, marking a significant stride in sensor technology. Its potential applications span across various fields, including highly precise gas monitoring in medical diagnostics, environmental studies, and sophisticated safety systems. Offering superior functionality compared to traditional gas sensors, the PANI/Gr-based sensor integrated with metal oxides emerges as a leading solution in the realm of ultra-sensitive gas detection, as supported by further studies (Zhang et al. 2020a; Lin et al. 2023). In addition, PANI/Gr-based nanocomposites, especially when augmented with metallic nanoparticles, are emerging as potent materials for biosensing applications. This includes the detection of hydrogen peroxide (H_2O_2), an essential analyte in a multitude of biological systems and processes. The unique attributes and adaptability of these PANI/Gr-based nanocomposites position them as valuable tools for a range of biosensing tasks. Their capability to accurately detect H_2O_2 not only broadens the scope of biosensor technology but also supports the detailed examination and tracking of biological processes. This has significant implications for enhancing biomedical research and healthcare practices (Du et al. 2017; Liu et al. 2019).

While numerous PANI/graphene, PANI/GO, and PANI/rGO nanocomposites have been successfully utilized in gas sensor development, PANI/GQDs have not been as extensively explored. Gavgani et al. (Gavgani et al. 2016) and Hakimi et al. (Hakimi et al. 2018) developed ammonia sensors using PANI/S, N-GQDs on PET substrates, and PANI/N-GQDs hybrids with silver (Ag) and aluminum (Al) electrodes. The response of PANI/S and N-GQDs to NH_3 increased by 42% and 385% respectively at 100 and 1000 ppm, with a response time of 115 seconds and a recovery time of 44 seconds at room temperature (Gavgani et al.

2016). The PANI/N-GQDs sensor with Ag contacts showed a 110.9% response at 1500 ppm NH3, outperforming the Al electrode sensor, which had an 86.9% response (Hakimi et al. 2018). In a recent study by Hong et al. (Hong et al. 2021), PANI/N-GQD/ hollow In_2O_3 nanofiber composites were synthesized through in-situ chemical oxidative polymerization for use as electrode materials in NH_3 gas sensors. These sensors effectively detected NH_3 concentrations between 0.6 and 2.0 ppm at 25°C. Notably, a 20 wt.% N-GQD composite showed a 15.1% response at 1 ppm NH_3, approximately 4.4 and 1.4 times higher than pure PANI and PANI/hollow In_2O_3 nanofiber composites, respectively. This suggests its potential application in detecting hepatic or renal diseases through human breath analysis.

The aforementioned research suggests enhanced sensing performance of PANI/graphene-based materials at room temperature. Table I.6 collects various studies that investigate the sensing attributes of PANI/graphene nanocomposites towards different target gases, such as NH_3, CH_4, acetone (CH_3COCH_3), and H_2S. Notably, PANI/GO nanocomposites, especially those with 10 wt.% GO, showed an NH_3 response that was 550% and 726% greater than responses to other gases, respectively (Javadian-Saraf et al. 2021). Figure I.19 presents selectivity data for PANI/GO/V_2O_5 nanocomposites at 100 ppm for gases like CO, H_2, formaldehyde (CH_2O), methanol (CH_3OH), ethanol (C_2H_5OH), CH_3COCH_3, and C_7H_8, in comparison to 10 ppm of H_2S and NH_3. This data demonstrates notably lower responses to gases other than NH_3 (Xing et al. 2022). Therefore, while PANI/graphene-based nanocomposites are promising for sensing a broad spectrum of gases, the majority of existing research has predominantly focused on NH_3 gas detection.

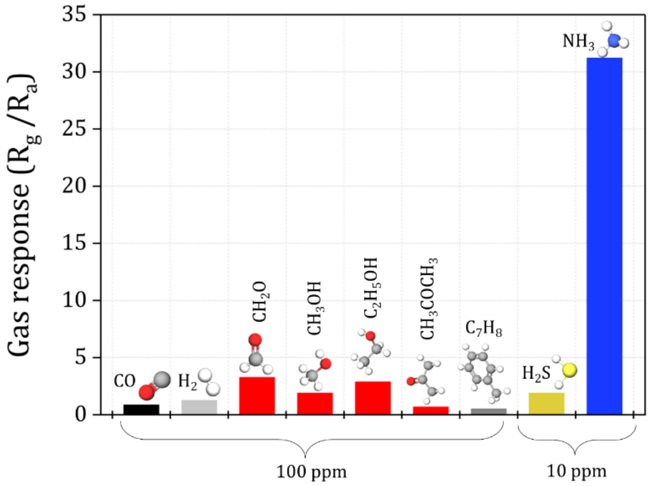

Figure I.19. The selectivity of PANI/GO/V_2O_5 nanocomposite of different gases (Xing et al. 2022).

Table I.6. Summary of gas detection properties of PANI, Graphene and its derivatives-based nanocomposites sensors.

Sensing nanocomposite	**Gas sensing**	**Operating temperature (℃)**	**Response time (s)**	**Recovery time (s)**	**Sensitivity or Response (% at x ppm)**	**References**
PANI/rGO	H_2	RT	-	-	$16.57 – 10^4$	(Al-Mashat et al. 2010)
PANI	NH_3	RT	8760	-	2.03 – 92	(Kebiche et al. 2012)
PANI/rGO	NH_3	RT	~1000	-	37.1 – 50	(Huang et al. 2013)
PANI/CrGO			-	240	59.2 – 50	
PANI	NO_2	RT	~11	420	~12.10 – 100	(Sonker et al. 2016)
PANI	NH_3	RT	-	144	13.4 – 50	(Huang et al. 2012)
rGO			-	140	5.2 – 50	
PANI/rGO			-	240	0.6 – 50	
PANI/Gr	NH_3	RT	50	23	4.7 – 50	(Wu et al. 2013b)
PANI/rGO	CH_4	RT	~85	~45	-	(Wu et al. 2013a)
PANI/Gr	$C_6H_5CH_3$	30	~660	-	8.4 – 100	(Parmar et al. 2013)
PANI/rGO/SnO_2	NH_3	RT	660	-	1.6 – 20	(Ye et al. 2015)
rGO	NO_2	RT	~10	~10	1.2 – 4	(Guo et al. 2018a)
			~ 7	~ 7	1.27– 20	
PANI/rGO	NH_3	12 – 40	18	36	4900 – 100	(Guo et al. 2016)
PANI/ In_2O_3	NH_3	RT	-	-	3.2 – 100	(Pang et al. 2017)
PANI/ S, N-GQDs	NH_3	RT	115	44	42.3 – 100	(Gavgani et al. 2016)
PANI/GO	NH_3	RT	61	10	14.63 – 50	(Wei et al. 2017)
PANI/GO/ZnO	NH_3	RT	2	164	1.307 – 300	(Gaikwad et al. 2017)
PANIHs/GO	NH_3	RT	102	186	31.8 – 100	(Li et al. 2018c)
PANI/Gr/SnO_2	NH_3	RT	8	33	2.78 – 10	(Bera et al. 2018)
PANI/rGO	NH_3	RT	96	1326	13 – 15	(Lee and Wang 2019)
PANI/Gr	$C_6H_5CH_3$	RT	8.6	16	90 – 5000	(Al-Hartomy et al. 2019)
PANI/rGO/SnO_2	H_2S	RT	80	88	9.1 – 0.1	(Zhang et al. 2019a)
PANI/N-rGO	NH_3	25	-	-	208 – 20	(Tanguy et al. 2019)
PANI/MWCNTs	NH_3	RT	9	30	92 – 100	(Maity and Kumar 2018)
PANI/P-rGO	NH_3	25	-	-	773 – 100	(Tanguy et al. 2020)
PANI/Gr/ In_2O_3	NH_3	RT	-	-	8.6 – 0.65	(Xu and Wu 2020)
PANI/rGO/SnO_2	NH_3	RT	35	40	56 – 100	(Saravanan et al. 2020)
PANI/GO	NH_3	RT	51	23	9.6 –70	(Mohammed et al. 2022)
	CO		-	-	31.26 – 230	
PANI/N-GQD/ In_2O_3	NH_3	RT	-	-	15.6 – 1	(Hong et al. 2021)
PANI/ Gr	NH_3	RT	~46	~198	60 – 1	(Wu et al. 2021)
V_2O_5/PANI/GO	NH_3	RT	70	520	31.2 ± 1.8 – 10	(Xing et al. 2022)
PANI/rGO/LCNF	NH_3	RT	-	-	745 – 60	(Tanguy et al. 2022)
PANI/N-GQD	CH_3OH	26	100	96	0.15 – 100	(Masemola et al. 2022)
	C_2H_5OH		85	62	0.66 – 100	
PANI/GCs	NH_3	RT	34	42	1.30 – 10	(Wang et al. 2019)

I.5. Computational insights into Polyaniline and graphene nanocomposites

The quest for high-performance nanocomposites necessitates precise control over synthesis and processing conditions. This control is essential for optimizing composition, morphology, and structure, and for devising novel characterization techniques at the nanoscale. Predicting the properties of PANI/graphene nanocomposites is particularly crucial, considering the vast array of possible material configurations. Traditional experimental methods, while effective, are often time-consuming and labor-intensive, involving the synthesis and analysis of numerous samples (Agrawal and Choudhary 2016; Boublia et al. 2022a).

Cutting-edge computational chemistry techniques, particularly density functional theory (DFT) and molecular dynamics (MD) simulations, has substantially refined our understanding of conducting polymers and graphene-based composites. These potent computational techniques are essential for dissecting the complex charge transfer dynamics and molecular interactions that are central to the materials' gas sensing capabilities. DFT and MD simulations unveil the nuanced electrochemical properties of PANI and their graphene-based counterparts, revealing how their selectivity and sensitivity can be meticulously engineered to detect a range of gas molecules with heightened precision (Shokuhi Rad et al. 2016; Oliveira et al. 2022; Riaz et al. 2022).

For instance, the research conducted by Ullah et al. (Ullah et al. 2013), assessed the PANI emeraldine salt's response to gases like NH_3, CO_2, and CO, across a range of phenyl ring configurations, using advanced computational levels to investigate the system's selectivity and sensitivity. They employed a combination of interaction energy, natural bond orbital, and Mulliken charge analyses to appraise the sensing efficacy, finding a particularly pronounced interaction with NH_3, as depicted in Figure I.20 (A). This reaction led to notable shifts in the PANI energy spectrum, indicating a heightened selectivity for NH_3, aligning well with empirical observations. Moreover, MD simulations have provided a microscopic view into the behavior of these sensors, with Pang et al. (Pang et al. 2021b) visualizing NH_3 distribution within a HCl-doped PANI system, offering a dynamic portrayal of gas molecule interactions at the nanoscale

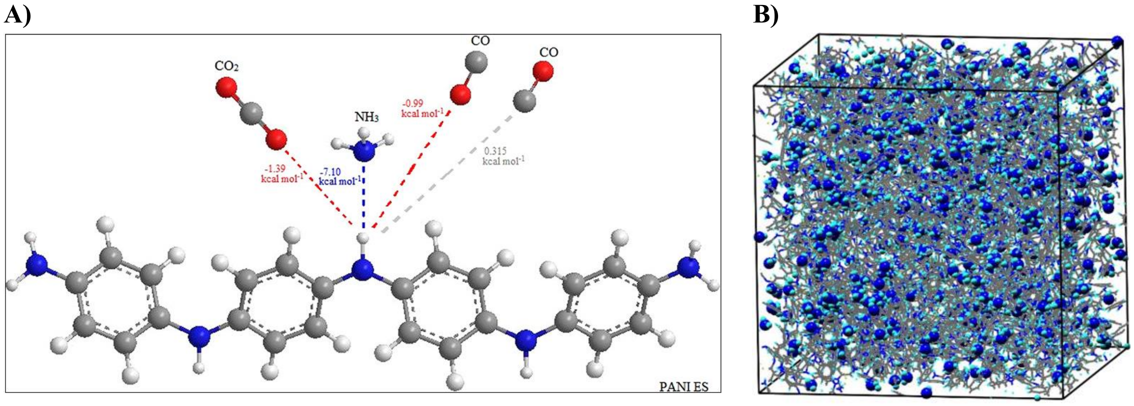

Figure I.20. (A) Comparative adsorption energies of different gases on polyaniline (Ullah et al. 2013), and (B) Molecular Dynamics visualization of NH_3 in a HCl-PANI system (Pang et al. 2021b).

Diving into the intricate world of PANI/graphene nanocomposite systems, Guo et al. (Guo et al. 2018b), expanded this inquiry into the interactions between gases like NH_3 and graphene/PANI composites. They deployed DFT and MD simulations to unravel the interactions between key gases—NH_3, NO, CO, and H_2—and the graphene/PANI composites. These studies provided valuable insights into the adsorptive behaviors of NH_3 on the nuanced surfaces of PANI and graphene, delineating specific sites of interaction as depicted in Figure I.21 (A). The simulation parameters were meticulously set, with MD simulations conducted at a granular 0.5 femtosecond timestep to shed light on the gas diffusion within these composites. The initial models used for their sorption isotherms and diffusion studies are elaborated in Figure I.21 (B), offering a comprehensive view of the dynamic process.

Thus, the findings from Guo et al.'s research (Guo et al. 2018b) underscored a remarkable enhancement in the sensitivity of graphene/PANI composites towards NH_3—a result of significant shifts in both the density of states (DOS) and electrical conductivity following NH_3 exposure. This sensitivity amplifies their potential as selective and sensitive platforms for ammonia detection, a testament to their prowess demonstrated in Figure I.21 (B).

Moreover, the composites' accelerated NH_3 detection capability, as evidenced by the diffusion studies, marks a substantial improvement over PANI alone. These insights present the graphene/PANI nanocomposites as promising contenders for the development of sophisticated ammonia sensors, capable of operating efficiently in multifaceted environments.

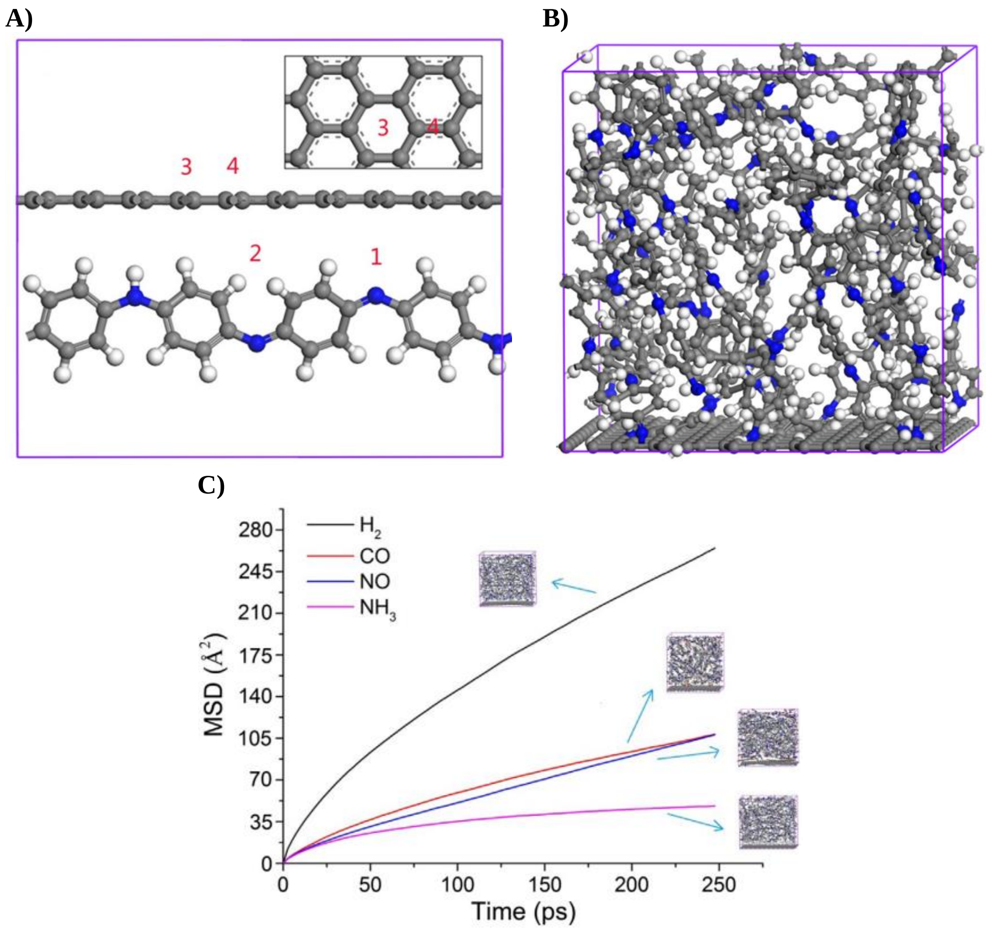

Figure I.21. Analytical visualization of gas interactions with graphene/PANI: (A) Energy profiles of gas adsorption, (B) Structural models for gas sorption and diffusion analysis, and (C) Comparative diffusion trajectories of key gases (Guo et al. 2018b).

In an insightful study, Farooqi et al. (Farooqi et al. 2020a) advanced our understanding of the sensing capabilities of graphene-PANI nanocomposites, particularly in detecting gases like methylamine and ammonia. Leveraging the M06-2X DFT level of theory, they meticulously explored the non-covalent interactions that play a pivotal role in gas detection. Their study reveals the intricate dance of attractive and repulsive forces that come into play when gases are adsorbed onto these composites, as depicted in Figure I.22. The visualization of these interactions in 3D iso-surfaces elucidates the nuanced mechanisms by which these materials respond to gas molecules.

Thus, the computational analysis applied in their research delineates how the unique electronic environment of graphene-PANI composites confers enhanced sensitivity towards NH_3. These findings are crucial, as they provide a foundational understanding necessary for designing gas sensors that are not only highly selective but also remarkably responsive to the presence of target gases.

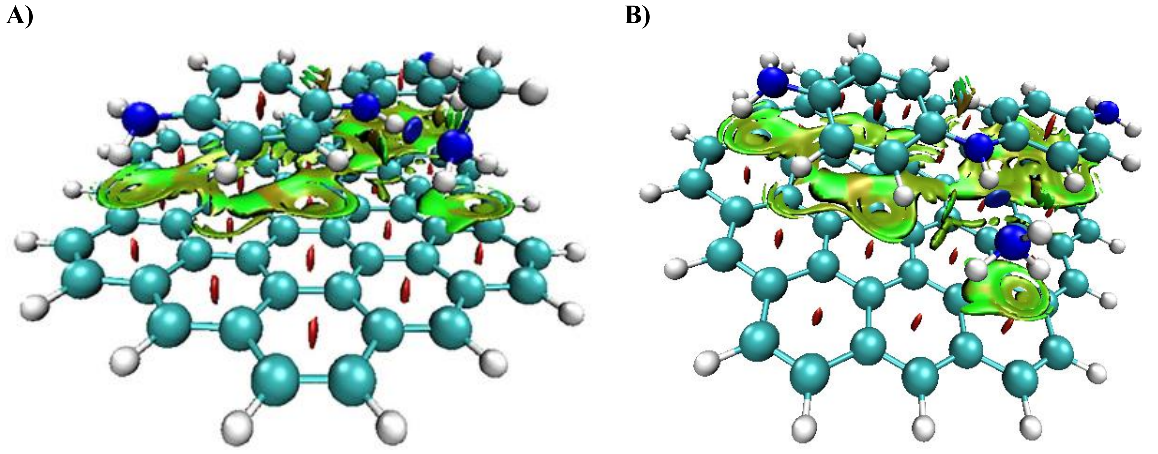

Figure I.22. Non-bonding interaction depictions in graphene-PANI structures with (A) methylamine and (B) ammonia (Farooqi et al. 2020a).

Despite these advancements, conventional models face accuracy and generalizability issues when applied to PANI/graphene composites with varying states and molecular structures. The integration of machine learning (ML) into this domain offers a new avenue for efficiently discovering structure-property relationships in nanomaterials. ML, a rapidly evolving branch of artificial intelligence, holds the potential to revolutionize material discovery and optimization processes (Chen et al. 2021b). By training ML models on extensive datasets of experimental or simulated materials, researchers can predict the properties of new materials based on their structural characteristics. These interpretable models can provide insights into the structural factors underlying specific material properties, enhancing our understanding of these complex systems (Audus and de Pablo 2017; Zhou et al. 2019).

ML's integration with experimental and theoretical approaches can significantly accelerate the development of tailored high-performance nanocomposites. The ability to predict polymer characteristics before synthesis could lead to energy and cost savings in industrial development, hastening the exploration of structure-property relationships among diverse polymers (Motevalli et al. 2020; Cencer et al. 2021).

ML's application in polymer research has already shown promising results, as evidenced by Biswas et al.'s development of a ML-based smart sensing platform utilizing a PANI-coated paper device for urinary pH sensing. This innovative approach combines DFT-based calculations with real-time pH prediction, demonstrating over 98% accuracy through a smart web app interface, a pioneering step in non-invasive health monitoring and clinical diagnostics (Biswas et al. 2022). However, it is worth noting that, as of now, there is no existing ML model specifically designed to predict the gas sensing or electrical properties of PANI/graphene composites. This gap highlights a potential area for future research, where the development of such predictive models could significantly advance the field of nanocomposite materials science.

I.6. Conclusion

This chapter has elucidated several key insights into the realm of PANI and functionalized graphene nanocomposites, marking significant strides in the field of materials science and engineering. The noticeable points derived from this chapter include:

- The narrative of this chapter meticulously charts the evolution and multifaceted applications of PANI and graphene-based nanocomposites. It ventures into their synthesis techniques, morphological intricacies, and the resultant synergistic properties that underscore their advanced electrical, mechanical, and sensory functionalities.
- It showcases an array of sophisticated synthesis techniques, including *in-situ* electropolymerization and interfacial polymerization, tailored to fortify the interaction between PANI and graphene. These methodologies culminate in nanocomposites endowed with distinct structural, electrical, and mechanical attributes, emphasizing the pivotal role of meticulous synthesis in realizing the composites' optimal functionalities.
- The discourse accentuates the remarkable electrical conductance, environmental durability, and pseudocapacitive traits of PANI. In concert with graphene's mechanical robustness and extensive surface area, these attributes amalgamate to endow the nanocomposites with superior electrochemical prowess. This synergy renders them exceedingly apt for diverse applications spanning electronic devices to energy storage solutions.
- Future perspectives delineated in the chapter spotlight the burgeoning avenues for PANI/graphene nanocomposites, aiming at amplifying their efficacy, environmental sustainability, biomedical applicability, and sensing capabilities. The ongoing advancements and investigative endeavors in these nanocomposites are anticipated to transcend the confines of existing technologies, ushering in groundbreaking solutions to intricate engineering and ecological quandaries.
- An exhaustive literature review within the chapter pinpoints pivotal factors that significantly sway the performance of PANI/graphene nanocomposites. Notable enhancements in synthesis protocols and the strategic incorporation of graphene

derivatives have been identified as key to augmenting the electrical conductance and overall utility of these materials, setting the stage for their extensive deployment in high-end electronics, supercapacitors, sensors, and beyond.

To sum up, this chapter provides a foundational description on the modeling and improvement of eco-friendly, multifunctional nanocomposite materials based on polyaniline and functionalized graphene. It heralds the profound impact of these nanocomposites on boosting forward the frontiers of material science and engineering, signaling an epoch of innovative technological breakthroughs and sustainable material solutions.

Chapter II

Chapter II: Research Theories and Methodologies

The aim of the present chapter is to provide an in-depth analysis of the theoretical approaches and methodological processes employed in the study of PANI and graphene-based nanocomposites. This chapter outlines the confluence of advanced computational tools and traditional experimental techniques that form the backbone of current research, facilitating the systematic development of materials with tailored properties.

II.1. Introduction

The exploration of PANI and graphene-based nanocomposites within the landscape of polymer nanocomposite science necessitates a deep dive into advanced research theories and methodologies. This survey delves into the sophisticated blend of computational and experimental techniques that form the cornerstone of contemporary material science research. The focus lies on leveraging advanced machine learning algorithms, intertwined with proven experimental design approaches, to unravel the complexities and fine-tune the properties of these cutting-edge nanocomposites.

Central to this exploration are the machine learning methods, serving as powerful instruments for analyzing and predicting the behavior of PANI and graphene nanocomposites with enhanced accuracy. These methods are instrumental in distributing the intricate behaviors of PANI and graphene nanocomposites, enabling researchers to predict outcomes with increased precision and reliability. Complementing these computational techniques are experimental design strategies like Response Surface Methodology, which play a crucial role in optimizing process variables and enhancing material performance.

Additionally, this chapter emphasizes the significance of characterization and electrochemical tools in providing comprehensive insights into the morphological, structural, and electrochemical attributes of the nanocomposites. Techniques ranging from spectroscopy and microscopy to advanced electrochemical analyses serve as key enablers in deciphering the nuanced interactions within these materials. The incorporation of these diverse methodologies not only enriches our understanding of PANI/graphene nanocomposites but also paves the way for their application in various technological domains, from energy storage to environmental sensing. Thus, this comprehensive approach to research methodologies underlines the importance of an integrated, multi-dimensional analysis in the field of nanocomposite science. It highlights the synergy between computational prowess and experimental ingenuity, necessary for the advancement of material science and engineering.

II.2. Computational Approaches

II.2.1. Machine Learning Methods

Machine Learning (ML) has paved its role as a cornerstone of computational algorithms, facilitating cognitive learning patterns akin to human intelligence. As the frontiers of data expand, ML has become an indispensable instrument for pattern detection, predictive analytics, and decision-making in a spectrum of sectors, encompassing visual recognition systems, financial modeling, and the realm of biomedical sciences. The hallmark of ML is its inherent capacity to undertake complex tasks autonomously, eschewing explicit programmatic instructions. Instead, ML algorithms fine-tune their parameters through an iterative learning process, aptly termed 'training.' Within this phase, algorithms assimilate patterns from datasets, enhancing their predictive acumen for fresh, uncharted data, thus bolstering their adaptability and precision progressively (Xu et al. 2022).

The collection of ML methodologies spans from the straightforward Multi Linear Regression (MLR) to the intricate Artificial Neural Networks (ANNs), with various intermediate algorithms like Multiple Non-Linear Regression (MLNR), Decision Tree (DT), Random Forest (RF), Gradient Boosting Machine (GBM), *k*-Nearest Neighbors (*k*-NN), and Support Vector Regression (SVR) enriching the mix. These methods are depicted in Figure II.1, and a systematic breakdown of their strengths and limitations is presented in Table II.1. This analytical comparison draws from a robust body of literature (Rashidian and Hassanlourad 2014; Belgiu and Drăguţ 2016; Song et al. 2017; Pandey et al. 2017; Fissa et al. 2019; Mienye et al. 2019; Quang et al. 2019; Maulud and Abdulazeez 2020; Bansal et al. 2022; Li et al. 2022b; Manoharan et al. 2022). These scholarly works are critical in identifying the most suitable ML approaches for analyzing and modeling the properties of polymeric nanocomposites, steering the selection of computational techniques that align with the sophisticated demands of polymer nanocomposite research.

Consequently, the integration of ML in nanocomposite research has shattered conventional limitations, unveiling a new realm of understanding into the complex attributes and functionalities of these materials. By carefully selecting and thoroughly validating ML algorithms, researchers are now poised to forge innovative nanocomposites, customized for avant-garde applications. The synergy between ML, experimental inquiry, and theoretical analysis promises a swifter path to discovering and designing nanocomposites with bespoke characteristics for targeted uses (Motevalli et al. 2020).

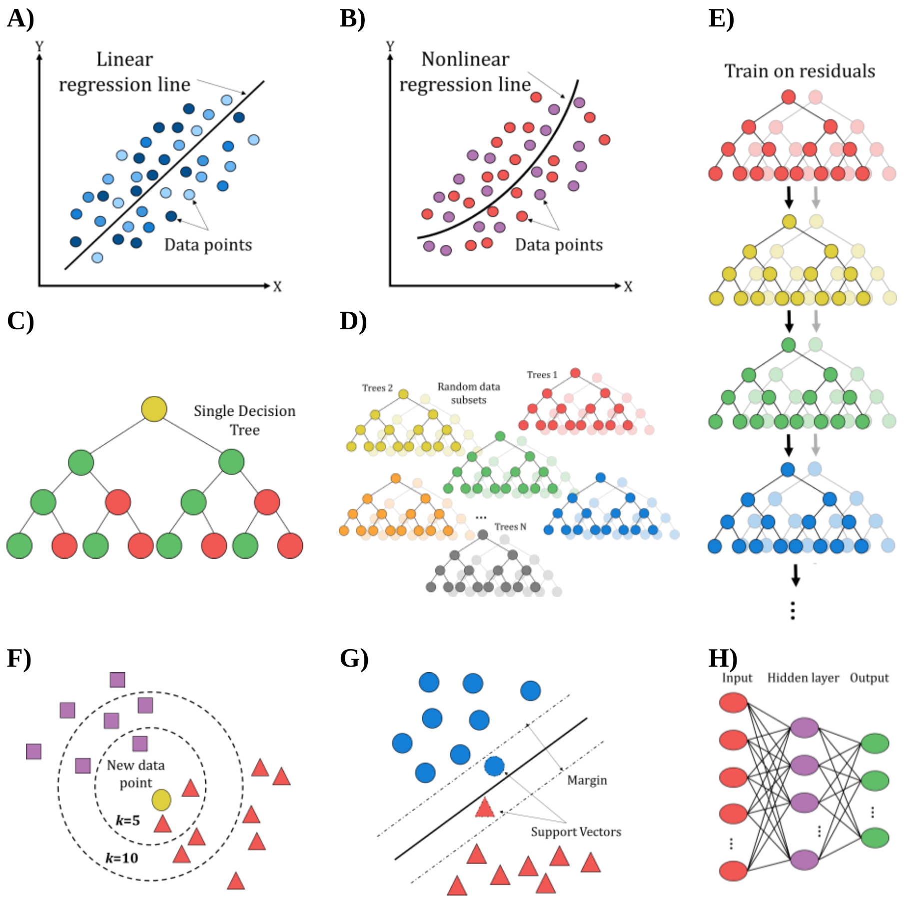

Figure II.1. Diagrammatic illustration of the ML algorithms: A) MLR, B) MLNR, C) DT, D) RF, E) GBM, F) *k*-NN, G) SVR, and H) ANN.

Given that the properties of polymer materials are intricately linked to a multitude of synthesis and processing parameters, ML emerges as a particularly valuable asset in polymer research. The predictive power of ML to foresee the traits of polymers prior to synthesis can lead to substantial savings in energy and production costs, thereby expediting the exploration of structure-property relationships across various polymer classes. This predictive prowess has catalyzed the widespread adoption of polymer-based materials in fields such as electrical engineering, medical technology, and manufacturing engineering (Audus and de Pablo 2017; Zhou et al. 2019). Scientists have embarked on a multitude of successful projects, leveraging ML to probe the synthesis processes and properties of polymers (Cencer et al. 2021). The application of ML in conjunction with mechanical properties of polymer composites (Altarazi et al. 2018; Hiraide et al. 2021), liquid crystal behavior of copolyether (Leon et al. 2007), thermal conductivity and dielectric behaviors (Wu et al. 2019; Chen et al. 2020; Liang et al. 2021; Armida et al. 2023), glass transition (T_g) (Chen et al. 2021a; Boublia et al. 2022c; Xing et al. 2022), melting (T_m) and degradation temperature (T_d), as well as quantum physical and chemical properties (Ma et al. 2019; Ma and Luo 2020; Kuenneth et al. 2021; Bejagam et al. 2022), marking a significant stride in the accuracy of such predictions.

Table II.1. Comparative analysis of machine learning algorithms and their implications for nanocomposite research.

Algorithm	Core Strengths	Potential Limitations	Relevance to nanocomposite research
MLR	Straightforward to implement and interpret; effective for datasets with clear linear trends; informative on variable interdependencies.	Assumes a linear relationship; may not capture complex, non-linear interactions; risk of overfitting with many variables.	Ideal for initial exploration of linear relationships in nanocomposite properties and synthesis parameters.
MNLR	Captures intricate, non-linear relationships; adaptable model for complex systems.	Higher risk of overfitting; may require substantial data to train effectively.	Suitable for modeling complex behaviors in nanocomposite synthesis and property analysis.
DT	Highly interpretable; versatile with various data types; effective at illustrating non-linear relationships.	Can overfit noisy or intricate data; sensitive to minor data variations; may necessitate pruning.	Useful for classifying nanocomposite types and understanding decision rules influencing properties.
RF	Aggregates multiple DTs to reduce overfitting; robust to noise; can handle a variety of data types.	Computationally intensive; potentially less interpretability due to ensemble nature.	Employed for enhanced predictive accuracy of nanocomposite performance under diverse conditions.
GBM	Sequential learning reduces error margins; less prone to overfitting; can handle diverse data types.	Computationally demanding; parameter tuning required; potential for reduced interpretability.	Applicable for optimizing nanocomposite formulations with iterative refinement.
k-NN	Handles linear and non-linear data; high prediction accuracy; intuitive classification based on proximity.	Computational load increases with dataset size; sensitive to irrelevant features and noise.	Effective in property prediction based on similarity measures among nanocomposite datasets.
SVM	Manages non-linear boundaries; robust to overfitting; effective with high-dimensional data.	Requires significant computational resources; selection of kernel and parameters is crucial.	Utilized for regression tasks in nanocomposite studies, particularly in high-dimensional compositional space.
ANN	Simulates complex brain-like processing; handles vast and complex datasets; models both linear and non-linear relationships.	Computationally demanding training process; may overfit with excessive complexity; can be challenging to interpret.	Integral for multifaceted modeling of synthesis and predictive analysis in advanced nanocomposite development.

II.2.2. Artificial Neural Networks

ANNs stand as a transformative branch of ML, offering computational analogs to the human brain's architecture and functionality. These networks are composed of a sequence of layers filled with interconnected processing units known as neurons, each contributing to the model's predictive capability. In this arrangement, the neurons are sequentially organized into input, hidden, and output layers, which process the incoming data and generate predictive outcomes (Rashidian and Hassanlourad 2014; Fissa et al. 2019; Quang et al. 2019). ANNs encompass a variety of configurations, including feedforward networks, radial basis function networks, and fuzzy networks, each suitable for different applications (Himmelblau 2000; Wang and Fu 2005). The potency of ANNs was highlighted by Hornik et al. (Hornik et al. 1989), who showed that even a single-layered feedforward network can approximate any conceivable function from multiple dimensions. This versatility has seen ANNs eclipse traditional modeling techniques in terms of predictive accuracy, particularly in complex engineering domains (Pirdashti et al. 2013; Susaimanickam et al. 2023).

The strength of ANNs lies in their nonparametric nature, allowing for model development devoid of any presuppositions regarding data distribution or variable interactions—requirements typically mandated by standard parametric statistical methods (Walczak and Cerpa 2019). In an ANN, each neuron receives weighted input signals, akin to synaptic inputs in a biological context (Bullock 1997), with the weights being analogous to synaptic strength. It is the optimization of these weights through a process known as 'training' that enables ANNs to learn and adapt.

Within the context of nanocomposite research, ANNs serve as a versatile modeling tool, adept at handling both linear and nonlinear multivariate regression challenges found in synthesis and fabrication processes (Boublia et al. 2022a). The network is crafted with layers populated by a predetermined number of artificial neurons, each characterized by weights and a transfer function. The input weights, calculated from the product of input units, undergo processing through the neuron's transfer function in what is known as a 'feedforward process'. This is followed by 'backpropagation', a training phase where the network fine-tunes its weights based on a set of input-response data pairs, aiming to minimize the mean square error between experimental and predicted outputs. The culmination of ANN modeling is in the validation and testing of datasets, an essential step in gauging the network's performance and reliability (Himmelblau 2000; Wang and Fu 2005). Thus, given their exceptional adaptability and precision, ANNs have emerged as an indispensable tool in the repertoire of nanocomposite researchers, providing a robust framework for probing the intricate behaviors and properties of these advanced materials.

II.2.3. Importance of Database

The establishment of a detailed materials database is the cornerstone of any successful ML model. It is a curated collection of material structures and properties, informed by empirical research or computational predictions. The ability of an ML model is intrinsically linked to the database's scope, diversity, and uniformity of data representation. These factors are vital for a model that aims to be predictive, offering reliable insights into new materials and phenomena. Remarkably, even databases of moderate size can yield highly accurate ML models, as evidenced by their applications in the design of energetic materials and thermal conductivity analyses for polymers.

When constructing a database from scratch is impractical due to resource demands, existing public databases offer a treasure trove of structured and property data. These databases are invaluable assets, as highlighted in Table II.2, where they serve as a foundation for various applications. An illustrative case is the assimilation of 1,442 homopolymer structures from assorted polymer families, with all property data for neat polymers sourced from the acclaimed PolyInfo database. Such comprehensive polymer databases empower ML algorithms to unearth deeper insights into polymer science and contribute to the evolution of polymer informatics.

Table II.2. Key public databases for accessing polymer and nanocomposite material data.

Database	**Short description**	**URL**
PoLyInfo	Comprehensive data for polymeric material design	https://polymer.nims.go.jp/
Polymer Genome	Informatics platform for polymer property prediction	https://www.polymergenome.org/
CROW Polymer Properties Database	Extensive polymer properties information	http://polymerdatabase.com/
Polymer Science Learning Center Spectral Database	Polymer IR and NMR spectral data	https://pslc/uwsp.edu
MATWEB Material Property Data	Properties of thermoplastics and thermosetting polymers	http://www.matweb.com
Polymer Property Predictor and Database	Flory–Huggins's interaction parameters and T_g for polymers	https://pppdb.uchicago.edu/
NanoMine	Open-source data resource for the nanocomposite's community.	https://materialsmine.org/nm#/

Nevertheless, there exists a void in databases encompassing detailed processing procedures or experimental metadata. The scientific community is thus encouraged to share their datasets and code openly, enhancing the collective knowledge base. When specific requirements exceed the scope of public databases, data extraction from scientific literature stands out as a viable strategy. An instance of this approach can be seen in organic solvent nanofiltration research by Wang et al. (Wang et al. 2023), where a dataset comprising 9,252 data points was compiled from 20 scholarly articles. This database, detailing chemical structures and optical properties, facilitated the discovery of high-efficiency thin-film nanocomposite membranes through rigorous high-throughput screening. Thus, the examples cited here exemplify the practicality and the innovative impact of data extraction in material science, setting the stage for both predictive performance modeling and the conceptualization of high-performance material designs for future exploration.

II.2.4. Molecular Descriptors

Molecular modeling is a cornerstone in the development of materials, providing a bridge between theoretical concepts and empirical findings. This tool enriches our understanding of material behavior at a microscopic level, offering detailed insights into the underlying mechanisms of materials' properties. For polymer nanocomposite research, the adept application of computational techniques is crucial for uncovering new potential and enhancing material functionalities (Patra 2022; Zhao et al. 2023). Molecular descriptors, a product of cross-disciplinary principles from quantum chemistry, information theory, organic chemistry, and graph theory, stand at the forefront of this computational endeavor. They offer a window into the intricate behaviors of polymer nanocomposites, serving as a simulation tool to predict material properties with a high degree of accuracy (Brown et al. 2006; Mallakpour et al. 2010). These descriptors are pivotal in accurately capturing the essence of molecular attributes, which is fundamental for refining synthesis and application strategies for advanced material development. The analysis of molecular descriptors is augmented by an arsenal of statistical, chemometric, and cheminformatics tools, enabling researchers to navigate through complex datasets to extract meaningful insights. This analytical prowess ensures that the exploration and innovation of polymers and nanocomposites are grounded in data-driven precision.

In the realm of ML, a recent work reported by (Boublia et al. 2023c) stands out, demonstrating the efficacy of the COSMO-RS-derived *σ-Profiles* inputs in constructing robust models for homo-polymers and co-polymers. These *σ-Profiles* are presented as a superior alternative to conventional molecular inputs traditionally cited in polymer literature. Their study culminated in the construction of a multitask ANN model adept at predicting critical thermal properties of materials, such as the T_g and T_m of polyhydroxyalkanoates, as depicted in Figure II.2. This model exemplifies the synergy between molecular modeling and ANN, paving the way for precise predictions that are crucial for material design and application.

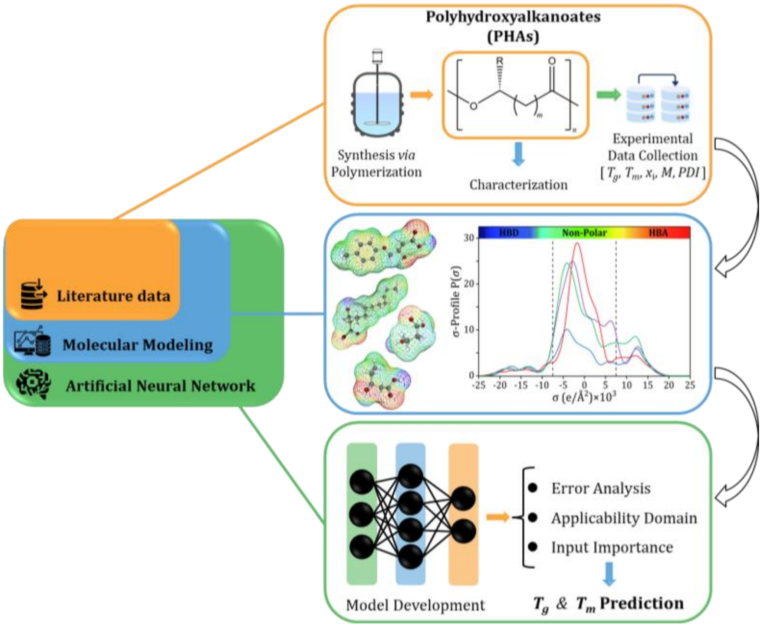

Figure II.2. COSMO-RS derived $\sigma_{Profiles}$ of the 24 monomers used as molecular descriptor to predict T_g and T_m of polyhydroxyalkanoates (Boublia et al. 2023c).

II.2.5. Model Evaluation

Model evaluation stands as a foundation stone in the application of ML within material science, serving as the litmus test for the predictive prowess and dependability of computational models. The domain's complex nature, which includes forecasting the behavior of nanocomposites and polymer materials, necessitates a comprehensive and nuanced approach to validation.

II.2.5.1. Evaluation Metrics

Model evaluation is an indispensable component of the machine learning pipeline, with its significance magnified in the domain of chemical engineering where predictive precision and reliability are paramount. The effectiveness of a machine learning model in forecasting the behaviors of nanocomposites or the outcomes of polymer reactions is fundamentally contingent upon a meticulous evaluation grounded in robust statistical measures and validation methodologies. Crucial to this process is the selection of appropriate evaluation metrics, which must be meticulously tailored to align with the specific requirements and nuances of the model's application. For regression tasks pivotal to material research, a suite of metrics—such as the Root Mean Square Error (RMSE), coefficient of determination (R^2), Average Standard Deviation (ASD), Average Absolute Relative Deviation (AARD), Mean Absolute Error (MAE), and Mean Squared Error (MSE)—is indispensable. These metrics, quantitatively detailed in Table II.3, offer a multi-faceted view into the model's predictive accuracy and the extent of deviation from actual observations, thereby underscoring the model's efficacy in real-world applications (Umehara et al. 2019; Lian et al. 2024).

Table II.3. Summary of evaluation metrics for machine learning models.

Metric	**Mathematical Definition**	**Description**
RMSE	$RMSE = \sqrt{\frac{\sum_1^N (Y_{exp} - Y_{pred})^2}{N}}$	A measure of the model's prediction error, calculating the square root of the average of squared differences between predicted and actual values. Lower values indicate better fit.
R^2	$R^2 = 1 - \frac{\sum_1^N (Y_{exp} - Y_{pred})^2}{\sum_1^N (Y_{exp} - \bar{Y})^2}$	Represents the proportion of variance in the dependent variable that is predictable from the independent variables, with values closer to 1 indicating a better model fit.
ASD	$ASD = \sqrt{\frac{\sum_1^k (Y_{pred} - \bar{Y})^2}{N}}$	Typically refers to the dispersion or variation of a set of values. Not a standard metric for ML model evaluation.
AARD	$AARD\ (\%) = \frac{100}{N} \times \sum_1^N \frac{\lvert (Y_{pred} - Y_{exp}) \rvert}{Y_{exp}}$	Evaluates the average error magnitude in relation to true values, serving as a standardized gauge of model accuracy. Smaller AARD values suggest higher predictive precision, especially useful for assessing models across diverse datasets.
MAE	$MAE = \frac{1}{N} \sum_1^N \lvert Y_{exp} - Y_{pred} \rvert$	Provides an intuitive gauge of average error magnitude in the data's units, preferring models with minimal MAE for their precision. Effective for continuous outcomes, it's robust against outliers, offering a clearer accuracy picture than RMSE.
MSE	$MSE = \frac{1}{N} \sum_1^N \left(Y_{exp} - Y_{pred}\right)^2$	Similar to RMSE but averages the squares of the prediction errors. It heavily penalizes larger errors, making it sensitive to outliers.

II.2.5.2. Validation Techniques

In terms of validation, simple hold-out methods provide an initial gauge of model performance by testing on unseen data. However, the *k*-fold cross-validation technique stands out for its robustness, methodically partitioning the dataset into '*k*' equal parts to iteratively train and validate the model, hence providing a holistic assessment of performance. For an exhaustive and rigorous validation, especially when precise prediction of nanocomposite properties is critical, the leave-one-out method, despite its computational demands, may be employed to ensure utmost accuracy and generalizability (Syed 2011).

Basically, the process of cross-validation is considered by the strategic omission of subsets of data from the dataset, subsequently employing the remaining data to construct a ML model. This model is then tasked with predicting the values of the omitted subset, offering an evaluation of the model's predictive power. The simplest variant of cross-validation, the leave-one-out method, involves the exclusion of a single data point at a time. To ascertain the robustness and applicability of our developed ML models, a *k*-fold cross-validation technique (Stone 1976) can be implemented. This approach involves partitioning the dataset into five equal subsets, rotating each as a test set while the rest serve as the training set, which includes a validation subset. The overarching aim of k-fold cross-validation is to train the model with diverse data segments and to assess its predictive prowess with the complementary test sets. By iterating this process five times, we gain a robust estimation of the model's performance, particularly in relation to data not included in the training folds. The model's final iteration is then selected based on its ability to yield the lowest average error rate across all the k-fold validations (refer to Figure II.3). This meticulous process is instrumental in thwarting the tendency of overfitting and offers a comprehensive evaluation of the model's adaptability to novel data, thus ensuring its readiness for deployment in real-world scenarios.

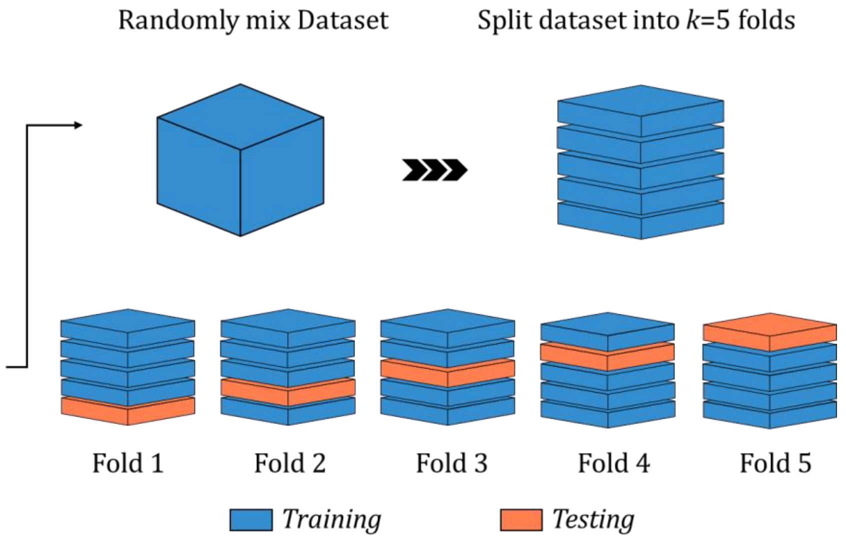

Figure II.3. Schematic illustration of the k-fold cross-validation (k=5) protocol.

II.4. Experimental Design Approaches

Response Surface Methodology (RSM), introduced by Box and Wilson (Box and Wilson 1992) in the mid-20th century, has been adopted in polymer-based materials for its efficacy in optimizing complex chemical processes. It is a robust statistical technique that integrates multiple variables to streamline the experimental workflow and enhance the desired outcome.

For instance, in polymers, conductivity is a key performance metric influenced by factors such as temperature "X_1," dopant concentration "X_2," polymerization time "X_3," and cross-linking degree "X_4." Continuous variation in these factors can lead to changes in the polymer's conductivity, which RSM can adeptly map and optimize. The relationship between conductivity "Y" and its influencing factors in a polymer system can be represented by the following equation:

$$Y = f(X_1) + f(X_2) + f(X_3) + f(X_4) + e \qquad \text{Eq. (8)}$$

Here, Y represents the conductivity (dependent variable), f signifies the functional responses, X_1 to X_4 are the independent variables affecting conductivity, and $\epsilon\epsilon$ captures the experimental error and other uncertainties.

The essence of RSM lies in its capacity to discern the optimal conditions within the landscape of the response surface, as illustrated in Figure II.4. It navigates through the terrain of maxima, minima, and saddle points to pinpoint the region yielding the most favorable response. Although RSM is a formidable analytical tool, it does not dictate the data collection methodology. It assesses variable interactions to identify the best operational parameters or a suitable range within the experimental domain (Bradley 2007).

Diverse RSM approaches include the Box-Behnken Design (BBD), Central Composite Design (CCD), Doehlert Matrix (DM), among others. These methods have been instrumental in revealing the intricate relations between dependent and independent variables in polymer research (Boublia et al. 2022a).

On the other hand, for a rigorous empirical assessment of the model's reliability, optimal conditions derived from RSM are experimentally validated and subjected to statistical scrutiny *via* *t*-tests or *Chi*-Square analysis. Model trustworthiness is affirmed when the *P*-value is below 0.05, lack of fit is above 0.05, R^2 exceeds 0.9, and adequacy precision surpasses 4. The Analysis of Variance (ANOVA) further corroborates the significance of the model's predictive power (Witek-Krowiak et al. 2014).

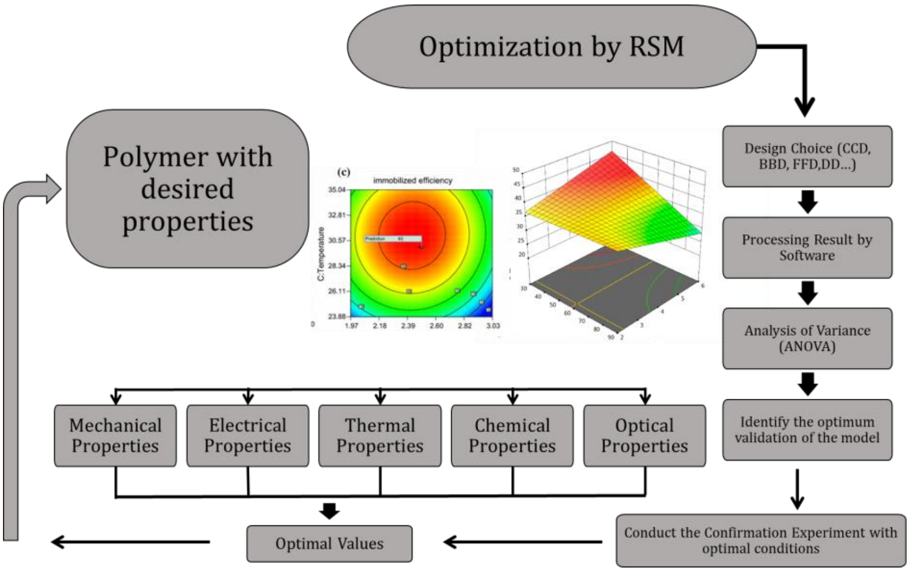

Figure II.4. Schematic workflow of response surface methodology in polymer optimization.

Furthermore, the systematic steps of RSM, summarized in Figure II.4, range from identifying optimization variables to experiment design, variable level determination, mathematical-statistical data processing, model evaluation, and optimal condition discovery.

Thus, different experimental design frameworks, such as full factorial, CCD, DM, and BBD, are considered based on their suitability for the given research objectives. The Table II.4 encapsulates the merits and drawbacks of these designs, aiding in the selection of the most appropriate RSM model for the task at hand.

Table II.4. Merits and drawbacks of RSM models: Full Factorial, CCD, DM, and BBD.

RSM Models	Advantages	Disadvantages
Full factorial	Comprehensive combination coverage; no factor or level limits	Challenging with multiple factors; high labor demand.
CCD	Excellent predictive scope; accommodates five levels per factor	Requires symmetrical spacing around the center, varying with factor count.
DM	Optimal for polynomial models; fewer runs needed	Limited use in common software applications.
BBD	Reduces experimental runs; ideal for second-order models	Limited to three or more factors; unsuitable for extreme condition experiments.

Within this context, BBD stands out for its efficiency in optimizing multifaceted systems. It significantly reduces experimental iterations, conserves resources, and carefully avoids the extremes of factor levels, thereby circumventing the potential for suboptimal experimental outcomes.

II.5. Characterization and electrochemical tools

In the landscape of advanced materials research, the characterization of PANI/graphene nanocomposites stands as a cornerstone for elucidating their multifaceted characteristics and unlocking their vast application potential. Employing a spectrum of sophisticated analytical techniques, researchers delve into the intricate dynamics of these nanocomposites, aiming to finely calibrate their properties to meet specific application needs. These characterization and electrochemical tools provide a window into the nanocomposites' morphological, structural, and electrochemical profiles, shedding light on pivotal aspects that dictate their overall performance (Divya et al. 2019; Babel and Hiran 2021). The integration of these diverse techniques paints a holistic picture of the nanocomposites, laying the groundwork for their tailored application in cutting-edge technologies.

PANI/graphene nanocomposites undergo thorough examination through methodologies such as UV-Visible Spectroscopy (Kumar et al. 2018a), Photoluminescence Spectroscopy (PL) (Beygisangchin et al. 2021), Fourier Transform Infrared Spectroscopy (FT-IR)(Usman et al. 2019), X-ray Diffraction (XRD) (Li et al. 2018a), and X-ray Photoelectron Spectroscopy (XPS) (Gabunada et al. 2019), alongside critical electrochemical and electrical analyses including

Electrical Conductivity (Xavier et al. 2019) and Cyclic Voltammetry (CV) (Gul et al. 2020). These approaches are complemented by thermal analysis through Thermogravimetric Analysis (TGA) (Parveen et al. 2016), providing insights into the thermal stability and degradation patterns of the nanocomposites.

Moreover, direct microscopy techniques such as Atomic Force Microscopy (AFM), Scanning Electron Microscopy (SEM), and Transmission Electron Microscopy (TEM) are instrumental in visualizing the micro to nanoscale architecture of these materials (Das et al. 2023). These microscopy methods are pivotal in investigating the dispersion level of graphene fillers within the PANI matrix—a challenge in both the fabrication and post-preparation phases of nanocomposites. Techniques like SEM, TEM, XRD, Raman spectroscopy, and AFM are routinely employed to evaluate filler dispersion, utilizing image analysis to examine the nanocomposite structure, particle distribution, aggregate size, and more (Javadian-Saraf et al. 2021).

Meanwhile, in light of increasing concerns about environmental conservation and industrial safety, the effectiveness of PANI/graphene nanocomposites in detecting gases has become highly significant. Techniques like conductometric (Li et al. 2024), chemoresistive (Pandey 2016; Zamiri and Haseeb 2020), and optical (Ismail and Sulaiman 2021) gas sensing are utilized for their sensitivity and selectivity towards environmental pollutants and hazardous gases. These materials demonstrate exceptional sensitivity and selectivity for various gases, making them essential tools for monitoring environmental pollution and safeguarding industrial environments.

To facilitate an efficient selection of these diverse techniques, Table II.5 provides a quick-reference framework that encapsulates the essence of each method, ranging from spectroscopic and microscopic analyses to thermal and electrochemical evaluations. It outlines not only the type of information each technique can reveal but also highlights the particular properties of PANI/graphene nanocomposites that can be explored. This structured overview is designed to streamline the decision-making process in the research of these complex materials, ensuring that the chosen methods align optimally with the intended research objectives and contribute effectively to the advancement of knowledge in the field of polymer nanocomposites.

Table II.5. Summary of characterization techniques for PANI/graphene nanocomposites.

Characterization Technique	Information Provided	Properties Analyzed	Applicability to PANI/graphene
UV-Visible Spectroscopy	Analyzes electronic transitions and band gaps	Optical properties, band gap	Assessing optoelectronic characteristics
Photoluminescence (PL)	Evaluates luminescent properties of materials.	Electron-hole recombination	Investigating light-emitting efficiency
Raman Spectroscopy	Vibrational modes, molecular interactions	Material structure, stress/strain analysis	Structural characterization and integrity
FT-IR Spectroscopy	Chemical bonds, functional groups	Compositional analysis	Chemical compatibility and bonding analysis
X-ray Diffraction (XRD)	Crystalline structure, graphitization level	Crystallinity, phase analysis	Structural phase and crystallinity assessment
X-ray Photoelectron Spectroscopy (XPS)	Surface chemistry, elemental composition	Surface chemistry, oxidation states	Surface composition and electronic structure
Atomic Force Microscopy (AFM)	Visualizes surface topology at the nanometer scale.	Surface morphology, mechanical properties	Nanostructural analysis and mechanical assessment
Electrical Conductivity Analysis	Measures the electrical conductivity of composites.	Conductivity, charge transport	Conductivity performance for electronics
Cyclic Voltammetry (CV)	Investigates redox behavior and electrochemical properties.	Electrochemical properties, redox potential	Evaluating charge storage and transfer
Thermogravimetric Analysis (TGA)	Assesses thermal stability and degradation.	Thermal stability, degradation temperature	Thermal analysis for processing and application
Scanning Electron Microscopy (SEM)	Examines surface morphology and topography.	Surface texture, morphological features	Morphological evaluation and dispersion quality
Transmission Electron Microscopy (TEM)	Provides detailed internal structure images.	Internal morphology, nanoparticle distribution	Nanostructural details and composite homogeneity
Conductometric, Chemoresistive, and Optical gas sensing techniques	Tests sensitivity and selectivity for gas detection.	Sensor response, selectivity	Gas sensor development for environmental monitoring

II.5. Conclusion

This chapter has provided a profound exploration into the integrative use of computational and experimental methodologies within the sphere of polymer nanocomposite research. Through a meticulous analysis of machine learning techniques in combination with sophisticated experimental design strategies, we have projected new directions for optimizing the utility and efficiency of PANI/graphene nanocomposites.

The expansive survey of characterization and electrochemical tools further accentuates the chapter’s pivotal role in deepening our comprehension of the intricate structural, morphological, and electrochemical attributes of these advanced materials.

This incorporated methodology not only sharpens our predictive accuracy but also extends our ability to customize nanocomposites for targeted technological endeavors. The findings presented herein underscore the critical importance of cross-disciplinary approaches in expanding the boundaries of material science.

By combining computational prowess with experimental rigor, this chapter heralds an era marked by significant breakthroughs in the development and application of polymer nanocomposites, setting the stage for future innovations in this dynamic field.

Chapter III

Chapter III: Enhancing Precision in PANI/Gr Nanocomposite Design: Robust Machine Learning Models, Outlier Resilience, and Molecular Input Insights for Superior Electrical Conductivity and Gas Sensing Performance

In this chapter we employed various machine learning algorithms to model the electrical conductivity and gas sensing responses of polyaniline/graphene (PANI/Gr) nanocomposites based on a comprehensive dataset gathered from over 100 references. Artificial neural networks (ANNs) demonstrated superior predictive accuracy among the models. The investigation delves into identifying and mitigating outliers, both structural and response-related, showcasing the robustness of the proposed ANN models. The study emphasizes the critical role of applicability domain (AD) analysis in evaluating model reliability. Results indicate high accuracy for electrical conductivity (RMSE: 0.408, R^2: 0.984) and gas sensing responses for ammonia, toluene, and benzene gases (RMSE: 0.350, 0.232, and 0.081, R^2: 0.967, 0.983, and 0.976, respectively). Input contribution analysis highlights key parameters influencing performance. The σ-Profiles of additives emerge as significant contributors, emphasizing the importance of molecular-input understanding in machine learning models. These findings contribute to developing high-performance PANI/Gr nanocomposites with implications for diverse applications like supercapacitors, gas sensors, and energy storage devices. The study underscores the need for further research to deepen the understanding of molecular inputs' impact on PANI/Gr system performance, enabling more precise material design.

III.1. Introduction

PANI/graphene-based nanocomposites have risen as up-and-coming materials due to their distinctive electrical and gas-sensing properties, rendering them well-suited for diverse industrial applications. However, developing PANI/graphene-based nanocomposites with enhanced properties and attaining a comprehensive comprehension of the interconnections between their properties and constituents necessitates in-depth analysis. Experimentally investigating every possible combination of PANI/graphene mixtures is challenging, time-consuming, and expensive. Hence, establishing prediction models for PANI/graphene-based nanocomposites' physicochemical features is critical. In this context, adopting ML techniques, particularly Artificial Neural Networks (ANNs), is an efficient and cost-effective alternative. ANNs, with their capacity to mimic the structure and function of the human brain, have garnered significant attention in this domain. ANNs are a type of ML algorithm capable of identifying patterns in datasets and making accurate predictions for new data based on these patterns. ANNs have demonstrated remarkable success across diverse fields, effectively addressing material design, optimization, and process control challenges. By using ANNs, researchers can build accurate predictive models that can simulate the behavior of complex systems, such as PANI/graphene-based nanocomposites, with remarkable accuracy and efficiency.

This research aims to thoroughly comprehend the performance prediction of PANI/graphene-based nanocomposites using ANNs and demonstrate the potential of this approach for designing and developing new high-performance nanocomposites. Twelve years of published data on PANI/graphene nanocomposites were utilized to build databases and create a data-driven platform to predict the electrical conductivity and gas sensing response performances of any new PANI/graphene-based nanocomposite. A comprehensive methodology is employed utilizing the COSMO-RS-derived *σ-profiles* of additives in the systems as inputs into eight different ML algorithms, including simple linear models such as Multi Linear regression (MLR), Multiple Non-Linear Regression (MLNR), Decision Tree (DT), Random Forest (RF), Gradient Boosting Machine (GBM), k-Nearest Neighbors (k-NN), Support Vector Regression (SVR), and ANNs. A thorough statistical evaluation and examination of the molecular space of applicability were performed to validate the predictive accuracy and robustness of the developed models. Furthermore, a bootstrap forest was employed to categorize PANI/graphene systems based on their inputs, unveiling insights into the influences of individual inputs on the enhancement or reduction of electrical conductivity and gas sensing response in the nanocomposite systems. This groundbreaking study introduces pioneering holistic models, showcasing their proof-of-concept potential that effectively map the properties of graphene-based nanocomposites. It is also the first reported model to predict the electrical conductivity and gas-sensing response of polyaniline/graphene-based nanocomposites. The model's outstanding performance underscores the prospect of this methodological approach in guiding the design of novel PANI/graphene systems, reduces the necessity for extensive experimental measurements, leading to a substantial reduction in the nanocomposite manufacturing cycle, thereby facilitating the design of tailor-made conducting nanocomposites for specific applications.

III.2. Methodologies

This research aims to build a machine-learning technique for estimating the performance of polyaniline and graphene nanocomposite systems in high-end applications based on their electrical and gas sensing properties. The accurate prediction of the performance of such systems is a significant and currently unresolved challenge that involves modeling various processes occurring at distinct time and length scales. Instead of pursuing a multi-scale approach, a different strategy focuses on the conditions that can be imposed on the polyaniline/graphene systems and accurately predicted. Figure III.1 represents the overall procedure used for the development of the models. The first and foremost step of the methodology involves generating a comprehensive dataset from published literature sources and organizing it in a readable format. Subsequently, machine learning algorithms were evaluated and validated utilizing *k*-fold cross-validation. The best model was selected based on its performance and then further hyper-tuned to improve accuracy. The final models were employed to predict the systems' conductivity, gas-sensing effectiveness, and responsiveness to various parameters. The methodology will be thoroughly discussed in the subsequent sections of the manuscript.

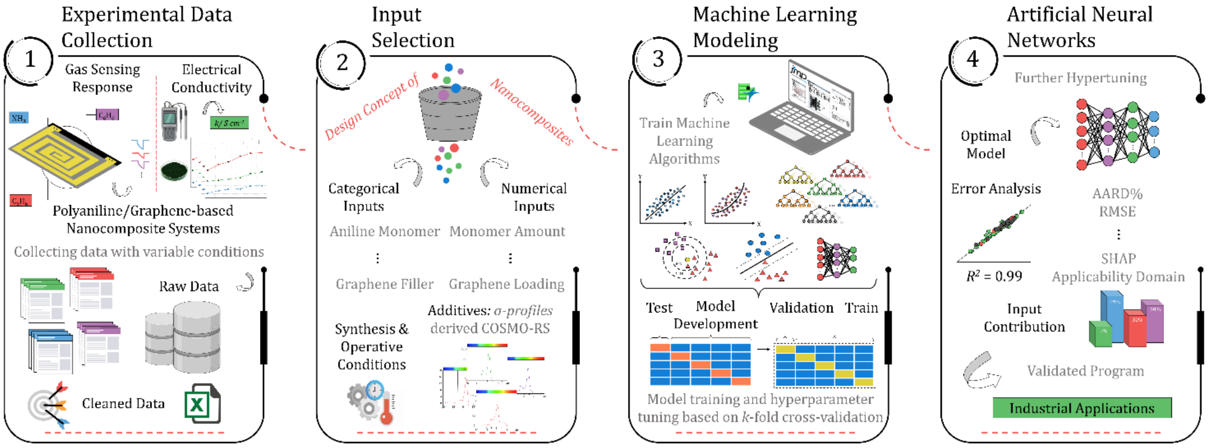

Figure III.1. A comprehensive summary of the ML-assisted workflow for developing robust models capable of predicting electrical conductivity and gas sensing response.

III.2.1. Datasets processing and treatment

One of the key steps in building a machine learning model is obtaining relevant datasets. To construct the datasets for this study, a comprehensive search was conducted to gather information on synthesis conditions that could affect the effectiveness of PANI and graphene nanocomposites. This was achieved by mining all available data published between 2010 and 2023 from credible sources such as Scopus, Google Scholar, and Web of Science using relevant keywords such as “polyaniline, PANI, graphene, nanocomposite, and PANI/graphene.” This study's performance evaluation of novel polyaniline/graphene nanocomposites was based on the collected experimental data. Data were sourced from tables and figures, while for specific figures where direct data retrieval proved challenging, a digitized image tool, in conjunction with the professional software Origin Lab® 2022b, was employed effectively to ascertain their values.

Furthermore, the resulting experimental data was systematically organized into two primary datasets: electrical conductivity and gas sensing response. The raw data points in each dataset varied due to the availability of information reported in the literature, including a sum of 989 data points for electrical conductivity and 931 data points for gas sensing. Within the extensive gas sensing dataset, 26 different gases were identified in the literature, encompassing a range of substances such as hydrogen, ammonia, methane, nitrogen dioxide, sulfur dioxide, hydrogen sulfide, carbon dioxide, carbon monoxide, benzene, toluene, among others. Upon a comprehensive examination of the gas-specific datapoints, it became evident that ammonia, benzene, and toluene gases have received considerable attention in the literature. This is reflected in the substantial number of datapoints associated with these gases, establishing a robust foundation for comparative analysis with existing research. Furthermore, the prominence of these gases in real-world applications underscores their relevance and renders them meaningful choices for in-depth investigation within the scope of our study. Furthermore, various parameters, such as the concentrations of the monomer, oxidant, and doping agents, the graphene filler's type and loading, the synthesis conditions (temperature and time), and the operative temperature, were extracted from each report. The gas sensors' response also considered the tested gas's type and concentration. The experimental data that met the criteria for analysis was then organized in Excel, and a percentage distribution was generated to aid in the examination. The next step in the process was data cleaning and pretreatment since most unprocessed data sets contain duplicate or even inaccurate information that can negatively impact the machine learning model's performance. All the data points collected for this study were obtained from *in situ* polymerization, which involves synthesizing the PANI/Gr nanocomposites directly on the graphene surface. This approach simplifies the systems and eliminates potential contamination from external sources, resulting in more reliable and accurate experimental data. Additionally, this methodology ensures a higher degree of homogeneity in the resulting nanocomposites. It reduces the variability in the measured properties, which is crucial for developing robust ML models for predicting the electrical conductivity and gas sensing response values. The final data utilized in this study consisted of 616 data points of various systems and synthesis conditions for electrical conductivity and 668 datapoints for gas sensing, with the gas sensing data further subdivided and analyzed for the presence of ammonia, benzene, and toluene gases (338, 146, and 122 datapoints, respectively).

Further, the datasets were converted and used on the logarithmic scale during training for all property sets used in the models to aid machine learning. Figure III.2 presents a comprehensive summary of the histogram distribution for the employed datasets, showcasing their frequency counts, averages, and one-sigma standard deviations. Utilizing a logarithmic scale during model training leads to a more uniform distribution, effectively mitigating any unbalanced skewness in the models.

A) Electrical conductivity **B) Ammonia Sensing response**

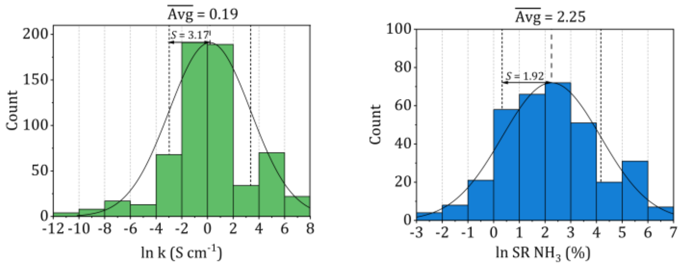

C) Toluene Sensing response **D) Benzene Sensing response**

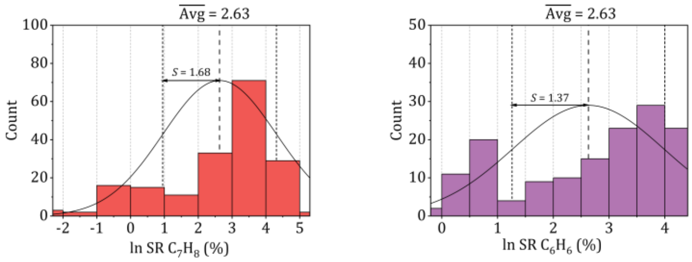

Figure III.2. Histogram distribution of the collected datasets utilized for A) Electrical conductivity, B) Ammonia (NH_3), C) Toluene (C_7H_8), and D) Benzene (C_6H_6) Sensing responses.

III.2.2. Input selection

When building an ML model, identifying relevant inputs is vital in ensuring the model's accuracy and effectiveness. To determine the relevant factors that affect the performance of polyaniline/graphene systems, a comprehensive literature review was conducted to identify commonly reported input parameters. These inputs were then incorporated into the ML models, considering the design concept of nanocomposites and experimental operation. As shown in Figure III.3, four sections were chosen as input descriptors. They are as follows: 1) matrix: aniline amount, type, and amount of oxidant, volume, and concentration of the doping agent, and additives, 2) filler: graphene filler type and loading, 3) synthesis conditions: temperature and time, and 4) operating conditions: temperature and gas concentration for the gas sensing response properties. It is worth noting that some inputs that may affect the electrical conductivity or gas response were not included in the datasets as they were either not widely reported in the literature or not uniformly documented. However, many of the inputs used in these datasets were categorical, and a short abbreviation was utilized to incorporate categorical data in the ML algorithms effectively. This involved assigning numerical values to the categorical inputs, such as the type of graphene nanofiller and doping agents. The numerical inputs, such as temperature and time, were entered as reported in the literature.

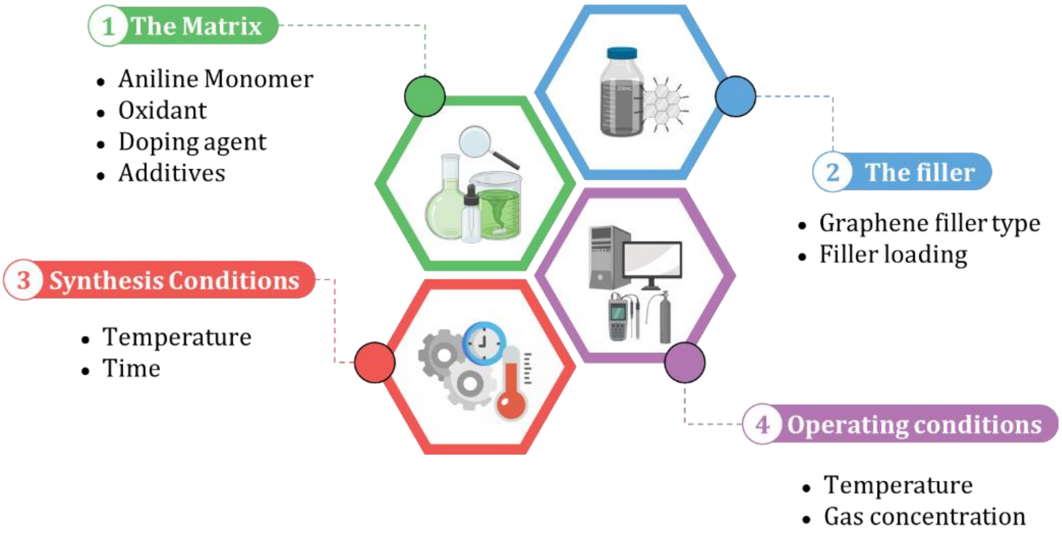

Figure III.3. The input selection process for machine learning models of polyaniline/graphene nanocomposites.

Given the limited number of variations for inputs, including monomers, oxidants, and graphene fillers, incorporating them as molecular inputs into the model would not significantly increase its complexity and result in overfitting. However, the wide range of various additives used in the systems can dramatically impact the material properties. To properly account for these impacts, it was crucial to include the additives as molecular inputs in the model. Utilizing sigma profiles derived from the COSMO-RS offered a powerful method for characterizing the complex mixture of additives in the system. This approach accurately describes the mixture and provides valuable insights into the behavior and properties of the material under study. This molecular method allows for a complete examination of the effects of additives on polyaniline/graphene systems, yielding a clearer understanding of their influence on material characteristics and behavior. The methodology behind the molecular inputs is thoroughly described in a subsequent section.

In this study, the density functional theory (DFT) computations were conducted using the DMol$_3$ code, part of the Material Studio® 2020 software developed by BIOVIA Corporation. This code employs localized numerical orbitals as basis functions and can predict the energy and structure of atoms without any experimental data inputs (Delley 1995, 2000; Moumeni et al. 2023; Yasmin et al. 2023). To improve upon the limitations of the LDA in accurately predicting bond energies and equilibrium distances, the GGA with the PBE method was used to treat the correlation (Dal Corso et al. 1996; Perdew et al. 1996). The GGA functional is known for its reliable numerical behavior and is commonly employed in DFT methodology. The computations were performed using the high-quality DNP basis set, including hexadecapole for multipolar expansion. Using a numerical basis set and precise DFT spherical atomic orbitals to mitigate any potential basis set superposition effects and enhance the accuracy of the system description, even for weak bonds. To optimize computational performance and achieve convergence efficiently, a thermal smearing of 5×10^{-3} Ha was utilized. Additionally, we set the density at 0.2 charges and 0.5 spins, respectively, to improve the overall computational efficiency. These computational approaches contributed to a more reliable and accurate analysis of the system under investigation. In addition, for the graphene-based compounds, we employed specific models to simulate their structures. The graphene (Gr) model contained 92 atoms and was adopted from previous studies (Legarreta-Mendoza et al. 2019). The model of graphene oxide (GO) consisted of 114 atoms, which include two epoxy groups ($\mathrm{C-O-C}$), two hydroxyl groups ($\mathrm{-OH}$), and four carboxyl groups ($\mathrm{-COOH}$) (Tabari and Farmanzadeh 2020). For reduced graphene oxide (rGO), a model of 93 atoms with the charge set at -2, where oxygen atoms bonded to 2 carbon atoms to represent the $\mathrm{C-O-C}$ group (Shi et al. 2020). After geometry optimization, energy computations were performed utilizing a conductor-like screening model for real solvents (COSMO-RS) solvation with a dielectric constant of 78.54, representative of water (Klamt 2018), to generate COSMO files. These files were subsequently leveraged to calculate sigma profiles (*σ-profiles*).

III.2.3. Machine learning models

This study aimed to identify polyaniline/graphene-based nanocomposites with high electrical conductivity and gas-sensing solid capabilities for ammonia, toluene, and benzene. To achieve this, we evaluated eight different ML algorithms concurrently, including simple linear models such as MLR, MLNR, DT, RF, GBM, *k*-NN, SVR, and ANN.

These ML algorithms, including MLR, MLNR, DT, RF, GBM, K-NN, SVR, and ANN models, were all implanted and directly programmed using the JMP® statistical software (version 16). To optimize the model hyperparameters, we employed several techniques, including stepwise parameter variation for MLR to achieve the smallest value of root mean squared error (RMSE), varying the number of splits between 1 and 100 for DT, using default settings with 100 trees for RF and GBM; performing *k*-NN regression for all *k*-values of 10; and adjusting the neuron's number in the first hidden layer of ANNs between 5 and 25.

Additionally, to further optimize the performance of the ANNs, we performed further adjustments by varying the configuration of neurons in the second hidden layer, along with their activation functions. These refinements were accomplished through a conventional iterative approach, systematically seeking the most effective settings (Matsukawa et al. 2021) through a seven-level factorial design, which evaluated 25 two-hidden layer configurations. All other software options in JMP® 16 were kept as default.

III.2.4. Criteria for model evaluation

To analyze the reliability and applicability of the developed ML models, a *k*-fold cross-validation technique was employed (Stone 1976). In this strategy, the dataset is divided into *k*=5 subsets of equal size, one of which serves as the test set, while the remaining *k*-1 subsets form the training set, which also includes the validation set. The primary objective of this technique is to train the model using different subsets of the data and evaluate its performance using the held-out test set. By repeating this process *k* times, we can estimate the model's performance using data not included in the specific fold. The final model is then selected based on the parameter set that provides the lowest average error across all *k* iterations. This method effectively prevents overfitting and gives a more thorough assessment of the models' capacity to adapt to new data.

Moreover, various metrics were employed to assess the models' reliability. These metrics encompass root mean square error ($RMSE$), coefficient of determination (R^2), the standard deviation (ASD), average absolute relative deviation ($AARD$), and Mean Absolute Error (MAE), which are determined through Eq. (1) – Eq. (5). In these equations, Y_{exp}, Y_{pred}, and $\bar{Y}$ are utilized to denote the target properties' experimental, predicted, and average values, respectively. The symbol N represents the total number of data points in the datasets.

$$RMSE = \sqrt{\frac{\sum_1^N (Y_{exp} - Y_{pred})^2}{N}} \qquad \text{Eq. (9)}$$

$$R^2 = 1 - \frac{\sum_1^N (Y_{exp} - Y_{pred})^2}{\sum_1^N (Y_{exp} - \bar{Y})^2} \qquad \text{Eq. (10)}$$

$$ASD = \sqrt{\frac{\sum_1^k (Y_{pred} - \bar{Y})^2}{N}} \qquad \text{Eq. (11)}$$

$$AARD\ (\%) = \frac{100}{N} \times \sum_1^N \frac{\left|(Y_{pred} - Y_{exp})\right|}{Y_{exp}} \qquad \text{Eq. (12)}$$

$$MAE = \frac{1}{N}\sum_{1}^{N}\left|Y_{exp} - Y_{pred}\right| \qquad \text{Eq. (13)}$$

Although all of these metrics are generally useful for evaluating model accuracy, it was found that the *RMSE* is mainly affected by a small number of highly inaccurate predictions. In practical applications, such predictions can have significant consequences. Therefore, *RMSE* has been adopted as the primary metric for quantifying accuracy in this study, in which the analysis of the current data sets indicates that the *RMSE* provides a conservative estimate of the model's performance, making it a suitable choice for evaluating the accuracy of the developed models.

III.2.5. Artificial neural network

Upon evaluating the constructed models, the most effective model, ANN, was chosen for interpretation. The hidden neurons within layers 1 and 2, denoted as $H_{n,l}$ and $HH_{n,l}$ respectively, are mathematically represented by Eq. (14) and Eq. (15). The weights between neurons *m* and *n*, denoted as $W_{m,n,l}$, along with the biases of neurons (b), are specified in the equations. The hyperbolic tangent function (*tanh*) utilized in Eq. (14) and Eq. (15) confines the neuron's activation or deactivation values within the range of [-1, 1]. Ultimately, the ANN model's output response (y_{pred}) is determined through Eq. (16), derived from Eq. (14) and Eq. (15) (Haykin 2009; Lemaoui et al. 2021).

$$H_{n,l} = tanh\left(\sum_{n=1}^{N}(W_{m,n,l})(I_m) + b_{n,l}\right) \qquad \text{Eq. (14)}$$

$$HH_{n,l} = tanh\left(\sum_{n=1}^{N}(W_{m,n,l})(H_{n,l}) + b_{n,l}\right) \qquad \text{Eq. (15)}$$

$$Y_{pred} = \sum_{n=1}^{N}(W_{m,n,3})(HH_{n,2}) + b_{n,3} \qquad \text{Eq. (16)}$$

The optimization process during ANN training involved the implementation of the Broyden-Fletcher-Goldfarb-Shanno (BFGS) algorithm, well-regarded for its efficacy in handling datasets. To ascertain the suitability of the dataset for training ANNs, a meticulous evaluation was conducted, considering factors such as the model's complexity, dimensionality of the input space, and intrinsic relationships within the data. Despite the considerable number of data points, we underscored the significance of scrutinizing the distribution across training, validation, and testing sets. To gauge the model's generalization performance, we employed appropriate cross-validation techniques, ensuring a robust assessment of the ANN training efficiency. The effectiveness of training ANNs with a specific number of hidden neurons underwent comprehensive testing and cross-validation procedures. This rigorous validation process guarantees the models' robustness and their ability to generalize effectively to new, unseen data. For internal validation, a k-fold of 5 was adopted, and an ANN network learning rate of 0.10 was set, employing squared penalty optimization $\left[\sum\left(Y_{exp} - Y_{pred}\right)^2\right]$ to enhance learning stability. The model weights were initialized randomly to ensure diversification in the preliminary state and prevent convergence to local minima. A maximum of 1,000 epochs were carried out throughout the training process, and early stopping was incorporated to avoid overfitting. The training was stopped if the validation loss did not improve in consecutive epochs. The model with the lowest achieved Mean Squared Error (MSE) value was chosen as the best, while all other settings in JMP 16 Pro® remained at their default values.

III.2.6. Applicability domain analysis

To determine the outliers in the datasets and establish the range of molecules/systems for accurate predictions, an applicability domain (AD) evaluation was conducted. The AD approach relies on two key specifications, namely, the leverage values h_i, and the SDR. The AD range is defined as $0 < h_i < h^*$, and $-3 < SDR < +3$. The critical leverage value h^* and the leverage value h_i are determined using Eq. (17), Eq. (18), and Eq. (19), respectively. A matrix represents the input parameters considered for this study x_i of dimensions $1 \times D$ while D is the number of input parameters. The training data points are represented by a matrix V of dimensions $N \times D$, where N is the total number of data points in the datasets, moreover, the superscript "T" signifies the transpose of matrices (Tropsha et al. 2003; Almi et al. 2020).

$$SDR = \frac{Y_{pred} - Y_{exp}}{\sqrt{\frac{\sum_{m=1}^{N}(Y_{pred} - Y_{exp})^2}{N}}} \qquad \text{Eq. (17)}$$

$$h_i = x_i(X^{\mathrm{T}}X)^{-1} * x_i{}^{\mathrm{T}} \qquad \text{Eq. (18)}$$

$$h^* = 3(\mathrm{D}+1)/\mathrm{N} \qquad \text{Eq. (19)}$$

The William plot is widely used to represent the applicability domain (AD) visually due to its simplicity (Tropsha et al. 2003; Mitra et al. 2010). It involves plotting the SDR versus h_i values to determine the AD coverage. the AD coverage is calculated using the following equation Eq. (20), where N_{inside} refers the count of data points that lie within the specified boundaries, while N_{total} represents the total number of data points considered for analysis.

$$AD_{coverage} = \frac{N_{inside}}{N_{total}} \times 100 \qquad \text{Eq. (20)}$$

III.3. Results and discussion

III.3.1. Database treatment and visualization

To develop accurate ML-based prediction models, it is necessary to visualize and analyze the constructed datasets to investigate the correlations and structures of each input. The collected datasets for both electrical conductivity and gas sensing capabilities of PANI/graphene nanocomposites involve several forms of nanocomposites based on various parameters such as aniline concentrations, oxidant types and concentrations, graphene types, and loading, dopant types and concentrations, and additive types. Including such comprehensive and diverse data is essential for developing reliable prediction models. The datasets consist of graphene-based nanofillers, including Gr, GO, and rGO. The commonly used oxidants and dopants for PANI/graphene nanocomposite fabrication are ammonium persulphate and hydrochloric acid, respectively. The loading of graphene varies from 0 to 50 *wt*%, with most loadings being between 0.1 to 3 *wt*%, although exceptional cases of high loading rates were noticed for GO fillers. Moreover, more information has been gathered about the concentrations of aniline monomers/oxidants, such as APS or potassium persulphate (KPS), which range from 10^{-3} to 2 M, with the majority of the concentrations ranging between 0.5 to 1 M. The aniline monomers/dopants include 9 different doping agents with concentrations ranging from 0.1 to 10 M, with most concentrations of 1M. We also observed high concentrations of formic acid as a dopant (10 M), which is not typically applied in experiments. The additives vary from organic solvents surfactants to nanoparticles, with different concentrations. The datasets underwent essential preprocessing steps to enhance the accuracy and reliability of ML models for predicting the performance of PANI/graphene nanocomposites. These steps encompassed handling missing data, detecting and removing outliers, and normalizing data to ensure equitable consideration of each input variable in the analysis. For instance, the deliberate selection of ammonia, benzene, and toluene as selected gases in this study was grounded in their prevalence in industrial and environmental contexts, aligning them closely with gas-sensing applications. Their distinct chemical properties permit an exploration of the versatility of polyaniline/graphene-based nanocomposites across diverse chemical environments (Wang et al. 2016; Tanguy et al. 2018). Moreover, the extensive literature on these gases serves as a robust foundation for comparative analysis, contributing meaningfully to existing research and advancing the understanding of gas-sensing materials. The practical significance of ammonia, benzene, and toluene in real-world applications, including environmental monitoring and industrial processes, further justifies their selection for in-depth investigation. While recognizing the importance of other gases, our focused exploration of ammonia, benzene, and toluene enables valuable insights into the materials' performance within the defined scope and objectives of this study.

Consequently, the application of such preprocessing steps is crucial for developing accurate prediction models by reducing noise and improving the reliability of results. The comprehensive information gathered about the inputs forms the basis for building highly accurate and reliable ML models. Such models aid in the design and optimization of new and innovative materials. Thus, the use of advanced visualization and data preprocessing techniques along with comprehensive datasets is essential for developing accurate prediction models.

III.3.2. Input selection

Input selection is a critical process that selects the key features that contribute most to the PANI/graphene systems. As mentioned earlier, the input variables were chosen based on the design principles of nanocomposites and the requirements of experimental operations. Although the number of variations for inputs, such as monomers, oxidants, and graphene fillers, is limited, incorporating them as molecular inputs into the model is still essential. This approach ensures that the model's complexity does not significantly increase and results in overfitting. However, using various additives in the systems can dramatically impact their material properties. Therefore, it is crucial to include the additives as molecular inputs in the model to account for these impacts properly. The following section will analyze the σ-Profiles of some selected additives and other features. This analysis will better understand the proportion of each input variable to the PANI/graphene systems' performance and behavior.

III.3.2.1 σ-Profiles analysis

The analysis of the additives in terms of molecular inputs *via σ-Profiles* offers a comprehensive understanding of the chemical makeup and behavior of the polyaniline/graphene systems. This technique provides a holistic view of the molecular interactions and composition, offering a more in-depth analysis than other methods. Indeed, the analysis of the *σ-Profiles* can provide valuable insights into the polarization and concentration of specific atoms within the nanocomposites, which can, in turn, inform their performance. By examining these profiles, we can gain insights into the distribution and arrangement of the atoms within the nanocomposites, which can be crucial in understanding how they interact and contribute to the material's properties. Therefore, this analysis can be a valuable tool in developing and optimizing polyaniline/graphene-based systems. Furthermore, the observed peaks in the *σ-Profiles* provide valuable information concerning the polarity and concentration of specific atoms within a molecule. Increased peak heights indicate higher concentrations, while the peak location offers insights into the corresponding polarity characteristics (Torrecilla et al. 2010). This analysis helps identify "polar" molecules, characterized by substantial peaks at σ values exceeding $\pm 0.008\ \mathrm{e}/\text{Å}^2$ (Adeyemi et al. 2020). In addition, the utilization of *σ-Profiles* offers a unique perspective into the relationships between organic components. Unlike conventional approaches that primarily focus on atom categories and their correlations, such as group contribution methodology or molecular fingerprinting, the *σ-Profiles* comprehensively depict molecules as assemblies of charged surface segments, offering a quantitative definition (Abranches et al. 2022). The use of *σ-Profiles* offers several advantages over other molecular inputs, including HOMO energy, LUMO energy, and topological indices. These profiles are an intuitive and easily understandable analysis tool with a robust quantum chemical foundation. *σ-Profiles* offer a unique capability to capture polarizability and asymmetric electron densities arising from covalent bonds between atoms with differing electronegativities. These attributes make *σ-Profiles* particularly valuable for characterizing non-covalent interactions between molecules and properties that depend significantly on intermolecular interactions (Awaja et al. 2023; Lemaoui et al. 2023b, a), such as electrical conductivity. By utilizing *σ-Profiles*, we can gain valuable insights into the molecular interactions that govern the behavior of nanocomposite materials, leading to advancements in material design and applications in various fields (Boublia et al. 2022b). An additional advantage of *σ-Profiles* lies in their capability to characterize molecules of varying sizes, facilitated by their unnormalized histograms comprising 61 points within the σ value range of $[-0.030, +0.030]\ \mathrm{e}/\text{Å}^2$(Boublia et al. 2022c). This inherent property ensures a consistent number of inputs for machine and deep learning applications, as it remains unaffected by variations in the molecular structure. Analyzing additives in the PANI/Gr system using *σ-Profiles* provides a comprehensive view of their chemical composition and behavior. However, simplifying this complexity, even with 61 dimensions of *σ-Profiles*, may overlook crucial details essential for a comprehensive system understanding. The decision to preserve the full complexity of *σ-Profiles* without reduction ensures complex details about the diverse contributions of different additives, aligning with principles of interpretability and specificity in this analysis. Additionally, reducing dimensionality carries the risk of compromising the ability to distinguish between various additive mixtures, a critical consideration for our comprehensive analysis. Therefore, the current dimensionality, including 61 dimensions dedicated to *σ-Profiles*, is a judicious choice, achieving a balance that ensures a comprehensive representation of the system. Figure III.4 (1) presents a graphical representation of a series of representative additives modeled in this study. The *σ-Profiles* of key components, such as the aniline monomer, two oxidants, three representative graphene fillers, and three dopants were also analyzed and graphically displayed in Figure III.4 (2).

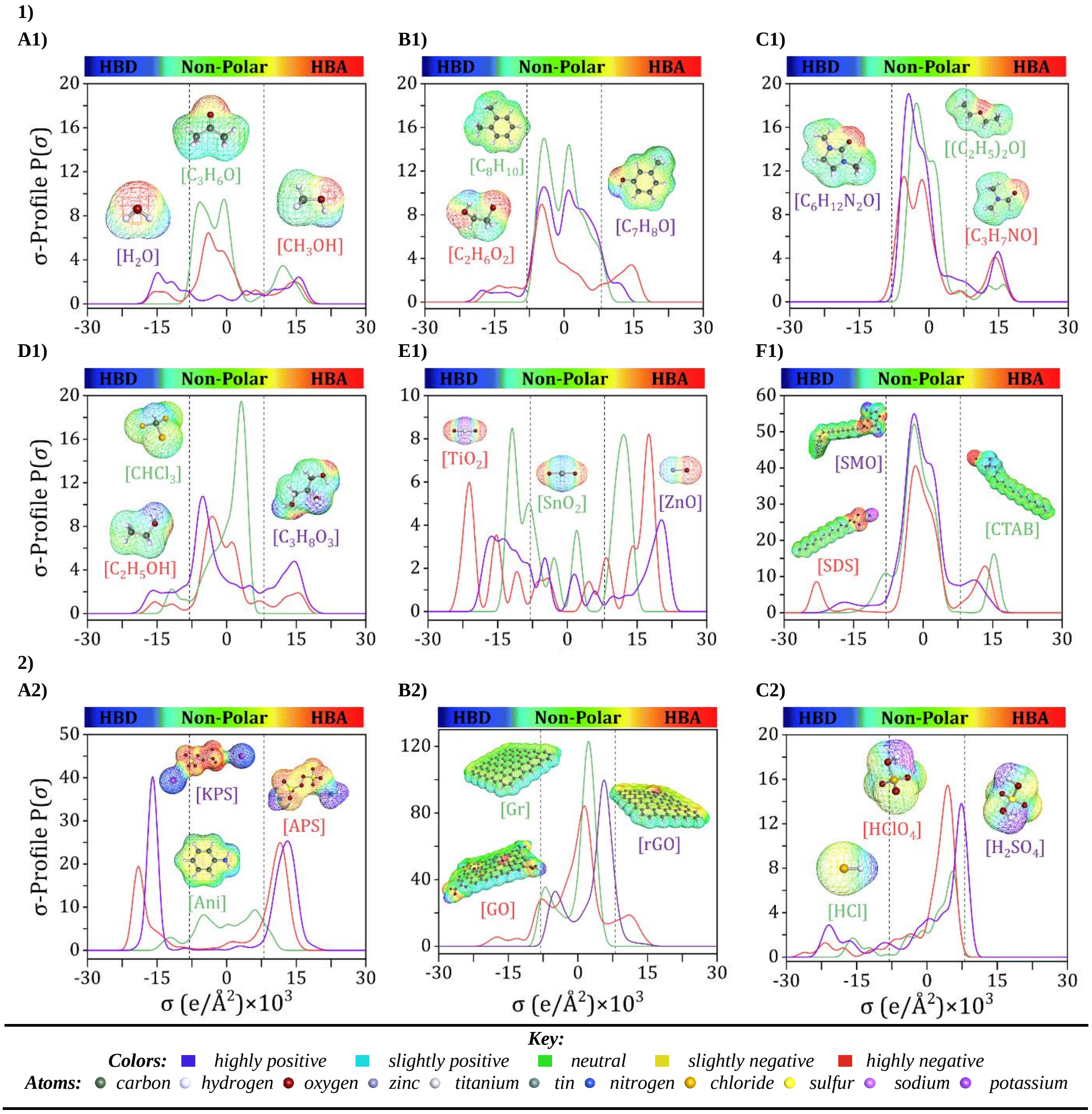

Figure III.4. COSMO-RS molecular structures and *σ-Profiles* of selected components: 1) Various additives (A1-F1), and 2) Aniline monomer, two oxidants, graphene fillers, and three dopants (A2-C2).

Upon observing Figure III.4, it becomes evident that the *σ-Profiles* can be classified into three distinct regions, each delineated by the electrostatic properties of the molecular surface. These regions are identified as the hydrogen bond donor (HBD) region ($-0.030 < \sigma < -0.008\ \mathrm{e/Å^2}$), the non-polar region $-0.0075 < \sigma < +0.008\ \mathrm{e/Å^2}$), and the hydrogen bond acceptor (HBA) region ($+0.008 < \sigma < +0.030\ \mathrm{e/Å^2}$)(Lemaoui et al. 2020, 2022; Uka et al. 2023). As depicted in Figure III.4, the HBD, non-polar, and HBA regions are clearly distinguished using vertical dashed lines. As described earlier, the peaks in the σ-Profile include more of a measure of the relative concentration of different atom types within the molecular system, therefore revealing underlying molecular insights into the behavior of compounds. The additives used in these systems can vary greatly, including solvents, inorganic nanoparticles, and surfactants. Solvents play a key aspect in the preparation and effectiveness of polyaniline/graphene systems. They serve a dual purpose as they are employed both for dissolving the polyaniline and graphene and for doping/dedoping the system, thereby affecting its conductivity. Additionally, solvents can also serve as washing agents. The choice of solvent has a major impact on the properties of the system, including its stability, dispersion, and conductivity (Goswami et al. 2023). Each of these solvents has unique properties and characteristics, such as boiling point, solubility, and polarity, which can affect the properties of the polyaniline/graphene system. In the case of water (H_2O), acetone (C_3H_6O), and methanol (CH_3OH), as shown in Figure III.4 (A1), The *σ-Profile* graphs exhibit wide peaks that span across both the HBA and HBD areas, showing the potential of these solvents to act as both HBAs and HBDs, this phenomenon is primarily governed by the concentration and polarization of the partially positive hydrogen ($\mathrm{H}^{\delta+}$) and partially negative oxygen ($\mathrm{O}^{\delta-}$) atoms in the molecule, respectively. The sigma profile graphs for xylene (C_8H_{10}), ethylene glycol ($C_2H_6O_2$), and m-cresol (C_7H_8O) show that these solvents also have the potential to act as both HBAs and HBDs, with distinct peaks and regions in their profiles (Figure III.4 (B1)). The exact nature of these peaks and regions depends on the specific functional groups in the molecule, includes the $-\mathrm{OH}$ group in ethylene glycol and the phenol group in m-cresol. Furthermore, dimethyl propylene urea ($C_6H_{12}N_2O$), ethyl ether ($(C_2H_5)_2O$), and dimethylformamide (C_3H_7NO) reveals small peaks in the HBA region and minimal or no presence in the HBD region (Figure III.4 (C1)). The presence of functional groups, such as amines and ethers, accounts for this observation, for instance, in the case of C_3H_7NO, it can be attributed to the nitrogen (N) atom, which has a relatively high electronegativity, allowing it to attract electrons and partially negative charges. However, these solvents have a weak HBA ability, suggesting that they can be classified as intermediate polar with different solubility properties. Further, the *σ-Profile* of ethanol (C_2H_5OH) and glycerol ($C_3H_8O_3$) suggest that they can act as both HBAs and HBDs, with distinctive peaks and regions in their profiles determined by the functional groups in the molecule. On the other hand, chloroform ($CHCl_3$) is dominated by a peak close to the HBA region, which is primarily attributed to the presence of a highly polarizable chloroform molecule due to the fact of a highly electronegative chlorine (Cl) atom in the molecule Figure III.4 (D1). This polarizability enables chloroform to act as an effective HBA, leading to the observed peak close to the HBA region. Inorganic nanoparticles are essential in controlling the properties and behavior of polyaniline/graphene systems, promoting oxidation and improving the material's conductivity for practical functionality. In terms of their *σ-Profiles*, as shown in Figure III.4 (E1), tin oxide (SnO_2), zinc oxide (ZnO), and titanium oxide (TiO_2) show unique peaks and regions in both HBD or HBA regions, which can influence the interactions between the polyaniline and graphene components. For example, due to its excellent conductivity-promoting properties, SnO_2 is a widely used oxidant in polyaniline/graphene systems. It is a wide bandgap semiconductor made up of tin and oxygen atoms and is commonly used in various fields, including catalysis, gas sensing, and environmental remediation (Arora et al. 2012). The *σ-Profile* of SnO_2 shows broad peaks in both the HBD and HBA areas, indicating that it can act as both an HBD and HBA. These peaks are primarily attributed to hydroxyl groups and oxygen atoms appearing on the SnO_2 surface. The −OH groups can act as HBDs by donating a hydrogen atom, while the oxygen atoms can act as HBAs by accepting a hydrogen atom. However, it is essential to note that these specific characteristics can vary depending on various factors, such as the nanoparticle synthesis process, particle size, and crystal structure (Krithika and Balavijayalakshmi 2022).

Moreover, considering surfactant substances as additives in these systems, it is essential to note that their *σ-Profile*, as represented by sodium dodecyl sulfate (SDS), sodium cetyltrimethylammonium bromide (CTAB), and sorbitan monooleate (SMO), will typically have a larger neutral region, indicating that they are not likely to participate in hydrogen bonding interactions with other substances (Figure III.4 (F1)). However, some HBD or HBA regions may be present, suggesting that these substances can form weak hydrogen bonds with other molecules due to their unique molecular structure. However, they are not typically considered strong HBDs or HBAs. Surfactant molecules tend to interact more strongly with each other through hydrophobic and VDW interactions rather than with H bonding with other molecules, owing to the polar head groups and nonpolar tails in their molecular structure. Despite not directly participating in hydrogen bonding interactions, surfactants are pivotal in improving the dispersion, stability, and characteristics of polyaniline/graphene nanocomposites, making them an essential component of these materials.

In the context of the statement provided, the *σ-Profiles* also yield significant insights into these components' molecular interactions and behavior, which are invaluable contributions to advancing the field. The key components analyzed in this study include an aniline monomer, two oxidants, three representative graphene fillers, and three dopants (Figure III.4 (2)). Even though these components may not be directly included as molecular inputs, their *σ-Profiles* offer a deeper understanding of their electronic structure and interactions with the surrounding environment. By analyzing Figure III.4 (A2), aniline, for example, can act as an HBD and an HBA. The HBD and HBA properties of aniline are essential in the polymerization process, as they allow for hydrogen bond creation between aniline monomers, which can facilitate the polymerization reaction. Specifically, the density of electrons on the nitrogen atom and the benzenoid and quinoid unit of aniline can contribute to its ability to undergo oxidative polymerization with oxidants, including ammonium persulfate (APS) or potassium persulfate (KPS). Alternatively, the *σ-Profiles* of APS and KPS can offer valuable information on their reactivity and capability to oxidize aniline monomers.

The electron density on the sulfate groups of these oxidants, as revealed by their *σ-Profiles*, can facilitate the H bond creation with the electron's lone pairs on the aniline nitrogen atom. Furthermore, the *σ-Profiles* can indicate the ability of these oxidants to accept electrons during the oxidation process. In the case of graphene and its derivatives (Figure III.4 (B2)), *σ-Profile* can give insight into the interactions between the graphene sheets and the surrounding solvent or other molecules. For Gr, *σ-Profile* shows a uniform electron density distribution around the sheet, with a slight electron density depletion at the edges. This is because the carbon-carbon bonds in Gr are powerful, and the electron density is uniformly dispersed over the sheet.

In contrast, GO shows a more significant variation in electron density, as the O-containing functional groups on the sheet surface can create regions of higher or lower electron density. These functional groups can interact with solvent molecules or other molecules in solution through hydrogen bonding or other interactions, which can affect the stability and reactivity of the GO (Prías Barragán et al. 2020). For rGO shows a decrease in electron density compared to GO, as the reduction process removes some of the oxygen-containing functional groups from the sheet surface. This can lead to a uniform electron density around the sheet, similar to Gr (Masson et al. 2017). Doping is a process in which impurities, or dopants, are intentionally introduced into a material to modify its properties. Hydrochloric acid (HCl), sulfuric acid (H_2SO_4), and perchloric acid ($HClO_4$) are widely recognized and used as dopants to modify the electronic and structural properties in the case of the polyaniline/graphene nanocomposite systems. When examining the *σ-Profile* (Figure III.4 (C2)) of HCl, H_2SO_4, and $HClO_4$, it can be observed that there are regions of high electron density around the sulfur, chlorine, and oxygen atoms. These regions of high electron density indicate that these atoms have a partial negative charge and are, therefore, capable of acting as HBAs. Therefore, these molecules can participate in H-bonding interactions with suitable donor molecules, which can play a key function in chemical reactions and the behavior of these compounds in various applications. Overall, *σ-Profiles* reveal important information about the electronic structure and interactions of key components in conducting polymer composites like polyaniline/graphene. This analysis can assist in designing and enhancing the material properties in wide variety of applications, including electronics and energy storage materials. Additionally, accurately predicting the hydrogen bonding ability of these molecules based on its *σ-Profile* can also be beneficial for gas sensing applications. This can aid in the discovery and development of gas sensors with improved sensitivity and selectivity, leading to better detection and identification of various gases in industrial and environmental settings.

III.3.2.2. Input contribution analysis

To understand the individual influence of each parameter on the nanocomposites' performance, the relative contributions of input parameters in the ML models and their effects on electrical conductivity and gas sensing responses were thoroughly examined. We utilized the "predictor screening" tool available in JMP Pro® SAS 16, incorporating the bootstrap forest approach, to evaluate the significance of variables in our predictive model. This approach involves generating multiple decision trees from different data subsets and then combining their results to recognize the most influential predictors in the model. To ascertain the significance of each feature, the model's accuracy is evaluated after removing individual features. The impact of each parameter is then visually represented in Figure III.5.

A) ln k

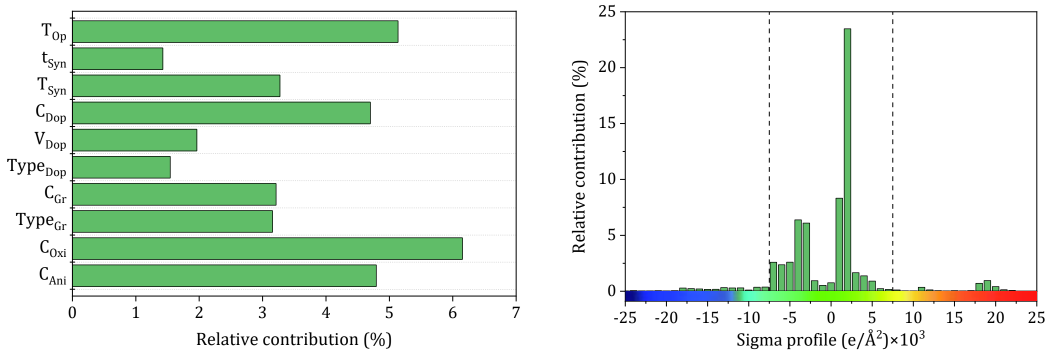

B) ln SR NH_3

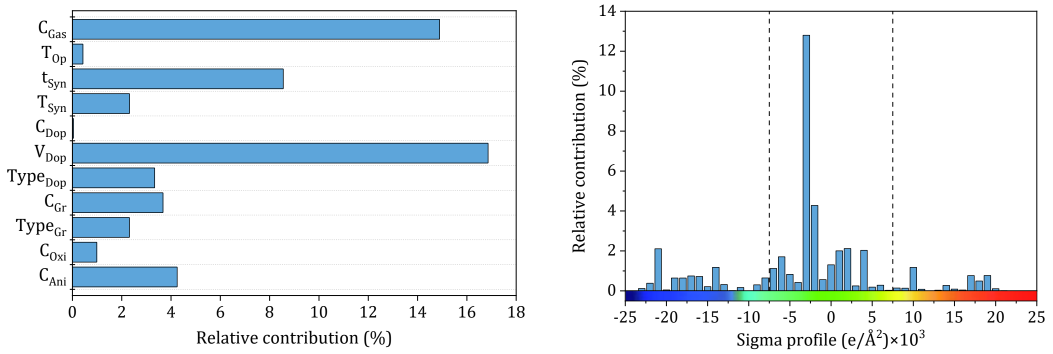

C) ln SR C_7H_8

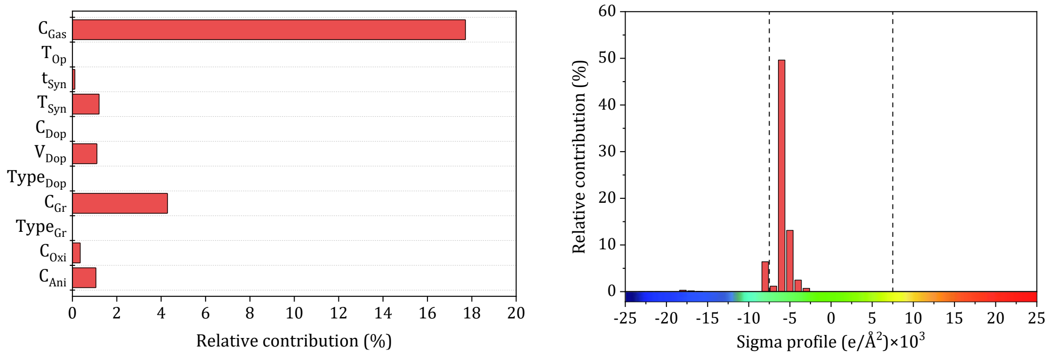

D) ln SR C_6H_6

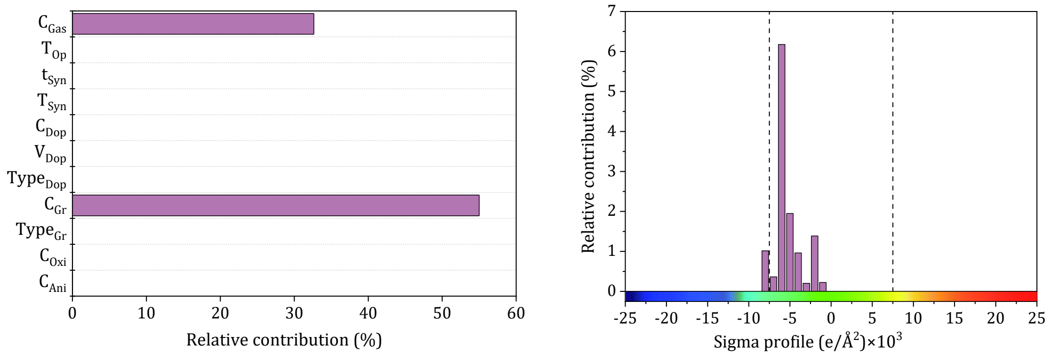

Figure III.5. Relative contribution of input parameters to accuracy (A) electrical conductivity, (B) NH_3, (C) C_7H_8, and (D) C_6H_6 Sensing response models.

To achieve high electrical conductivity and gas sensing response values, it is essential to understand the influences of synthesis and operational conditions and use them to reduce the generation of undesired properties. For electrical conductivity (Figure III.5 (A)), the oxidant amount, aniline amount, doping agent concentration, and operating temperature were the most critical features, followed by graphene filler type with corresponding loading and synthesis conditions, including temperature and time. This indicates that synthesis and operating conditions play important roles in the electrical conductivity property. For instance, According to Zheng *et al*. (Zheng et al. 2021), PANI's electrical conductivity increases with the rise in the oxidant (APS) molar ratio, attributed to higher concentrations of cation radicals and increased PANI chain length. These factors contribute to the enhancement of interchain transfer in electrical conductivity. However, an increase in APS concentration above 0.5 M leads to the production of phenazine, which reduces the electrical conductivity (Jelmy et al. 2013; Reza et al. 2019). Additionally, Nazari *et al*. (Nazari and Arefinia 2019) demonstrated that the conductivity of PANI shows an initial increase with an aniline amount of up to 0.15 M, but it decreases with further additions of aniline. Moreover, the rise in PANI particle conductivity with Oxi/Ani ratio can be attributed to an augmentation in both the crystalline regions and the doping level of microstructures. Extensive investigations into the impact of diverse dopants on electrical conductivities have been conducted, revealing a positive correlation between each dopant's concentration and PANI's electrical conductivity (Rahman et al. 2021). Significantly, the electrical conductivity of PANI experiences a notable decline with increasing the DBSA/Ani ratio, indicating that the intramolecular mobility of charged species along the chain exerts a more substantial impact on electrical conductivity than the intermolecular hopping of charge carriers within crystalline regions. However, at very high DBSA concentrations (DBSA/Ani= 3), a more pronounced reduction in conductivity can be achieved by simultaneously reducing both the doping level and crystallinity (Neelgund and Oki 2011). Additionally, the electrical conductivity of PANI/Gr nanocomposites was evaluated across different operating temperatures and varying loadings of graphene. The observed enhancement in conductivity with increasing temperature can be attributed to thermally-assisted charge carrier hopping, a characteristic commonly found in disordered materials. Al-Hartomy *et al.* (Al-Hartomy et al. 2019) assessed the electrical conductivity of PANI-Gr systems at various temperatures and diverse Gr loadings. Incorporating Gr into the PANI matrix remarkably enhances the composite's conductivity, attributed to the synergetic interactions between PANI and Gr phases involving charge transfer between delocalized *P*-orbitals. The system's conductivity demonstrates an increasing trend up to a 6 *wt*% content of Gr in PANI, after which it exhibits a subsequent decrease (Badi et al. 2016; Al-Hartomy et al. 2019). Moreover, the synthesis time and temperature can also impact the size and structure of the PANI/Gr nanocomposites, which in turn affect the electrical conductivity. Longer synthesis times and lower temperatures can lead to larger and more well-defined PANI/Gr systems, typically exhibiting higher electrical conductivity. The gas concentration is the most significant input affecting all gas sensing properties, including NH_3, C_7H_8, and C_6H_6. As gas concentration decreases, a stepwise reduction trend is observed in the actual sensor resistance values. Additionally, the sensor's resistance decreases with rising temperature. Higher gas concentrations result in gas molecules covering the largest surface area of the sensor, promoting an increased surface reaction. This, in turn, leads to higher resistance and a more pronounced response from the sensor. Conversely, lower gas concentrations result in fewer gas molecules adsorbing on the sensor's surface, diminishing surface reactions and reducing the sensor's resistance (Tanguy et al. 2018). Additionally, for NH_3 gas sensing response (Figure III.5 (B)), the most critical features contributing to high sensitivity are the dopant amount and synthesis time. These input variables are followed by aniline amount, graphene filler type with its corresponding loading, dopant type, and synthesis temperature. Doping PANI changes it from an insulator to a conductor, increasing its sensitivity to gases. This phenomenon arises from the protonation/deprotonation process of PANI, wherein the introduction of a proton acid stabilizes the regular and output resistance response curve. Consequently, the system's conductivity and NH_3 adsorption capacity exhibit an increase (Li et al. 2022a, 2023). For instance, during the in-situ polymerization of PANI with the addition of HCl as a dopant, a doping reaction (protonation) takes place, leading to neutral PANI molecules gaining protons and forming N^+-H bonds. Subsequently, as NH_3 molecules adsorb on the PANI surface and interact with one another, PANI loses protons and converts into an emeraldine base, resulting in a sharp increase in resistance (deprotonation) and NH_3 transforming into ion (NH_4^+) (Fratoddi et al. 2015b). According to a previous study, the response values of five different samples of 1 *wt*% PANI/rGO produced from varying HCl molarities (0.1, 0.5, 1, 1.5, and 2 M) exhibit varying trends, with response values changing with HCl concentration, particularly at the lowest and highest NH_3 concentrations. Response values are observed to decrease on either side of this optimal concentration, which has been found that 1*wt*% PANI/rGO sensors prepared using a 1 M HCl concentration demonstrate good NH_3 response capabilities, with different sensing response values increasing with increasing NH_3 concentration (Kundu et al. 2023). The introduction of GO in the PANI/GO system was observed to improve its response values, similar to the enhancement observed in electrical conductivity. The optimal loading of 1 *wt*% GO resulted in the strongest response value, reaching 31.2 ± 1.8% (Xing et al. 2022). Notably, Gr has shown to play a beneficial role in C_7H_8 and C_6H_6 gases typically similar to NH_3 sensing measurements which achieved a significantly higher maximum response compared to other nanocomposite samples (Xu and Wu 2020). Several experimental studies have demonstrated that PANI/Gr-based gas sensors are more suitable for measuring room temperature gases, as they are less affected by operating temperatures and maintain reliable gas response sensing properties (Liu et al. 2022). Additionally, it should be noted that there is a lack of experimental data in relation to the influence of other input variables on the sensing properties of C_7H_8 and C_6H_6 gases (Figure III.5 (C) and (D)). Hence, further research is required to comprehensively understand the behavior of PANI/Gr nanocomposites towards these gases and to identify the crucial input variables that can be optimized to improve gas sensing properties. Such studies could facilitate the advancement of more effective and reliable gas sensors for detecting C_7H_8 and C_6H_6, which are important industrial pollutants. Therefore, in addition to synthesis and operational conditions, the *σ-Profiles* of additives play a pivotal role in predicting the electrical conductivity and gas sensing responses of PANI/Gr systems. These additives exert a substantial influence on both the preparation and performance of nanocomposites. The types of additives used in PANI/Gr systems can vary greatly, including solvents, inorganic nanoparticles, or surfactants. Interestingly, for both electrical conductivity and gas sensing response values, the nonpolar regions of the additive molecules were observed as the most significant inputs. This can be attributed to the fact that most additives act as solvents (*e.g.*, H_2O, C_3H_6O or CH_3OH) as washing agents to remove any unreacted aniline or other compounds from the system. This study imparts invaluable insights into the structural features of PANI/Gr nanocomposites, enabling the optimization of both electrical conductivity and gas sensing response values. By prioritizing the significance of synthesis and operational conditions, along with additives possessing specific *σ-Profile* features, the design of new PANI/Gr nanocomposites with exceptional electrical conductivities and NH_3, C_7H_8, and C_6H_6 sensing responses becomes feasible. This approach facilitates the selection of more focused and efficient PANI/Gr prospects, presenting the opportunity for the advancement of highly effective gas sensor technologies.

III.3.3. ML algorithms analysis

After analyzing the input parameters, eight different ML algorithms were utilized to predict the electrical conductivity and gas sensing responses (NH_3, C_7H_8, and C_6H_6) of PANI/Gr nanocomposite systems. These algorithms include MLR, MLNR, DT, RF, GBM, *k*-NN, SVR, and ANN, each of which requires the selection of hyperparameters to ensure optimal performance (MacKay 1996). These algorithms include MLR, MLNR, DT, RF, GBM, *k*-NN, SVR, and ANN, each of which requires the selection of hyperparameters to ensure optimal performance. These hyperparameters were determined through train and test sets. The R^2, ASD, and residual error used for evaluation of the robustness and cognitive ability of each developed ML model. Table III.1 shows the predictive performance of the electrical conductivity and gas sensing response models trained by the different ML algorithms. The average R^2 from the various models ranged from 0.616 to 0.998. As shown in Table III.1, some of the developed ML models demonstrated good training performance for predicting the different properties, while others did not achieve high accuracy.

Table III.1. Performance evaluation of 8 tuned ML models in train and test sets and optimum key parameters.

	Electrical Conductivity		**Ammonia Sensing Response**		**Toluene Sensing Response**		**Benzene Sensing Response**	
	R^2	***ASD (±)***	***R^2***	***ASD (±)***	***R^2***	***ASD (±)***	***R^2***	***ASD (±)***
MLR								
	45 parameters		37 parameters		26 parameters		25 parameters	
Train	0.9166	0.4320	0.7827	0.4692	0.9276	0.2543	0.8872	0.2161
Test	0.8811	0.5069	0.6160	0.5779	0.7872	0.3303	0.8744	0.2693
MNLR								
	73 parameters		54 parameters		37 parameters		34 parameters	
Train	0.9667	0.2642	0.9231	0.2738	0.9356	0.2361	0.9192	0.1760
Test	0.9538	0.2947	0.8667	0.3387	0.8082	0.3039	0.9102	0.2224
DT								
	42 splits		31 splits		12 splits		16 splits	
Train	0.9040	0.3781	0.8723	0.3490	0.8085	0.2617	0.9346	0.1682
Test	0.8900	0.3835	0.8107	0.4426	0.6309	0.3013	0.9254	0.1817
RF	94 trees		81 trees		70 trees		73 trees	
Train	0.9528	0.2548	0.9290	0.2476	0.9543	0.1630	0.9511	±0.1679
Test	0.9448	0.2716	0.8908	0.3210	0.8153	0.2403	0.9314	±0.1907
GBM								
	122 trees		113 trees		104 trees		98 trees	
Train	0.9562	0.2119	0.9061	0.3038	0.9137	0.2529	0.9205	0.1784
Test	0.9477	0.2315	0.8610	0.3736	0.7663	0.3205	0.8899	0.2221
k-NN								
	3 neighbors		3 neighbors		2 neighbors		2 neighbors	
Train	0.9611	0.2054	0.9693	0.1257	0.9750	0.1275	0.9550	0.1632
Test	0.9525	0.2364	0.9203	0.1731	0.9560	0.1784	0.9245	0.1878
SVR								
	C=4.84, γ=0.434		C=4.40, γ=0.495		C=4.36, γ=0.423		C=4.41, γ=0.495	
Train	0.9642	0.2282	0.9574	0.1862	0.9685	0.1369	0.9583	0.1156
Test	0.9601	0.2313	0.9275	0.2138	0.9556	0.1451	0.9377	0.1788
ANN								
	20–20 neurons		20–10 neurons		10–10 neurons		15–5 neurons	
Train	0.9850	0.1064	0.9725	0.1339	0.9877	0.0721	0.9977	0.0346
Test	0.9776	0.1307	0.9444	0.1799	0.9692	0.1166	0.9919	0.0631

To select the best model among the developed ML algorithms, a visualization of their prediction residual errors (RSE) can be displayed using a violin plot, as shown in Figure III.6. A fatter plot in the violin plot indicates that the distribution of the prediction residual errors is more spread out, which suggests higher variability and potentially larger errors in the model predictions. Conversely, a thinner plot indicates a more centralized distribution, which suggests lower variability and potentially more accurate predictions.

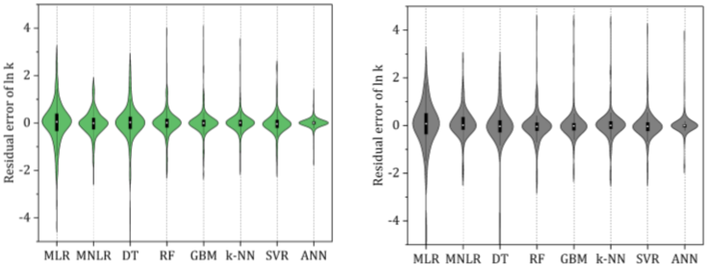

Electrical Conductivity

A) Train

B) Test

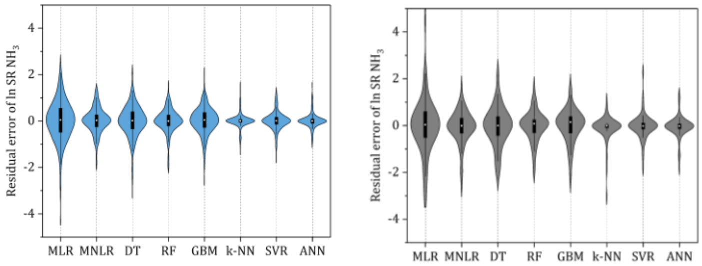

Ammonia Sensing Response

C) Train

D) Test

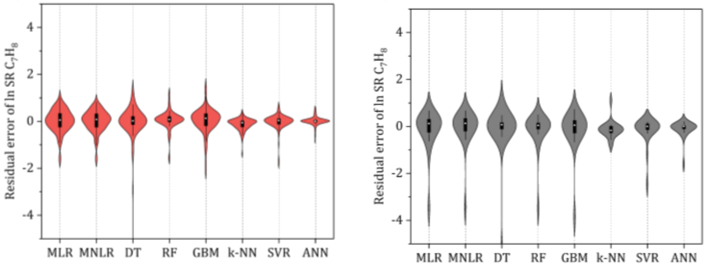

Toluene Sensing Response

E) Train

F) Test

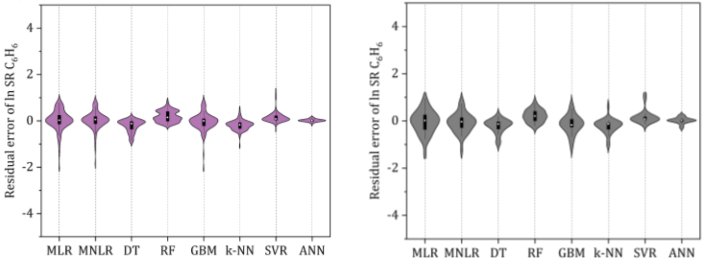

Benzene Sensing Response

G) Train

H) Test

Figure III.6. An in-depth assessment of ML model performance on electrical conductivity and sensing response properties for NH_3, C_7H_8, and C_6H_6 predicted by different ML algorithms. Violin plots visually depict error probability density. Green, blue, red, and purple segments show train set errors, while gray segments represent test set errors. Box plots within each violin indicate extrema (whisker edges), interquartile range (box boundaries), and median (white dot) of error.

By analyzing Table III.1 and Figure III.6, it can be observed that while MLR is one of the algorithms that were tested, its R^2 values for the test set analysis of electrical conductivity,

NH_3, C_7H_8, and C_6H_6 models are only 0.881, 0.616, 0.787, and 0.874, respectively. Furthermore, the corresponding ASD of the testing sets is between 0.2 and 0.5. Based on these results, it can be confirmed that linear models are unsuitable for accurate electrical conductivity and gas sensing response prediction, except for very narrow ranges of conditions where the problem might be nearly linear.

Furthermore, the nonlinear ML models examined demonstrated significantly superior effectiveness to the linear ones. Based on the evaluation of the different nonlinear models, it was found that the *k*-NN, SVR, and ANN models provided lower ASD values compared to the tree-based and other models. However, when considering the testing set standard deviations, the ANN model outperformed the k-NN or SVR models. This, along with the high R^2 value of over 0.98, and the excellent fit demonstrated by the ANN model makes it the best candidate for further hypertuning. Hence, the ANN algorithm was selected for further optimization.

III.3.4. ANN Hypertuning

III.4.4.1 Second hidden layer

In recognizing the pivotal role of hyperparameter optimization experiments for diverse ML algorithms, we deliberately directed our focus toward ANN optimization. This deliberate choice stems from the inherent suitability of ANN in modeling the intricate interactions within our datasets. The primary objective was to highlight the efficacy of ANN within the specific context of our study, rather than embarking on an exhaustive comparison across a diverse array of algorithms. Numerous studies have delved into the exploration of multiple hidden layers in ANNs, consistently demonstrating that the incorporation of such layers enhances prediction accuracy across a wide spectrum of properties (Kakkar et al. 2021; Matsukawa et al. 2021). This underscores the significance of considering the depth of ANN architectures to effectively capture and model complex relationships within datasets—a critical factor in achieving superior predictive performance. The capability of multiple hidden layers to capture intricate relationships between inputs and outputs is a key contributing factor to the improved predictive capabilities of ANNs.

Achieving the optimal network architecture requires meticulous tuning of the number of hidden layers and neurons in each layer to suit the specific problem under investigation precisely. To investigate the influence of the second hidden layer's neuron count on network performance, we conducted a seven-level factorial design for both the first and second layers, with the number of neurons varying from 5 to 25. This resulted in 25 different network configurations, with the 5-5 architecture being the simplest and the 25-25 architecture being the most intricate. Consequently, the results of this study have been meticulously showcased through the use of contour maps in Figure III.7, providing a comprehensive and intuitive representation of the findings. These maps illustrate the *RMSE* of the 25 ANN configurations, based on the training set, for predicting electrical conductivity and the three gas sensing response properties.

Figure III.7 (A) shows that the two-layer ANN configuration with 20–20 neurons best predicted electrical conductivity, with a lower *RMSE* in the test set, exhibiting a value of 0.3876 S cm^{-1}. Regarding the gas sensing response properties, Figure III.7 (B), (C), and (D) show that the ANN models with 20–10, 10–10, and 15–5 neurons, respectively, outperformed other models and had the lowest *RMSE* values of 0.3170, 0.1862, and 0.0642% for ammonia, toluene, and benzene gases, respectively. The presented findings underscore the promising potential of ANNs in effectively predicting the electrical conductivity and gas-sensing response properties of polyaniline-graphene nanocomposites with high accuracy.

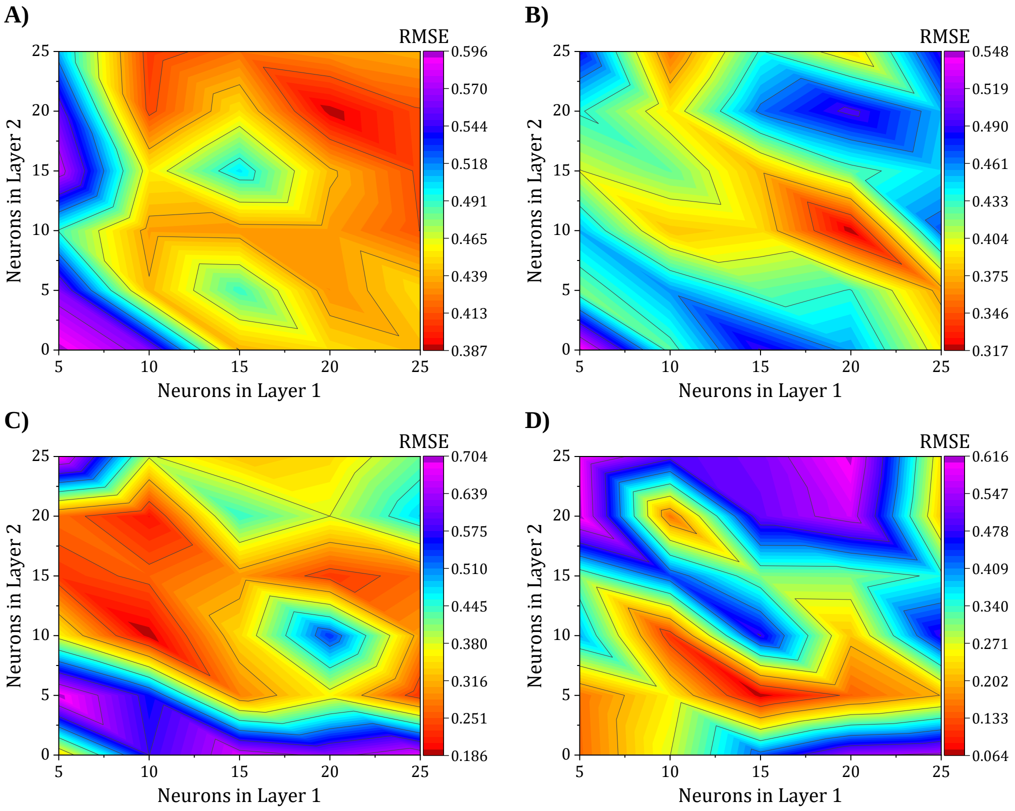

Figure III.7. 2D Surface plots representing the *RMSE* values for all the analyzed ANN architectures in the training set for the (A) Electrical conductivity, (B) NH_3, (C) C_7H_8, and (D) C_6H_6 Sensing response models.

The findings emphasize the importance of meticulous optimization of neuron count per layer and thoughtful selection of suitable activation functions when employing ANNs for predictive modeling. The configurations that demonstrated the highest accuracy and reliability were the 62–20–20–1, 63–20–10–1, 63–10–10–1, and 63–15–5–1 ANN configurations, which are illustrated clearly and concisely in Figure III.8. Hence, this methodology can significantly facilitate the rational design and exploration of innovative multifunctional nanocomposite systems. These systems can be precisely customized to fulfill specific requirements in diverse applications, including electronics, sensors, and energy storage.

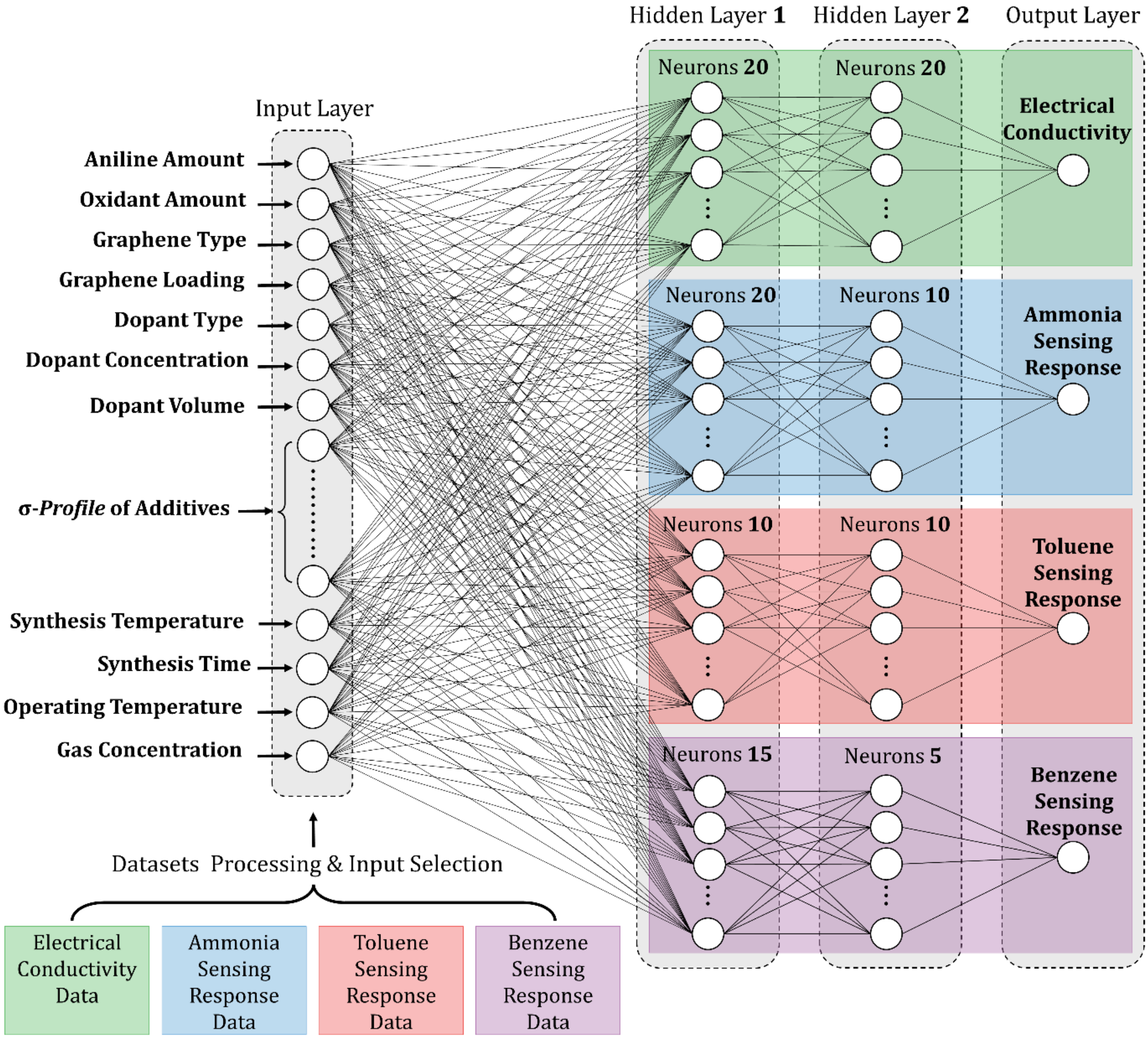

Figure III.8. Schematic representation of the hypertuned ANN architectures (62–20–20–1, 63–20–10–1, 63–10–10–1, and 63–15–5–1) for electrical conductivity and gas sensing response prediction models.

III.3.5. Model analysis

III.3.5.1. Error evaluation

Following the meticulous selection of the optimal ANN configurations, the models underwent a rigorous evaluation to assess their performance in predicting electrical conductivity properties and gas-sensing responses. As indicated in Table III.2, the ANN models exhibited exceptional accuracy in their predictions of the testing sets, with R^2 values of 0.978, 0.944, 0.969, and 0.992 for electrical conductivity, ammonia, toluene, and benzene gas sensing response, respectively. These high R^2 values are a testament to the effectiveness of the ANN models in capturing the complex relationships between the input features and target properties of polyaniline-graphene nanocomposites. However, this accuracy is critical for advancing our understanding of these materials. It has the prospect of influencing the design and implementation of novel nanocomposites for a broad spectrum of applications.

Table III.2. Statistical parameters for evaluating the effectiveness of modeled ANNs.

Parameter	**Electrical conductivity**	**Ammonia Sensing response**	**Toluene Sensing response**	**Benzene Sensing response**
Training				
R^2_{train}	0.985	0.973	0.988	0.998
RMSE	0.388	0.317	0.186	0.064
ASD	±0.1064	±0.1339	±0.0721	±0.035
MAE	0.1505	0.1893	0.1019	0.0489
Testing				
R^2_{test}	0.978	0.944	0.969	0.992
RMSE	0.479	0.459	0.358	0.127
ASD	±0.1307	±0.1799	±0.1166	±0.0631
MAE	0.1848	0.2544	0.1649	0.0892
Total				
R^2	0.984	0.967	0.983	0.996
RMSE	0.408	0.350	0.232	0.081
ASD	±0.1113	±0.1431	±0.0812	±0.0404
MAE	0.1574	0.2024	0.1148	0.0572

To validate the performance of the ANN models, scatter plots of the training and testing sets were meticulously examined, as depicted in Figure III.9. Each joint scheme consists of 5 plots, including a scatter plot and four marginal distribution plots. For instance, in Figure III.9 (A), the gray and green-colored scatter plots demonstrate the correlation between experimental and predicted electrical conductivity values in both the training and testing sets. Additionally, the four marginal distribution plots on the top and right-hand side offer a comprehensive insight into the distribution of experimental and predicted values in their respective sets. The findings reveal excellent agreement of the ANN models, with data points mostly aligning along the y = x diagonal, exhibiting minimal dispersion and scattering. For the electrical conductivity model, as shown in Figure III.9 (A), the ANN model achieved an *RMSE* of 0.338 and R^2 of 0.985 for the train set and 0.479 and 0.978 for the testing set, respectively.

Similarly, in the case of the ammonia gas model (Figure III.9 (B)), the ANN model achieved *RMSE* and R^2 values of 0.317 and 0.973 for the train set and 0.459 and 0.944 for the testing set, respectively. For the gas sensing response of toluene and benzene gases, as presented in Figure III.9 (C) and (D), the ANN models achieved higher accuracy, with all data points closely centered around the perfect fitting line and lower *RMSE* values of 0.193 and 0.064 and higher R^2 values, reaching 0.988 and 0.998 for the train sets and 0.350 and 0.127 and 0.961 and 0.992 for the testing sets, respectively. These findings demonstrate the ANN models' exceptional performance, which suggests the models' substantial accuracy and reliability in predicting the conductivity and gas sensing performances of all three gases, including ammonia, toluene, and benzene.

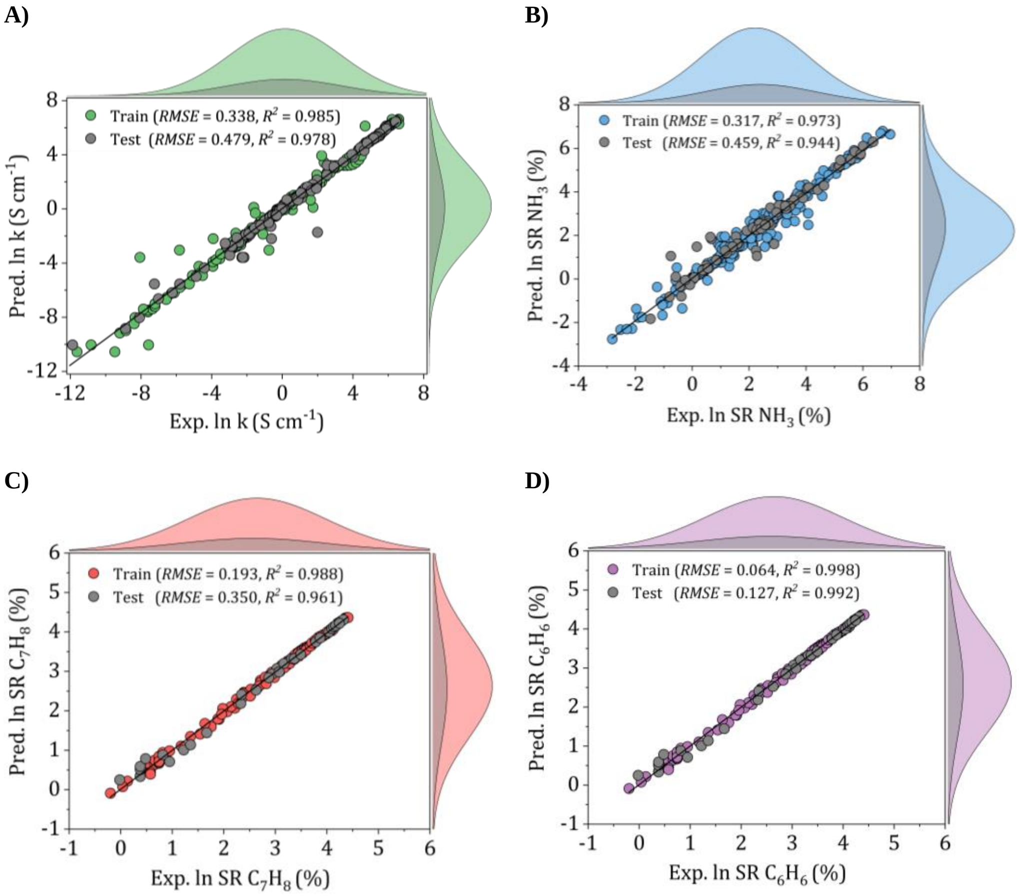

Figure III.9. Scatter plots for the (A) electrical conductivity, (B) NH_3, (C) C_7H_8, and (D) C_6H_6 sensing response properties, *RMSE*s, and R^2 are indicated in each plot. The heights of the marginal distributions represent the counts of data points.

III.3.5.2. Input attribution through SHAP analysis

In this study, the SHapley Additive exPlanations (SHAP) method was employed to interpret the output of the ANN, a critical step in validating model performance and unraveling the intricate processes underlying ANN predictions. As ANNs inherently possess a 'black box' nature due to their complex, non-linear interactions, understanding the individual inputs' influence becomes paramount for ensuring model transparency and interpretability. SHAP, rooted in game theory, serves as a robust framework for attributing importance scores to each input feature concerning specific predictions (Meyer et al. 2022; Mosca et al. 2022; Martin and Audus 2023).

To achieve this, we employed the 'Kernel Explainer' method from the SHAP toolkit in Python, designed to handle intricate and computationally intensive models like ANNs. This method utilizes a unique kernel function to compute SHAP values, allowing an in-depth analysis of the model by approximating the contribution of each input to the final prediction. The primary objective of integrating SHAP was to enhance the interpretability of the ANN, making its decision-making process more transparent and understandable. One significant advantage of SHAP is its ability to reflect the impact of each input in each sample, showcasing both positive and negative impacts. The SHAP values for each input were then summarized and ranked based on their mean values, as depicted in Figure III.10.

A) ln k

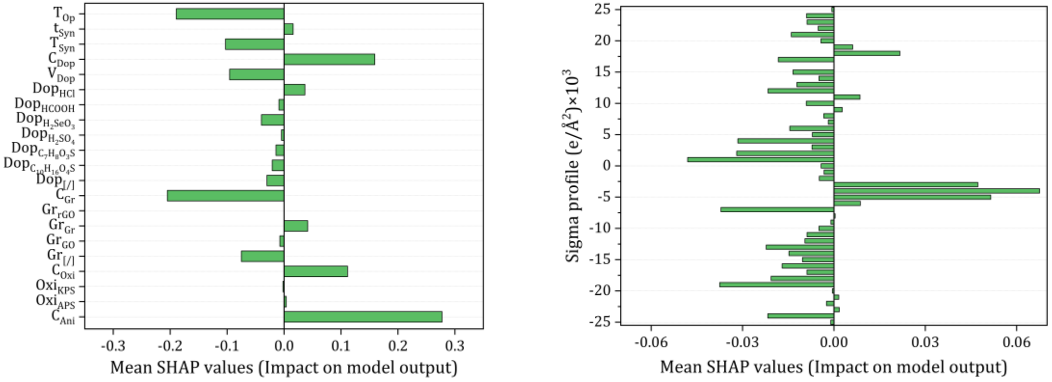

B) ln SR NH_3

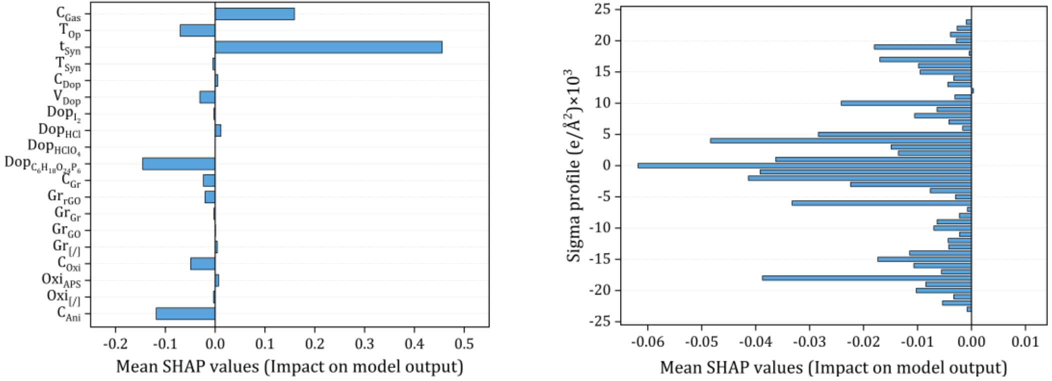

C) ln SR C_7H_8

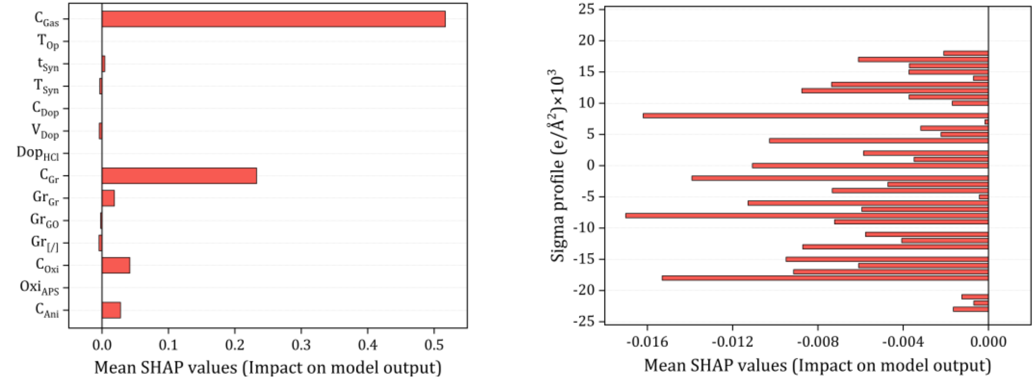

D) ln SR C_6H_6

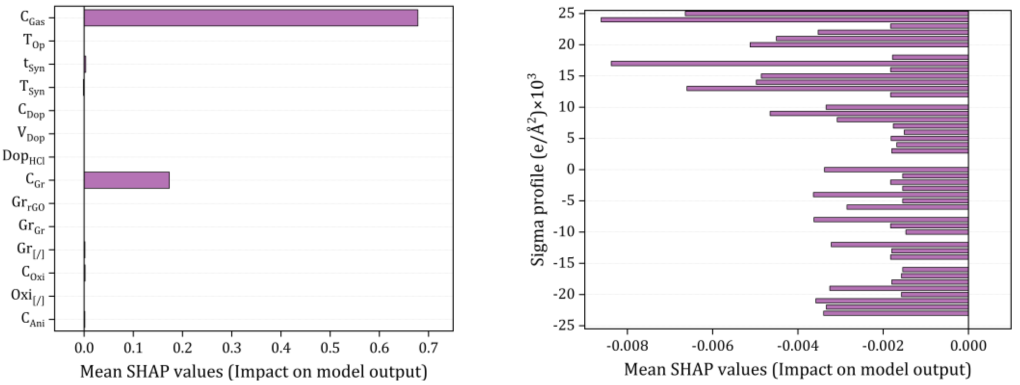

Figure III.10. SHAP input importance to accuracy (A) electrical conductivity, (B) NH_3, (C) C_7H_8, and (D) C_6H_6 Sensing response models.

The SHAP values for each input are summarized with a bar char are ranked according to the mean value of SHAP as shown in Figure III.10. Specifically, concerning electrical conductivity (Figure III.10 (A)), crucial inputs such as oxidant amount, aniline amount, doping agent concentration, and operating temperature emerged as the most critical contributors. Synthesis and operating conditions played pivotal roles in influencing electrical conductivity, with varying effects observed for different input parameters. For instance, aniline amount, oxidant amount, Gr filler, HCl doping agent, doping agent concentration, and synthesis time exhibited a positive impact on electrical conductivity, whereas systems without Gr filler ($Gr_{[/]}$) and doping agent, GO filler, dopant volume, and other doping agents had a negative effect. The influence of temperature was also explored, revealing that an increase in synthesis and operating temperature tended to decrease electrical conductivity, aligning with both input contribution analysis and existing literature reports (Neelgund and Oki 2011; Jelmy et al. 2013; Al-Hartomy et al. 2019; Nazari and Arefinia 2019; Reza et al. 2019; Rahman et al. 2021; Zheng et al. 2021). Turning to NH_3 gas sensing response ((Figure III.10 (C)), synthesis time and gas concentration emerged as pivotal inputs positively affecting the sensing response. Conversely, aniline and oxidant amount, camphorsulfonic acid ($C_{10}H_{16}O_4S$) doping agent, dopant volume, and operating temperature were identified as inputs exerting a negative impact on the sensing response. The role of doping agents in transforming PANI from an insulator to a conductor, particularly through the protonation/deprotonation process, was discussed, with the impact on NH_3 adsorption capacity well-established in the literature (Fratoddi et al. 2015b; Li et al. 2022a, 2023). For the prediction of C_7H_8 and C_6H_6 sensing response (Figure III.10 (C) and (D)), it was highlighted that a lack of experimental data regarding the influence of other input features necessitates further research. Comprehensive studies are required to unravel the behavior of PANI/Gr nanocomposites towards these gases and identify crucial input variables for optimization. Such endeavors hold the promise of advancing more effective and reliable gas sensors for detecting C_7H_8 and C_6H_6, crucial industrial pollutants.

Conclusively, as elucidated in earlier sections, the *σ-Profiles* of additives play a pivotal role alongside synthesis and operational conditions in predicting the electrical conductivity and gas sensing responses of PANI/Gr systems. These additives, including solvents, inorganic nanoparticles, or surfactants, exert a substantial influence on both the synthesis and performance of nanocomposites. Intriguingly, for electrical conductivity, nonpolar regions of additive molecules emerged as the most significant inputs, predominantly influencing conductivity positively. Conversely, HBA and HBD regions were identified as exerting a negative impact on conductivity. This observed phenomenon can be attributed to the solvent-like role of most additives, acting as washing agents to eliminate any unreacted aniline or other compounds from the system. In terms of gas sensing responses, all regions of additive molecules were noted to negatively affect the gas sensing response. In addition, the SHAP analysis also revealed that, even with 61 dimensions of *σ-Profiles*, other inputs played more crucial roles in the ANN predictions. This underscores the complexity of our system and emphasizes the need for a multifaceted approach. Consequently, the extensive SHAP analysis aligns with the input contribution analysis, shedding light not only on the intricate relationships between input variables and model predictions but also providing actionable insights for the future optimization of gas sensors. This contribution adds to the ongoing discourse, advancing our understanding and strategies for enhancing the performance of PANI/Gr nanocomposite systems.

III.3.5.3. Applicability domain results

AD is a crucial theory in ML for ensuring that models generate reliable predictions. It refers to the space in which a model can operate with dependable accuracy, and accurate identification is key to informed decision-making. A standardization theory is implemented to identify and eliminate outliers from the training set and define inputs outside the AD in the test set. This process is especially critical for ANNs, complex models dependent on the range of molecules analyzed. Quantitative evaluation of the AD provides valuable information on the range of molecules for which ANNs can generate accurate predictions. The range of molecules or systems for which ANNs can generate accurate predictions can be determined by precisely defining the AD. This knowledge is invaluable across various applications, from electrocapacitors and gas sensors to materials science and beyond, where ANNs are increasingly used to model complex systems and predict outcomes (Almi et al. 2020;

Oluwaseye et al. 2020; Lemaoui et al. 2021). In determining the AD of ANN models, various methods can be applied. However, among numerous approaches, the leverage method strategy is the most widely employed technique for identifying outliers in datasets (Tropsha et al. 2003; Mitra et al. 2010). The ADs of the proposed ANNs are visually depicted in Figure III.11 using William's graphs, where the AD boundaries are illustrated within the range of $0 < h_i < h^*$ (vertical dashed line) and $-3 < SDR < +3$ (filled-colored line) for all the models.

A) Electrical conductivity **B) Ammonia Sensing response**

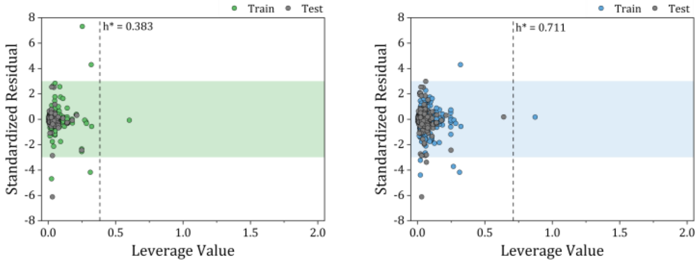

C) Toluene Sensing response **D) Benzene Sensing response**

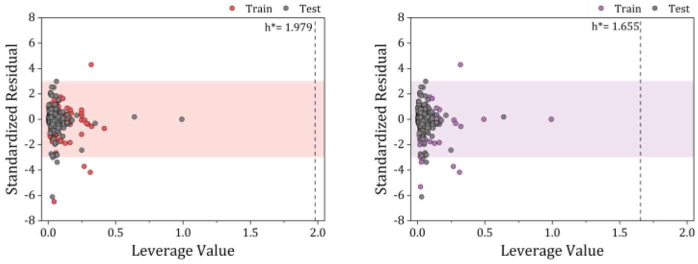

Figure III.11. Applicability Domain Assessment using William Plots: (A) Electrical Conductivity, (B) Ammonia Sensing Response, (C) Toluene Sensing Response, and (D) Benzene Sensing Response Models.

Figure III.11 (A), (B), (C), and (D) provide a helpful comparison of the applicability domains of various models, including the electrical conductivity model and models for sensing response to ammonia, toluene, and benzene. Upon examining these models, it becomes evident that the critical leverage of the toluene sensing model exceeds that of the other models, with the benzene sensing model showing the second-highest critical leverage value ($h_{C_7H_8}{}^{*} = 1.6552 > h_{C_6H_6}{}^{*} = 1.9794 > h_{NH_3}{}^{*} = 0.7111 > h_k{}^{*} = 0.3834$). However, despite the differences in critical leverage among the models, the analysis reveals that the majority of data points (over 97%) conform within the AD boundaries, signifying the dataset's limited inclusion of outliers based on the leverage method (*i.e.*, $h_i > h^*$), this metric holds significant importance in evaluating the data quality employed to train ML models. As presented in Table III.3, the electrical conductivity model has a lower percentage of structural outliers (0.16%) compared to the ammonia sensing model (0.30%). These findings suggest that the electrical conductivity model may be more reliable in its predictions than the ammonia sensing model. Furthermore, it is essential to highlight that both the toluene and benzene sensing models exhibited no structural outliers, as their leverages consistently remained below the critical boundary of $h_i < h^*$. This observation is consistent with the expected behavior of well-trained ANN models. It supports their reliability for predicting the toluene and benzene sensing properties of polyaniline/graphene systems within their AD.

In addition to the structural outliers discussed earlier, response outliers were also identified in the models. Specifically, specific data points at exception compositions and conditions were identified as outliers based on their SDR values exceeding the acceptable ± 3 SDR boundary. As a result, the coverage of the models within their AD was reduced to 99.03%, 98.52%, 98.36%, and 97.95% for the electrical conductivity, ammonia, toluene, and benzene sensing response models, respectively. Outliers can substantially influence the accuracy of model predictions, emphasizing the criticality of meticulous identification and evaluation of the AD of models to ensure dependable and precise predictions. It is worth emphasizing that the absence of data points in the double outlier region (*i.e.*, $h_i > h^*$ and $SDR_i > \pm 3$) as illustrated in Figure III.11. This observation underscores the robustness of the proposed ANN models, indicating minimal impact from outliers on their performance.

In summary, accounting and identifying structural and response outliers are crucial for improving the reliability and accuracy of ANN models in chemical engineering applications. This study underscores the significance of the AD method as an invaluable instrument for assessing data quality during model training, enabling the identification and evaluation of outliers that could potentially impact model predictions. The concurrent use of k-fold validation and AD analysis provides a robust framework for the holistic evaluation of our models. It is important to note that the AD analysis, in particular, considers the distribution of training data and helps identify how different a data point is from the majority of the points. This method has been chosen deliberately to enhance the understanding of model performance within specific boundaries. Consequently, the findings from this study indicate that the predictions of new polyaniline/graphene systems, falling within the same domain of applicability, can be deemed reliable for preliminary polymer nanocomposite investigations, even without experimental data. This highlights the significance of dependable and precise predictions for advancing new nanocomposites, mainly when the properties of the materials are challenging to measure experimentally.

Table III.3. Applicability domain parameters for the electrical conductivity, ammonia, toluene, and benzene sensing response models.

Parameter	**Electrical conductivity**	**Ammonia Sensing response**	**Toluene Sensing response**	**Benzene Sensing response**
h^*	0.3834	0.7111	1.9794	1.6552
Training				
Structural outliers	0.16%	0.30%	0.0%	0.0%
Response outliers	0.65%	0.89%	0.82%	2.05%
$AD_{coverage}$	99.19%	98.82%	99.18%	97.95%
Testing				
Structural outliers	0.81%	0.30%	0.0%	0.0%
Response outliers	0.81%	1.47%	4.0%	0.0%
$AD_{coverage}$	99.19%	97.06%	96%	100%
Total				
Structural outliers	0.16%	0.30%	0.0%	0.0%
Response outliers	0.81%	1.18%	1.64%	2.05%
$AD_{coverage}$	99.03%	98.52%	98.36%	97.95%

III.3.5.4. Systematic predictions and comparative analysis

Systematic predictions of the effect of aniline concentration, dopant type and its concentration, graphene loading on conductivity, and gas type and concentration, along with the influence of graphene loading and operating temperature on gas sensing responses using the developed ANNs were evaluated and compared with the experimental data as shown in Figure III.12. The results showcase the multifaceted behavior of PANI/Gr in varying experimental conditions, providing insights into the potential applications of these composites in sensor technology. The conductivity exhibits a non-linear response to the concentration of aniline, which suggests a threshold behavior where the conductivity stabilizes beyond a certain concentration (Cao and Wang 2018). While the ANN models capture this phenomenon to some extent, there is a noticeable divergence from experimental data. This discrepancy suggests the intricate nature of molecular-level interactions that might not be entirely accounted for by the ANN. Molecularly, this can be associated with increased π-π stacking between the aniline-derived PANI chains and the graphene sheets, leading to improved charge transport pathways (Imran et al. 2014). When considering dopant effects, the nature of the dopant and its concentration have pronounced effects on the conductivity of PANI (Alesary et al. 2018). The protonation of the nitrogen atoms in the PANI backbone by acid dopants like HCl and H_2SeO_3 enhances the delocalization of electrons, which is crucial for conductivity (Tung et al. 2011). The temperature dependence of conductivity is consistent with a semiconducting behavior where thermal energy aids in the hopping of charge carriers, enhancing conductivity (Badi et al. 2016; Gaikwad et al. 2017; Al-Hartomy et al. 2019).

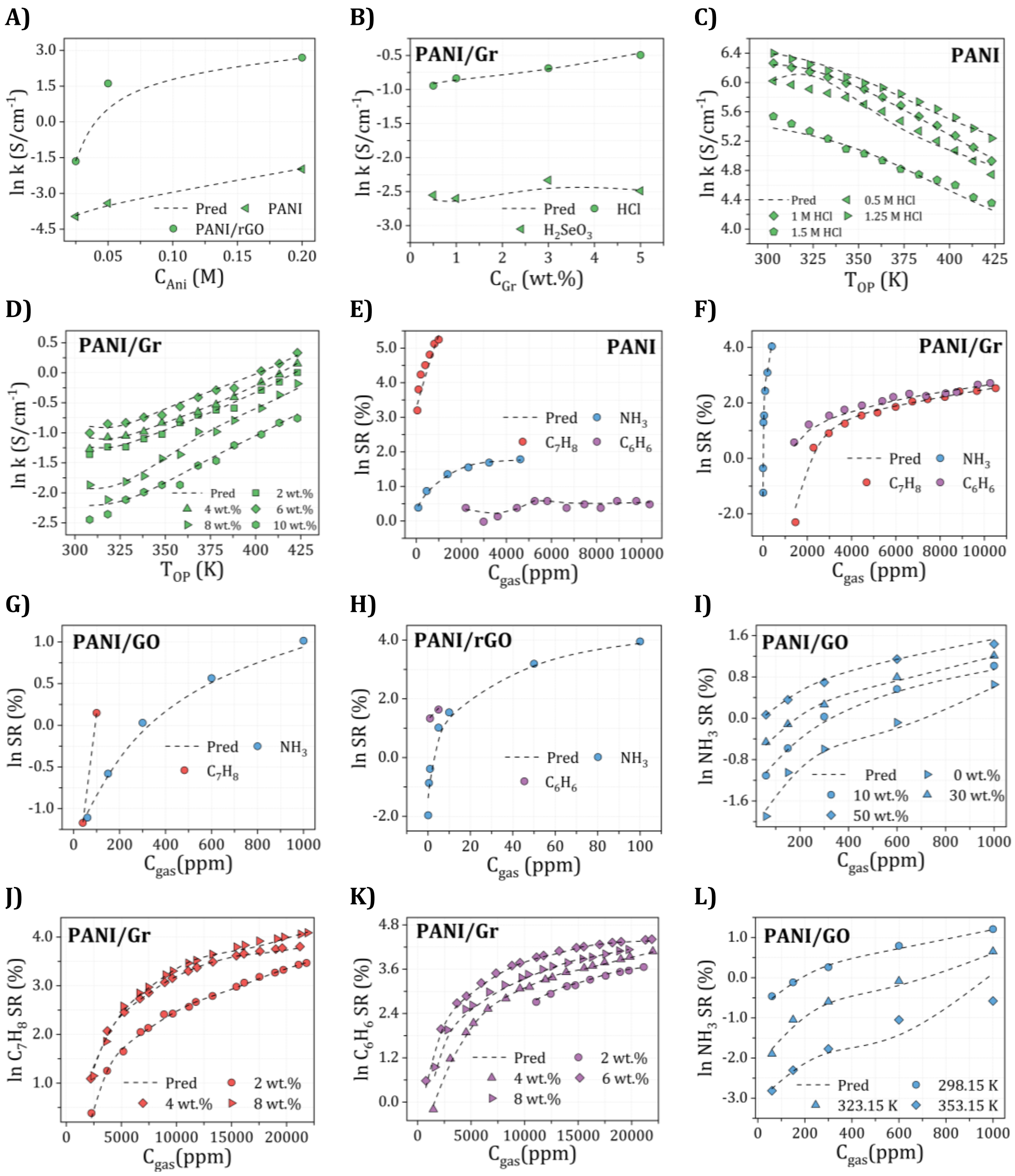

Figure III.12. Comparative analysis of experimental (symbols) and ANN-predicted (dashed lines) electrical conductivity and gas sensing responses: effect of aniline concentration (A), dopant type and its concentration (B and C), graphene loading and operating temperature (D) on electrical conductivity, and gas type and concentration (E–H), along with the influence of graphene loading (I–K) and operating temperature on gas sensing response (L).

Thus, the ANN predictions closely follow the experimental data, suggesting that the temperature effect is well-characterized by the network parameters, capturing the thermally activated processes within the material. In terms of gas sensing, the nanocomposites exhibit distinct responses to NH_3, C_7H_8 and C_6H_6. The molecular interactions between these gases and the PANI/Gr nanocomposite are crucial for the sensing mechanism (Liu et al. 2022). NH_3, being a polar molecule with a lone pair of electrons, can interact with the π-electron rich regions of the composites, likely forming charge transfer complexes. This interaction alters the distribution of charge carriers in the PANI chains, leading to a measurable change in conductivity which is utilized for sensing (Huang et al. 2013; Ansari et al. 2014b). C_7H_8 and C_6H_6, being aromatic compounds, may also interact with the nanocomposite through π-π stacking interactions. The presence of the methyl group in toluene introduces steric hindrance and a slight electron-donating effect, potentially altering its interaction with the nanocomposite compared to C_6H_6. The differential sensing response between C_6H_6 or C_7H_8 can be attributed to the size and electron density of these molecules, which influences their adsorption onto the system surface and subsequent interaction with the conductive network (Murugan et al. 2014; Xu et al. 2014; Subramanian et al. 2018). The enhancement in gas response with increasing graphene content can be rationalized by the expanded surface area provided by graphene, which facilitates greater adsorption of gas molecules. Additionally, graphene's high electron mobility may contribute to more efficient charge transfer upon interaction with gas molecules, leading to a stronger sensing response. Meanwhile, the response to gases such as NH_3, C_7H_8, and C_6H_6 indicates that the nanocomposites are sensitive to changes in gas concentration, with the response magnitude varying according to the type of gas (Tanguy et al. 2018). The response to NH_3 is especially significant, which is a desirable trait for sensors targeting this gas. However, the ANN predictions are less accurate at higher concentrations, potentially due to saturation effects that are not fully represented in the mode.

Consequently, the experimental findings enriched by molecular insights into the nanocomposite's interaction with aniline, dopants, temperature, and gases, demonstrate the complexity and potential of PANI/Gr as a material for gas sensors. Although ANNs prove valuable in predicting overarching trends and behaviors, the existing disparities between experimental and predicted data emphasize the imperative for further model refinement. Supplementary approaches such as molecular dynamics simulations or quantum mechanical modeling could complement ANN predictions, offering a more thorough understanding of the intricate interactions involved. The imperative for further refinement is driven by the complex and dynamic nature of nanocomposites' responses, necessitating a nuanced comprehension. These findings not only yield insights into the intricate behavior of PANI/Gr nanocomposites but also lay the foundation for optimizing these materials for specific applications, particularly in the domain of sensitive and selective gas detection.

III.4. Conclusions

In conclusion, this study comprehensively explores machine learning models for predicting the properties of polyaniline/graphene (PANI/Gr) nanocomposites, leveraging a rich dataset from numerous sources. The ANN models emerge as highly accurate tools for forecasting electrical conductivity and gas sensing responses, with meticulous attention given to identifying and handling outliers. The robustness of these models, particularly in the face of structural and response outliers, underscores their reliability.

The input contribution analysis provides crucial insights into the key parameters shaping the performance of PANI/Gr nanocomposites, highlighting the significance of oxidant, aniline, doping agent concentration, and operating temperature. Complementing this, the SHAP analysis reveals intricate relationships among input variables and model predictions, offering valuable insights for gas sensor optimization and contributing to the ongoing discourse on enhancing PANI/Gr nanocomposite systems' performance. Furthermore, the study underscores the influential role of molecular inputs, particularly the *σ-Profiles* of additives, in predicting material properties.

Applicability domain (AD) analysis is a critical facet of model evaluation, revealing high coverage percentages and emphasizing the models' dependability within specific parameter ranges. The significance of understanding and managing outliers is highlighted, as they can significantly impact model predictions. Notably, the absence of data points in the double outlier region underscores the resilience of the proposed ANN models.

The implications of this research extend to the practical development of high-performance PANI/Gr nanocomposites, offering valuable contributions to fields such as supercapacitors, gas sensors, and energy storage devices. The call for further investigations into the nuanced impacts of molecular inputs on material performance reflects the ongoing pursuit of precision in nanocomposite design. Overall, this study significantly advances our understanding of machine learning applications in chemical engineering, providing a foundation for informed decision-making and reliable predictions in developing novel materials.

Chapter IV

Chapter IV: Comprehensive investigation of multifunctional polyaniline/reduced graphene oxide nanocomposites synthesized from deep eutectic solvents: Experimental, RSM, ANN and computational studies

This chapter reports a comprehensive investigation into the synthesis, modeling, and characterization of multifunctional polyaniline/reduced graphene oxide (PANI/rGO) nanocomposites, with a focus on their synthesis using deep eutectic solvents (DES). Leveraging an in-situ chemical polymerization method, PANI/rGO nanocomposites were successfully synthesized, introducing a novel approach employing DES as the electrolyte. The study utilized Response Surface Methodology (RSM), Artificial Neural Networks (ANN), and molecular simulation techniques to model, optimize, and characterize the nanocomposites comprehensively. RSM analysis disclosed the impact of APS/ANI molar ratio, rGO loading, and polymerization time on electrical conductivity, with optimal conditions identified: APS/ANI molar ratio of 0.75, 3 wt.% rGO loading, and a 6-hour polymerization time, yielding a high electrical conductivity of 4.975 × 10^{-3} S cm^{-1}. Integration of ANN techniques enhanced predictive accuracy, reaching an electrical conductivity of 4.988 × 10^{-3} S cm^{-1}, surpassing RSM. Characterization techniques including UV-vis, PL, Raman, FTIR, and XRD highlighted structural changes, while XPS analysis revealed intensified CN peaks in PANI/rGO, indicating a denser nanocomposite coating. Electrochemical studies showcased superior capacitance at 145.79 F g^{-1}, surpassing individual components, and TGA analysis unraveled enhanced thermal stability. Molecular-level insights provided a nuanced understanding of the PANI-rGO system through FMO, COSMO-RS, NCI, and QTAIM analyses. The study not only presents an innovative synthesis method but also positions PANI/rGO nanocomposites as promising materials for supercapacitors and gas sensors, offering potential for advancements in green chemistry and eco-friendly innovations.

IV.1. Introduction

The synthesis of PANI/rGO nanocomposites conventionally relies on *in-situ* chemical oxidative polymerization, a preferred method for its efficiency (Gospodinova and Terlemezyan 1998; Ćirić-Marjanović 2013). However, the quest for elevated electrical conductivity demands a meticulous manipulation of various parameters (Boublia et al. 2023a, 2024). These encompass critical factors such as GO filler loading, the oxidant-to-monomer ratio, the nature and concentration of dopant acids, reaction temperature, monomer purity, and polymerization time (Ameen et al. 2010; Pang et al. 2021a). The traditional approach to optimization, involving the alteration of one parameter at a time, is time-intensive and resource-draining. Conducting numerous experiments, each adjusting a single factor while keeping others constant, consumes considerable time and energy resources. To overcome these limitations, a more efficient approach involves the collective optimization of all pertinent parameters. This is accomplished through an empirical design based on statistical methodologies, illustrated by the implementation of Response Surface Methodology (RSM) (Sharifi et al. 2018; Boublia et al. 2022a). RSM, combining mathematical and statistical methods, plays a significant role in process modeling and optimization studies (Silva et al. 2018). It discerns the impact of independent variables, either in isolation or combination, on the synthesis processes. An inherent strength of RSM lies in its capacity to reduce the number of experiments needed for an in-depth statistical analysis, especially in scenarios involving numerous factors. This modeling approach utilizes polynomials to locally approximate, resulting in the derivation of a mathematical expression that succinctly expresses the complex interplay between the response and the independent variables (Boublia et al. 2022a).

A thorough literature review was conducted to pinpoint the key factors influencing the electrical conductivity of PANI/rGO. The investigation revealed that the electrical conductivity of PANI experiences an increase with a higher oxidant molar ratio. Such enhancement in conductivity is attributed to a rise in the density of cation radicals and the extension of PANI chain length. These factors facilitate an enhanced interchain transfer, thereby increasing the carrier mobility (Zheng et al. 2021). Nevertheless, concentrations of oxidant exceeding 0.5 M resulted in phenazine production, causing a reduction in electrical conductivity (Jelmy et al. 2013; Reza et al. 2019). Moreover, studies demonstrated an initial increase in PANI conductivity with an aniline amount of up to 0.15 M, followed by a decrease with further additions of aniline (Nazari and Arefinia 2019). The investigation of the oxidant-to-aniline ratio indicated that an optimal PANI conductivity and yield were achieved with a ratio close to 1. Higher ratios, however, led to over-oxidation, resulting in a decrease in both conductivity and yield (Adams et al. 1996). Diverse dopants were explored for their impact on electrical conductivity, showing a positive correlation between dopant concentration and PANI's conductivity (Rahman et al. 2021). Although, an increase in the dopant/aniline ratio resulted in a notable decline in PANI conductivity, emphasizing the influence of intramolecular mobility of charged species along the chain on electrical conductivity, surpassing the impact of intermolecular hopping within crystalline regions (Cao et al. 1989; Sengupta and Adhikari 2007; Sapurina and Stejskal 2008). At extremely elevated dopant concentrations, a substantial decline in conductivity was accomplished through concurrent reductions in doping levels and crystallinity (Neelgund and Oki 2011). Evaluation of PANI/rGO nanocomposites across different temperatures and rGO loadings demonstrated enhanced conductivity as temperature rises, linked to thermally-assisted charge carrier hopping in disordered materials. The integration of rGO into the PANI matrix notably enhanced the conductivity of the nanocomposite. This improvement can be attributed to synergistic interactions between the PANI and rGO phases, involving charge transfer among delocalized *P*-orbitals (Sreeja et al. 2019). the duration and temperature of the synthesis process played a crucial role in determining the size and structure of PANI/rGO nanocomposites, directly influencing their electrical conductivity. Extended synthesis times and lower temperatures yielded larger and well-defined PANI/rGO systems with enhanced electrical conductivity. Previous studies emphasized that the yield and electrical conductivity remain unaffected by the polymerization temperature when maintained below 0°C. Conversely, elevated temperatures were found to induce more defects, resulting in diminished conductivity (Cao et al. 1989). Consequently, a polymerization temperature of approximately 0°C was considered optimal for the synthesis of PANI/rGO.

In light of the reviewed literature, despite numerous studies on PANI synthesis, a specific optimization of PANI/rGO conductivity using RSM techniques, particularly in scenarios involving the nanoscale, taking into account the interactions and synthesis factors at play, remains unexplored. This study addresses this gap by identifying key factors influencing PANI electrical conductivity, including rGO loading, oxidant-to-monomer molar ratio, and polymerization time. Notably, PANI/rGO was synthesized *via in-situ* polymerization in a choline chloride/triethylene glycol-based deep eutectic solvent (DES) acting as an electrolyte. Employing BBD-RSM and ANN methodologies, we systematically assessed various nanocomposite synthesis conditions, analyzing the intricate relationship between electrical conductivity and these factors. Beyond optimization, we conducted a comprehensive analysis of the synthesized nanocomposites using Ultraviolet–visible Spectroscopy (UV-Vis), photoluminescence Spectroscopy (PL), Raman Spectroscopy, Fourier-transform infrared Spectroscopy (FTIR), X-ray diffraction (XRD), X-ray Photoelectron Spectroscopy (XPS), Cyclic voltammetry (CV), and thermogravimetric (TGA) analyses, exploring their structural, optical, and electrochemical properties. Significantly, our tailored computational models for PANI and rGO align with experimental data, enhancing the credibility of our findings. Theoretical analyses, including Frontier Molecular Orbital (FMO), COnductor like Screening MOdel for Real Solvents (COSMO-RS), Non-Covalent Interaction (NCI) based on the Reduced Density Gradient (RDG), and Quantum Theory of Atoms in Molecules (QTAIM) deepen our understanding of bonding interactions, providing insights for potential applications in nanocomposite technology. This combined computational and experimental methodology strives to provide an in-depth understanding of PANI/rGO nanocomposites for the creation of efficient, versatile, and eco-friendly materials.

IV.2. Experimental section

IV.2.1. Materials

Choline chloride (ChCl) ($[(CH_3)_3NCH_2CH_2OH]^+Cl^-$, Sigma-Aldrich, 99%), tetraethylene glycol (TEG) ($HO(CH_2CH_2O)_3CH_2CH_2OH$, Aldrich, 99%), Natural graphite powder was consummated by using graphite as a powder with particle size of the order of 10 µm. Sulfuric acid (H_2SO_4, Aldrich, 98%), sodium nitrate ($NaNO_3$, Aldrich, 99%), hydrogen peroxide (H_2O_2, Aldrich, 30%), hydrazine monohydrate (N_2H_4, Sigma-Aldrich, > 99%), aniline monomer (ANI)($C_6H_5NH_2$, Sigma-Aldrich, $\geq$ 99.5%), ammonium persulfate (APS) ($(NH_4)_2S_2O_8$, Sigma-Aldrich, 98%) was utilized as an oxidant and hydrochloric acid (HCl, Fisher chemical, 37%). All materials were employed in their as-received state, and aniline was saved under refrigeration at 4°C when not in use.

IV.2.2. Sample preparation

Three different DES formulations were prepared by combining ChCl with TEG in varying molar ratios (1:1, 1:2, and 1:3). The mixtures were heated at 60°C with continuous stirring. After 30 minutes, the resulting DESs became a homogeneous colorless liquid. Figure V.1 provides a schematic representation of the DES preparation process. Only the DES with a 1:2 molar ratio exhibited stability and was selected for further experimentation. The preparation of GO followed our prior work (Guezzout et al. 2017, 2023) and for the reduction of GO to rGO, a hydrazine chemical reduction method was then employed.

The synthesis of PANI/rGO nanocomposites was carried out according to previously established procedures (Lamiel et al. 2015; Usman et al. 2019). Initially, a dispersion of rGO was prepared by weighing the appropriate amount, adding distilled water, and subjecting it to ultrasonication for 1 hour. Simultaneously, an APS solution was prepared by dissolving it in fresh 1 M HCl/DES solution. The synthesis of PANI/rGO commenced with the dissolution of pure aniline and rGO in a 1 M HCl/DES solution, leading to the formation of an aniline-rGO suspension. This suspension was then subjected to 20 minutes of ultrasonication and placed in an iced bath, maintaining a temperature range of 05°C while being mechanically stirred (as depicted in Figure IV.1). The oxidant (APS solution) was carefully added drop by drop to the aniline-rGO suspension, following a two-step process to prevent excessive temperature elevation. The ratio of oxidant to aniline was carefully controlled throughout this synthesis. Approximately 20−30 minutes after the initial addition of the oxidant, the solution's color underwent a transition from blackish-blue to progressively greener, reflecting the progression of the reaction. The resultant nanocomposites and pure PANI were separated by centrifugation and subjected to thorough washing with 1 M HCl, fresh distilled water, and acetone. The compounds were subsequently dried in an oven at 50°C for a period of 48 hours. Details regarding the polymerization time, the aniline to rGO ratio, and the aniline to APS ratio are provided in the experimental design strategy outlined below.

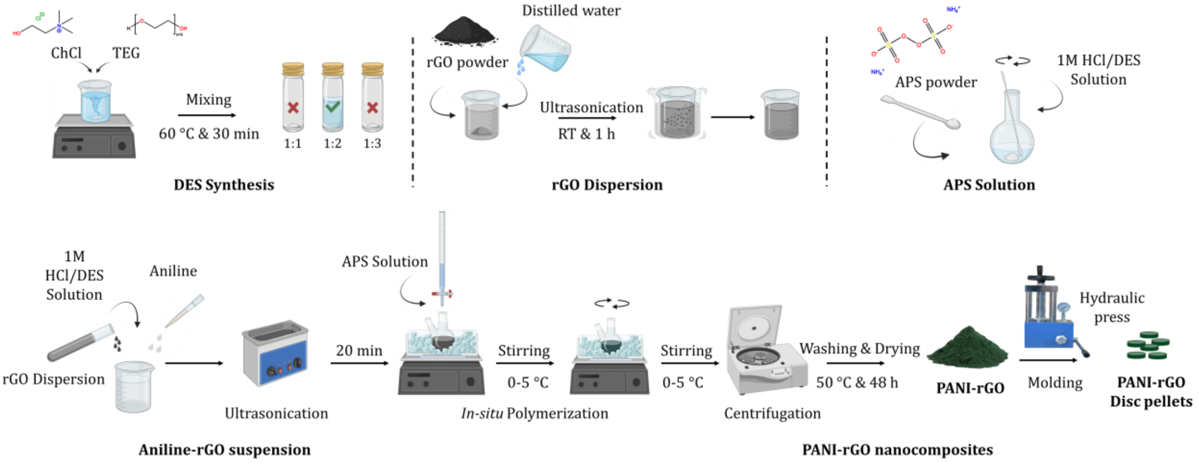

Figure IV.1. Flowchart illustrating of the experimental methodology used in this work.

IV.2.3. Experimental design by response surface methodology

Data analysis investigation is a valuable tool for uncovering concealed insights and constructing predictive models. The RSM, initially introduced by Box and Wilson (Silva et al. 2018), stands out as a robust approach for scrutinizing interactive influences within a system and for optimizing its performance. RSM typically employs specific experimental designs, with the most commonly employed ones being the Box-Behnken Design (BBD) and the Central Composite Design (CCD) (Silva et al. 2018). In the context of this study, we employed the BBD design to explore the impact of variables such as molar ratio of APS/ANI, rGO loading, and polymerization time on the electrical conductivity of PANI/rGO-based nanocomposites. Within the BBD framework, each factor is systematically assigned one of three equidistant values. The experimental conditions are represented by points positioned at the midpoint of the edges in the experimental space, which can be visualized as a cube, as well as at the center (as depicted in Figure IV.2). The total number of experiments, N, the variables under consideration, k, and the central points, C_0, can be calculated using the following Eq (21):

$$N = 2k\,(k-1) + C_0 \qquad \text{Eq. (21)}$$

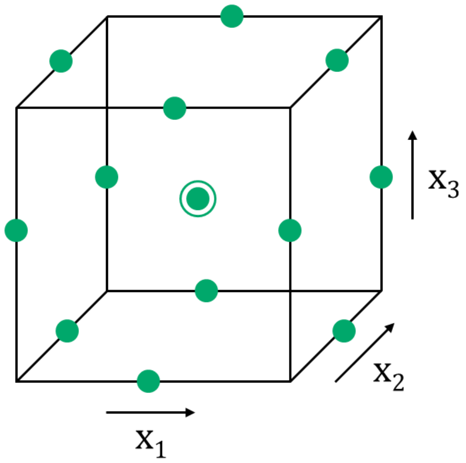

Figure IV.2. Configuration of the Box-Behnken design for a three-factor system.

Table IV.1 provides an overview of the experimental design using the BBD model. This design incorporates three factors, each with three levels, and we have included both actual and coded values for better understanding. The three optimized independent variables are APS/ANI ratio (X_1), rGO loading (X_2), and polymerization time (X_3). For each independent variable, we employed a horizontal encoding scheme, which assigns three values: 1, 0, and 1. This encoding facilitates the systematic exploration of the experimental space. The actual ranges for these variables are X_1: 0.25–0.75; X_2: 1–5 *wt.*%; X_3: 2–6 h, respectively.

Table IV.1. Factors Investigated in the Box-Behnken Design Experiment.

Factors	**Coded**	**Levels**		
		-1	0	1
Molar ratio of APS/ANI	X_1	0.25	0.5	0.75
rGO loading (*wt.*%)	X_2	1	3	5
Time (h)	X_3	2	4	6

The relationship and interactions between the independent variables and the response factors were thoroughly investigated using a second-order polynomial equation (Eq (2)):

$$y = \beta_0 + \sum_{j=1}^{k} \beta_j X_j + \sum_{j=1}^{k} \beta_{jj} X_j^2 + \sum_{i<j}^{k} \beta_{ij} X_i X_j \qquad \text{Eq. (22)}$$

Here, y represents the predicted value of the response, β_0 is the offset term, *j*, *ij*, and *jj* correspond to the linear coefficients, the cross-product coefficients, and the quadratic coefficients, respectively. X_i and X_i are the independent factors. To carry out this analysis, we employed JMP SAS Pro® 16 software. This robust software facilitated the evaluation of experimental data and the execution of analysis of variance (ANOVA) to ascertain the model's fitting accuracy. This statistical analysis is essential for understanding the impact and significance of the independent variables on our response factors.

IV.2.4. Artificial neural network

In the present study, we harnessed the power of Artificial Neural Networks (ANNs) to predict the intricate, non-linear relationship between our input parameters (X_1, X_2, and X_3) and the response variable (y), utilizing an experimental dataset derived from the BBD design. Our network architecture was meticulously constructed using JMP SAS Pro® 16 software (SAS Institute, Cary, NC), ensuring the efficacy of the feed-forward ANN. The configuration of the neural network holds a pivotal role in shaping the ANN model's capacity for generalization. It essentially comprises three key layers: input, hidden, and output, with each layer accommodating an array of neurons. The quantity of neurons in the input and output layers directly corresponds to the count of input and output variables. Consequently, we evaluated eight different ANN architectures, each equipped with a single hidden layer containing varying neuron counts ranging from 3 to 24. To ensure the model's robustness and reliability, we divided our datasets into training and testing subsets, following an 80%:20% ratio. This strategy allowed us to systematically explore various ANN architectures, ultimately selecting the optimal setup based on superior performance with the testing dataset. The equations within the ANN model incorporate various parameters that elucidate the neural network's behavior. These parameters encompass the weights (W_m) connecting neurons, the inputs (x) to specific neurons (n), considerations of the hidden layer (l), and the biases (b) associated with each neuron. Additionally, we incorporated the hyperbolic tangent ($tanh$) function into the expressions, effectively confining the output of each neuron to the variety of [1, 1]. This interval signifies the extent of activation or deactivation, ensuring meticulous control over the network's dynamics and results. The mathematical representation of the output of neuron (j) arises from the synergistic interplay of these parameters:

$$H_{n,l} = tanh\left(\sum_{m=1} (W_{m,n,l})(X_{n,l})\, b_{n,l}\right) \qquad \text{Eq. (23)}$$

To assess the effectiveness of both ANN and RSM models, performance metrics including root mean square error ($RMSE$), coefficient of determination (R^2), average absolute relative deviation ($AARD$), and mean absolute error (MAE) were applied where their expressions are shown in Eqs. (24−27), respectively. Where σ_{exp}, σ_{pred}, and $\bar{\sigma}$ indicate the experimental, predicted, and average values, while p denotes the total count of experimental data points.

$$R^2 = 1 - \frac{\sum_1^p (\sigma_{exp} - \sigma_{pred})^2}{\sum_1^p (\sigma_{exp} - \bar{\sigma})^2} \qquad \text{Eq. (24)}$$

$$RMSE = \sqrt{\frac{\sum_1^p (\sigma_{exp} - \sigma_{pred})^2}{p}} \qquad \text{Eq. (25)}$$

$$AARD\ (\%) = \frac{100}{p} \times \sum_1^p \frac{|(\sigma_{pred} - \sigma_{exp})|}{\sigma_{exp}} \qquad \text{Eq. (26)}$$

$$MAE = \frac{1}{p} \sum_1^p |\sigma_{pred} - \sigma_{exp}| \qquad \text{Eq. (27)}$$

IV.2.5. Characterization and morphology

The Ultraviolet–visible (UV-Vis) were recorded with V-650 JASCO spectrophotometer equipped with an integrating sphere. The photoluminescence (PL) investigation was carried out on the spectrofluorometer HORIBA FL3-DFX-iHR320 model. Raman was recorded with an invia microscope spectrometer (RENISHAW). Fourier-transform infrared (FTIR) spectroscopy was analyzed by the V-650 JASCO spectrophotometer equipped with an integrating sphere. X-ray diffraction (XRD) analysis was performed with Cu Ka X-ray sources on a D/Max-2400 powder diffractometer (Japanese Physical Company). The surface analysis of the synthesized materials was examined through means of an X-ray Photoelectron Spectroscopy (XPS) (Escalab THERMO SCIENTIFIC).

Cyclic voltammetry (CV) experiments were performed utilizing a Volta Lab PGZ 301 apparatus with Volta Master 40 software, employing a standard three-electrode configuration. The setup comprised a counter electrode made of platinum, a reference electrode of Ag/AgCl, and a working electrode made of platinum with modifications. A solution of 0.1 M lithium perchlorate ($LiClO_4$) in dimethylformamide (DMF) served as the electrolyte support in the analytical protocol. The electrochemical performances of PANI/rGO nanocomposites were explored through CV within a potential window with a range of 0.8 V to 1.6 V.

Thermal stability study of the PANI/rGO nanocomposites were conducted under nitrogen atmosphere (N_2) at room temperature up to 1000 °C with a heating rate of 10 °C minutes through thermogravimetric (TGA) analysis.

IV.2.6. Electrical conductivity measurements

The four-point probe method was employed to assess the electrical conductivity of pure PANI, rGO, and PANI/rGO nanocomposites. Digital micrometers were used to determine the thickness of the samples, which were shaped into discs with a diameter of approximately 12 mm. The electrical measurements were performed using a Keithley 195 current source and a Keithley 197 electrometer, both computer-controlled. For these measurements, the disc pellet samples were placed on an insulated test bed, connected to a PRF-912 probe model (as represented in Figure IV.3). This test was primarily focused on quantifying the sample's surface resistance. The reciprocal of resistivity (ρ) determined the electrical conductivity (σ) of the disc pellet samples, as expressed in Eq (28):

$$\sigma = \frac{1}{\rho} \qquad \text{Eq. (28)}$$

Where σ represents electrical conductivity in Siemens per centimeter (S $\mathrm{cm^{-1}}$), while ρ denotes resistivity measured in ohm-centimeters (Ω cm).

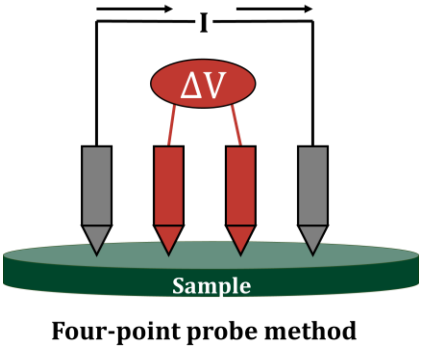

Figure IV.3. Schematic illustration of the four-point probe method utilized in this study.

IV.2.7. Computational methodology

This study involved comprehensive calculations concerning geometric parameters, internal energies, and electronic properties of the nanocomposite. Initially, we utilized the Material Studio software (Shankar et al. 2022) to perform MD simulations aimed at assessing the interaction energy between the PANI molecule and rGO sheet. The initial simulation box was constructed by placing the rGO sheet alongside the PANI molecule to investigate the inherent interactions between these components. Accordingly, the box's geometry was optimized to relax the entire molecular system. Subsequently, the box underwent NVT dynamics for approximately 2000 picoseconds, utilizing a 1 femtosecond time step at a temperature of 298 Kelvin. These simulations employed the COMPASS forcefield. After the NVT dynamics, a second MD simulation was conducted using the NPT thermodynamic ensemble for 20,000 picoseconds, also with a 1 femtosecond time step at 298 Kelvin. The outcome of this simulation led to another round of geometric optimization (Bousba et al. 2024). Energies were calculated for approximately of a hundred resulting conformations or more. Among these conformations, the one with the lowest energy was selected as the model for subsequent analysis. The selected model was further optimized *via* the DFT M06-2X functional (Moltved and Kepp 2019) and the TZVP basis set (Darwish et al. 2023; Mouffok et al. 2023; Uka et al. 2023), and this optimization was carried out with the Turbomole software (Boublia et al. 2022b, 2023c; Lemaoui et al. 2022, 2023a; AlYammahi et al. 2023). To delve deeper into the characteristics of the PANI/rGO system and their interactions, the COSMO-RS methodology was applied. This involved utilizing the COSMOThermx program to calculate pertinent parameters. In addition, the optimization process allowed us to determine geometrical parameters as well as various QTAIM and RDG topological parameters.

To represent the PANI conducting polymer, an oligomer was employed, comprising four monomer units of aniline. This oligomer includes 4 phenyl rings and a total of 48 atoms. In our model, rGO was selected. It's composed of 55 carbon atoms and 11 oxygen atoms, with open ends saturated by hydrogen atoms. rGO is essentially the reduced form of GO, featuring oxygen-containing groups like carboxyl acid (–COOH), hydroxy (–OH), and epoxy (–O–) functional groups that are haphazardly affixed to the edges and surface. The portrayal of rGO's structure lacks precision due to the erratic distribution of these oxygen-containing functional groups and the notable structural disarray within the framework (Dreyer et al. 2010). Both rGO and PANI underwent neutral optimization. This optimization allowed us to determine various electronic properties, including charge distribution, energies associated with the highest and the lowest occupied molecular orbitals (HOMO and LUMO, respectively), as well as band gap (E_g), which was estimated using the HOMO and LUMO energies through the following equation (Eq (29)):

$$E_g = E_{LUMO} - E_{HOMO} \qquad \text{Eq. (29)}$$

To comprehensively investigate weak interactions within a three-dimensional framework, our study employs an illuminating approach focused on the analysis of NCI (Johnson et al. 2010; Kr et al. 2022). Several theoretical models, including NCI-RDG and QTAIM, were applied. The RDG analysis relies on fundamental electron density (ρ) and reduced density gradients (RDGs), expressed in mathematical terms using Eq (30), where ρ denotes the electron density, and $\nabla\rho$ signifies its initial derivative. This method is particularly effective for identifying van der Waals interactions and weak non-covalent interactions, including hydrogen bonding and steric repulsions, which become significant at specific distances and can significantly influence the system as a whole (Boutouil et al. 2020; Mandal et al. 2023).

$$s = \frac{1}{2(3\pi^2)^{1/3}} \frac{|\nabla\rho|}{\rho^{4/3}} \qquad \text{Eq. (30)}$$

For NCI analyses based on the RDG and QTAIM, we incorporated the Molden input from Turbomole and utilized the computational tool Multiwfn (Lu and Chen 2012) to explore and identify potential weak interactions within the analyzed system.

To visualize the results, we generated RDG plots and QTAIM maps *via* the Visual Molecular Dynamics (VMD) interface (Humphrey et al. 1996). Furthermore, color scatter plots were created with the assistance of gnuplot (Williams et al. 2017). These advanced computational techniques facilitated an in-depth examination of weak interactions within the system under investigation.

IV.3. Results and discussion

IV.3.1. Response Surface Methodology results

In this investigation, a series of 15 experiments was executed using RSM-BBD, involving three repeated experiments that incorporated three input variables and three center points. Each experiment was replicated twice, and the mean value was determined. The design matrix for the experiments and the predicted outcomes are detailed in Table IV.2. Notably, the center point runs (#4, #10, and #15) exhibited minimal variations in the electrical conductivity, indicative of excellent experimental repeatability.

Furthermore, a comprehensive evaluation of the experimental outcomes involved an in-depth analysis of multiple regression models. After assessing various models, the quadratic model emerged as the most suitable fit for all design points.

To understand the effects of the variables and their interactions, Analysis of Variance (ANOVA) was performed, and the findings are reported in Table IV.3. It was observed that a linear effect (X_1) and a quadratic effect (X_3^2) were statistically significant, with a *p*-value < 0.05.

Table IV.2. RSM-BBD design matrix with its corresponding responses of electrical conductivity.

#Run	**Code values**			**Real values**			**Electrical conductivity σ x 10^{-3} (S cm^{-1})**
	X_1	**X_2**	**X_3**	**X_1**	**X_2**	**X_3**	
1	+	−	0	0.75	1	4	3.142
2	0	−	−	0.5	1	2	3.203
3	0	+	+	0.5	5	6	2.958
4	0	0	0	0.5	3	4	2.472
5	−	0	−	0.25	3	2	2.189
6	−	+	0	0.25	5	4	1.756
7	−	0	+	0.25	3	6	2.277
8	−	−	0	0.25	1	4	1.893
9	0	+	−	0.5	5	2	2.122
10	0	0	0	0.5	3	4	2.250
11	0	−	+	0.5	1	6	3.739
12	0	0	0	0.75	5	4	3.295
13	+	0	−	0.75	3	2	3.715
14	+	0	+	0.75	3	6	**4.975**
15	0	0	0	0.5	3	4	2.122

Nevertheless, the other linear and interaction terms, along with all quadratic terms, were considered statistically insignificant (*p*-value > 0.05). The experimental data exhibited a favorable agreement with the formulated model equation, evident from the lack of fit result with a *p*-value > 0.05. Subsequently, a second-order polynomial function, represented by Eq (31), was deduced to approximate the σ of PANI/rGO nanocomposites:

$$\begin{aligned}\sigma\ =\ & 2.28144 + 0.87651\, X_1 - 0.23076\, X_2 + 0.33983\, X_3 + 0.07224\ X_1X_2 \\ & + 0.29292\, X_1X_3 + 0.07501\, X_2X_3 + 0.26177\, X_1^2 - 0.02154\, X_2^2 \\ & + 0.74556\, X_3^2\end{aligned} \qquad \text{Eq. (31)}$$

Here, σ, X_1, X_2, and X_3 represent the electrical conductivity of PANI/rGO nanocomposites, coded forms of the APS/ANI ratio, rGO loading, and the time of polymerization, respectively.

The results from the ANOVA analysis, presented in Table IV.3, reveal an exceptionally low *p*-value (<0.0001), signifying a highly significant alignment of the model with the experimental data. Moreover, the lack of fit value (0.1212) substantiates the model's aptitude in capturing the experimental trends, thereby confirming its bona fide predictive power. Moreover, the model demonstrates excellent predictive performance, supported by the elevated adjusted and predicted R^2 values of 0.8041 and 0.9301, respectively, highlighting the precision and dependability of its predictions.

Additionally, to verify the adequacy of the model and ensure it meets the analysis assumptions, residual analysis was conducted. Given the dispersion of residuals observed in Figure IV.5, the data points scatter randomly about the center line, devoid of any apparent systematic trends or patterns. This randomness is indicative of the model's adequacy in capturing the inherent variability of the experimental data. Furthermore, the scatter of residuals displayed uncorrelated and random distribution on both sides of the center line, indicating constant variance. These robust findings provide compelling evidence that the model is appropriate and indeed satisfies the assumptions of the analysis.

Table IV.3. Statistical analysis (ANOVA) for the quadratic model of electrical conductivity in PANI/rGO nanocomposites.

Parameter	D_f	**Sum of Squares**	**Mean Square**	**F Ratio**	**Prob.> F**
Intercept	9	10.123	1.125	7.3866	0.0002*
X_1 (Molar ratio of APS/ANI)	1	6.147	6.147	40.3646	0.0014*
X_2 (rGO loading)	1	0.426	0.426	2.7974	0.1553
X_3 (Time)	1	0.924	0.924	6.0671	0.057
X_1*X_2	1	0.021	0.021	0.1371	0.7264
X_1*X_3	1	0.343	0.343	2.2538	0.1936
X_2*X_3	1	0.023	0.023	0.1478	0.7165
X_1^2	1	0.253	0.253	1.6615	0.2538
X_2^2	1	0.002	0.002	0.0113	0.9196
X_3^2	1	2.052	2.052	13.4778	0.0144*
Lack of fit	3	0.699	0.233	7.4106	0.1212
Pure error	2	0.063	0.031		
Total	14	10.885			

**Significant at 95% confidence interval.*

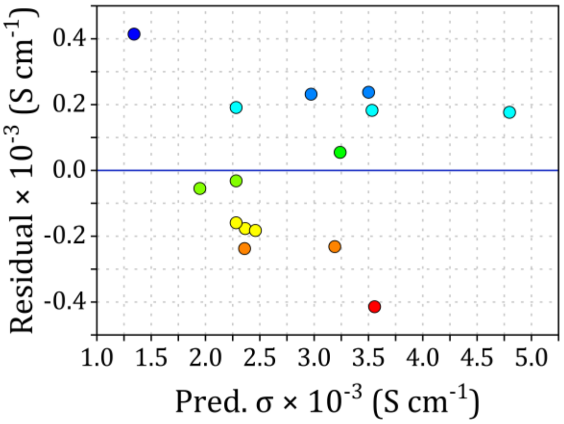

Figure IV.4. Correlation between residuals and predicted values for the electrical conductivity of PANI/rGO nanocomposites.

To understand the interaction effects of two variables while maintaining the other variables at their central point value (zero level), we created 2D contour and 3D surface plots using Eq (31). Figure IV.5 (A) and (D) depict the influence of the APS/ANI ration and rGO loading at a constant polymerization time of 4 h. It is evident that the electrical conductivity increases as the APS/ANI ratio and rGO loading vary from 0.5 to 0.75 and 3 to 5 *wt*.%, respectively. However, at higher APS/ANI ratios and increased rGO loading, the electrical conductivity shows a decreasing trend. This behavior can be attributed to the increased amount of APS (oxidant), resulting in the generation of a higher number of radical cations, which consequently accelerates the chemical oxidative polymerization of ANI. As acknowledged, the electrical conductivity of PANI is contingent on the protonation degree or the effective conjugation length of PANI chains (Qiu et al. 2020). In addition, the higher content of rGO in the nanocomposites hinders the orderly arrangement of PANI chains, inducing a higher structural disorder and creating more conjugated defects, ultimately contributing to lower conductivity (Sreeja et al. 2019).

Likewise, Figure IV.5 (B) and (E) exhibit the combined impact of APS/ANI ratio and polymerization time (h) on electrical conductivity while keeping the rGO loading fixed at 3 *wt*.%. It is evident that electrical conductivity continues to rise with an increase in the polymerization time, consistent with previous reports (Zhou et al. 2015; Sharifi et al. 2018). Finally, Figure IV.5 (C) and (F) demonstrate the linear influence of rGO loading and polymerization time on the electrical conductivity, suggesting their minor impact on the overall electrical conductivity.

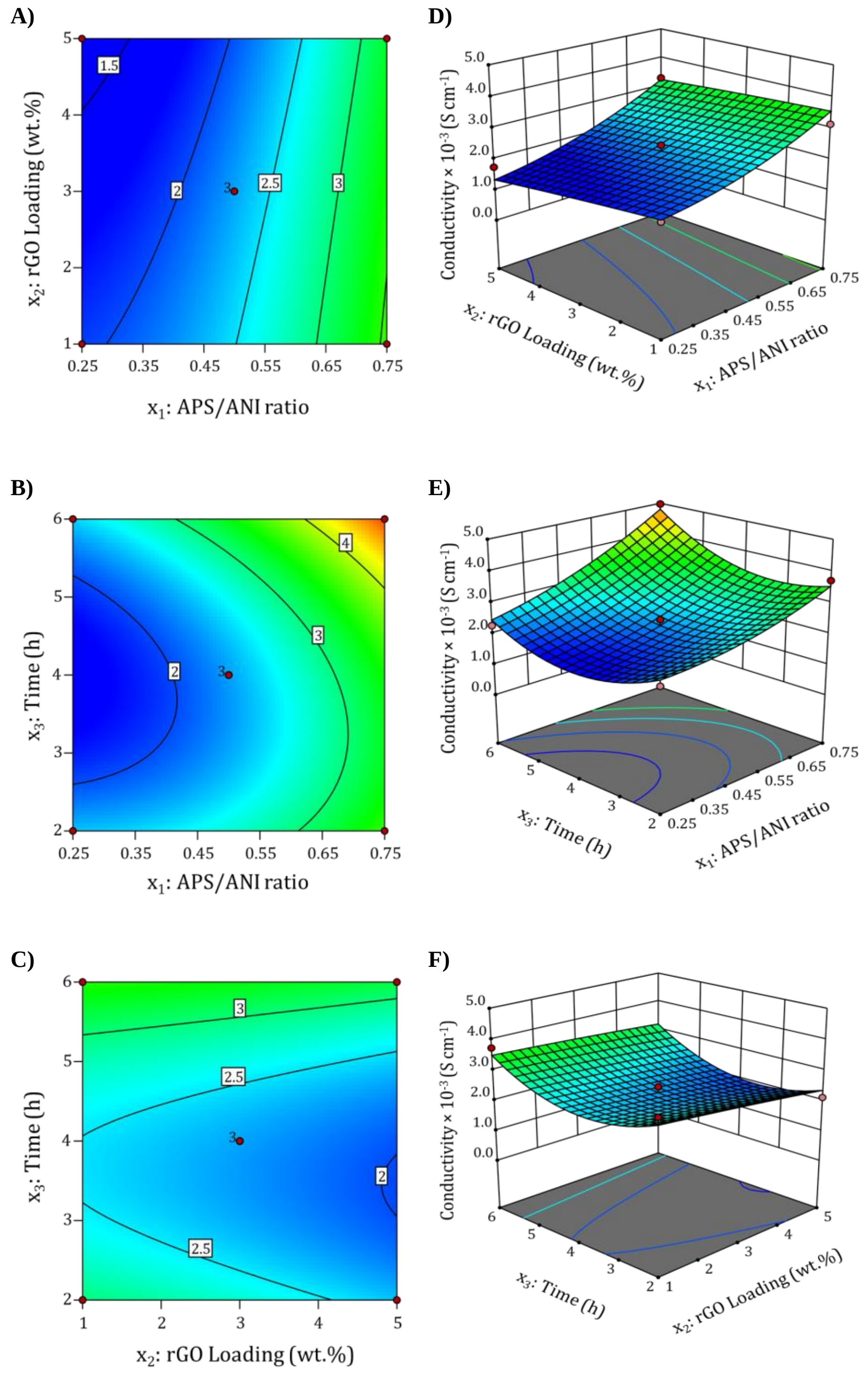

Figure IV.5. Two-dimensional (2D) contour and three-dimensional (3D) surface plots illustrating the combined impact on electrical conductivity. Interplay of APS/ANI ratio and rGO loading (A, D), APS/ANI ratio and polymerization time (B, E), and rGO loading and polymerization time (C, F).

IV.3.2. Artificial Neural Network Modeling

In this study, an ANN was constructed to capture the intricate non-linear associations among three independent variables (molar ratio of APS/ANI, rGO loading, and polymerization time) and the desired output (electrical conductivity) through the application of the Broyden-Fletcher-Goldfarb-Shanno (BFGS) algorithm. configuration that yielded the lowest *RMSE* and the highest R^2 values. following this analysis, we determined the final architecture of the ANN model, adopting a 3-12-1 configuration, where the hidden layer comprises 12 neurons. Figure IV.6 (A) illustrates the statistical metrics *RMSE* and R^2 for different architectures, revealing that the 3-12-1 architecture yields lower *RMSE* and higher R^2 values, indicating superior predictive performance. The proposed ANN structure is schematically depicted in Figure IV.6 (B).

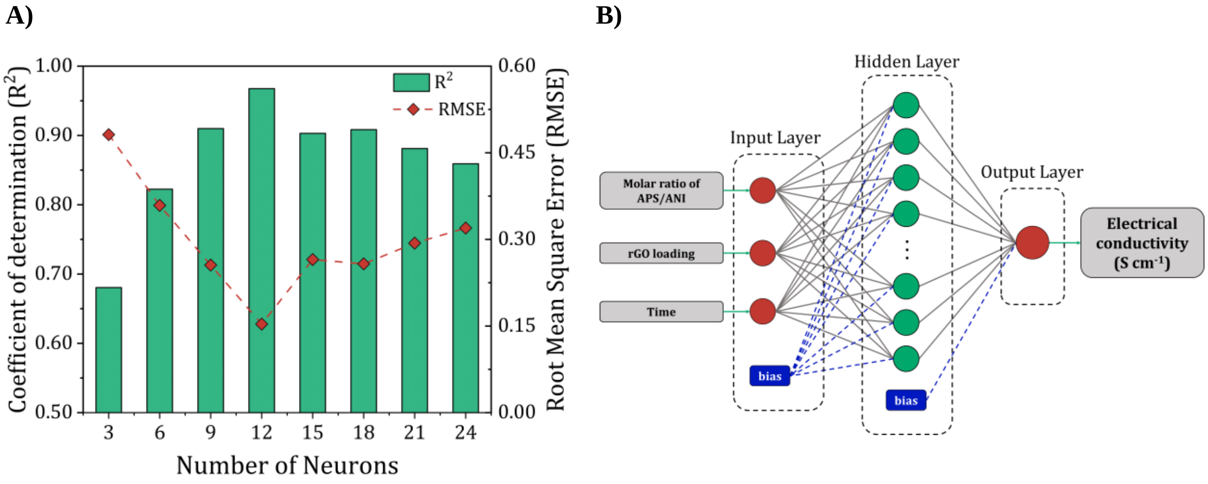

Figure IV.6. A) Performance of the developed ANN model with respect to the neurons' number in the hidden layer, and B) Schematic representation of the 3-12-1 ANN architecture.

IV.3.3. Comparison between RSM and ANN models

The effectiveness of the proposed approaches has been validated, establishing the superiority of the methods in depicting the PANI/rGO nanocomposites' electrical conductivity. To compare the predictions of the respective models (RSM-BBD and ANN), a comprehensive error analysis was performed, and key performance metrics, including R^2, *RMSE*, *AARD*, *MAE*, and relative deviation (*RD%*), were computed using the equations detailed in the methodology section. As depicted in Figure IV.7 (A) and (B), the scatter plots for both models illustrated strong concordance with the experimental data, substantiated by the elevated R^2 values of 0.93 and 0.97 for RSM and ANN, correspondingly. Notably, the ANN demonstrated superior accuracy in fitting the experimental data when contrasted with the RSM model, as indicated by the plot of *RD%* in Figure IV.7 (C). This higher predictive accuracy of the ANN model highlights its superior performance. However, it is crucial to recognize that the ANN model, in its standard form, does not inherently elucidate the influence of input parameters on the response; this understanding typically necessitates further analysis, such as a query strategy for selecting informative training data or post-hoc interpretability methods. In contrast, the primary advantage of RSM lies in its capacity to demonstrate factor contributions through coefficients in the regression model.

Evaluation metrics listed in Table IV.4, incorporating metrics such as R^2, *AARD*, and *RMSE* provides additional validation of the robust alignment between the ANN-predicted and experimental values, surpassing the performance achieved by the RSM model. The enhanced predictive prowess of ANNs can be ascribed to their adeptness in approximating non-linear systems, a capability beyond the scope of RSM, which is confined to approximating systems using second-order polynomials.

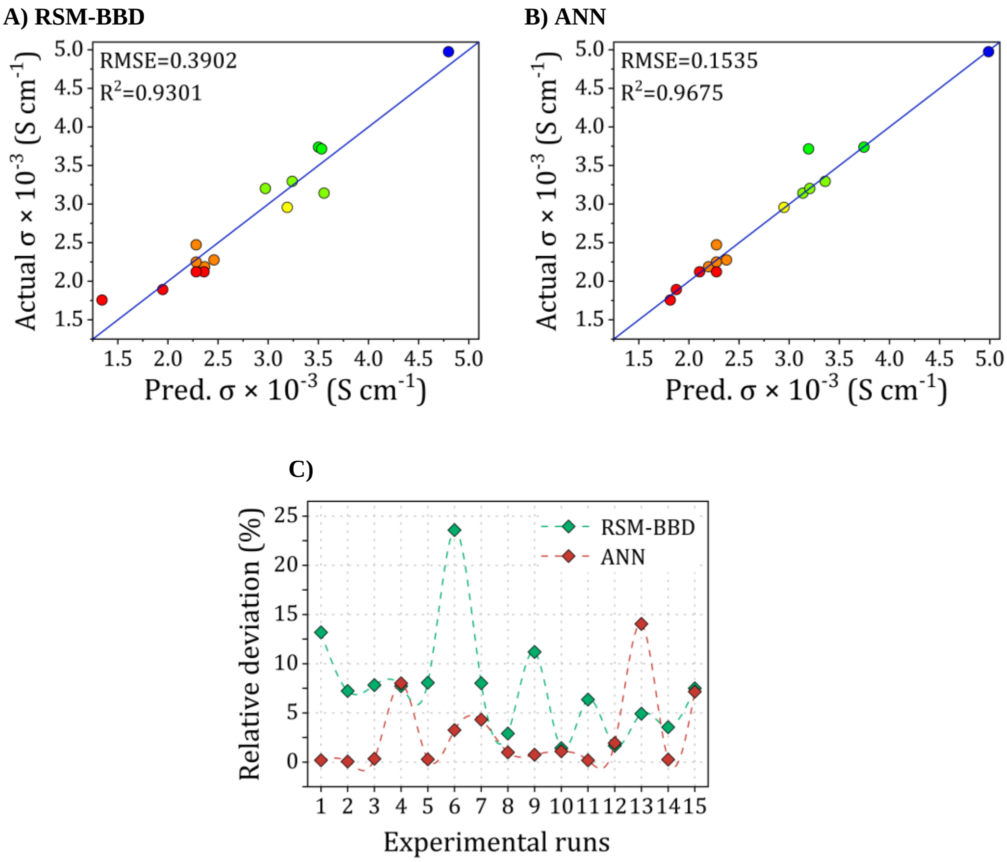

Figure IV.7. Regression analysis between actual and predicted electrical conductivity using A) RSM-BBD and B) ANN models, and C) Relative deviation plot for the predictions of electrical conductivity by RSM-bbd and ANN models.

Table IV.4. Comparative assessment of predictive performance between RSM and ANN models.

Metric	Model	
	BBD	**ANN (3-12-1)**
R^2	0.9301	0.9675
RMSE	0.3902	0.1535
AARD (%)	7.68	2.86
MAE	0.1985	0.0797

IV.3.4. Electrical conductivity optimization of the PANI/rGO nanocomposites

In our endeavor to improve the electrical conductivity of PANI/rGO nanocomposites, we harnessed the power of a response surface optimization approach and ANN predictive model. These methodologies are intricately crafted to identify the optimal position within the design space, whether it involves a minimum, a maximum, or a specific region characterized by a stable response. The main objective in this investigation was to maximize the electrical conductivity of PANI/rGO nanocomposites. To accomplish this, we relied on the RSM and ANN models. Through meticulous analysis, we uncovered the precise conditions that lead to the highest electrical conductivity. These optimal conditions were revealed to be an APS/ANI molar ratio of 0.75, an rGO loading of 3 *wt.*%, and a polymerization time of 6 hours.

Following this optimization, a comprehensive analysis using various techniques, encompassing UV-visible, Raman, FTIR, PL, XRD, XPS, CV, and TGA analyses were performed for the PANI/rGO samples. These analyses provided in-depth insights into the structural, optical, and electrochemical performances of the investigated PANI/rGO nanocomposites.

IV.3.5. Compositional and structural analyses

IV.3.5.1. UV-visible spectroscopy

Extensive investigations have been undertaken to comprehensively analyze the optical properties of PANI/rGO (1, 3, and 5 *wt.*%) nanocomposites, as depicted in Figure IV.8. The UV-Visible spectrum of pure PANI, revealed in Figure IV.8 (A), unveils the existence of two significant absorbance peaks around 270 nm and 655 nm. The initial peak at 270 nm is attributed to the π–π^* electron orbital transition of the benzenoid ring within PANI structure. This transition reflects the movement of electrons within the conjugated system, shedding light on the electronic properties associated with the benzenoid moiety (Ansari et al. 2014a; Mitra et al. 2015). On the other hand, the UV-Vis spectrum of rGO demonstrates enhanced and uniform absorption spanning the range of 240 to 800 nm, indicating the occurrence of a restricted number of oxygen groups or graphitic domains on the graphene planes. This observation can be attributed to the $n \rightarrow \pi^*$ transition arising from the occurrence of bonds in carbonyl or carboxyl groups within rGO, which occur as a result of partial reduction (Habib et al. 2022). This absorbance profile is characteristic of graphene materials and indicates the restoration of electronic conjugation within rGO sheets (Li et al. 2008; Bhattacharya et al. 2018).

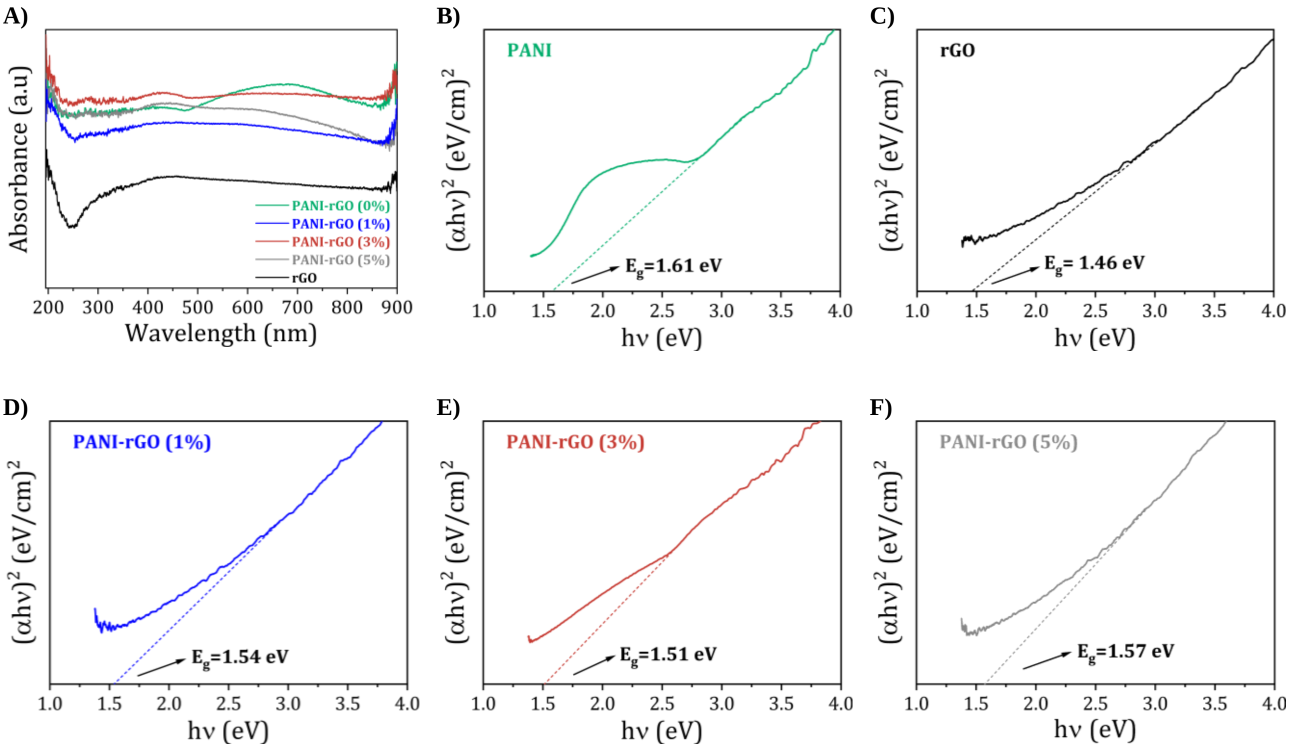

Figure IV.8. A) UV–Visible adsorption spectra (A) with its corresponding Tauc plots for pure PANI, rGO, and PANI/rGO nanocomposites (B, C, D, E, and F).

The enhanced absorption and absence of distinct peaks within this range indicate the formation of a continuous, highly conjugated graphene structure in rGO. Regarding the PANI/rGO nanocomposites in varying ratios, it is noteworthy that compared to the pure PANI or rGO samples, it displays three robust absorbance peaks at 210 nm, 270 nm, and 655 nm, each showing a shift with respect to the peaks observed in the pure materials. These peaks are shifted, suggesting a relatively complex interaction between PANI and rGO. The observed peak at approximately 210 nm is attributed to a π–π^* aromatic transition (Abd Razak et al. 2021). The wide peak ranging from 240 to 320 nm in the PANI/rGO spectra is associated with the benzenoid π–π^* transition. Additionally, a shoulder is observed, likely stemming from the Polaron–π^* transition of quinoid-imine functional groups due to protonation. These findings affirm the presence of diverse interactions, involving hydrogen bonding and π-π coordination among the PANI and rGO (Lin et al. 2013; Lu et al. 2013; Geethalakshmi et al. 2014).

Moving on, Figure IV.8 (B, C, D, E, and F) show the corresponding Tauc plot, $(\alpha h\nu)^2$ with hν, for pure PANI, rGO, and PANI/rGO (1, 3, and 5 *wt.*%) samples, with h representing the Planck constant and ν denoting the frequency. The energy gap (E_g) can be estimated by determining the x-intercept of the extrapolated Tauc plot (Choudhary and Verma 2019). For pure PANI and rGO, the band gap is found to be approximately 1.61 and 1.46 eV, respectively (Figure IV.8 (B and C)). Furthermore, as the rGO loading increases up to 3 *wt.*%, the optical band gap of the composite decreases to 1.51 eV. In PANI/rGO nanocomposites, the integration of rGO leads to the formation of new energy levels known as trap states. These states are typically located near the valence band and arise due to the complex interaction between PANI and rGO, introducing localized states or defect levels within the composite structure. These trap states play a pivotal role in the electronic properties of the nanocomposite (Figure 8 (D and E)). While electron delocalization within the conjugated PANI chains is a contributing factor, the primary mechanism for the reduced energy gap (E_g) and increased conductivity lies in these trap states. These states provide a pathway for electrons to move from the valence band to the conduction band with minimal energy input. Essentially, the trap states create a 'stepping stone' effect, allowing electrons to 'hop' between these states. This hopping mechanism is less energy-intensive than the direct transition across the full band gap in a pristine material. As a result, the presence of these trap states in PANI/rGO nanocomposites facilitates easier and more efficient electron movement, leading to enhanced electrical conductivity. However, it is important to note that this is a nuanced balance. An excessive concentration of trap states or rGO can lead to increased scattering and localization effects, potentially countering the benefits of enhanced conductivity. Nevertheless, as shown in Figure IV.8 (F), with a continued increase in rGO loading (5 wt.%), barriers are formed within the PANI chain, hindering electron delocalization and resulting in a corresponding increase in the band gap (1.57 eV)) (Sreeja et al. 2019). Thus, incorporating 3 *wt.*% rGO into the PANI matrix promotes electron delocalization, broadening the absorption range, and enhancing electrical conductivity (Konwer 2016; Kandulna et al. 2019). Meanwhile, the reduction in the energy gap compared to rGO alone is particularly significant which expands the absorption range into the visible area of the electromagnetic spectrum, thereby improving the light harvesting efficiency of PANI/rGO nanocomposites. Consequently, the incorporation of rGO facilitates increased delocalization of electrons within the PANI chains, allowing for the absorption of a wider range of photons (Choudhary and Kandulna 2019). As a result, the PANI/rGO nanocomposites exhibit improved electrical conductivity, as observed in the present study.

IV.3.5.2. Photoluminescence studies (PL)

Photoluminescence (PL) spectra provide valuable insights into the recombination efficiency of photo-generated electrons and holes, which can be inferred from the fluorescence intensity. A strong PL intensity signifies a rapid recombination of photo-generated charge carriers with a short lifetime. Conversely, a higher separation efficiency of the photo-generated carriers, i.e., electrons (e^-) and holes (h^+), resulting in longer lifetimes, leads to a reduction in the intensity observed in the PL spectra (Chaudhary et al. 2019). Figure IV.9 illustrates the PL spectrum of pure PANI, rGO, as well as rGO-PANI nanocomposite samples (1, 3, and 5 *wt.*%), recorded using an excitation wavelength of 320 nm. The PL spectrum for pure PANI exhibits two broad peaks in the wavelength range of 420-440 nm and 510-535 nm. These PL peaks, specifically located at approximately 436.1 nm and 535 nm, correspond to the π–π^* transition and $\pi^* \rightarrow$ Polaron transition, respectively (Banerjee et al. 2009; Geethalakshmi et al. 2014). In rGO, a significant broad peak appears within the wavelength range of 400-450 nm, signifying the formation of additional sp^2 carbon atoms resulting from the reduction of GO. Moreover, a broad peak is observed in the range of 510-535 nm, suggesting a reduction in the quantity of disorder-induced states within the π–π^* energy gap of rGO. This decrease in disorder-induced states contributes to the enrichment of small-sized sp^2 clusters in the rGO structure (Singh et al. 2022). Moving forward to discuss PANI/rGO nanocomposites, the emission peaks predominantly originate from the π–π^* transition of the benzenoid unit, transitioning from the polaronic band to the π band structures of PANI. This emission also signifies the presence of electronic states involved in the photoexcitation process. The arrangement of quinoid and benzenoid units in PANI facilitates the formation of singlet excitons, which subsequently undergo photonic emission as they decay to the ground state. Consequently, excitons significantly contribute in the photoluminescence behavior of conjugated polymers. This effect primarily stems from the inherent structure of the conjugated systems, where the delocalization of π-electrons facilitates more efficient charge carrier movement (Sreeja et al. 2019). In PANI/rGO nanocomposites, the interaction between PANI and rGO creates an environment conducive to increased carrier mobility. The conjugation within PANI allows for a smoother transition of charge carriers, enhancing the overall electrical conductivity of the composite. This enhancement is particularly significant when considering the separation between electrons (e^-) and holes (h^+), which directly impacts the mobility of excitons (electron-hole pairs). The presence of rGO in the composite also plays a pivotal role. rGO, with its high surface area and conductive nature, provides additional pathways for charge transfer, further augmenting the mobility of charge carriers within the composite material. This enhancement in excitons significantly contributes to a more pronounced PL. Interestingly, the PL intensity shows a remarkable amplification with the incorporation of rGO up to a specific threshold (3 *wt.*%), beyond which a slight reduction is observed. This observation could be attributed due to improved charge transfer and reduced electron-hole recombination, excessive rGO can lead to the formation of non-radiative recombination centers, thus diminishing the PL intensity. The slight deviation in the emission peak in PANI/rGO nanocomposites is mainly influenced by variations in the arrangement of quinoid and benzenoid units within PANI (Souza Jr et al. 2006; Lai et al. 2012; Maruthamani et al. 2016; Choudhary and Verma 2019). As a result, these findings, in agreement with the UV-visible spectroscopy findings, afford compelling evidence of the substantial impact of rGO on the optical properties of PANI/rGO nanocomposites.

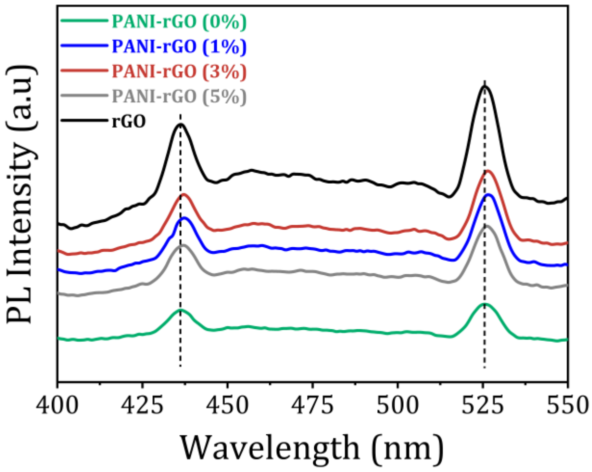

Figure IV.9. PL spectrum of PANI, rGO, and PANI/rGO nanocomposites.

IV.3.5.3. Raman spectroscopy

Raman spectroscopy serves as a rapid and nondestructive characterization method, providing valuable insights into the lattice structure, structural disorders, crystallization, and defects of carbon-based materials (Wu et al. 2018a). In this study, Raman analysis was utilized to explore the structural alterations in PANI throughout de-doping and redoping procedures, as well as to analyze the vibrational spectrum of nonpolar bonds, particularly the C–C interactions within the PANI backbone and the basal planes of rGO. Figure IV.10 (A) presents the Raman spectra for rGO, PANI, and PANI/rGO (1, 3, and 5 *wt.*%) nanocomposites.

The Raman spectra of rGO shows two discernible peaks with significance: one at 1351 cm^{-1} associated with the D mode, suggesting defects in graphitic carbon, and the other at 1580 cm^{-1} (G mode), aligning with the first-order scattering of the E_{2g} mode commonly observed in *sp*^{2}-carbon fields (Wu et al. 2009; Kim et al. 2014). The extent of disorder in carbon materials is commonly assessed using the I_D/I_G ratio. In this case, the low I_D/I_G ratio of rGO (0.516) suggests a reduction in structural defects compared to its precursor material, GO. Literature reports suggest that the high I_D/I_G ratio in GO is indicative of a distorted lattice and a significant number of sp^3-like defects resulting from the oxidation process during its preparation (Maulana et al. 2017). The presence of oxygen-containing chemical moieties or groups during oxidation causes disturbances in the graphene lattice and leads to the formation of sp^3 carbon domains in GO. Nevertheless, during the reduction process, some of these defects are repaired, leading to a more ordered lattice in rGO defects by restoring the sp^2 hybridized carbon network and reducing the sp^3 domains, as evidenced by a lower I_D/I_G ratio. This process, however, might not completely eliminate all defects, leaving some residual disruptions in the lattice structure. The removal of oxygen-containing functional groups during reduction restores sp^2 carbon domains and recovers the graphene-like structure. As a consequence, the I_D/I_G ratio in rGO decreases, representing a reduction in the number of sp^3-like defects and an increase in the relative abundance of sp^2 carbon fields (Wang et al. 2010; Kim et al. 2014).

The Raman spectrum of pristine PANI reveals distinct bands linked to the doped polymer, including C–H bending in the quinoid ring at 1161 cm^{-1}, $C–N^+$ stretching at 1329 cm^{-1}, and C=C stretching in the quinonoid ring at 1590 cm^{-1}. In PANI/rGO nanocomposites, the Raman spectra exhibits characteristic peaks consistent with those of pure PANI, corroborated by prior research, providing further evidence of the presence of PANI in the nanocomposites (Louarn et al. 1996; Niaura et al. 2004; Salunkhe et al. 2014). Interestingly, As the rGO content increases in the PANI/rGO nanocomposites, the vibration intensity at approximately 1470 cm^{-1} (corresponding to C=N quinoid stretching) undergoes changes, signifying that the addition of rGO encourages the prevalence of the quinoid form of PANI, promoting a conjugated planar arrangement. This finding is additionally substantiated by analyzing the intensity ratio of the C–H vibration in the quinoid unit (1150 cm^{-1}) relative to that of the consistent benzenoid (1160 cm^{-1}) (Pereira da Silva et al. 2000; Jain and Annapoorni 2010). The stabilization of quinoid rings in the PANI/rGO nanocomposites is facilitated by π–π interactions with the basal planes of rGO, resulting in an increased level of polymer chain ordering within the hybrids (Wang et al. 2010). This enhanced polymer chain ordering promotes stronger interactions and facilitates more effective charge transfer between rGO and PANI.

IV.3.5.4. Fourier transformation infrared spectroscopy (FTIR)

To complement the Raman data and gain insights into the interaction between rGO and PANI, FTIR spectroscopy was employed in this study. Figure IV.10 (B) showcases the FTIR spectra of PANI, rGO, as well as PANI/rGO nanocomposites (at 1, 3, and 5 *wt.*% rGO) in the region between 1800 and 1000 cm^{-1}. This zoomed-in view allows for the identification of peaks resulting from the interactions between rGO and PANI. For further reference, Figure A.1 and Figure A.2 in the Appendix display the FTIR spectra of rGO and pure PANI, respectively.

Remarkably, the FTIR spectrum of rGO exhibited distinct changes, with a novel peak emerging at 1565 cm^{-1}, attributed to sp^2 hybridized CC, and the disappearance of the peak at 1050 cm^{-1}, indicative of epoxide groups. These observations proved the successful reduction of GO to rGO, aligning with similar FTIR spectra reported in the literature for rGO (Kumar et al. 2018b). In the FTIR spectrum of PANI and PANI/rGO nanocomposites, prominent absorption peaks are observed at 3277, 1623, 1428, and 1318 cm^{-1}, corresponding to N-H, C=N, C=C, and C−N stretching, correspondingly (Mostafaei and Zolriasatein 2012). Notably, the intensity ratio of the PANI bands (1623 and 1428 cm^{-1}) is indicative of the occurrence of reduced (benzenoid) and oxidized (quinoid) repeat units. These characteristic bands serve as compelling evidence for the presence of the emeraldine salt phase of PANI in the nanocomposites (Jain et al. 2016). The emeraldine salt phase represents the conductive state of PANI, featuring alternating benzenoid and quinoid repeat units. This conductive state is crucial for optimizing the electrical properties of PANI/rGO nanocomposites. In the structure of polyaniline, the alternating arrangement of benzenoid and quinoid units plays a crucial role in defining its electrical properties. This structural configuration facilitates the delocalization of π electrons across the benzenoid units, which is essential for the intrinsic conductivity of the polymer. This delocalization contributes to the overall electronic structure of PANI, allowing for a certain degree of electron mobility within the polymer chain. Simultaneously, the presence of quinoid units introduces sites for potential charge transfer interactions. These interactions are not purely based on the delocalization of π electrons but involve hopping mechanisms, where charge carriers, such as polarons and bipolarons, move between localized states along the polymer chain. This charge transfer process is influenced by the degree of oxidation (doping) of PANI and is critical in applications where PANI undergoes redox reactions or interacts with other materials, such as graphene in composites. Therefore, the electrical conductivity in PANI is a result of a complex interplay between the delocalization of π electrons, predominantly within the benzenoid segments, and charge transfer mechanisms, facilitated by the quinoid structures and doping levels. This interplay enables PANI to exhibit a range of conductive behaviors, adapting to different environmental conditions and applications. As a result, the presence of the emeraldine salt phase enables the efficient flow of electrons, contributing to improved electrical conductivity and enhanced performance of the nanocomposites in various applications, including energy storage devices, sensors, and conductive coatings.

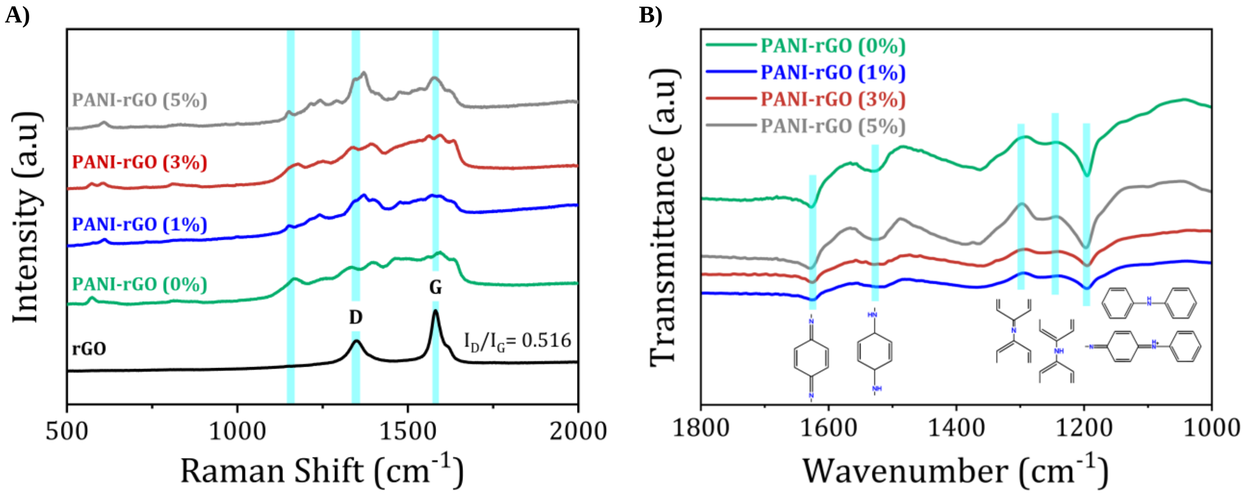

Figure IV.10. A) Raman spectra and B) FT-IR spectrum of pure PANI, rGO, and PANI/rGO nanocomposites.

Interestingly, the FTIR spectrum of PANI/rGO nanocomposites did not exhibit the functional groups present on the rGO. This finding indicated that the surface of rGO was effectively coated with PANI through precise interactions, such as π–π electron stacking and H- bonding among the amine group of PANI and the oxygen groups in rGO (Xu et al. 2010; Imran et al. 2014). Notably, the polymerization process involving aniline in the presence of rGO follows a specific mechanism. Aniline undergoes oxidation, consequential in the construction of oxidized radicals. These radicals then undergo a reductive elimination of $2H^+$ to form an α,α-aniline dimer. Subsequently, these dimers can propagate to longer chain lengths through repeated oxidation and reaction with generated aniline radicals *via* oxidation (Gospodinova et al. 1993). These interactions not only ensure the uniform dispersion of rGO within the PANI matrix but also contribute significantly to the improved electrical properties and overall performance of the PANI/rGO nanocomposites.

V.3.5.5. X-ray diffraction analysis (XRD)

The structures of the PANI/rGO nanocomposites were further elucidated through powder X-ray diffraction (XRD) analyses. These analyses were conducted to investigate the elemental composition, carbon bonding, morphology, and crystallinity of the nanocomposites (Vinet and Zhedanov 2011). Figure IV.11 illustrates the XRD patterns of pure rGO and PANI, as well as PANI/rGO (1, 3, and 5 *wt.*%) nanocomposites. The XRD measurements were conducted over an angular range of $10° \leq 2\theta \leq 60°$, utilizing a scanning rate of 6° min^{-1} with a step size of 0.02°. In the XRD analysis of PANI, small diffraction peaks were observed at 15.20°, 20.20°, and a distinct peak at 25.50°, corresponding to the (011), (020), and (200) Bragg's reflections, correspondingly. These peaks are indicative of the crystalline planes associated with the emeraldine salt state of PANI (Yan et al. 2010). The XRD pattern of rGO displayed peaks at 2θ = 26.51° and 44.40°, representing the characteristic (002) and (100) peaks of graphite-like structures, respectively. The intensities of these peaks amplified as a result of the interaction between rGO and PANI chains in different proportions (Abd Razak et al. 2021).

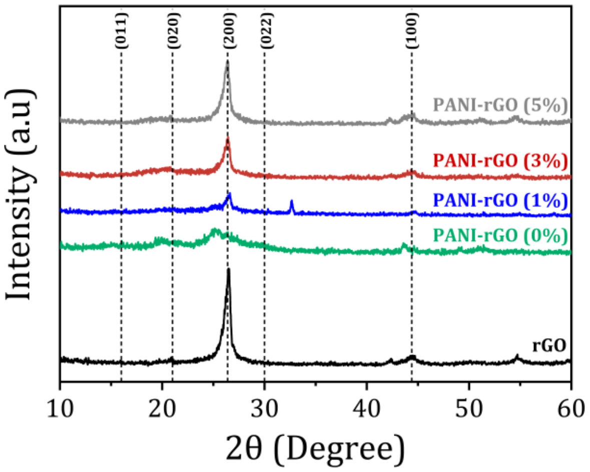

Figure IV.11. XRD patterns of pure PANI, rGO, and PANI/rGO nanocomposites.

Upon forming the PANI/rGO nanocomposites, new peaks surfaced, demonstrating a shift compared to the pristine rGO peaks. This shift is ascribed to the π–π bond stacking of the benzene rings in PANI with rGO. Particularly, the peak at 2θ = 25.50° in pure PANI shifted to 26.60° when PANI was blended with rGO, signifying a substantial interaction between rGO particles and PANI chains (Mitra et al. 2015). Moreover, the XRD analysis of rGO/PANI nanocomposites revealed diffraction peaks similar to those observed in PANI or rGO, suggesting the absence of additional crystalline structures in the nanocomposite samples. Based on these outcomes, it can be resolved that the characteristic diffraction peaks indicate extensive physical and chemical interactions between rGO and PANI chains. These interactions include H-bonds, electrostatics, and π-π coordination interactions (Abd Razak et al. 2021).

IV.3.6. X-ray photoelectron spectroscopy (XPS)

The investigation of elemental composition was advanced by X-ray photoelectron spectroscopy (XPS), providing deeper insights into the samples. The comprehensive survey spectra, as depicted in Figure IV.12 (A), distinctively portray the characteristic chemical profiles of pure PANI, rGO, and PANI/rGO nanocomposite samples, featuring discernible signals consistent to carbon (C 1s), nitrogen (N 1s), and oxygen (O 1s) for each respective material. Additionally, it is noteworthy that besides the detection of C KLL and O KLL Auger electron emissions in the high binding energy region, the oxygen signal present in the PANI sample may have arisen from residual APS as well as water molecules adsorbed onto the surface (Moyseowicz and Gryglewicz 2019). This oxygen signal might also stem from the rGO component within the PANI/rGO samples. Intriguingly, a subtle yet noteworthy N 1s peak observed in the rGO spectrum can be ascribed to doped nitrogen resulting from the hydrazine reduction process, thus further enriching our understanding of these intricate materials (Lamiel et al. 2015; Yu et al. 2023).

Meanwhile, the N1s spectrum at high resolution for both PANI and PANI/rGO reveals four discernible components, as illustrated in Figure IV.12 (B) and (C). The peaks at binding energies of 398.1 and 399.2 eV are indicative of imine (-N=) and amine (-NH-) groups, respectively, while those at 401.6 and 405.1 eV are associated with positively charged nitrogen groups N^+ and $-NH^+$, respectively. PANI is predominantly composed of amine groups, suggesting its protoemeraldine form (Vallés et al. 2011; Li et al. 2020). Throughout synthesis, PANI undergoes oxidation, leading to the partial conversion of amine to imine nitrogen. This transformation is explicable by the simultaneous reduction of GO oxygen functionalities and PANI nitrogen groups, facilitated by superheated water and the hydrothermal process (Xu et al. 2011), also *via* hydrothermal process (Moyseowicz and Gryglewicz 2019). The heightened fraction of positively charged nitrogen can be attributed to the interactions between PANI and rGO, inducing a restructuring of the benzenoid amine structure of PANI. Moreover, the elevated doping level of PANI in this composite is expected to augment its electrical and electrochemical performance. The C 1s spectra' deconvolution for PANI, PANI/rGO nanocomposite, and rGO samples is presented in Figure IV.12 (D).

Upon closer examination of the primary peak line of PANI, as shown in Figure IV.12 (D), a decomposition into four distinct peak lines becomes evident. Specifically, PANI displays a peak at 284.6 eV attributed to C–C and C=C bonds. Furthermore, characteristic peaks associated with carbon-nitrogen interactions manifest as follows: C–N, C–N+, C=N, and C=O, each corresponding to binding energies of approximately 285.6, 286.7, as well as 287.9 eV, respectively. The presence of carbonyl functional groups within PANI can be ascribed to the generation of benzoquinone and hydroquinone, resulting from partial surface oxidation (Zou et al. 2018).

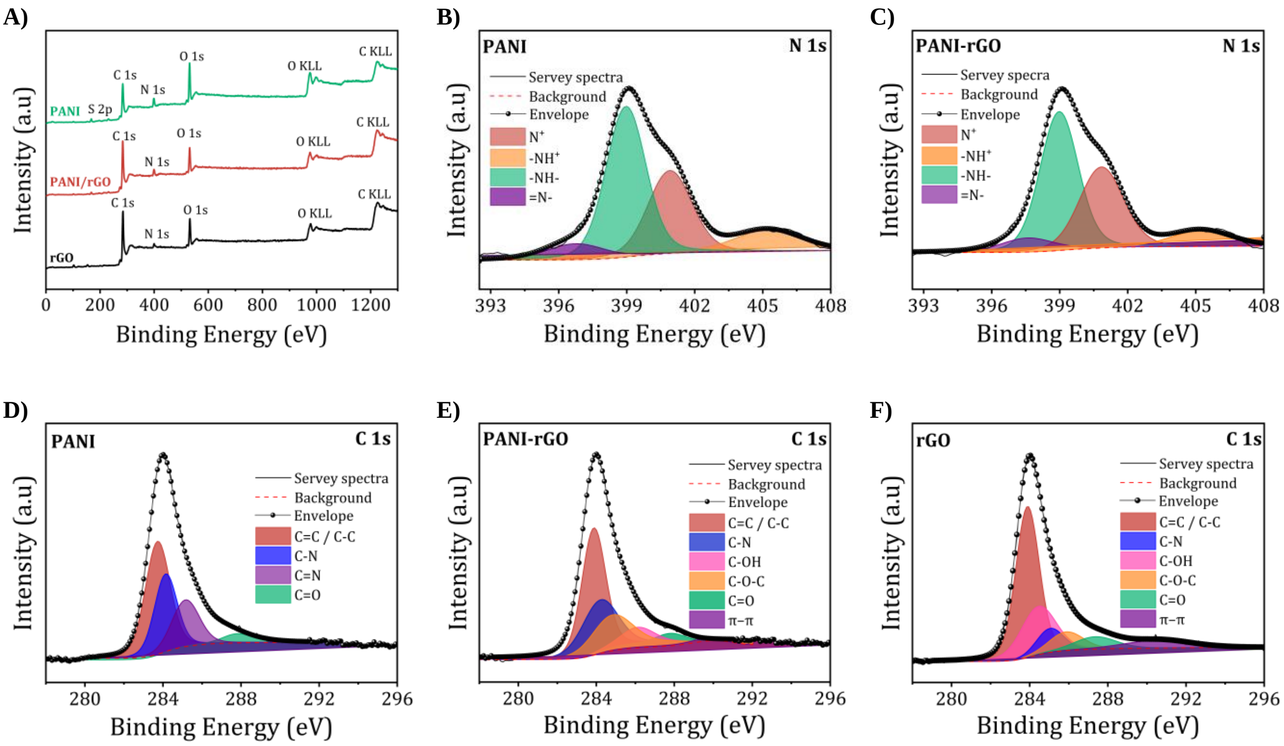

Figure IV.12. XPS surveys with the broad high-resolution spectrum of the C 1s and N 1s areas for pure PANI, rGO, and PANI/rGO nanocomposites (3 *wt.*%).

Turning attention to Figure IV.12 (E and F), the C 1s spectrum for PANI/rGO and rGO display six discernible peak lines: C=C and C-C (284.31 eV), C-N (285.4 eV), C-OH (285.7 eV), C-O-C (286.6 eV), C=O bonds (288.1 eV), and $\pi-\pi$ stacking (290.4 eV) (Fujimoto et al. 2016; Yu et al. 2023). Notably, the C-N peaks are more prominent in the PANI/rGO spectra than in the rGO sample. While inherent oxygen defects may exist in the raw rGO sample, the majority of the oxygen in the PANI/rGO nanocomposite coating likely originates from slight rGO oxidation during synthesis. This oxygen content acts as active sites, facilitating PANI polymerization. In this context, it is reasonable to infer that rGO contributes to the formation of a more comprehensive and densely structured PANI/rGO nanocomposite coating. This observation holds significant implications for the structural and functional properties of the resultant nanocomposite material.

IV.3.7. Electrochemical behavior of PANI/rGO nanocomposites

To comprehend the electrochemical redox behavior of PANI/rGO nanocomposites, a conventional cyclic voltammetry (CV) test was performed. Figure IV.13 illustrates the cyclic voltammograms of rGO, pure PANI, and PANI/rGO nanocomposites. When scanned at a rate of 25 mV s^{-1}, the CV of pure PANI exhibited the existence of two sets of redox peaks. These peaks correspond to specific transitions within the PANI structure, notably the shift from the fully-reduced PANI form (leucoemeraldine) to the partially-oxidized PANI form (emeraldine), as well as the transition among emeraldine and the fully-oxidized PANI form (pernigraniline) (Salunkhe et al. 2014; Silva et al. 2018; Boublia et al. 2023a).

In contrast, the CV of PANI exhibits a single pair of redox peaks when scanned at rates ranging across 25 to 175 mV s^{-1}. It is important to note that as the scan rate rises from 25 to 175 mV s^{-1}, there is a proportional increase in current density. This increase can be ascribed to the interior resistance within the electrode. CV curves for PANI/rGO nanocomposites share a similar overall shape to that of pure PANI, but there is a noticeable difference in current densities. Specifically, the current densities of PANI/rGO nanocomposite samples are somewhat lower compared to PANI at equivalent potential scan rates. Moreover, by altering the weight percentage (*wt.*%) of rGO in the PANI/rGO nanocomposites, significant changes in the profiles of the CV curves and current densities were observed. An increase in the rGO *wt.*% from 3 *wt.*% resulted in a substantial rise in current density. However, this trend was reversed as the rGO content was further increased to 5 *wt.*%.

Using the CV data, the specific capacitances (C_p, F g^{-1}) were calculated for various potential scan rates (ν, mV s^{-1}) through the application of the following formula:

$$Specific\ capacitance\ (C_p) = \frac{\int I(V)\ \times dV}{m\ \times\ \Delta V \times \nu} \qquad \text{Eq. (32)}$$

Here, $\int I(V)\ dV$ signifies the integration of current over time, as acquired from the cyclic voltammogram, m denotes the mass of the sample, which, in this case, corresponds to the PANI/rGO nanocomposites, and is expressed in grams. ΔV represents the potential window, while v represents the scan rate.

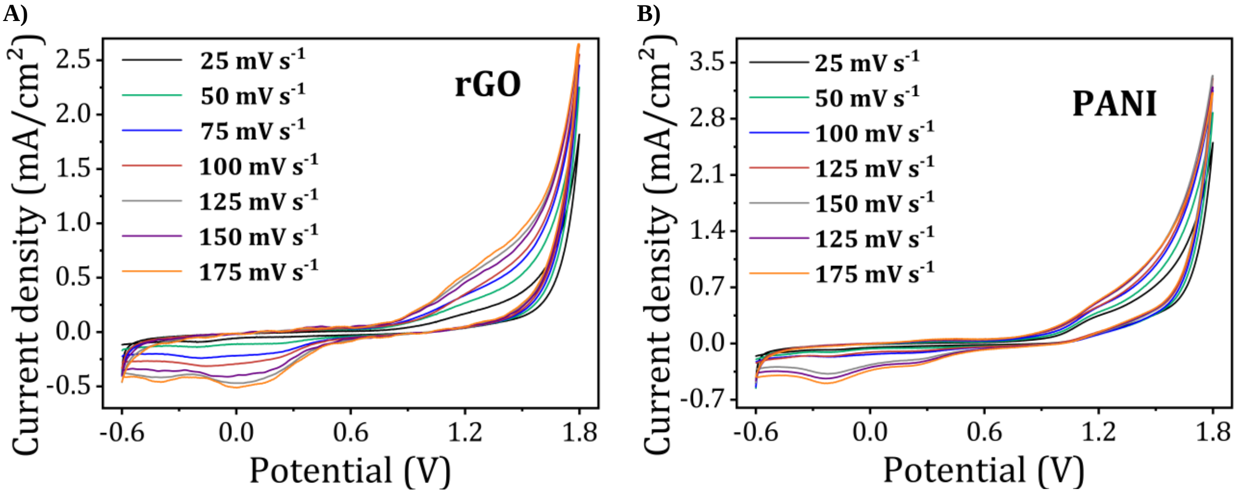

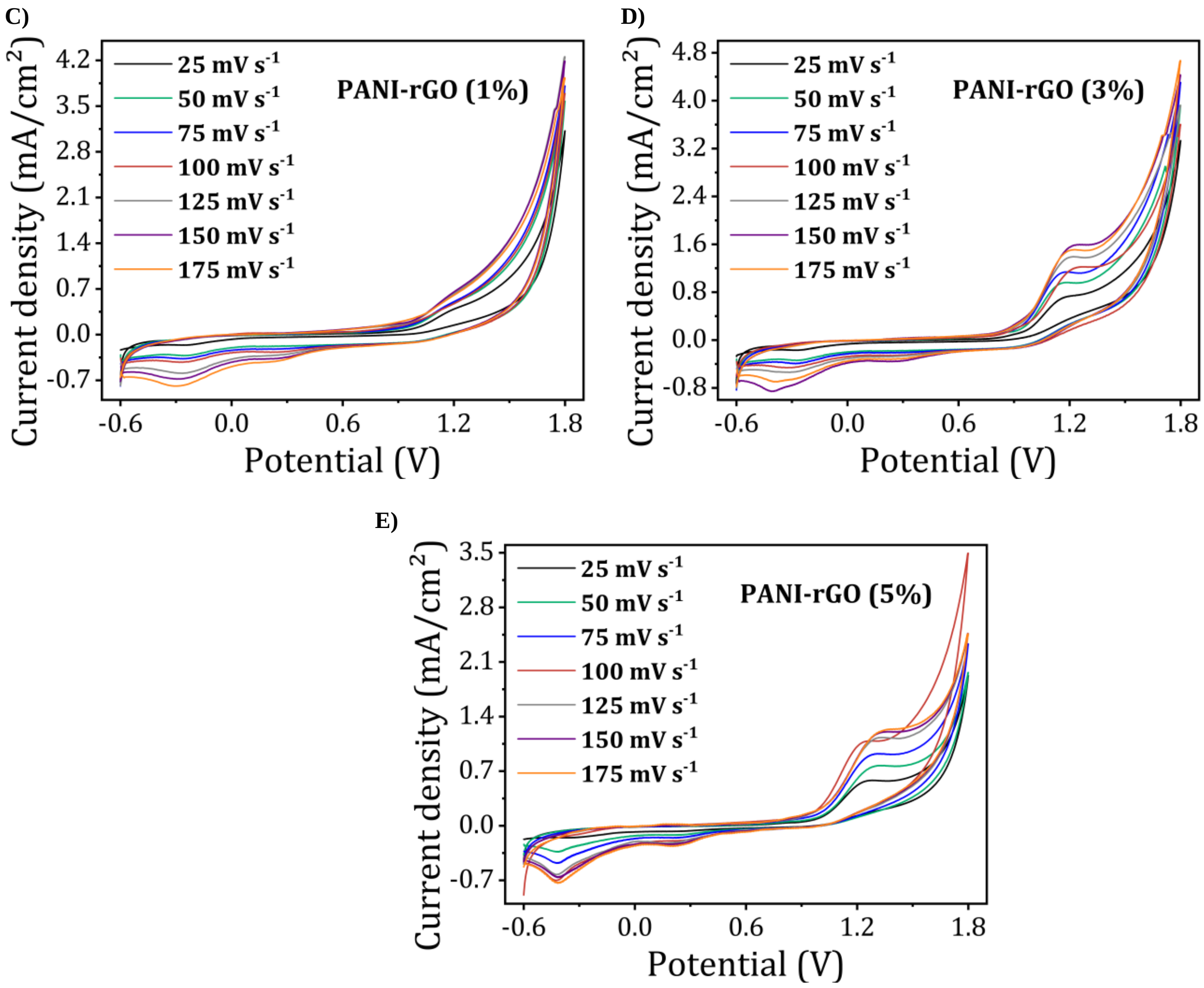

Figure IV.13. Cyclic voltammograms of A) rGO, B) PANI, and PANI/rGO nanocomposites (C, D, & E) at different scan rates.

Figure IV.14 offers an insightful evaluation by comparing the CV curves at a scan rate of 25 mV s^{-1} and the computed specific capacitances of pure PANI, rGO, and PANI/rGO nanocomposites. Notably, the trends in current density at 25 mV s^{-1} (Figure IV.14 (A)) and the specific capacitance (Figure IV.14 (B), as detailed in Table IV.5) align consistently. The order is as follows: PANI/rGO (3 *wt.*%) < PANI/rGO (1 *wt.*%) < PANI < PANI/rGO (5 *wt.*%) < rGO. At a scan rate of 25 mV s^{-1}, the PANI/rGO (3 *wt.*%) nanocomposite exhibits the highest specific capacitance, reaching a remarkable 145.79 F g^{-1}.

This finding underscores the exceptional electrochemical behavior of PANI/rGO (3 *wt.*%), which holds great promise for diverse sensor and energy storage applications.

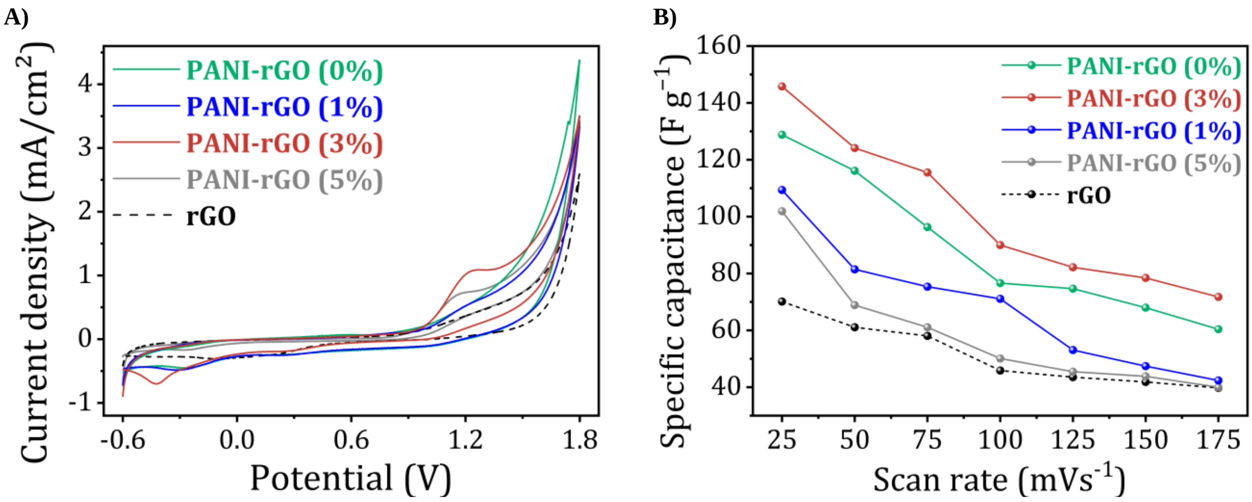

Figure IV.14. A) CV curves at a scan rate of 25 mV s^{-1} and B) the computed specific capacitance of rGO, pure PANI, and rGO/PANI nanocomposites across various scan rate.

Table IV.5. Specific capacities of pure PANI, rGO, and PANI/rGO at a scan rate of 25 mV s^{-1}.

Sample	Specific capacitance (F g^{-1})
PANI	101.87
PANI/rGO (1 *wt.*%)	128.80
PANI/rGO (3 *wt.*%)	**145.79**
PANI/rGO (5 *wt.*%)	109.36
rGO	70.13

IV.3.8. Thermo-gravimetric analysis (TGA)

Thermogravimetry analysis (TGA) proves instrumental in discerning dopants and water content within polymers, offering valuable insights into thermal degradation patterns, structural characteristics, and thermal stability (Veloso et al. 2022). The progressive degradation at each step of the curve can be delineated through the mass loss profile. Employing TGA, we investigated the thermal stability of rGO, PANI, and PANI/rGO from room temperature up to 1000 °C (Figure IV.15).

In the case of rGO, a significantly lower weight loss of approximately 11% was noted at 600 °C, demonstrating its heightened stability. The consistent weight reduction observed throughout the temperature spectrum emphasizes the enduring stability of rGO. The initial weight decline in rGO (~2%) below 100 °C is ascribed to the evaporation of adsorbed solvent molecules. Subsequently, a minor weight loss of ~5% and ~7% was observed in rGO between 100-300 °C and >300 °C, correspondingly. The gradual loss at temperatures exceeding 300 °C is linked to the elimination of more stable oxides, particularly –COOH groups, with the partial presence of oxides validating the successful preparation of rGO (Gebreegziabher et al. 2019).

In PANI, a weight loss approximately 260 °C links to the evaporation of moisture content and dopants, initiating the breakdown of the PANI backbone beyond 260 °C (Park et al. 2020). PANI/rGO experiences rapid mass loss at approximately 390 °C, attributed to the decomposition of oxygen-containing groups such as –OH, –CO–, and –COOH (Wang et al. 2013). Furthermore, Figure IV.15 depicts that the thermal stability of the nanocomposite is shifted towards elevated temperatures in contrast to pure PANI. While PANI experiences complete decomposition at 767 °C, PANI/rGO nanocomposites exhibit decomposition temperatures of 838, 870, and 878 °C for PANI/rGO at 1%, 3%, and 5% *wt*., respectively. This enhanced thermal stability can be attributed to the covalent bonding among rGO and the PANI backbone (Li and Zheng 2018). Moreover, these covalent bonds foster a substantial π–π stacking force amongst the basal plane of rGO and the PANI backbone, further reinforcing the nanocomposite's thermal stability (Gupta et al. 2016).

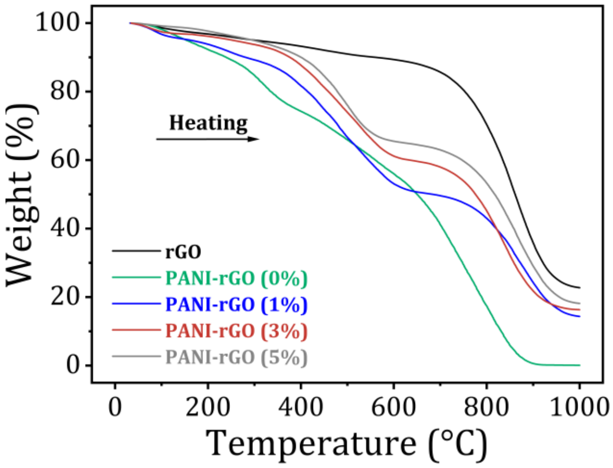

Figure IV.15. The TGA profiles of pure PANI, rGO, and PANI/rGO nanocomposites.

IV.3.10. Computational calculations

In the pursuit of advancing materials science and engineering, the choice of appropriate models for the constituents of a nanocomposite material is paramount. In this study, a specific model for PANI and a distinct model for rGO were selected to comprehensively investigate the PANI-rGO nanocomposite. The overarching aim of this study is to align computational results with experimental findings. By selecting these tailored models for PANI and rGO, we aim to compare and confirm our computational outcomes with experimental data, reinforcing the credibility and applicability of our calculations. This holistic approach bridges the gap between theory and practice, fostering a deeper understanding of the PANI-rGO nanocomposite's structural and electronic properties, with significant implications for materials design and engineering applications.

IV.3.10.1. Frontier molecular orbital (FMO) analysis

An advanced computational approach was employed to delve into the intricate interaction configurations and characteristics of PANI/rGO nanocomposites. Specifically, FMO analysis was utilized to pinpoint the most favorable interaction geometry. The optimized structures of PANI, rGO, and PANI/rGO are visually represented in Figure IV.16. This investigation revealed a compelling inclination of rGO to establish intimate contact with the nitrogen (N) atoms of PANI, significantly, Figure IV.16 (C) distinctly illustrates the close contact formed by rGO with the N atoms of PANI. These critical findings, illustrated in Figure IV.16, provide invaluable insights into the optimized geometry of both PANI, rGO and the PANI/rGO nanocomposite.

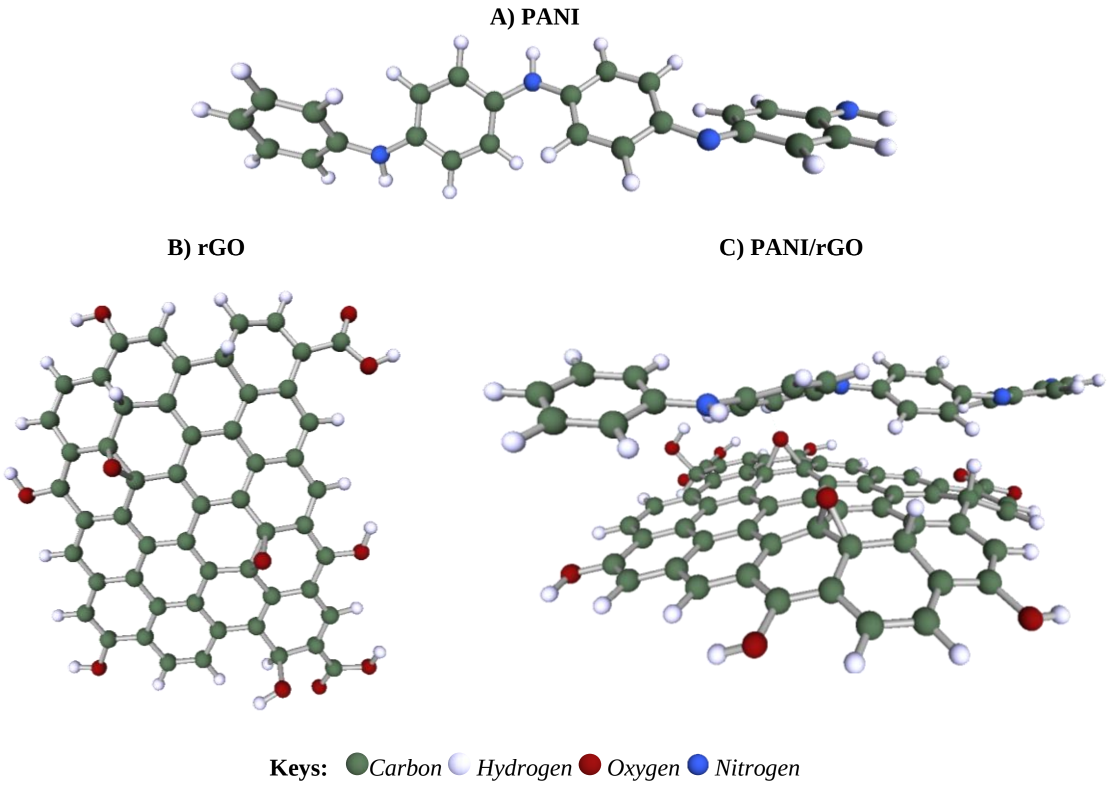

Figure IV.16. Optimized geometry for A) rGO sheet and B) PANI-rGO nanocomposite.

The interaction among rGO and PANI, as elucidated in the optimized structure, assumes paramount importance in comprehending the electronic and molecular characteristics of this nanocomposite material. To evaluate the comparative stability and reactivity of the optimized structures, a range of parameters were systematically computed. These parameters include the interaction energy, energies of the E_{HOMO}, E_{LUMO}, and E_g. The interaction energy was systematically evaluated by subtracting the electronic energies of the resulting complex from the electronic energies of the initial components. A negative interaction energy indicates the formation of the complex through an exothermic reaction (Boulechfar et al. 2023a; Yasmin et al. 2023) The determined interaction energy for the PANI/rGO nanostructures was 12.566 eV, suggesting that the formation of these structures was thermodynamically favorable.

Figure IV.17 provides a comprehensive overview of the E_{HOMO} and E_{LUMO}, along with the energy gap, for the PANI, rGO, and PANI-rGO structures, all meticulously optimized in their most stable forms. The energy gap of a molecular structure is widely acknowledged as a crucial indicator of its electron transport properties (Farooqi et al. 2020b). Specifically, a lower energy gap in molecular structures suggests enhanced ease of electron transport. As illustrated in Figure IV.17, the optimized configurations of PANI, rGO, and PANI-rGO exhibit energy gaps of 0.96 eV, 1.36 eV, and 2.15 eV, respectively. This observation aligns seamlessly with the experimental findings outlined in section V.3.5.1. This insight further underscores the potential of the PANI/rGO nanocomposite in facilitating efficient electron transport, a key attribute in various electronic applications.

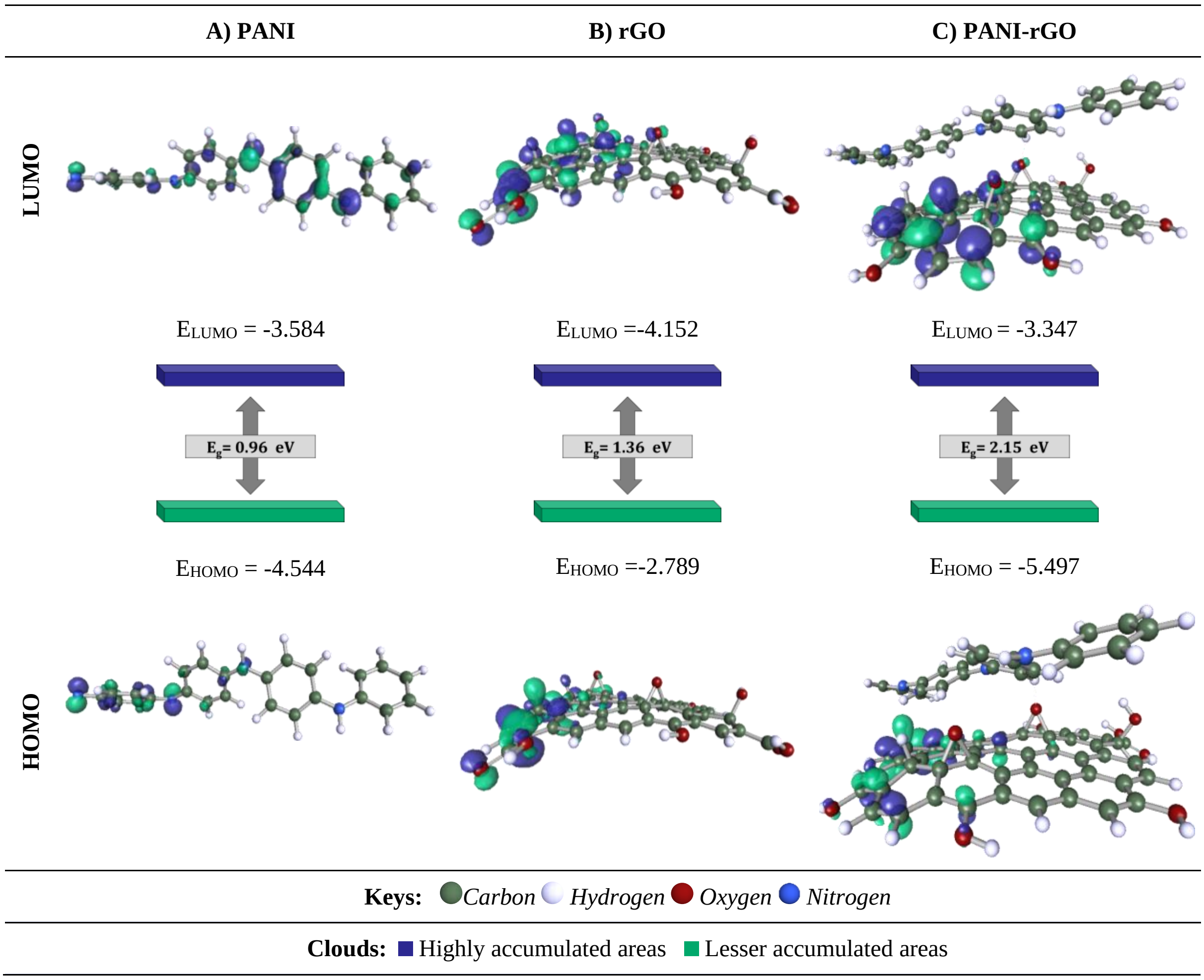

Figure IV.17. Frontier molecular orbitals of A) PANI, B) rGO and C) PANI-rGO nanocomposite.

IV.3.10.2. COSMO-RS approach

Unveiling the structure-property relationship within molecular structures stands as a primary objective of COSMO-RS. COSMO-RS, an advanced computational technique, utilizes quantum chemical computations and statistical thermodynamics to anticipate the thermodynamic attributes of both individual substances and their combinations (Lemaoui et al. 2021). It relies solely on details about the atoms in pure compounds, encompassing their geometry and charge shielding density, rendering it independent of experimental data (Paduszyński 2018; Lemaoui et al. 2023b). The COSMO-RS charge distribution in the interacting system of PANI, rGO, and PANI-rGO is visually depicted on the COSMO surfaces, as illustrated in Figure IV.18. Here, non-polar areas are represented in green, the acceptor of the hydrogen bond (HBA) location is shown in red, and the hydrogen bond donor is signified by the blue (HBD) region (Lemaoui et al. 2022; Mouffok et al. 2023; Boublia et al. 2023b).

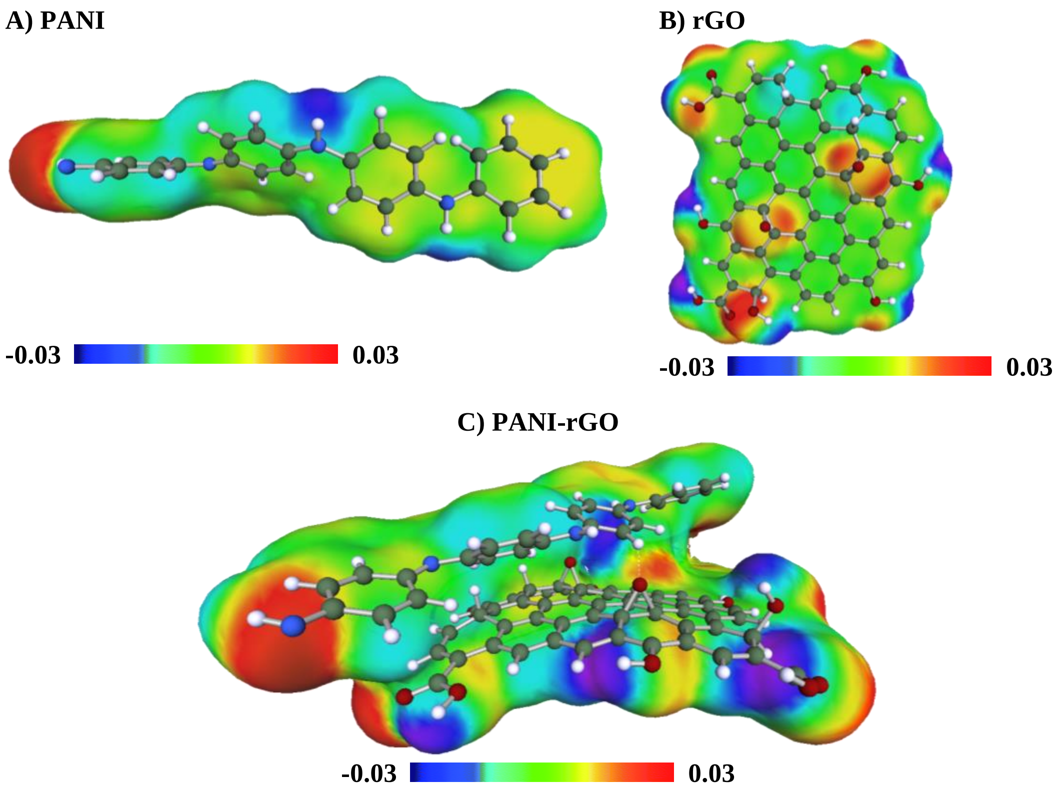

Keys: ● *Carbon* ○ *Hydrogen* ● *Oxygen* ● *Nitrogen*

Colors: ■ *highly positive* ■ *slightly positive* ■ *neutral* ■ *slightly negative* ■ *highly negative*

Figure IV.18. Optimized COSMO-RS 3D structures of PANI, rGO, and PANI-rGO models.

In chemistry, sigma profiles and sigma potentials (σ-profiles and σ-potentials, respectively) are fundamental tools for studying the distribution of electrostatic potential around molecules and ions. They are pivotal in characterizing a molecule's electronic structure and chemical properties, aiding in predicting reactivity, stability, and other key attributes (Kahlen et al. 2010; Szabo and Ostlund 2012). Within the COSMO-RS methodology, σ-profiles (P(σ)) offer graphical representations of charge shielding density on a molecular surface, providing insights into specific charge shielding densities in different regions. σ-potentials (μ(σ)), on the other hand, measure a molecule's interaction affinity by assessing the electrostatic potential energy at a exact point within the molecule, considering the surrounding solvent environment (Boublia et al. 2022b, 2023c; Mouffok et al. 2023). This metric helps evaluate the tendency of components in a mixture to interact with polar surfaces and establish hydrogen bonds. The electron density distribution is categorized into three regions: the HBD area ($\sigma < -0.0082\ e/Å^2$), the non-polar area ($-0.0082\ e/Å^2 < \sigma < 0.0082\ e/Å^2$), and the HBA area ($\sigma > 0.0082\ e/Å^2$). Positive μ(σ) values indicate a higher occurrence of repulsive interactions, while negative values indicate more significant interactions among molecules (Słupek et al. 2021). The horizontal axis, with increasing positive and negative values representing H-bond thresholds, delineates areas within a molecule where HBDs interact with HBAs (Man et al. 2017).

In this investigation, Figure IV.19 provides a compelling visualization of the σ-profiles as well as σ-potentials for both PANI and rGO, which offer profound insights into their unique characteristics.

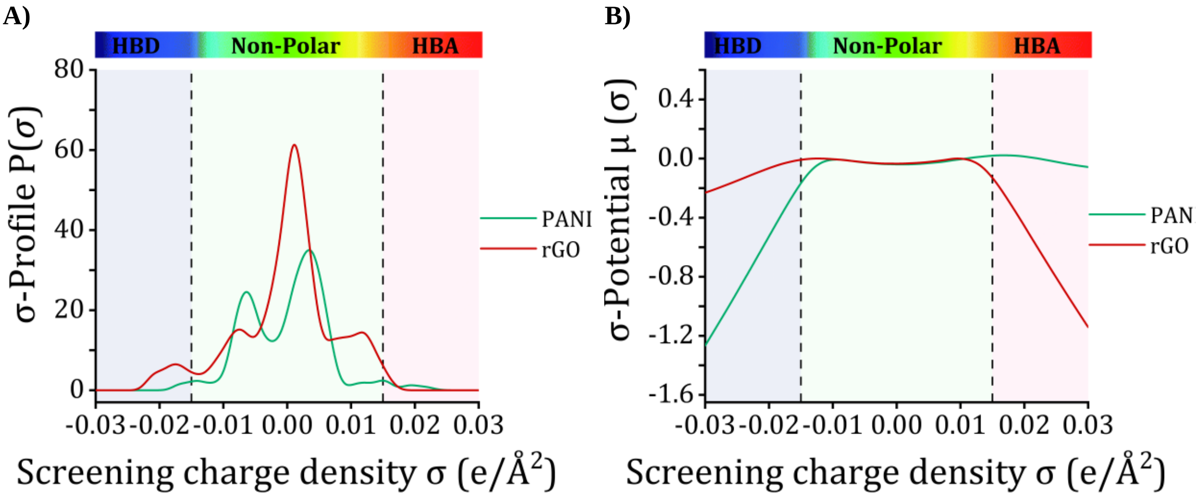

Figure IV.19. A) σ-profiles and B) σ-potentials derived by COSMO-RS for PANI and rGO models investigated in this study.

Upon scrutiny of the σ-profiles, it becomes evident that the PANI structure and rGO sheets predominantly exhibit nonpolar attributes, with discernible regions exhibiting a propensity for HBA, notably linked to the oxygen atoms within the rGO structure. Within the

P(σ), the central sector corresponds to nonpolar or weakly polar segments of the molecules, whereas the right-hand side reveals strongly polar areas, suggesting potential involvement in hydrogen bonding (Figure IV.19 (A)). On the left-hand side, HBD regions emerge. Within the carbon-rich zones, nonpolar characteristics prevail, denoted by the green regions in the surface charge distribution representations, signifying areas predominantly associated with exposed carbon atom surfaces. Peaks positioned within the HBA regions link to the presence of oxygen atoms, depicted as red areas in the surface charge density; for rGO, this red area is correlated with the epoxy groups (as observed in Figure IV.18 (B)). In contrast, peaks within the HBS area of the σ-profile align with hydrogen atoms present in the alkyl side chains and hydroxyl groups, illustrated as light blue areas (Prías Barragán et al. 2020). Moreover, a meticulous examination of the σ-potentials emphasizes that the primary interaction between PANI and rGO transpires within the polar region, encompassing both HBA and HBD sites. This phenomenon can be largely attributed to rGO's demonstrated capacity to establish hydrogen bonds, as indicated by positive μ(s) values (Behloul et al. 2022; Boulechfar et al. 2023b, a). Additionally, it is worth noting that viable interactions are not confined solely to the polar realm; they can also manifest within the nonpolar area, where rGO exhibits a negative μ(s) value (Figure IV.19 (B)). This observation underscores the intricate nature of the interaction between PANI and rGO, which bridges both polar and nonpolar domains. Accordingly, the σ-profiles and σ-potentials of these distinct compounds provide appreciated insights into their chemical composition, accounting for polarization and their potential for hydrogen bonding. This comprehensive understanding significantly augments our understandings into the plausible interactions among the targeted PANI and rGO structures.

IV.3.10.3. Non-covalent interaction (NCI) analysis

NCI analysis is an advanced theoretical approach widely used to unravel intermolecular interactions and characterize weak forces in molecular systems. This method employs visualization indicators based on electron density and appropriate metrics color-coded to represent the strength of these interactions using RDG values at low electron densities (Zhang et al. 2021; Murmu et al. 2022). The NCI method assesses the electron density (ρ) by multiplying it with the sign of the second-highest eigenvalue (λ_2) of the Hessian matrix of the electron density at each point on the isosurface (Ferkous et al. 2023). This product, represented as $(\lambda_2) \times \rho$, serves as a valuable indicator of whether intermolecular forces are attractive or repulsive. A negative sign of $(\lambda_2) \times \rho$ signifies basically attractive interactions, often linked with the formation of H-bonds, which are crucial in molecular associations. Conversely, a positive sign of $(\lambda_2) \times \rho$ indicates the presence of steric repulsion or non-bonding interactions, which are essential for understanding how molecules interact while maintaining their structural integrity (Zhang et al. 2021; Adekoya et al. 2022).

Figure IV.20 illustrates the NCI-RDG plots resulting from the density analysis of PANI, rGO, and their interaction (PANI/rGO). In this context, hydrogen bonding, van der Waals forces, and steric repulsive interactions are respectively represented by the colors blue, green, and red. The RDG isovalue, ranging from 0.035 to 0.020 a.u., along with the sign of provides insights into the strength and nature of these interactions. For PANI, the analysis indicates intramolecular van der Waals forces, noticeable as green surfaces in the 3D plot, with a spike at -0.01 (a.u.) in the 2D s(ρ) plot. The rest of the spikes are linked with repulsive forces with PANI, and no strong electrostatic forces are observed. In the case of PANI/rGO, a cluster of RDG spikes lies among 0.00 and 0.01 (a.u.), representing weak forces, also revealed as green iso surfaces in the 3D plot. Similar to PANI, no strong electrostatic forces are observed between PANI and rGO in the PANI/rGO. It is primarily VDW forces that contribute to the formation and stability of the PANI-rGO nanocomposite.

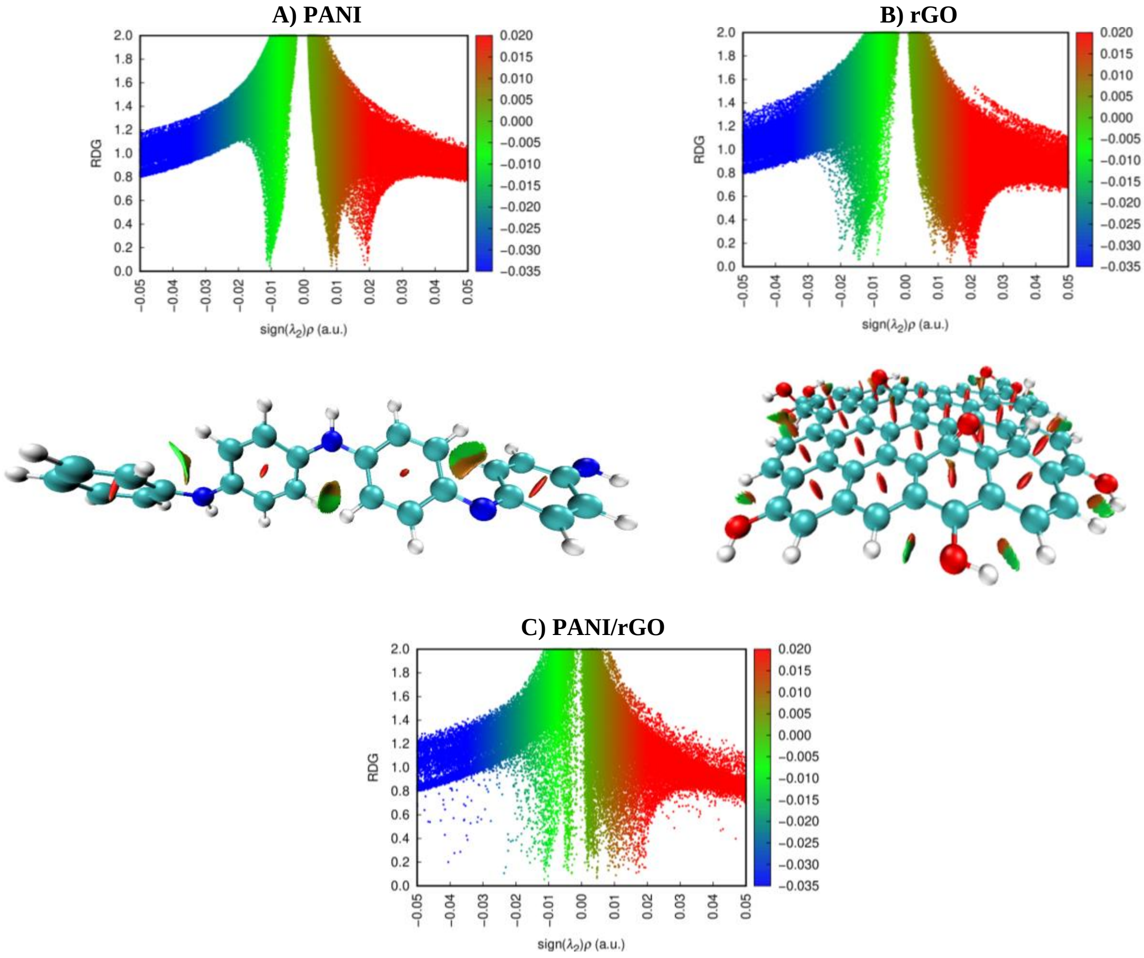

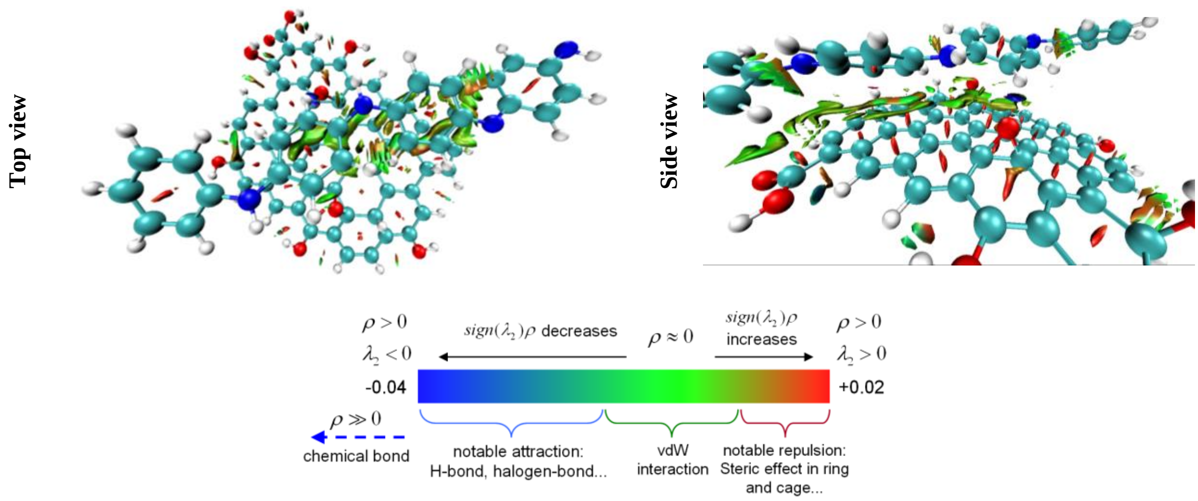

Figure IV.20. Scatter plots for RDG (upper) and NCI (bottom) isosurfaces (*s* = 0.5 a.u.) of A) PANI, B) rGO, and C) PANI/rGO isosurfaces (IGM = 0.01 a.u.). The isosurfaces' colors correspond to the sign values (λ_2) ρ, ranging from −0.05 to 0.05 a.u.

IV.3.10.4. Quantum theory of atoms in molecules (QTAIM) results

The QTAIM framework serves as a robust computational tool for characterizing the strength and nature of interactions among chemical compounds (Fuster and Grabowski 2011; Popelier 2014; Gabsi et al. 2023). Within Figure IV.21, we present representations of the PANI/rGO system, highlighting the presence of bond critical points (BCPs) and bond paths. The existence of BCPs in each system substantiates the transfer of electron density and unequivocally approves the establishment of chemical bonds among PANI and rGO. To pinpoint BCPs with precision, we identify the (3, 1) CPs, also recognized as saddle points, situated among interacting atoms of two fragments or along the path connecting analyte atoms to the surface (Garg and Goel 2023). BCPs play a pivotal role in probing non-covalent interactions within two-fragment systems. By employing BCPs, we can assess critical parameters including electron density (ρ(r)), Laplacian of the electron density ($\Delta^2\rho(r)$), potential energy density (V(r)), Lagrangian kinetic energy (G(r)), and total energy density (H(r)). The values of these parameters at BCPs are meticulously outlined in Table IV.6. To investigate the strength of intermolecular bonds among PANI and rGO, we classify them based on the and H(r) values. Positive and negative values for both parameters signify weak and strong interactions, correspondingly. In contrast, a negative H(r) combined with a positive denotes medium-strength interactions (Sattar et al. 2022).

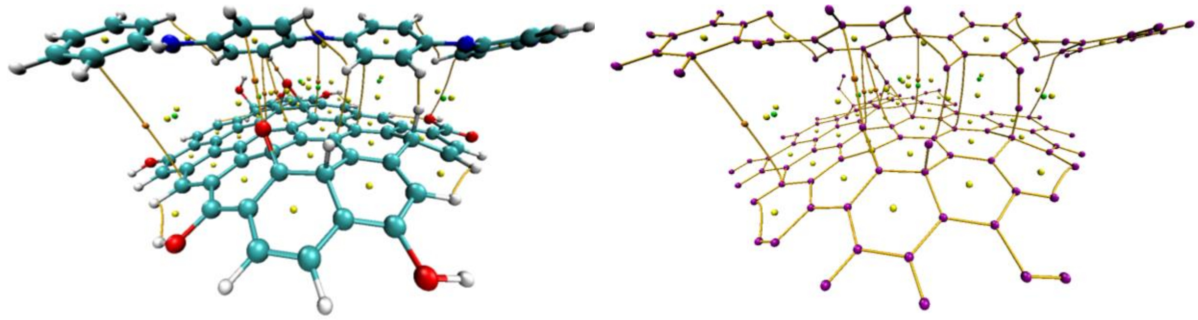

Figure IV.21. QTAIM molecular graphs showing bond paths and critical points for PANI/rGO complex. Orange, yellow, and green dots signify BCP points, ring-critical points, and cage-critical points, correspondingly.

Table IV.6. QTAIM characteristics of the interaction sites (in a.u.) at selected BCPs in PANI/rGO complex.

BCP	**X Y**	**ρ(r)**	**$\Delta^2\rho(r)$**	**V(r)**	**G(r)**	**|V(r)|/G(r)**	**H(r)**
164	91(C) -- 40(C)	0.000274	0.001532	-0.000132	0.000257	-0.511626	0.000126
175	54(O) -- 97(C)	0.005454	0.018768	-0.003213	0.003952	-0.812856	0.000740
247	100(C) -- 32(C)	0.004964	0.000702	-0.002328	0.003031	-0.768261	0.000702
248	100(C) -- 33(C)	0.004954	0.015022	-0.002333	0.003044	-0.766277	0.000711
274	102(N) -- 21(C)	0.004138	0.012777	-0.002290	0.002742	-0.835106	0.000452
284	125(H) -- 88(O)	0.041559	0.176644	-0.041626	0.042893	-0.970443	0.001268

As detailed in Table IV.6, reveal significant insights into the nature of interactions within the PANI-rGO system. Notably, ρ(r) values with positive indicative of hydrogen bond interactions, prominently illustrated in the case of 125(H) -- 88(O). Furthermore, the analysis indicated that rGO demonstrated a pronounced tendency to closely interact with the nitrogen (N) atoms of PANI, illustrated by the BCP of 274: 102(N) -- 21(C). This observation aligns with the concept that the electrons' tendency to combine, denoted as V(r), is outweighed by their propensity to disperse, represented by G(r), as showed by the |V(r)|/G(r) ratio being less than 1. This ratio, G(r)/|V(r)|, can further serve to anticipate atomic interactions: a G(r)/|V(r)| exceeding 1 suggests noncovalent electrostatic interactions, while a range of 0.5 < G(r)/|V(r)| < 1 indicates covalent interactions, and values within 0.5 < G(r)/|V(r)| < 0 point to highly covalent interactions (Sattar et al. 2022). The G(r)/|V(r)| values of PANI-rGO system are consistently < 0, indicative of an electrostatic type of interaction throughout PANI and rGO sheets. This comprehension offers valuable insights into the bonding interactions' nature within these systems and illuminates their potential in nanocomposite technology.

IV.4. Conclusion

In the current work, we achieved the successful synthesis of PANI/rGO nanocomposites through an *in-situ* chemical polymerization process facilitated by a deep eutectic solvent (DES) serving as an electrolyte. A thorough investigation was conducted, integrating Response Surface Methodology (RSM), Artificial Neural Networks (ANN), and molecular modeling techniques for the comprehensive modeling, optimization, and characterization of PANI/rGO nanocomposites. The collaborative implementation of optimization methods and meticulous characterization uncovered profound insights into the multifaceted characteristics of these nanocomposites. From this integrative approach, several key outcomes have emerged:

- RSM analysis elucidated the impact of APS/ANI molar ratio, rGO loading, and polymerization time on electrical conductivity, culminating in a second-order polynomial function. Optimal conditions for maximum electrical conductivity were identified as an APS/ANI molar ratio of 0.75, 3 *wt.%* rGO loading, and a 6-hour polymerization time, yielding a high conductivity of 4.975×10^{-3} S cm^{-1}. ANN analysis exhibited enhanced conductivity of 4.988×10^{-3} S cm^{-1}, showcasing the superior predictive accuracy of the ANN model over RSM.
- Comprehensive characterization through UV-vis, PL, Raman, FTIR, and XRD elucidated significant structural changes in PANI/rGO nanocomposites, emphasizing the transformative impact of rGO on PANI.
- XPS analysis unveiled distinctive elemental compositions, with the deconvolution of C 1s spectra highlighting intensified C-N peaks in PANI/rGO, indicating a denser nanocomposite coating and promising structural enhancements.
- Electrochemical studies through cyclic voltammetry showcased superior capacitance in PANI/rGO, reaching an impressive 145.79 F g^{-1}, surpassing individual PANI or rGO components.
- TGA analysis affirmed the enhanced thermal stability of PANI/rGO, with decomposition temperatures notably higher than pure PANI, attributed to synergistic covalent bonding and substantial π–π stacking forces.
- Molecular-level insights through FMO, COSMO-RS, NCI, and QTAIM analyses provided a nuanced understanding of the PANI-rGO system, highlighting the dominant role of VDW forces in nanocomposite formation and stability.

Conclusion and Future Perspectives

Conclusion and Future Perspectives

This dissertation, conducted throughout the PhD research, centered on developing multifunctional, eco-friendly nanocomposites using polyaniline (PANI) and functionalized graphene. Aiming to deeply understand these materials, the research integrated experimental methodologies with computational and machine learning techniques. The primary goal was to clarify the complexities of PANI/graphene nanocomposites, focusing on synthesis, structural characterization, and performance enhancement. Each chapter systematically contributes to this goal, weaving a narrative that reveals the sophisticated processes in the synthesis, characterization, and enhancement of these nanocomposites.

Summary of The Thesis

The thesis starts with a detailed review of PANI and graphene-based nanocomposites, emphasizing their significance in electrical conductivity and gas sensing, and highlighting recent research progress. This is complemented by an exploration of the integration of computational and experimental techniques in polymer nanocomposite research. The synergy of machine learning with experimental design unfolds new potential in optimizing PANI/graphene nanocomposites, enhancing our grasp of their complex structural, morphological, and electrochemical traits.

A notable contribution of this PhD thesis is the development of new holistic models for predicting the electrical conductivity and gas-sensing responses of PANI/graphene nanocomposites. This breakthrough modeling approach sets a new standard in material science, showcasing the potential of these models in guiding future nanocomposite technology research and applications.

Thus, key achievements include:

- A detailed review of PANI and graphene-based nanocomposites, highlighting their electrical conductivity and gas sensing capabilities. This included a focus on recent advancements and the exploration of gas detection mechanisms.
- The integration of computational and experimental techniques in polymer nanocomposite research. This involved combining machine learning with experimental design to optimize PANI/graphene nanocomposites, enhancing understanding of their structural, morphological, and electrochemical attributes.

- The introduction of the first ML models for predicting electrical conductivity and gas-sensing responses in PANI/graphene nanocomposites. This marked a major milestone in material science, demonstrating the models' potential to accurately map nanocomposite properties.
- Successful synthesis of PANI/graphene nanocomposites using *in-situ* chemical polymerization with a deep eutectic solvent and extensive characterization to understand their structural and electrochemical properties.
- The thorough applicability domain analysis underscored the robustness and dependability of the ANN models within specific parameter ranges, emphasizing their practical relevance in the development of high-performance materials.
- The research effectively synthesized PANI/rGO nanocomposites, employing *in-situ* chemical polymerization with a deep eutectic solvent. Comprehensive characterization techniques provided detailed insights into their structural and electrochemical properties
- Employing RSM, ANN, and molecular simulations for optimizing electrical conductivity and performance of the nanocomposites.

Overall, this thesis offers a comprehensive understanding into the advanced applications of PANI and graphene-based nanocomposites, bridging the gap between advanced material science and sustainable applications. It stands as a testament to innovative approaches in synthesizing, characterizing, and optimizing these nanocomposites, thereby unlocking their potential in diverse areas like supercapacitors, gas sensors, and energy storage systems. This body of work not only propels forward the domain of sustainable materials science but also paves the way for future technological breakthroughs in nanocomposite applications.

Innovative Contributions to The Field

The innovative contributions of this dissertation in the field of PANI/graphene nanocomposites are multi-dimensional, reflecting a comprehensive integration of methodologies and insights:

- **Development of Predictive Models:** A ground-breaking achievement in this research is the development of a robust ML model. This model, a first of its kind, adeptly predicts the electrical conductivity and gas-sensing properties of PANI/graphene nanocomposites, establishing a new benchmark in polymer science modeling.
- **Advanced Synthesis Techniques:** The thesis marks significant advancements in synthesis methods, notably *in-situ* polymerization utilizing deep eutectic solvents. This approach

enhances the interaction between PANI and rGO, yielding nanocomposites with superior structural and functional attributes.

- **Synergy of Computational and Experimental Techniques:** A notable innovation is the harmonious blend of computational models, including ANNs, with traditional experimental approaches. This integration has led to increased precision in predictions and greater customization possibilities in nanocomposite development.
- **Comprehensive Characterization and Electrochemical Analysis:** The thesis provides an in-depth exploration of various characterization techniques, offering detailed insights into the structural, morphological, and electrochemical properties of PANI/graphene nanocomposites.
- **Molecular Simulation Insights:** Employing advanced techniques like DFT and MD simulations, the research deepens our understanding of charge transfer mechanisms and molecular interactions within these materials.

Future Works

In the future research and development, we believe that the following aspects are worth further efforts:

1. Expanding Applications

Future research directions will explore the extensive applications of PANI/graphene nanocomposites in diverse fields. Central to these endeavors will be the empirical assessment of the gas-sensing capabilities of our PANI/rGO nanocomposites. This experimental validation will serve to substantiate the theoretical models, bridging the gap between computational predictions and real-world effectiveness. By doing so, the research will not only broaden the practical applications of these nanocomposites but also contribute significantly to areas of sustainable development and environmental monitoring. Additionally, this hands-on approach will pave the way for further innovations in nanocomposite technology, driving forward the frontiers of materials science.

2. Advanced Material Design

Future advancements in this research will focus on the innovative design of PANI/graphene nanocomposites, with a particular emphasis on refining synthesis techniques and exploring new graphene derivatives. A key area of exploration will be the experimental functionalization of graphene and rGO using deep eutectic solvents. This approach aims to enhance the performance and broaden the utility of these nanocomposites. By strategically modifying the surface chemistry of graphene, it is expected that these alterations will lead to substantial improvements in the properties of the nanocomposites, potentially unlocking new applications across various fields. This strategic functionalization, combined with the use of deep eutectic solvents, presents an exciting opportunity to push the boundaries of material science in novel and sustainable ways.

3. Interdisciplinary Approaches

In the future, this research will explore an array of interdisciplinary approaches to further advance the field of polymer nanocomposites. One key area will be the exploration of diverse machine learning models to enhance predictive capabilities and optimize material properties of PANI/graphene systems. Additionally, molecular dynamics simulations will be undertaken to gain deeper insights into the nanoscale interactions and behaviors of these materials. This combined computational-experimental strategy will enable us to develop more sophisticated and effective solutions for complex material science challenges, pushing the boundaries of what's achievable in the realm of advanced nanocomposites.

4. Sustainability and Eco-Friendliness

This research will strongly emphasize sustainability and eco-friendliness, aligning with the urgent need for environmental responsibility and technological advancements. This approach will involve developing PANI/graphene nanocomposites using sustainable methods and materials, with a keen focus on reducing environmental impact. The exploration will include identifying and employing green synthesis techniques, integrating renewable resources, and minimizing waste and toxic by-products. By prioritizing eco-friendly practices and materials, the research aims to contribute significantly to sustainable development, addressing the global environmental challenges.

This PhD thesis underscores the significance of interdisciplinary approaches in propelling polymer nanocomposite science. It lays a solid groundwork for further investigations and innovations within material science and engineering. By combining various scientific methodologies, this PhD thesis not only enhances our comprehension of PANI/graphene nanocomposites but also paves the way for new technological advancements in this ever-evolving domain.

Appendix

Appendix

Appendix A

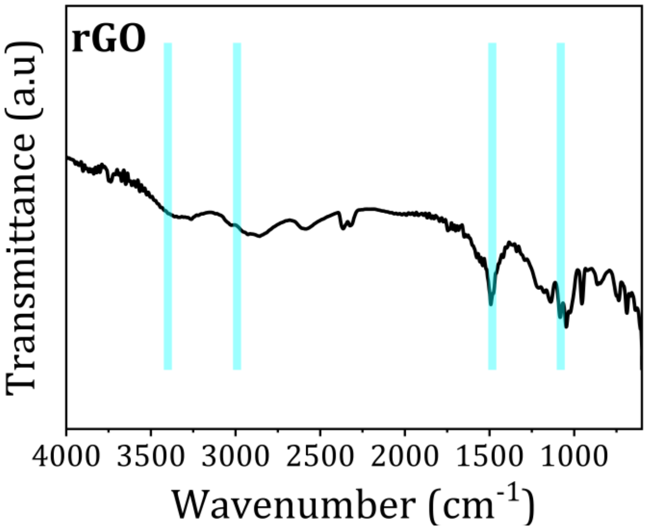

Figure A.1. FT-IR spectra showing the various functional groups present in rGO.

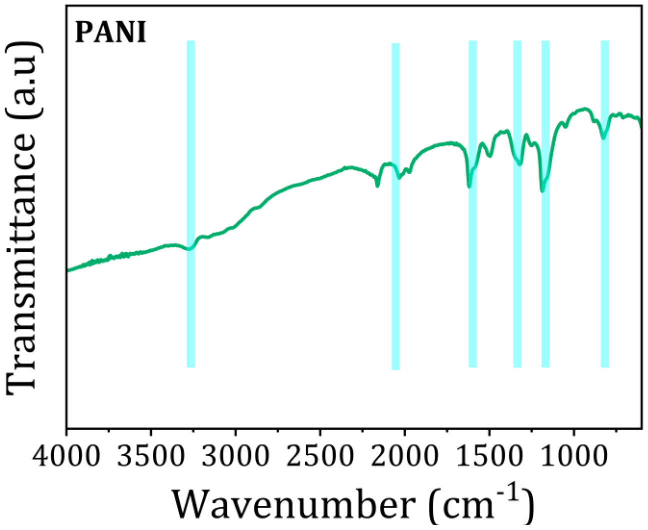

Figure A.2. FT-IR spectra showing the various functional groups present in pure PANI.

Appendix B

The main results of this PhD work have been published in papers:

B.1. Publication of Chapter I

CRITICAL REVIEWS IN SOLID STATE AND MATERIALS SCIENCES
https://doi.org/10.1080/10408436.2023.2274900

Taylor & Francis
Taylor & Francis Group

REVIEW ARTICLE

Check for updates

The curious case of polyaniline-graphene nanocomposites: a review on their application as exceptionally conductive and gas sensitive materials

Abir Boublia[a], Zahir Guezzout[b], Nacerddine Haddaoui[a], Michael Badawi[c], Ahmad S Darwish[d], Tarek Lemaoui[e], Seif El Islam Lebouachera[f,g], Krishna Kumar Yadav[h,i], Maha Awjan Alreshidi[j], Jari S. Algethami[k,l], Mohamed Abbas[m], Fawzi Banat[d], Inas M AlNashef[d], Byong-Hun Jeon[n], and Yacine Benguerba[e]

[a]Laboratoire de Physico-Chimie des Hauts Polymères (LPCHP), Département de Génie des Procédés, Faculté de Technologie, Université Ferhat ABBAS Sétif-1, Sétif, Algeria; [b]Unité de Recherche sur les Matériaux Emergents –Sétif- URMES, Equipe de Valorisation Des Polymères, Université Ferhat ABBAS Sétif-1, Sétif, Algeria; [c]Laboratoire de Physique et Chimie Théoriques (LPCT), UMR 7019 CNRS, Université of Lorraine, Nancy, France; [d]Department of Chemical Engineering, Khalifa University of Science and Technology, Abu Dhabi, United Arab Emirates (UAE); [e]Laboratoire de Biopharmacie Et Pharmacotechnie (LPBT), Ferhat Abbas Sétif 1 University, Sétif, Algeria; [f]Université de Pau Et Des Pays de L'Adour, E2S UPPA, CNRS, Total Energies, LFCR, Allée du Parc Montaury, Anglet, France; [g]Institut des Sciences Analytiques et de Physico-Chimie pour l'Environnement et les Matériaux, IPREM, UMR 5254, CNRS Université de Pau et des Pays de l'Adour/E2S, 2 Avenue P. Angot, Technopôle Hélioparc, Pau, France; [h]Faculty of Science and Technology, Madhyanchal Professional University, Bhopal, India; [i]Environmental and Atmospheric Sciences Research Group, Scientific Research Center, Al-Ayen University, Nasiriyah, Iraq; [j]Department of Chemistry, University of Hail, Hail, Saudi Arabia; [k]Department of Chemistry, College of Science and Arts, Najran University, Najran, Saudi Arabia; [l]Advanced Materials and Nano-Research Centre (AMNRC), Najran University, Najran, Saudi Arabia; [m]Electrical Engineering Department, College of Engineering, King Khalid University, Abha, Saudi Arabia; [n]Department of Earth Resources & Environmental Engineering, Hanyang University, Seoul, Republic of Korea

ABSTRACT
This review presents a brief overview of the electrical and gas-sensor properties of polyaniline (PANI) and graphene-based nanocomposites, their application as gas detection materials, and their underlying sensing mechanisms. Several studies have shown that graphene-based PANI gas sensors perform remarkably well at ambient temperatures, are energy efficient, and are inexpensive. The electrical and gas sensing properties of PANI/graphene nanocomposites offer improved responsiveness, durability, and other detection capabilities in sensor-based devices at room temperature. Moreover, the electrical conductivity and gas sensor properties may be controlled by the synthesis methods and the form and type of graphene. This review provides a new framework for the development of new nanomaterials based on PANI/graphene, which will advance their development and industrialization in the environment.

KEYWORDS
PANI/graphene nanocomposites; graphene; electrical properties; gas sensing properties

GRAPHICAL ABSTRACT

CONTACT Krishna Kumar Yadav envirokrishna@gmail.com

B.2. Publication of Chapter II

Polymer Bulletin
https://doi.org/10.1007/s00289-022-04398-6

REVIEW PAPER

State-of-the-art review on recent advances in polymer engineering: modeling and optimization through response surface methodology approach

Abir Boublia[1] · Seif El Islam Lebouachera[2] · Nacerddine Haddaoui[1] · Zahir Guezzout[3] · Mohammed Abdelfetah Ghriga[4] · Mahdi Hasanzadeh[5] · Yacine Benguerba[6] · Nadjib Drouiche[7]

Received: 14 March 2022 / Revised: 2 June 2022 / Accepted: 22 June 2022

Abstract

Composites, blends, and polymer membranes are all examples of processes that may benefit from response surface methodology (RSM) to optimize material characteristics. RSM is a convenient technique for determining the effect of several variables and their interactions on single or multiple response variables. The theoretical foundations and practical applications of RSM including the advantages and disadvantages of some design models are thoroughly explained. The RSM technique is shown to be relevant for the first time in polymer science and engineering research. We'll divide it into three sections: RSM may be used in some scenarios for polymerization, manufacturing, and evaluating the characteristics of polymers. The paper also compares RSM and other optimization techniques to an artificial neutral network. This review should be beneficial to anyone involved in polymer RSM and optimization.

Graphical abstract

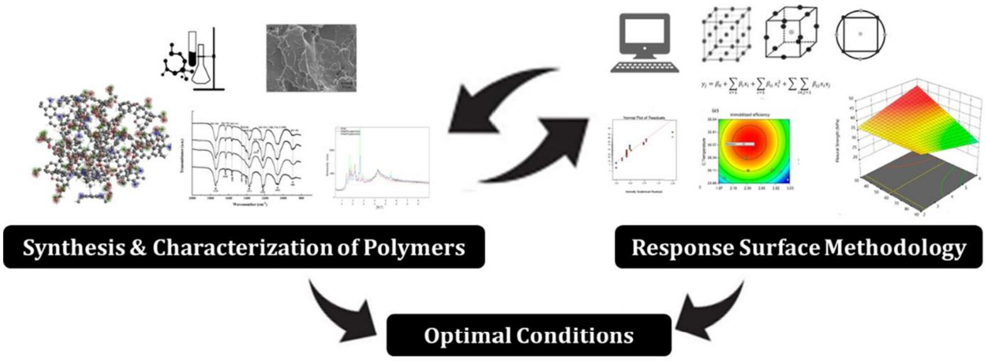

Extended author information available on the last page of the article

B.3. Publication of Chapter III

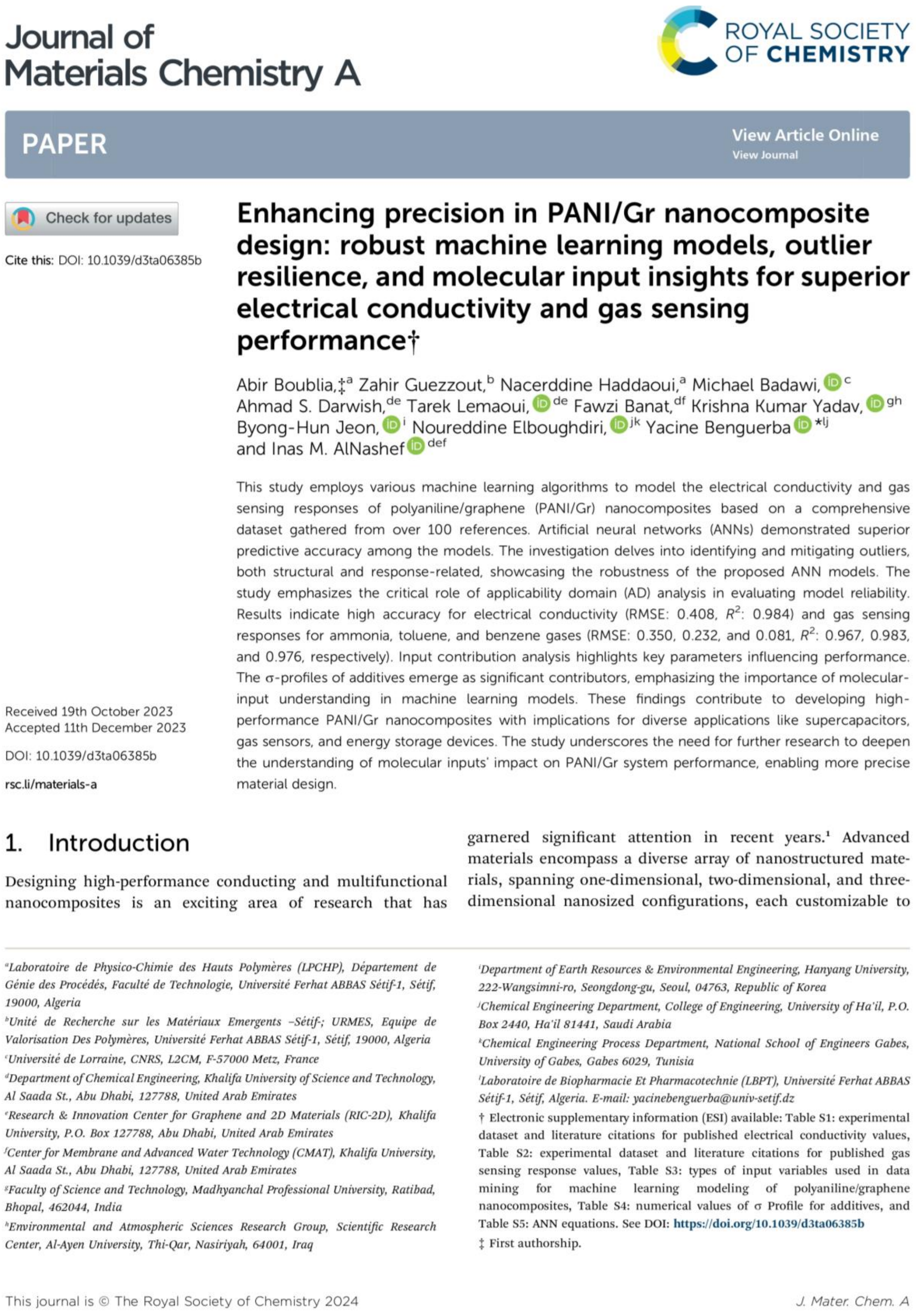

Journal of
Materials Chemistry A

ROYAL SOCIETY
OF CHEMISTRY

PAPER

View Article Online
View Journal

Check for updates

Cite this: DOI: 10.1039/d3ta06385b

Enhancing precision in PANI/Gr nanocomposite design: robust machine learning models, outlier resilience, and molecular input insights for superior electrical conductivity and gas sensing performance†

Abir Boublia,‡[a] Zahir Guezzout,[b] Nacerddine Haddaoui,[a] Michael Badawi,[c]
Ahmad S. Darwish,[de] Tarek Lemaoui,[de] Fawzi Banat,[df] Krishna Kumar Yadav,[gh]
Byong-Hun Jeon,[i] Noureddine Elboughdiri,[jk] Yacine Benguerba*[lj]
and Inas M. AlNashef[def]

This study employs various machine learning algorithms to model the electrical conductivity and gas sensing responses of polyaniline/graphene (PANI/Gr) nanocomposites based on a comprehensive dataset gathered from over 100 references. Artificial neural networks (ANNs) demonstrated superior predictive accuracy among the models. The investigation delves into identifying and mitigating outliers, both structural and response-related, showcasing the robustness of the proposed ANN models. The study emphasizes the critical role of applicability domain (AD) analysis in evaluating model reliability. Results indicate high accuracy for electrical conductivity (RMSE: 0.408, R^2: 0.984) and gas sensing responses for ammonia, toluene, and benzene gases (RMSE: 0.350, 0.232, and 0.081, R^2: 0.967, 0.983, and 0.976, respectively). Input contribution analysis highlights key parameters influencing performance. The σ-profiles of additives emerge as significant contributors, emphasizing the importance of molecular-input understanding in machine learning models. These findings contribute to developing high-performance PANI/Gr nanocomposites with implications for diverse applications like supercapacitors, gas sensors, and energy storage devices. The study underscores the need for further research to deepen the understanding of molecular inputs' impact on PANI/Gr system performance, enabling more precise material design.

Received 19th October 2023
Accepted 11th December 2023

DOI: 10.1039/d3ta06385b

rsc.li/materials-a

1. Introduction

Designing high-performance conducting and multifunctional nanocomposites is an exciting area of research that has garnered significant attention in recent years.[1] Advanced materials encompass a diverse array of nanostructured materials, spanning one-dimensional, two-dimensional, and three-dimensional nanosized configurations, each customizable to

---

[a] Laboratoire de Physico-Chimie des Hauts Polymères (LPCHP), Département de Génie des Procédés, Faculté de Technologie, Université Ferhat ABBAS Sétif-1, Sétif, 19000, Algeria

[b] Unité de Recherche sur les Matériaux Emergents –Sétif-; URMES, Equipe de Valorisation Des Polymères, Université Ferhat ABBAS Sétif-1, Sétif, 19000, Algeria

[c] Université de Lorraine, CNRS, L2CM, F-57000 Metz, France

[d] Department of Chemical Engineering, Khalifa University of Science and Technology, Al Saada St., Abu Dhabi, 127788, United Arab Emirates

[e] Research & Innovation Center for Graphene and 2D Materials (RIC-2D), Khalifa University, P.O. Box 127788, Abu Dhabi, United Arab Emirates

[f] Center for Membrane and Advanced Water Technology (CMAT), Khalifa University, Al Saada St., Abu Dhabi, 127788, United Arab Emirates

[g] Faculty of Science and Technology, Madhyanchal Professional University, Ratibad, Bhopal, 462044, India

[h] Environmental and Atmospheric Sciences Research Group, Scientific Research Center, Al-Ayen University, Thi-Qar, Nasiriyah, 64001, Iraq

[i] Department of Earth Resources & Environmental Engineering, Hanyang University, 222-Wangsimni-ro, Seongdong-gu, Seoul, 04763, Republic of Korea

[j] Chemical Engineering Department, College of Engineering, University of Ha'il, P.O. Box 2440, Ha'il 81441, Saudi Arabia

[k] Chemical Engineering Process Department, National School of Engineers Gabes, University of Gabes, Gabes 6029, Tunisia

[l] Laboratoire de Biopharmacie Et Pharmacotechnie (LBPT), Université Ferhat ABBAS Sétif-1, Sétif, Algeria. E-mail: yacinebenguerba@univ-setif.dz

† Electronic supplementary information (ESI) available: Table S1: experimental dataset and literature citations for published electrical conductivity values, Table S2: experimental dataset and literature citations for published gas sensing response values, Table S3: types of input variables used in data mining for machine learning modeling of polyaniline/graphene nanocomposites, Table S4: numerical values of σ Profile for additives, and Table S5: ANN equations. See DOI: https://doi.org/10.1039/d3ta06385b

‡ First authorship.

B.4. Publication of Chapter IV (Future publication)

Chapter IV of this thesis, dedicated to the synthesis, modeling, and characterization of PANI/rGO nanocomposites, is being prepared as the fourth paper for future publication (currently under review). This chapter, with its focus on DES for synthesis, showcases an innovative approach in the field of nanocomposite technology. It comprehensively covers novel synthesis methods, and the application of RSM, ANNs, and molecular simulations. The chapter's findings on electrical conductivity, structural dynamics, and electrochemical properties highlight the potential of PANI/rGO nanocomposites in supercapacitors and gas sensors, making it a valuable addition to green chemistry and sustainable material science literature.

Curriculum Vitae

Abir BOUBLIA a dedicated researcher in polymer engineering, earned her Master of Science degree from Ferhat Abbas University, Sétif, Algeria in 2020. Her academic journey is marked by a deep engagement with machine learning and molecular modeling applications in material development, particularly polymers and nanocomposites. Currently, she is advancing her expertise as a Ph.D. candidate in polymer engineering at the same institution, focusing on the innovative design of polyaniline/graphene nanocomposites for gas sensing applications. Her research, under the esteemed guidance of Prof. Zahir GUEZZOUT, Prof. Nacerddine HADDAOUI, and Prof. Yacine BENGUERBA, has led to multiple peer-reviewed publications and presentations at international forums. Abir's academic contributions include several peer-reviewed publications and presentations at international conferences, predominantly in the fields of Environmental Science and Technology, and Sustainable Development. Her research interests span machine learning, polymer informatics, molecular screening, COSMO-RS, and graphene technology. In addition to her research endeavors, Abir plays an active role in academia, contributing to teaching and supervising undergraduate and master's students. Her work in this dissertation encapsulates her profound insights and significant contributions to the field of polymer-graphene nanocomposite research.

Bibliography

Abd Razak J, Hasib H, Khalid NA, et al (2021) Influence of Graphene Nanoplatelets Loading into Physical and Morphological Characteristics of Polyaniline Nanocomposites. Springer Singapore

Abranches DO, Zhang Y, Maginn EJ, Colón YJ (2022) Sigma profiles in deep learning: towards a universal molecular descriptor. Chem Commun 5630–5633. https://doi.org/10.1039/d2cc01549h

Adams PN, Laughlin PJ, Monkman AP (1996) Synthesis of high molecular weight polyaniline at low temperatures. Synth Met 76:157–160

Adekoya OC, Adekoya GJ, Sadiku RE, et al (2022) Density Functional Theory Interaction Study of a Polyethylene Glycol-Based Nanocomposite with Cephalexin Drug for the Elimination of Wound Infection. ACS Omega 7:33808–33820. https://doi.org/10.1021/acsomega.2c02347

Adeyemi I, Sulaiman R, Almazroui M, et al (2020) Removal of chlorophenols from aqueous media with hydrophobic deep eutectic solvents: Experimental study and COSMO RS evaluation. J Mol Liq 311:113180. https://doi.org/10.1016/j.molliq.2020.113180

Adrian LCO, Mariatti M, Lockman Z (2019) Effect of Dodecylbenzenesulfonic acid as a Surfactant on the Properties of Polyaniline/Graphene Nanocomposites. Mater Today Proc 17:864–870. https://doi.org/https://doi.org/10.1016/j.matpr.2019.06.382

Agrawal A, Choudhary A (2016) Perspective: Materials informatics and big data: Realization of the “fourth paradigm” of science in materials science. Apl Mater 4:53208

Ahmadi Z, Chauhan NPS, Zarrintaj P, et al (2019) Experimental procedures for assessing electrical and thermal conductivity of polyaniline. Elsevier Inc.

Al-Haidary QN, Al-Mokaram AM, Hussein FM, Ismail AH (2021) Development of polyaniline for sensor applications: A review. In: Journal of Physics: Conference Series. IOP Publishing, p 12062

Al-Hartomy OA, Khasim S, Roy A, Pasha A (2019) Highly conductive polyaniline/graphene nano-platelet composite sensor towards detection of toluene and benzene gases. Appl Phys A Mater Sci Process 125:1–9. https://doi.org/10.1007/s00339-018-2317-7

Al-Mashat L, Shin K, Kalantar-zadeh K, et al (2010) Graphene/Polyaniline Nanocomposite for Hydrogen Sensing. J Phys Chem C 114:16168–16173. https://doi.org/10.1021/jp103134u

Alesary HF, Ismail HK, Khudhair AF, Mohammed MQ (2018) Effects of dopant ions on the properties of polyaniline conducting polymer. Orient J Chem 34:2525

Ali MK, Hessein A, Hassan MA, et al (2021) Heteroatom-doped reduced graphene oxide/polyaniline nanocomposites with improved n-type thermoelectric performance. J Appl Polym Sci 138:50852

Almi I, Belaidi S, Zerroug E, et al (2020) QSAR investigations and structure-based virtual screening on a series of nitrobenzoxadiazole derivatives targeting human glutathione-S-transferases. J Mol Struct 1211:128015. https://doi.org/10.1016/j.molstruc.2020.128015

Alruwais RS, Adeosun WA, Marwani HM, et al (2021) Novel aminosilane (APTES)-grafted polyaniline@ graphene oxide (PANI-GO) nanocomposite for electrochemical sensor. Polymers (Basel) 13:2562

Altarazi S, Ammouri M, Hijazi A (2018) Artificial neural network modeling to evaluate polyvinylchloride composites' properties. Comput Mater Sci 153:1–9. https://doi.org/https://doi.org/10.1016/j.commatsci.2018.06.003

AlYammahi J, Darwish AS, Lemaoui T, et al (2023) Molecular Guide for Selecting Green Deep Eutectic Solvents with High Monosaccharide Solubility for Food Applications. ACS Omega. https://doi.org/10.1021/acsomega.3c03326

Ameen S, Shaheer Akhtar M, Husain M (2010) A review on synthesis processing, chemical and conduction properties of polyaniline and its nanocomposites. Sci Adv Mater 2:441–462

Amu-Darko JNO, Hussain S, Gong Q, et al (2023) Highly sensitive In2O3/PANI nanosheets gas sensor for NO2 detection. J Environ Chem Eng 11:109211. https://doi.org/https://doi.org/10.1016/j.jece.2022.109211

Andre RS, Mercante LA, Facure MHM, et al (2019) Enhanced and selective ammonia detection using In2O3/reduced graphene oxide hybrid nanofibers. Appl Surf Sci 473:133–140

Ansari MO, Khan MM, Ansari SA, et al (2014a) pTSA doped conducting graphene/polyaniline nanocomposite fibers: Thermoelectric behavior and electrode analysis. Chem Eng J 242:155–161. https://doi.org/https://doi.org/10.1016/j.cej.2013.12.033

Ansari MO, Khan MM, Ansari SA, et al (2014b) Enhanced thermoelectric performance and ammonia sensing properties of sulfonated polyaniline/graphene thin films. Mater Lett 114:159–162. https://doi.org/https://doi.org/10.1016/j.matlet.2013.09.098

Armida SA, Ebrahimibagha D, Ray M, Datta S (2023) Assessing thermoelectric performance of quasi 0D carbon and polyaniline nanocomposites using machine learning. Adv Compos Mater 1–23

Arora R, Srivastav A, Mandal UK (2012) Polyaniline based polymeric nanocomposite containing TiO2 and SnO2 for environmental and energy applications. Int J Mod Eng Res 2:2384–2395

Audus DJ, de Pablo JJ (2017) Polymer informatics: Opportunities and challenges. ACS Macro Lett 6:1078–1082

Awaja NE, Almustafa G, Darwish AS, et al (2023) Molecular-based artificial neural networks for selecting deep eutectic solvents for the removal of contaminants from aqueous media. Chem Eng J 146429. https://doi.org/https://doi.org/10.1016/j.cej.2023.146429

Babel V, Hiran BL (2021) A review on polyaniline composites: Synthesis, characterization, and applications. Polym Compos 42:3142–3157

Badi N, Khasim S, Roy AS (2016) Micro-Raman spectroscopy and effective conductivity studies of graphene nanoplatelets/polyaniline composites. J Mater Sci Mater Electron 27:6249–6257

Bai S, Zhao Y, Sun J, et al (2015) Ultrasensitive room temperature NH 3 sensor based on a graphene–polyaniline hybrid loaded on PET thin film. Chem Commun 51:7524–7527

Banerjee S, Sarmah S, Kumar A (2009) Photoluminescence studies in HCl-doped polyaniline nanofibers. J Opt 38:124–130

Bansal M, Goyal A, Choudhary A (2022) A comparative analysis of K-Nearest Neighbor, Genetic, Support Vector Machine, Decision Tree, and Long Short Term Memory algorithms in machine learning. Decis Anal J 3:100071. https://doi.org/https://doi.org/10.1016/j.dajour.2022.100071

Behloul H, Ferkous H, Bougdah N, et al (2022) New insights on the adsorption of CI-Reactive Red 141 dye using activated carbon prepared from the ZnCl2-treated waste cotton fibers: Statistical physics, DFT, COSMO-RS, and AIM studies. J Mol Liq 364:119956. https://doi.org/10.1016/j.molliq.2022.119956

Bejagam KK, Lalonde J, Iverson CN, et al (2022) Machine Learning for Melting Temperature Predictions and Design in Polyhydroxyalkanoate-Based Biopolymers. J Phys Chem B 126:934–945. https://doi.org/10.1021/acs.jpcb.1c08354

Belgiu M, Drăguţ L (2016) Random forest in remote sensing: A review of applications and future directions. ISPRS J Photogramm Remote Sens 114:24–31. https://doi.org/https://doi.org/10.1016/j.isprsjprs.2016.01.011

Bera S, Kundu S, Khan H, Jana S (2018) Polyaniline coated graphene hybridized SnO2 nanocomposite: Low temperature solution synthesis, structural property and room temperature ammonia gas sensing. J Alloys Compd 744:260–270. https://doi.org/https://doi.org/10.1016/j.jallcom.2018.02.034

Beygisangchin M, Abdul Rashid S, Shafie S, Sadrolhosseini AR (2021) Polyaniline synthesized by different dopants for fluorene detection via photoluminescence spectroscopy. Materials (Basel) 14:7382

Bhadra S, Khastgir D, Singha NK, Lee JH (2009) Progress in preparation, processing and applications of polyaniline. Prog Polym Sci 34:783–810. https://doi.org/https://doi.org/10.1016/j.progpolymsci.2009.04.003

Bhadra S, Singha NK, Khastgir D (2007) Electrochemical synthesis of polyaniline and its comparison with chemically synthesized polyaniline. J Appl Polym Sci 104:1900–1904

Bhattacharya S, Ghorai A, Raval S, et al (2018) A comprehensive dual beam approach for broadband control of ultrafast optical nonlinearity in reduced graphene oxide. Carbon N Y 134:80–91. https://doi.org/https://doi.org/10.1016/j.carbon.2018.03.082

Bhuyan M, Alam S, Uddin M, et al (2016) Synthesis of graphene. Int Nano Lett 6:65–83

Biswas S, Pal A, Chakraborty P, et al (2022) Machine learning based urinary pH sensing using polyaniline deposited paper device and integration of smart web app interface: Theory to application. Biosens Bioelectron 211:114332. https://doi.org/10.1016/j.bios.2022.114332

Bogue R (2014) Graphene sensors: a review of recent developments. Sens Rev

Bolotin KI, Sikes KJ, Jiang Z, et al (2008) Ultrahigh electron mobility in suspended graphene. Solid State Commun 146:351–355. https://doi.org/https://doi.org/10.1016/j.ssc.2008.02.024

Bolto BA, McNeill R, Weiss DE (1963) Electronic conduction in polymers. III. Electronic properties of polypyrrole. Aust J Chem 16:1090–1103

Boublia A, El S, Lebouachera I, Haddaoui N (2022a) State - of - the - art review on recent advances in polymer engineering : modeling and optimization through response surface methodology approach. Springer Berlin Heidelberg

Boublia A, Guezzout Z, Haddaoui N, et al (2023a) The curious case of polyaniline-graphene nanocomposites: a review on their application as exceptionally conductive and gas sensitive materials. Crit. Rev. Solid State Mater. Sci. 0:1–25

Boublia A, Guezzout Z, Haddaoui N, et al (2024) Enhancing Precision in PANI/Gr Nanocomposite Design: Robust Machine Learning Models{,} Outlier Resilience{,} and Molecular Input Insights for Superior Electrical Conductivity and Gas Sensing Performance. J Mater Chem A. https://doi.org/10.1039/D3TA06385B

Boublia A, Lemaoui T, Abu Hatab F, et al (2022b) Molecular-based artificial neural network for predicting the electrical conductivity of deep eutectic solvents. J Mol Liq 366:120225. https://doi.org/https://doi.org/10.1016/j.molliq.2022.120225

Boublia A, Lemaoui T, Almustafa G, et al (2023b) Critical Properties of Ternary Deep Eutectic Solvents Using Group Contribution with Extended Lee-Kesler Mixing Rules. ACS Omega. https://doi.org/10.1021/acsomega.3c00436

Boublia A, Lemaoui T, AlYammahi J, et al (2022c) Multitask Neural Network for Mapping the Glass Transition and Melting Temperature Space of Homo-and Co-Polyhydroxyalkanoates Using σProfiles Molecular Inputs. ACS Sustain Chem Eng

Boublia A, Lemaoui T, AlYammahi J, et al (2023c) Multitask Neural Network for Mapping the Glass Transition and Melting Temperature Space of Homo- and Co-Polyhydroxyalkanoates Using σProfiles Molecular Inputs. ACS Sustain Chem Eng 11:208–227. https://doi.org/10.1021/acssuschemeng.2c05225

Boulechfar C, Ferkous H, Delimi A, et al (2023a) Corrosion Inhibition of Schiff Base and their Metal Complexes with [Mn (II), Co (II) and Zn (II)]: Experimental and Quantum Chemical Studies. J Mol Liq 121637

Boulechfar C, Ferkous H, Delimi A, et al (2023b) Schiff Bases and Their Metal Complexes: A review on the history, synthesis, and applications. Inorg Chem Commun 110451. https://doi.org/https://doi.org/10.1016/j.inoche.2023.110451

Bousba D, Sobhi C, Zouaoui E, et al (2024) Efficient biodiesel production from recycled cooking oil using a NaOH / CoFe 2 O 4 magnetic nano-catalyst : synthesis , characterization , and process enhancement for sustainability. Energy Convers Manag 300:118021. https://doi.org/10.1016/j.enconman.2023.118021

Boutouil A, Laamari MR, Elazhary I, et al (2020) Towards a deeper understanding of the inhibition mechanism of a new 1,2,3-triazole derivative for mild steel corrosion in the hydrochloric acid solution using coupled experimental and theoretical methods. Mater Chem Phys 241:122420. https://doi.org/https://doi.org/10.1016/j.matchemphys.2019.122420

Box GEP, Wilson KB (1992) On the experimental attainment of optimum conditions. In: Breakthroughs in statistics. Springer, pp 270–310

Bradley N (2007) The response surface methodology. Indiana University South Bend

Brown WM, Martin S, Rintoul MD, Faulon J-L (2006) Designing novel polymers with targeted properties using the signature molecular descriptor. J Chem Inf Model 46:826–835

Brownson DAC, Banks CE (2012) The electrochemistry of CVD graphene: progress and prospects. Phys Chem Chem Phys 14:8264–8281

Bullock TH (1997) Signals and signs in the nervous system: The dynamic anatomy of electrical activity is probably information-rich. Proc Natl Acad Sci U S A 94:1–6.

https://doi.org/10.1073/pnas.94.1.1

Cao J, Wang C (2018) Highly conductive and flexible silk fabric via electrostatic self assemble between reduced graphene oxide and polyaniline. Org Electron 55:26–34

Cao Y, Andreatta A, Heeger AJ, Smith P (1989) Influence of chemical polymerization conditions on the properties of polyaniline. Polymer (Guildf) 30:2305–2311. https://doi.org/https://doi.org/10.1016/0032-3861(89)90266-8

Cencer MM, Moore JS, Assary RS (2021) Machine learning for polymeric materials: an introduction. Polym Int

Chakraborty P, Chien Y-A, Chiu W-T, et al (2020) Design and development of amperometric gas sensor with atomic Au–Polyaniline/Pt composite. IEEE Sens J 20:12479–12487

Chang J, Zhang X, Wang Z, et al (2021) Polyaniline-reduced graphene oxide nanosheets for room temperature NH3 detection. ACS Appl Nano Mater 4:5263–5272

Chaudhary N, Khanuja M, Islam SS (2019) Broadband photodetector based on 3D architect of MoS2-PANI hybrid structure for high photoresponsive properties. Polymer (Guildf) 165:168–173

Chauhan NPS, Mozafari M, Chundawat NS, et al (2016) High-performance supercapacitors based on polyaniline-graphene nanocomposites: Some approaches, challenges and opportunities. J Ind Eng Chem 36:13–29. https://doi.org/10.1016/j.jiec.2016.03.003

Chee WK, Lim HN, Huang NM, Harrison I (2015) Nanocomposites of graphene/polymers: a review. Rsc Adv 5:68014–68051

Chen G, Tao L, Li Y (2021a) Predicting polymers' glass transition temperature by a chemical language processing model. Polymers (Basel) 13:1–14. https://doi.org/10.3390/polym13111898

Chen H, Zhuo F, Zhou J, et al (2023a) Advances in Graphene-based Flexible and Wearable Strain Sensors. Chem Eng J 142576

Chen L, Kim C, Batra R, et al (2020) Frequency-dependent dielectric constant prediction of polymers using machine learning. npj Comput Mater 6:30–32. https://doi.org/10.1038/s41524-020-0333-6

Chen L, Li N, Yu X, et al (2023b) A general way to manipulate electrical conductivity of graphene. Chem Eng J 462:142139

Chen L, Pilania G, Batra R, et al (2021b) Polymer informatics: Current status and critical next steps. Mater Sci Eng R Reports 144:100595. https://doi.org/https://doi.org/10.1016/j.mser.2020.100595

Chen W, Yan L, Bangal PR (2010) Preparation of graphene by the rapid and mild thermal reduction of graphene oxide induced by microwaves. Carbon N Y 48:1146–1152. https://doi.org/https://doi.org/10.1016/j.carbon.2009.11.037

Chen Y, Li Y, Yip M, Tai N (2013) Electromagnetic interference shielding efficiency of polyaniline composites filled with graphene decorated with metallic nanoparticles. Compos Sci Technol 80:80–86. https://doi.org/https://doi.org/10.1016/j.compscitech.2013.02.024

Chiang CK, Fincher Jr CR, Park YW, et al (1977) Electrical conductivity in doped polyacetylene. Phys Rev Lett 39:1098

Cho S, Lee JS, Jun J, et al (2014) Fabrication of water-dispersible and highly conductive PSS-doped PANI/graphene nanocomposites using a high-molecular weight PSS dopant and their application in H2S detection. Nanoscale 6:15181–15195. https://doi.org/10.1039/c4nr04413d

Choudhary RB, Kandulna R (2019) 2-D rGO impregnated circular-tetragonal-bipyramidal structure of PPY-TiO2-rGO nanocomposite as ETL for OLED and supercapacitor electrode materials. Mater Sci Semicond Process 94:86–96

Choudhary RB, Verma A (2019) Augmented structural, optical and electrical properties of CdS decorated PANI/rGO nanohybrids. Opt Mater (Amst) 96:109310

Christopholi LP, da Cunha MRP, Spada ER, et al (2020) Reduced graphene oxide and perylene derivative nanohybrid as multifunctional interlayer for organic solar cells. Synth Met 269:116552. https://doi.org/https://doi.org/10.1016/j.synthmet.2020.116552

Ćirić-Marjanović G (2013) Recent advances in polyaniline research: Polymerization mechanisms, structural aspects, properties and applications. Synth Met 177:1–47

Clemons CB, Roberts MW, Wilber JP, et al (2010) Continuum plate theory and atomistic modeling to find the flexural rigidity of a graphene sheet interacting with a substrate. J Nanotechnol 2010:. https://doi.org/10.1155/2010/868492

Company BB, Laureates N (2003) In Electroactive Polymers for Corrosion Control; Zarras, P., et al.; ACS Symposium Series; American Chemical Society: Washington, DC, 2003. Corrosion

Cong H-P, Ren X-C, Wang P, Yu S-H (2013) Flexible graphene–polyaniline composite paper for high-performance supercapacitor. Energy Environ Sci 6:1185–1191

D Ghuge A, R Shirode A, J Kadam V (2017) Graphene: a comprehensive review. Curr Drug Targets 18:724–733

Dal Corso A, Pasquarello A, Baldereschi A, Car R (1996) Generalized-gradient approximations to density-functional theory: A comparative study for atoms and solids.

Phys Rev B 53:1180

Darwish AS, Lemaoui T, AlYammahi J, et al (2023) Molecular Insights into Potential Hydrophobic Deep Eutectic Solvents for Furfural Extraction Guided by COSMO-RS and Machine Learning. J Mol Liq 121631

Das P, Deoghare AB, Ranjan Maity S (2023) Fabrication and characterization of polyaniline (PANI) modified with reduced graphene oxide (RGO) nanosheets. Mater Today Proc 72:2306–2314. https://doi.org/10.1016/j.matpr.2022.09.397

Delley B (1995) DMol, a standard tool for density functional calculations: review and advances. Theor Comput Chem 2:221–254

Delley B (2000) From molecules to solids with the DMol 3 approach. J Chem Phys 113:7756–7764

Díez-Pascual AM, Luceño-Sánchez JA (2021) Antibacterial activity of polymer nanocomposites incorporating graphene and its derivatives: A state of art. Polymers (Basel) 13:. https://doi.org/10.3390/polym13132105

Divya P, Prithiba A, Rajalakshmi R (2019) A comprehensive review on the nanocomposites of graphene and its derivatives in the application of supercapacitors. Rasayan J Chem 12:214–231

Dreyer DR, Park S, Bielawski CW, Ruoff RS (2010) The chemistry of graphene oxide. Chem Soc Rev 39:228–240. https://doi.org/10.1039/b917103g

Du X, Chen Y, Dong W, et al (2017) A nanocomposite-based electrochemical sensor for non-enzymatic detection of hydrogen peroxide. Oncotarget 8:13039–13047. https://doi.org/10.18632/oncotarget.14308

Du Y, Cai K, Shen SZ (2013) Facile preparation and characterization of graphene nanosheet/polyaniline nanofiber thermoelectric composites. Funct Mater Lett 6:1340002

Farooqi BA, Ashraf A, Farooq U, Ayub K (2020a) Comparative study on sensing abilities of polyaniline and graphene polyaniline composite sensors toward methylamine and ammonia. Polym Adv Technol 31:3351–3360. https://doi.org/10.1002/pat.5058

Farooqi BA, Yar M, Ashraf A, et al (2020b) Graphene-polyaniline composite as superior electrochemical sensor for detection of cyano explosives. Eur Polym J 138:. https://doi.org/10.1016/j.eurpolymj.2020.109981

Ferkous H, Sedik A, Delimi A, et al (2023) A comparative study of novel synthesized sulfamide compounds: Electrochemical, morphological, XPS, and theoretical investigations on copper corrosion inhibition in 1.0 M HCl. J Mol Liq 123781. https://doi.org/https://doi.org/10.1016/j.molliq.2023.123781

Firdaus SM, Anasyida AS, Zubir SA, Mariatti M (2020) Graphene/polyaniline nanocomposites: effect of in-situ polymerization and solvent blending methods with dodecylbenzene sulfonic acid surfactant. J Mater Sci Mater Electron 31:15805–15821

Fissa MR, Lahiouel Y, Khaouane L, Hanini S (2019) QSPR estimation models of normal boiling point and relative liquid density of pure hydrocarbons using MLR and MLP-ANN methods. J Mol Graph Model 87:109–120

Fratoddi I, Venditti I, Cametti C, Russo MV (2015a) Chemiresistive polyaniline-based gas sensors: A mini review. Sensors Actuators, B Chem 220:534–548. https://doi.org/10.1016/j.snb.2015.05.107

Fratoddi I, Venditti I, Cametti C, Russo MV (2015b) Chemiresistive polyaniline-based gas sensors: A mini review. Sensors Actuators B Chem 220:534–548

Fu S, Sun Z, Huang P, et al (2019) Some basic aspects of polymer nanocomposites: A critical review. Nano Mater Sci 1:2–30

Fujimoto A, Yamada Y, Koinuma M, Sato S (2016) Origins of sp3C peaks in C1s X-ray photoelectron spectra of carbon materials. Anal Chem 88:6110–6114

Fuster F, Grabowski SJ (2011) Intramolecular hydrogen bonds: the QTAIM and ELF characteristics. J Phys Chem A 115:10078–10086

Gabsi M, Ferkous H, Delimi A, et al (2023) The curious case of polyphenols as green corrosion inhibitors: a review on their extraction, design, and applications. Environ Sci Pollut Res 1–25

Gabunada JC, Vinothkannan M, Kim DH, et al (2019) Magnetite Nanorods Stabilized by Polyaniline/Reduced Graphene Oxide as a Sensing Platform for Selective and Sensitive Non-enzymatic Hydrogen Peroxide Detection. Electroanalysis 31:1524–1533. https://doi.org/10.1002/elan.201900134

Gaikwad G, Patil P, Patil D, Naik J (2017) Synthesis and evaluation of gas sensing properties of PANI based graphene oxide nanocomposites. Mater Sci Eng B 218:14–22. https://doi.org/https://doi.org/10.1016/j.mseb.2017.01.008

Gao C, Li W, Morimoto H, et al (2006) Magnetic carbon nanotubes: synthesis by electrostatic self-assembly approach and application in biomanipulations. J Phys Chem B 110:7213–7220

Gao W, Alemany LB, Ci L, Ajayan PM (2009) New insights into the structure and reduction of graphite oxide. Nat Chem 1:403–408

Garg S, Goel N (2023) Encapsulation of heavy metal ions via adsorption using cellulose/ZnO composite: First principles approach. J Mol Graph Model 124:.

https://doi.org/10.1016/j.jmgm.2023.108566

Gautam SK, Gokhale NA, Panda S (2022) Mechanism of NH3 gas sensing by SnO2/PANI nanocomposites: charge transport and temperature dependence study. Flex Print Electron 7:35022

Gavgani JN, Hasani A, Nouri M, et al (2016) Highly sensitive and flexible ammonia sensor based on S and N co-doped graphene quantum dots/polyaniline hybrid at room temperature. Sensors Actuators B Chem 229:239–248. https://doi.org/https://doi.org/10.1016/j.snb.2016.01.086

Gebreegziabher GG, Asemahegne AS, Ayele DW, et al (2019) One-step synthesis and characterization of reduced graphene oxide using chemical exfoliation method. Mater Today Chem 12:233–239

Geethalakshmi D, Muthukumarasamy N, Balasundaraprabhu R (2014) Effect of dopant concentration on the properties of HCl-doped PANI thin films prepared at different temperatures. Optik (Stuttg) 125:1307–1310. https://doi.org/10.1016/j.ijleo.2013.08.014

Geim A, Novoselov K (2010) The nobel prize in physics 2010. Nat Phys 6:836

Gerard M, Chaubey A, Malhotra BD (2002) Application of conducting polymers to biosensors. Biosens Bioelectron 17:345–359

Goenka S, Sant V, Sant S (2014) Graphene-based nanomaterials for drug delivery and tissue engineering. J Control Release 173:75–88. https://doi.org/https://doi.org/10.1016/j.jconrel.2013.10.017

Gómez-Navarro C, Weitz RT, Bittner AM, et al (2007) Electronic transport properties of individual chemically reduced graphene oxide sheets. Nano Lett 7:3499–3503

Gospodinova N, Terlemezyan L (1998) Conducting polymers prepared by oxidative polymerization: polyaniline. Prog Polym Sci 23:1443–1484

Gospodinova N, Terlemezyan L, Mokreva P, Kossev K (1993) On the mechanism of oxidative polymerization of aniline. Polymer (Guildf) 34:2434–2437

Goswami S, Nandy S, Fortunato E, Martins R (2023) Polyaniline and its composites engineering: A class of multifunctional smart energy materials. J Solid State Chem 317:123679. https://doi.org/https://doi.org/10.1016/j.jssc.2022.123679

Gubler U, Concilio S, Bosshard C, et al (2002) Third-order nonlinear optical properties of in-backbone substituted conjugated polymers. Appl Phys Lett 81:2322–2324

Guezzout Z, Boublia A, Haddaoui N (2023) Enhancing thermal and mechanical properties of polypropylene - nitrile butadiene rubber nanocomposites through graphene oxide functionalization. J Polym Res 1–16. https://doi.org/10.1007/s10965-023-03585-x

Guezzout Z, Doufnoune R, Haddaoui N (2017) Effect of graphene oxide on the properties of compatibilized polypropylene/ethylene-propylene-rubber blend. J Polym Res 24:1–15

Gul H, Shah AUHA, Krewer U, Bilal S (2020) Study on direct synthesis of energy efficient multifunctional polyaniline–graphene oxide nanocomposite and its application in aqueous symmetric supercapacitor devices. Nanomaterials 10:. https://doi.org/10.3390/nano10010118

Guo L, Hao Y-W, Li P-L, et al (2018a) Improved NO2 gas sensing properties of graphene oxide reduced by two-beam-laser interference. Sci Rep 8:1–7

Guo Y, Wang T, Chen F, et al (2016) Hierarchical graphene-polyaniline nanocomposite films for high-performance flexible electronic gas sensors. Nanoscale 8:12073–12080. https://doi.org/10.1039/c6nr02540d

Guo Z, Liao N, Zhang M, Xue W (2018b) Theoretical approach to evaluate graphene/PANI composite as highly selective ammonia sensor. Appl Surf Sci 453:336–340. https://doi.org/10.1016/j.apsusc.2018.05.108

Gupta B, Kumar N, Panda K, et al (2016) Molecular-Pillar-Supported Functionalized Reduced Graphene-Oxide for Energy Efficient Lubrication. Adv Mater Interfaces 3:1600161

Gupta V, Miura N (2006) High performance electrochemical supercapacitor from electrochemically synthesized nanostructured polyaniline. Mater Lett 60:1466–1469. https://doi.org/https://doi.org/10.1016/j.matlet.2005.11.047

Habib H, Wani IS, Husain S (2022) High performance nanostructured symmetric reduced graphene oxide/polyaniline supercapacitor electrode: effect of polyaniline morphology. J Energy Storage 55:105732. https://doi.org/https://doi.org/10.1016/j.est.2022.105732

Hadano FS, Gavim AEX, Stefanelo JC, et al (2021) Nh3 sensor based on rgo-pani composite with improved sensitivity. Sensors 21:. https://doi.org/10.3390/s21154947

Hakimi M, Salehi A, Boroumand FA, Mosleh N (2018) Fabrication of a room temperature ammonia gas sensor based on polyaniline with N-doped graphene quantum dots. IEEE Sens J 18:2245–2252

Harun MH, Saion E, Kassim A, et al (2007) Conjugated conducting polymers: A brief overview. UCSI Acad J J Adv Sci Arts 2:63–68

Haykin S (2009) Neural networks and learning machines, 3/E. Pearson Education India

He F, Lam K-H, Fan J, Chan LH (2014) Improved dielectric properties for chemically functionalized exfoliated graphite nanoplates/syndiotactic polystyrene composites prepared by a solution-blending method. Carbon N Y 80:496–503. https://doi.org/https://doi.org/10.1016/j.carbon.2014.08.089

Heeger AJ, MacDiarmid AG, Shirakawa H (2000) "The Nobel Prize in Chemistry 2000." https://www.nobelprize.org. Accessed 20 Aug 2022

Heme HN, Alif MSN, Rahat SMSM, Shuchi SB (2021) Recent progress in polyaniline composites for high capacity energy storage: A review. J Energy Storage 42:103018

Himmelblau DM (2000) Applications of artificial neural networks in chemical engineering. Korean J Chem Eng 17:373–392

Hiraide K, Hirayama K, Endo K, Muramatsu M (2021) Application of deep learning to inverse design of phase separation structure in polymer alloy. Comput Mater Sci 190:110278. https://doi.org/10.1016/j.commatsci.2021.110278

Hirata M, Sun L (1994) Characteristics of an organic semiconductor polyaniline film as a sensor for NH3 gas. Sensors Actuators A Phys 40:159–163. https://doi.org/https://doi.org/10.1016/0924-4247(94)85024-0

Hong S-Z, Huang Q-Y, Wu T-M (2021) The Room Temperature Highly Sensitive Ammonia Gas Sensor Based on Polyaniline and Nitrogen-Doped Graphene Quantum Dot-Coated Hollow Indium Oxide Nanofiber Composite. Polymers (Basel) 13:3676

Hong X, Fu J, Liu Y, et al (2019) Recent progress on graphene/polyaniline composites for high-performance supercapacitors. Materials (Basel) 12:1451

Hornik K, Stinchcombe M, White H (1989) Multilayer feedforward networks are universal approximators. Neural networks 2:359–366

Hosseingholipourasl A, Hafizah Syed Ariffin S, Al-Otaibi YD, et al (2020) Analytical approach to study sensing properties of graphene based gas sensor. Sensors 20:1506

Hu N, Yang Z, Wang Y, et al (2013) Ultrafast and sensitive room temperature NH3 gas sensors based on chemically reduced graphene oxide. Nanotechnology 25:25502

Huang J, Virji S, Weiller BH, Kaner RB (2003) Polyaniline nanofibers: facile synthesis and chemical sensors. J Am Chem Soc 125:314–315

Huang W-S, Humphrey BD, MacDiarmid AG (1986) Polyaniline, a novel conducting polymer. Morphology and chemistry of its oxidation and reduction in aqueous electrolytes. J Chem Soc Faraday Trans 1 Phys Chem Condens Phases 82:2385–2400

Huang X, Hu N, Gao R, et al (2012) Reduced graphene oxide-polyaniline hybrid: Preparation, characterization and its applications for ammonia gas sensing. J Mater Chem 22:22488–22495. https://doi.org/10.1039/c2jm34340a

Huang X, Hu N, Zhang L, et al (2013) The NH3 sensing properties of gas sensors based on aniline reduced graphene oxide. Synth Met 185–186:25–30. https://doi.org/https://doi.org/10.1016/j.synthmet.2013.09.034

Huang Z, Li L, Wang Y, et al (2018) Polyaniline/graphene nanocomposites towards high-performance supercapacitors: A review. Compos Commun 8:83–91. https://doi.org/10.1016/j.coco.2017.11.005

Huh SH (2011) Thermal reduction of graphene oxide. Phys Appl graphene-experiments 19:73–90

Humphrey W, Dalke A, Schulten K (1996) VMD: Visual molecular dynamics. J Mol Graph 14:33–38. https://doi.org/https://doi.org/10.1016/0263-7855(96)00018-5

Idumah CI (2021) Novel trends in conductive polymeric nanocomposites, and bionanocomposites. Synth Met 273:116674

Imran SM, Kim Y, Shao GN, et al (2014) Enhancement of electroconductivity of polyaniline/graphene oxide nanocomposites through in situ emulsion polymerization. J Mater Sci 49:1328–1335

Iskandar F, Hikmah U, Stavila E, Aimon AH (2017) Microwave-assisted reduction method under nitrogen atmosphere for synthesis and electrical conductivity improvement of reduced graphene oxide (rGO). RSC Adv 7:52391–52397. https://doi.org/10.1039/c7ra10013b

Islam MA, Khan ME, Hossain MM, Hasan M (2016) Electrical conductivity retention and electrochemical activity of CSA doped graphene/gold nanoparticle@ polyaniline composites. Prog Nat Sci Mater Int 26:341–346. https://doi.org/https://doi.org/10.1016/j.pnsc.2016.06.001

Ismail AH, Sulaiman Y (2021) Review on the utilisation of sensing materials for intrinsic optical NH3 gas sensors. Synth Met 280:116860

Ismail HK, Alesary HF, Mohammed MQ (2019) Synthesis and characterisation of polyaniline and/or MoO2/graphite composites from deep eutectic solvents via chemical polymerisation. J Polym Res 26:1–12

Jain M, Annapoorni S (2010) Raman study of polyaniline nanofibers prepared by interfacial polymerization. Synth Met 160:1727–1732

Jain R, Sinha A, Kumari N (2016) A polyaniline/graphene oxide nanocomposite as a voltammetric sensor for electroanalytical detection of clonazepam. Anal methods 8:3034–3045

James DK, Tour JM (2013) Graphene: powder, flakes, ribbons, and sheets. Acc Chem Res 46:2307–2318

Javadian-Saraf A, Hosseini E, Wiltshire BD, et al (2021) Graphene oxide/polyaniline-based microwave split-ring resonator: A versatile platform towards ammonia sensing. J Hazard

Mater 418:126283. https://doi.org/10.1016/j.jhazmat.2021.126283

Jelmy EJ, Ramakrishnan S, Devanathan S, et al (2013) Optimization of the conductivity and yield of chemically synthesized polyaniline using a design of experiments. J Appl Polym Sci 130:1047–1057

Jindal S, Anand R, Sharma N, et al (2022) Sustainable Approach for Developing Graphene-Based Materials from Natural Resources and Biowastes for Electronic Applications. ACS Appl Electron Mater. https://doi.org/10.1021/acsaelm.2c00097

Johnson ER, Keinan S, Mori-Sánchez P, et al (2010) Revealing noncovalent interactions. J Am Chem Soc 132:6498–6506

Kahlen J, Masuch K, Leonhard K (2010) Modelling cellulose solubilities in ionic liquids using COSMO-RS. Green Chem 12:2172–2181

Kakkar S, Kwapinski W, Howard CA, Kumar KV (2021) Education for Chemical Engineers Deep neural networks in chemical engineering classrooms to accurately model adsorption equilibrium data. Educ Chem Eng 36:115–127. https://doi.org/10.1016/j.ece.2021.04.003

Kandulna R, Choudhary RB, Singh R (2019) Free Exciton Absorptions and Quasi-reversible Redox Actions in Polypyrrole–Polyaniline–Zinc Oxide Nanocomposites as Electron Transporting Layer for Organic Light Emitting Diode and Electrode Material for Supercapacitors. J Inorg Organomet Polym Mater 29:730–744. https://doi.org/10.1007/s10904-018-1047-9

Kar KK, Rana S, Pandey J (2015) Handbook of polymer nanocomposites processing, performance and application. Springer

Kar P, Choudhury A (2013) Carboxylic acid functionalized multi-walled carbon nanotube doped polyaniline for chloroform sensors. Sensors actuators B Chem 183:25–33

Kaur G, Adhikari R, Cass P, et al (2015) Electrically conductive polymers and composites for biomedical applications. Rsc Adv 5:37553–37567

Kausar A (2021) Polyaniline/graphene nanoplatelet nanocomposite towards high-end features and applications. Mater Res Innov 1–13

Kazemi F, Naghib SM, Zare Y, Rhee KY (2021) Biosensing Applications of Polyaniline (PANI)-Based Nanocomposites: A Review. Polym Rev 61:553–597. https://doi.org/10.1080/15583724.2020.1858871

Kebiche H, Debarnot D, Merzouki A, et al (2012) Relationship between ammonia sensing properties of polyaniline nanostructures and their deposition and synthesis methods. Anal Chim Acta 737:64–71. https://doi.org/https://doi.org/10.1016/j.aca.2012.06.003

Kebiche H, Debarnot D, Merzouki A, et al (2013) Ammonia gas sensors based on in situ and drop-coated polyaniline nanostructures. In: Advanced materials research. Trans Tech Publ, pp 134–138

Kebiche H, Poncin-Epaillard F, Haddaoui N, Debarnot D (2020) A route for the synthesis of polyaniline-based hybrid nanocomposites. J Mater Sci 55:5782–5794

Khan AA, Khalid M (2010) Synthesis of nano-sized ZnO and polyaniline-zinc oxide composite: Characterization, stability in terms of DC electrical conductivity retention and application in ammonia vapor detection. J Appl Polym Sci 117:1601–1607

Kim M, Lee C, Jang J (2014) Fabrication of highly flexible, scalable, and high-performance supercapacitors using polyaniline/reduced graphene oxide film with enhanced electrical conductivity and crystallinity. Adv Funct Mater 24:2489–2499

Klamt A (2018) The COSMO and COSMO-RS solvation models. Wiley Interdiscip Rev Comput Mol Sci 8:e1338

Konwer S (2016) Graphene oxide-polyaniline nanocomposites for high performance supercapacitor and their optical, electrical and electrochemical properties. J Mater Sci Mater Electron 27:4139–4146

Konwer S, Guha AK, Dolui SK (2013) Graphene oxide-filled conducting polyaniline composites as methanol-sensing materials. J Mater Sci 48:1729–1739

Kr S, Murmu M, Chandra N, Banerjee P (2022) Benzothiazolylhydrazine azomethine derivatives for efficient corrosion inhibition of mild steel in acidic environment : Integrated experimental and density functional theory cum molecular dynamics simulation approach. J Mol Liq 364:120033. https://doi.org/10.1016/j.molliq.2022.120033

Krithika S, Balavijayalakshmi J (2022) Investigation of structural, morphological and electrochemical properties of mos2/pani/sno2 nanocomposites for energy storage applications. Inorg Chem Commun 110324

Kuenneth C, Schertzer W, Ramprasad R (2021) Copolymer Informatics with Multitask Deep Neural Networks. Macromolecules 54:5957–5961. https://doi.org/10.1021/acs.macromol.1c00728

Kukla AL, Shirshov YM, Piletsky SA (1996) Ammonia sensors based on sensitive polyaniline films. Sensors Actuators B Chem 37:135–140. https://doi.org/https://doi.org/10.1016/S0925-4005(97)80128-1

Kulkarni HB, Tambe P, M. Joshi G (2018) Influence of covalent and non-covalent modification of graphene on the mechanical, thermal and electrical properties of epoxy/graphene nanocomposites: a review. Compos Interfaces 25:381–414

Kulkarni VG (1993) Processing of polyanilines. In: Intrinsically conducting polymers: an emerging technology. Springer, pp 45–50

Kulkarni VG, Campbell LD, Mathew WR (1989) Thermal stability of polyaniline. Synth Met 30:321–325

Kumar A, Jangir LK, Kumari Y, et al (2016) Electrical behavior of dual-morphology polyaniline. J Appl Polym Sci 133:

Kumar A, Kumar R, Pandey G (2018a) Synthesis, Characterization of Titania/Polyaniline/GO Nanocomposites, and Its Photocatalytic Activity Under UV-Visible Light. In: Macromolecular Symposia. Wiley Online Library, p 1600192

Kumar NA, Baek JB (2014) Electrochemical supercapacitors from conducting polyaniline-graphene platforms. Chem Commun 50:6298–6308. https://doi.org/10.1039/c4cc01049c

Kumar S, McEvoy N, Kim H, et al (2011) CVD growth and processing of graphene for electronic applications. Phys status solidi 248:2604–2608

Kumar V, Gupta RK, Gundampati RK, et al (2018b) Enhanced electron transfer mediated detection of hydrogen peroxide using a silver nanoparticle-reduced graphene oxide-polyaniline fabricated electrochemical sensor. RSC Adv 8:619–631. https://doi.org/10.1039/c7ra11466d

Kumar V, Mirzaei A, Bonyani M, et al (2020) Advances in electrospun nanofiber fabrication for polyaniline (PANI)-based chemoresistive sensors for gaseous ammonia. TrAC Trends Anal Chem 129:115938

Kundu S, Majumder R, Bhagat BR, et al (2023) An in situ synthesis of polyaniline/reduced graphene oxide nanocomposite flexible thin film on PET for the room temperature detection of trace level ammonia at ppb level. J Mater Sci 1–24

Kwak D, Lei Y, Maric R (2019) Ammonia gas sensors: A comprehensive review. Talanta 204:713–730

Kyomuhimbo HD, Feleni U (2023) Electroconductive Green Metal-polyaniline Nanocomposites: Synthesis and Application in Sensors. Electroanalysis 35:e202100636

Ladrón-de-Guevara A, Boscá A, Pedrós J, et al (2019) Reduced graphene oxide/polyaniline electrochemical supercapacitors fabricated by laser. Appl Surf Sci 467:691–697

Lai Q, Zhu S, Luo X, et al (2012) Ultraviolet-visible spectroscopy of graphene oxides. AIP Adv 2:

Lamiel C, Kharismadewi D, Shim J-J (2015) Covalently bonded reduced graphene oxide/polyaniline composite for electrochemical sensors and capacitors. J Electroanal Chem 758:148–155

Lee CT, Wang YS (2019) High-performance room temperature NH3 gas sensors based on polyaniline-reduced graphene oxide nanocomposite sensitive membrane. J Alloys Compd 789:693–696. https://doi.org/10.1016/j.jallcom.2019.03.124

Lee XJ, Hiew BYZ, Lai KC, et al (2019) Review on graphene and its derivatives: Synthesis methods and potential industrial implementation. J Taiwan Inst Chem Eng 98:163–180

Legarreta-Mendoza A, Flores-Holguín N, Lardizabal-Gutiérrez D (2019) A proposal based on quantum phenomena for the ORR mechanism on nitrogen-doped carbon-based electrocatalysts. Int J Hydrogen Energy 44:12374–12380. https://doi.org/https://doi.org/10.1016/j.ijhydene.2018.10.232

Lemaoui T, Abu Hatab F, Darwish AS, et al (2021) Molecular-Based Guide to Predict the pH of Eutectic Solvents: Promoting an Efficient Design Approach for New Green Solvents. ACS Sustain Chem Eng 9:5783–5808. https://doi.org/10.1021/acssuschemeng.0c07367

Lemaoui T, Boublia A, Darwish AS, et al (2022) Predicting the Surface Tension of Deep Eutectic Solvents Using Artificial Neural Networks. ACS Omega

Lemaoui T, Boublia A, Lemaoui S, et al (2023a) Predicting the CO2 Capture Capability of Deep Eutectic Solvents and Screening over 1000 of their Combinations Using Machine Learning. ACS Sustain Chem Eng

Lemaoui T, Darwish AS, Almustafa G, et al (2023b) Machine learning approach to map the thermal conductivity of over 2,000 neoteric solvents for green energy storage applications. Energy Storage Mater 59:102795. https://doi.org/10.1016/j.ensm.2023.102795

Lemaoui T, Darwish AS, Hammoudi NEH, et al (2020) Prediction of Electrical Conductivity of Deep Eutectic Solvents Using COSMO-RS Sigma Profiles as Molecular Descriptors: A Quantitative Structure–Property Relationship Study. Ind Eng Chem Res 59:13343–13354. https://doi.org/10.1021/acs.iecr.0c02542

Leon F, Curteanu S, Lisa C, Hurduc N (2007) Machine learning methods used to predict the liquid-crystalline behavior of some copolyethers. Mol Cryst Liq Cryst 469:1–22. https://doi.org/10.1080/15421400701431232

Letheby H (1862) XXIX.—On the production of a blue substance by the electrolysis of sulphate of aniline. J Chem Soc 15:161–163

Li B, Li Y, Ma P (2022a) Synthesis of H2SO4-doped polyaniline materials and behavior of enhancing gas sensing properties. J Mater Sci Mater Electron 33:18673–18685

Li B, Li Y, Ma P (2023) Synthesis of different inorganic acids doped polyaniline materials and behavior of enhancing NH3 gas sensing properties. Org Electron 114:106749. https://doi.org/https://doi.org/10.1016/j.orgel.2023.106749

Li D, Huang J, Kaner RB (2009) Polyaniline nanofibers: a unique polymer nanostructure for versatile applications. Acc Chem Res 42:135–145

Li D, Müller MB, Gilje S, et al (2008) Processable aqueous dispersions of graphene nanosheets. Nat Nanotechnol 3:101–105

Li J, Tang X, Li H, et al (2010) Synthesis and thermoelectric properties of hydrochloric acid-doped polyaniline. Synth Met 160:1153–1158. https://doi.org/https://doi.org/10.1016/j.synthmet.2010.03.001

Li J, Zhao H, Wang Y, Zhou Y (2024) Approaches for Selectivity Improvement of Conductometric Gas Sensors: An Overview. Sensors & Diagnostics

Li M, Dai L, Hu Y (2022b) Machine Learning for Harnessing Thermal Energy: From Materials Discovery to System Optimization. ACS Energy Lett 7:3204–3226. https://doi.org/10.1021/acsenergylett.2c01836

Li R, Xu H, Fu R, et al (2018a) Preparation of 3D reduced graphene oxide/carbon nanospheres/polyaniline ternary nanocomposites as supercapacitor electrode. React Funct Polym 125:101–107. https://doi.org/10.1016/j.reactfunctpolym.2018.02.011

Li S, Lin P, Zhao L, et al (2018b) The room temperature gas sensor based on Polyaniline@ flower-like WO3 nanocomposites and flexible PET substrate for NH3 detection. Sensors Actuators B Chem 259:505–513

Li S, Wang T, Yang Z, et al (2018c) Room temperature high performance NH3 sensor based on GO-rambutan-like polyaniline hollow nanosphere hybrid assembled to flexible PET substrate. Sensors Actuators B Chem 273:726–734. https://doi.org/https://doi.org/10.1016/j.snb.2018.06.072

Li Y, Xia Z, Gong Q, et al (2020) Green synthesis of free standing cellulose/graphene oxide/polyaniline aerogel electrode for high-performance flexible all-solid-state supercapacitors. Nanomaterials 10:1–18. https://doi.org/10.3390/nano10081546

Li Y, Zheng Y (2018) Preparation and electrochemical properties of polyaniline/reduced graphene oxide composites. J Appl Polym Sci 135:1–8. https://doi.org/10.1002/app.46103

Lian Z, Ma Y, Li M, et al (2024) Discovery Precision: An effective metric for evaluating performance of machine learning model for explorative materials discovery. Comput Mater Sci 233:112738

Liang H (2014) Mid-infrared response of reduced graphene oxide and its high-temperature coefficient of resistance. Aip Adv 4:107131

Liang J, Xu S, Hu L, et al (2021) Machine-learning-assisted low dielectric constant polymer discovery. Mater Chem Front 5:3823–3829. https://doi.org/10.1039/d0qm01093f

Lin J, Kilani M, Mao G (2023) Recent Advances in Integrating 1D Nanomaterials into Chemiresistive Gas Sensor Devices. Adv Mater Technol 2202038

Lin S-J, Sun H-J, Peng T-J, Jiang L-H (2014) Synthesis of high-performance polyaniline/graphene oxide nanocomposites. High Perform Polym 26:790–797

Lin Y-C, Hsu F-H, Wu T-M (2013) Enhanced conductivity and thermal stability of conductive polyaniline/graphene composite synthesized by in situ chemical oxidation polymerization with sodium dodecyl sulfate. Synth Met 184:29–34. https://doi.org/https://doi.org/10.1016/j.synthmet.2013.10.001

Liu T, Guo Y, Zhang Z, et al (2019) Fabrication of hollow CuO/PANI hybrid nanofibers for non-enzymatic electrochemical detection of H2O2 and glucose. Sensors Actuators B Chem 286:370–376

Liu X, Zheng W, Kumar R, et al (2022) Conducting polymer-based nanostructures for gas sensors. Coord Chem Rev 462:214517. https://doi.org/https://doi.org/10.1016/j.ccr.2022.214517

Louarn G, Lapkowski M, Quillard S, et al (1996) Vibrational properties of polyaniline isotope effects. J Phys Chem 100:6998–7006

Lu T, Chen F (2012) Multiwfn: A multifunctional wavefunction analyzer. J Comput Chem 33:580–592

Lu Y, Song Y, Wang F (2013) Thermoelectric properties of graphene nanosheets-modified polyaniline hybrid nanocomposites by an in situ chemical polymerization. Mater Chem Phys 138:238–244. https://doi.org/https://doi.org/10.1016/j.matchemphys.2012.11.052

Luo Y, Wang X (2018) Industry-viable metal anticorrosion application of polyaniline. In: Conductive Polymers. CRC Press, pp 107–128

Ma R, Liu Z, Zhang Q, et al (2019) Evaluating Polymer Representations via Quantifying Structure-Property Relationships. J Chem Inf Model 59:3110–3119. https://doi.org/10.1021/acs.jcim.9b00358

Ma R, Luo T (2020) PI1M: A benchmark database for polymer informatics. J Chem Inf Model 60:4684–4690. https://doi.org/10.1021/acs.jcim.0c00726

MacDiarmid AG (2001) “Synthetic metals”: a novel role for organic polymers. Curr Appl Phys 1:269–279

Macdiarmid AG, Chiang JC, Richter AF, Epstein AJ (1987) Polyaniline: a new concept in conducting polymers. Synth Met 18:285–290. https://doi.org/https://doi.org/10.1016/0379-6779(87)90893-9

MacDiarmid AG, Jones WE, Norris ID, et al (2001) Electrostatically-generated nanofibers of electronic polymers. Synth Met 119:27–30. https://doi.org/https://doi.org/10.1016/S0379-6779(00)00597-X

MacKay DJC (1996) Hyperparameters: optimize, or integrate out? Maximum Entropy Bayesian Methods St Barbar California, USA, 1993 43–59

Madurani KA, Suprapto S, Machrita NI, et al (2020) Progress in graphene synthesis and its application: History, challenge and the future outlook for research and industry. ECS J Solid State Sci Technol 9:93013

Mahmoudi T, Wang Y, Hahn Y-B (2018) Graphene and its derivatives for solar cells application. Nano Energy 47:51–65

Maity D, Kumar RTR (2018) Polyaniline Anchored MWCNTs on Fabric for High Performance Wearable Ammonia Sensor. ACS Sensors 3:1822–1830. https://doi.org/10.1021/acssensors.8b00589

Majeed AH, Mohammed LA, Hammoodi OG, et al (2022) A Review on Polyaniline: Synthesis, Properties, Nanocomposites, and Electrochemical Applications. Int. J. Polym. Sci. 2022

Malik N, Arfin T, Khan AU (2019) Graphene nanomaterials: chemistry and pharmaceutical perspectives. In: Nanomaterials for drug delivery and therapy. Elsevier, pp 373–402

Mallakpour S, Hatami M, Golmohammadi H (2010) Prediction of inherent viscosity for polymers containing natural amino acids from the theoretical derived molecular descriptors. Polymer (Guildf) 51:3568–3574

Man MS, Abdullah MAM, Abdullah SB, Yaacob Z (2017) Screening cation and anion of ionic liquid for dissolution of silicon dioxide using COSMO-RS. Indian J Sci Technol 10:1–6

Mandal S, Bej S, Banerjee P (2023) Insights into the uses of two azine decorated d10-MOFs for corrosion inhibition application on mild steel surface in saline medium: Experimental as well as theoretical investigation. J Mol Liq 381:121789. https://doi.org/10.1016/j.molliq.2023.121789

Manoharan A, Begam KM, Aparow VR, Sooriamoorthy D (2022) Artificial Neural Networks, Gradient Boosting and Support Vector Machines for electric vehicle battery state estimation: A review. J Energy Storage 55:105384. https://doi.org/https://doi.org/10.1016/j.est.2022.105384

Martin TB, Audus DJ (2023) Emerging Trends in Machine Learning: A Polymer Perspective. ACS Polym Au

Martins VHN, Siqueira NMS, Fonsaca JES, et al (2021) Ternary nanocomposites of reduced graphene oxide, polyaniline, and iron oxide applied for energy storage. ACS Appl Nano Mater 4:5553–5563

Maruthamani D, Divakar D, Harshavardhan M, Kumaravel M (2016) Evaluation of bactericidal activity of reduced graphene oxide supported titania nanoparticles under visible light irradiation. J Chem Pharm Res 8:236–244

Masemola CM, Moloto N, Tetana ZN, et al (2022) N-doped graphene quantum dot-modified polyaniline for room-temperature sensing of alcohol vapors. Mater Chem Phys 287:126229. https://doi.org/https://doi.org/10.1016/j.matchemphys.2022.126229

Masson S, Vaulot C, Reinert L, et al (2017) Thermodynamic study of seven micropollutants adsorption onto an activated carbon cloth: Van't Hoff method, calorimetry, and COSMO-RS simulations. Environ Sci Pollut Res 24:10005–10017. https://doi.org/10.1007/s11356-016-7614-0

Matsukawa H, Kitahara M, Otake K (2021) Fluid Phase Equilibria Estimation of pure component parameters of PC-SAFT EoS by an artificial neural network based on a group contribution method. Fluid Phase Equilib 548:113179. https://doi.org/10.1016/j.fluid.2021.113179

Mattson EC, Johns JE, Pande K, et al (2014) Vibrational excitations and low-energy electronic structure of epoxide-decorated graphene. J Phys Chem Lett 5:212–219

Maulana A, Nugraheni AY, Jayanti DN, et al (2017) Defect and magnetic properties of reduced graphene oxide prepared from old coconut shell. In: IOP Conference Series: Materials Science and Engineering. IOP Publishing, p 12021

Maulud D, Abdulazeez AM (2020) A Review on Linear Regression Comprehensive in Machine Learning. J Appl Sci Technol Trends 1:140–147. https://doi.org/10.38094/jastt1457

Meer S, Kausar A, Iqbal T (2016) Trends in conducting polymer and hybrids of conducting polymer/carbon nanotube: a review. Polym Plast Technol Eng 55:1416–1440

Meng F-L, Guo Z, Huang X-J (2015) Graphene-based hybrids for chemiresistive gas sensors. TrAC Trends Anal Chem 68:37–47. https://doi.org/https://doi.org/10.1016/j.trac.2015.02.008

Meyer TA, Ramirez C, Tamasi MJ, Gormley AJ (2022) A user's guide to machine learning for polymeric biomaterials. ACS Polym Au 3:141–157

Mienye ID, Sun Y, Wang Z (2019) Prediction performance of improved decision tree-based algorithms: a review. Procedia Manuf 35:698–703

Mirzaei A, Hashemi B, Janghorban K (2016) α-Fe2O3 based nanomaterials as gas sensors. J Mater Sci Mater Electron 27:3109–3144

Mirzaei A, Janghorban K, Hashemi B, Neri G (2015) Metal-core@ metal oxide-shell nanomaterials for gas-sensing applications: a review. J Nanoparticle Res 17:1–36

Mishra AK (2018) Conducting polymers: concepts and applications. J At Mol Condens Matter Nano Phys 5:159–193

Mitra I, Saha A, Roy K (2010) Exploring quantitative structure-activity relationship studies of antioxidant phenolic compounds obtained from traditional Chinese medicinal plants. Mol Simul 36:1067–1079. https://doi.org/10.1080/08927022.2010.503326

Mitra M, Kulsi C, Chatterjee K, et al (2015) Reduced graphene oxide-polyaniline composites—synthesis, characterization and optimization for thermoelectric applications. RSC Adv 5:31039–31048

Mohammed HY, Farea MA, Sayyad PW, et al (2022) Selective and sensitive chemiresistive sensors based on polyaniline/graphene oxide nanocomposite: A cost-effective approach. J Sci Adv Mater Devices 7:. https://doi.org/10.1016/j.jsamd.2021.08.004

Moltved KA, Kepp KP (2019) Performance of density functional theory for transition metal oxygen bonds. ChemPhysChem 20:3210–3220

Moon S, Jung YH, Kim DK (2015) Enhanced electrochemical performance of a crosslinked polyaniline-coated graphene oxide-sulfur composite for rechargeable lithium–sulfur batteries. J Power Sources 294:386–392. https://doi.org/https://doi.org/10.1016/j.jpowsour.2015.06.011

Mosca E, Szigeti F, Tragianni S, et al (2022) SHAP-based explanation methods: a review for NLP interpretability. In: Proceedings of the 29th International Conference on Computational Linguistics. pp 4593–4603

Mostafaei A, Zolriasatein A (2012) Synthesis and characterization of conducting polyaniline nanocomposites containing ZnO nanorods. Prog Nat Sci Mater Int 22:273–280

Motevalli B, Sun B, Barnard AS (2020) Understanding and Predicting the Cause of Defects in Graphene Oxide Nanostructures Using Machine Learning. J Phys Chem C 124:7404–7413. https://doi.org/10.1021/acs.jpcc.9b10615

Mouffok A, Bellouche D, Debbous I, et al (2023) Synergy of garlic extract and deep eutectic solvents as promising natural Antibiotics: Experimental and COSMO-RS. J Mol Liq 375:121321. https://doi.org/https://doi.org/10.1016/j.molliq.2023.121321

Moumeni O, Mehri M, Kerkour R, et al (2023) Experimental and detailed DFT/MD simulation of α-aminophosphonates as promising corrosion inhibitor for XC48 carbon steel in HCl environment. J Taiwan Inst Chem Eng 147:104918

Moyseowicz A, Gryglewicz G (2019) Hydrothermal-assisted synthesis of a porous polyaniline/reduced graphene oxide composite as a high-performance electrode material for supercapacitors. Compos Part B Eng 159:4–12

Mozafari M, Mehraien M, Vashaee D, Tayebi L (2012) Electroconductive nanocomposite scaffolds: a new strategy into tissue engineering and regenerative medicine. INTECH Open Access Publ 369–392

Murmu M, Murmu NC, Ghosh M, Banerjee P (2022) Density functional theory, Monte Carlo simulation and non-covalent interaction study for exploring the adsorption and corrosion inhibiting property of double azomethine functionalised organic molecules. J Adhes Sci Technol 36:2732–2760

Murugan C, Subramanian E, Padiyan DP (2014) Enhanced sensor functionality of in situ synthesized polyaniline–SnO2 hybrids toward benzene and toluene vapors. Sensors Actuators B Chem 205:74–81

Navazani S, Shokuhfar A, Hassanisadi M, et al (2018) Fabrication and characterization of a sensitive, room temperature methane sensor based on SnO2@reduced graphene oxide-polyaniline ternary nanohybrid. Mater Sci Semicond Process 88:139–147. https://doi.org/https://doi.org/10.1016/j.mssp.2018.08.006

Nazari H, Arefinia R (2019) An investigation into the relationship between the electrical conductivity and particle size of polyaniline in nano scale. Int J Polym Anal Charact 24:178–190

Neelgund GM, Oki A (2011) A facile method for the synthesis of polyaniline nanospheres and the effect of doping on their electrical conductivity. Polym Int 60:1291–1295

Nguyen VH, Shim J-J (2015) Ultrasmall SnO2 nanoparticle-intercalated graphene@polyaniline composites as an active electrode material for supercapacitors in different electrolytes. Synth Met 207:110–115. https://doi.org/https://doi.org/10.1016/j.synthmet.2015.06.010

Niaura G, Mažeikien R, Malinauskas A (2004) Structural changes in conducting form of polyaniline upon ring sulfonation as deduced by near infrared resonance Raman spectroscopy. Synth Met 145:105–112

Nicolas-Debarnot D, Poncin-Epaillard F (2003) Polyaniline as a new sensitive layer for gas sensors. Anal Chim Acta 475:1–15. https://doi.org/https://doi.org/10.1016/S0003-2670(02)01229-1

Novoselov KS, Geim AK, Morozov S V, et al (2004) Electric field effect in atomically thin carbon films. Science (80-) 306:666–669

Oliveira GP, Barboza BH, Batagin-Neto A (2022) Polyaniline-based gas sensors: DFT study on the effect of side groups. Comput Theor Chem 1207:113526.

https://doi.org/10.1016/j.comptc.2021.113526

Oluwaseye A, Uzairu A, Shallangwa GA, Abechi SE (2020) Quantum chemical descriptors in the QSAR studies of compounds active in maxima electroshock seizure test. J King Saud Univ - Sci 32:75–83. https://doi.org/10.1016/j.jksus.2018.02.009

Paduszyński K (2018) Extensive evaluation of the conductor-like screening model for real solvents method in predicting liquid–liquid equilibria in ternary systems of ionic liquids with molecular compounds. J Phys Chem B 122:4016–4028

Pandey PK, Nyori T, Pandey V (2017) Estimation of reference evapotranspiration using data driven techniques under limited data conditions. Model Earth Syst Environ 3:1449–1461. https://doi.org/10.1007/s40808-017-0367-z

Pandey S (2016) Highly sensitive and selective chemiresistor gas/vapor sensors based on polyaniline nanocomposite: A comprehensive review. J Sci Adv Mater Devices 1:431–453. https://doi.org/10.1016/j.jsamd.2016.10.005

Pang AL, Arsad A, Ahmadipour M (2021a) Synthesis and factor affecting on the conductivity of polypyrrole: a short review. Polym Adv Technol 32:1428–1454

Pang Z, Nie Q, Wei A, et al (2017) Effect of In2O3 nanofiber structure on the ammonia sensing performances of In2O3/PANI composite nanofibers. J Mater Sci 52:686–695

Pang Z, Yildirim E, Pasquinelli MA, Wei Q (2021b) Ammonia sensing performance of polyaniline-coated polyamide 6 nanofibers. ACS omega 6:8950–8957

Park J, Yang X, Wickramasinghe D, et al (2020) Functionalization of pristine graphene for the synthesis of covalent graphene–polyaniline nanocomposite. RSC Adv 10:26486–26493

Park S, An J, Jung I, et al (2009) Colloidal suspensions of highly reduced graphene oxide in a wide variety of organic solvents. Nano Lett 9:1593–1597

Park S, An J, Potts JR, et al (2011) Hydrazine-reduction of graphite- and graphene oxide. Carbon N Y 49:3019–3023. https://doi.org/https://doi.org/10.1016/j.carbon.2011.02.071

Parmar M, Balamurugan C, Lee D-W (2013) PANI and graphene/PANI nanocomposite films—Comparative toluene gas sensing behavior. Sensors 13:16611–16624

Partridge AC, Jansen ML, Arnold WM (2000) Conducting polymer-based sensors. Mater Sci Eng C 12:37–42

Parveen N, Mahato N, Ansari MO, Cho MH (2016) Enhanced electrochemical behavior and hydrophobicity of crystalline polyaniline@graphene nanocomposite synthesized at elevated temperature. Compos Part B Eng 87:281–290. https://doi.org/https://doi.org/10.1016/j.compositesb.2015.10.029

Patra TK (2022) Data-Driven Methods for Accelerating Polymer Design. ACS Polym Au 2:8–

26. https://doi.org/10.1021/acspolymersau.1c00035

Perdew JP, Burke K, Ernzerhof M (1996) Generalized gradient approximation made simple. Phys Rev Lett 77:3865

Pereira da Silva JE, De Faria DLA, Córdoba de Torresi SI, Temperini MLA (2000) Influence of thermal treatment on doped polyaniline studied by resonance Raman spectroscopy. Macromolecules 33:3077–3083

Pionteck J, Pionteck J, Wypych G (2007) Handbook of antistatics. ChemTec Publishing

Pirdashti M, Curteanu S, Kamangar MH, et al (2013) Artificial neural networks: applications in chemical engineering. Rev Chem Eng 29:205–239

Plutnar J, Pumera M, Sofer Z (2018) The chemistry of CVD graphene. J Mater Chem C 6:6082–6101

Popelier PLA (2014) The QTAIM perspective of chemical bonding. Chem Bond Fundam Asp Chem Bond 271–308

Prías Barragán JJ, Gross K, Darío Perea J, et al (2020) Graphene Oxide Thin Films: Synthesis and Optical Characterization. ChemistrySelect 5:11737–11744. https://doi.org/10.1002/slct.202002481

Qiu B, Wang J, Li Z, et al (2020) Influence of acidity and oxidant concentration on the nanostructures and electrochemical performance of polyaniline during fast microwave-assisted chemical polymerization. Polymers (Basel) 12:310

Quang NM, Mau TX, Ai Nhung NT, et al (2019) Novel QSPR modeling of stability constants of metal-thiosemicarbazone complexes by hybrid multivariate technique: GA-MLR, GA-SVR and GA-ANN. J Mol Struct 1195:95–109. https://doi.org/https://doi.org/10.1016/j.molstruc.2019.05.050

Rahman MM, Mahtab T, Mukhlish MZ Bin, et al (2021) Enhancement of electrical properties of metal doped polyaniline synthesized by different doping techniques. Polym Bull 78:5379–5397

Raji M, Zari N, El Kacem Qaiss A, Bouhfid R (2019) Functionalized Graphene Nanocomposites and their Derivatives

Ramakrishnan S (2011) Conducting Polymers. IntechOpen

Rangel-Olivares FR, Arce-Estrada EM, Cabrera-Sierra R (2021) Synthesis and characterization of polyaniline-based polymer nanocomposites as anti-corrosion coatings. Coatings 11:653

Rashidian V, Hassanlourad M (2014) Application of an artificial neural network for modeling the mechanical behavior of carbonate soils. Int J Geomech 14:142–150

Rasmussen SC (2017) The early history of polyaniline: discovery and origins. Substantia 1:99–109

Raza S, Li X, Soyekwo F, et al (2021) A comprehensive overview of common conducting polymer-based nanocomposites; Recent advances in design and applications. Eur Polym J 160:110773. https://doi.org/https://doi.org/10.1016/j.eurpolymj.2021.110773

Reddy KR, Sin BC, Ryu KS, et al (2009) In situ self-organization of carbon black–polyaniline composites from nanospheres to nanorods: Synthesis, morphology, structure and electrical conductivity. Synth Met 159:1934–1939. https://doi.org/https://doi.org/10.1016/j.synthmet.2009.06.018

Reza M, Srikandi N, Amalina AN, et al (2019) Variation of Ammonium Persulfate Concentration Determines Particle Morphology and Electrical Conductivity in HCl Doped Polyaniline. In: IOP Conference Series: Materials Science and Engineering. IOP Publishing, p 12002

Riaz U, Singh N, Banoo S (2022) Theoretical studies of conducting polymers: a mini review. New J Chem 46:4954–4973. https://doi.org/10.1039/d1nj05352c

Roth S, Graupner W (1993) Conductive polymers: evaluation of industrial applications. Synth Met 57:3623–3631

Saeed M, Alshammari Y, Majeed SA, Al-Nasrallah E (2020) Chemical vapour deposition of graphene—Synthesis, characterisation, and applications: A review. Molecules 25:3856

Salunkhe RR, Hsu SH, Wu KCW, Yamauchi Y (2014) Large-scale synthesis of reduced graphene oxides with uniformly coated polyaniline for supercapacitor applications. ChemSusChem 7:1551–1556. https://doi.org/10.1002/cssc.201400147

Samaddar P, Son Y-S, Tsang DCW, et al (2018) Progress in graphene-based materials as superior media for sensing, sorption, and separation of gaseous pollutants. Coord Chem Rev 368:93–114. https://doi.org/https://doi.org/10.1016/j.ccr.2018.04.013

Sapurina I, Stejskal J (2008) The mechanism of the oxidative polymerization of aniline and the formation of supramolecular polyaniline structures. Polym Int 57:1295–1325

Saravanan KK, Siva Karthik P, Mirtha PR, et al (2020) A one-pot hydrothermal-induced PANI/SnO2 and PANI/SnO2/rGO ternary composites for high-performance chemiresistive-based H2S and NH3 gas sensors. J Mater Sci Mater Electron 31:8825–8836

Sattar N, Sajid H, Tabassum S, et al (2022) Potential sensing of toxic chemical warfare agents (CWAs) by twisted nanographenes: A first principle approach. Sci Total Environ 824:153858. https://doi.org/https://doi.org/10.1016/j.scitotenv.2022.153858

Sen T, Mishra S, Shimpi NG (2016) Synthesis and sensing applications of polyaniline nanocomposites: A review. RSC Adv 6:42196–42222. https://doi.org/10.1039/c6ra03049a

Sengupta PP, Adhikari B (2007) Influence of polymerization condition on the electrical conductivity and gas sensing properties of polyaniline. Mater Sci Eng A 459:278–285

Sengupta PP, Barik S, Adhikari B (2006) Polyaniline as a gas-sensor material. Mater Manuf Process 21:263–270

Shankar U, Gogoi R, Sethi SK, Verma A (2022) Introduction to Materials Studio Software for the Atomistic-Scale Simulations. In: Forcefields for Atomistic-Scale Simulations: Materials and Applications. Springer, pp 299–313

Sharifi H, Zabihzadeh SM, Ghorbani M (2018) The application of response surface methodology on the synthesis of conductive polyaniline/cellulosic fiber nanocomposites. Carbohydr Polym 194:384–394

Shi Q, Yan L, Jing C (2020) Oxidation of Arsenite by Epoxy Group on Reduced Graphene Oxide/Metal Oxide Composite Materials. Adv Sci 7:1–8. https://doi.org/10.1002/advs.202001928

Shoaie N, Daneshpour M, Azimzadeh M, et al (2019) Electrochemical sensors and biosensors based on the use of polyaniline and its nanocomposites: a review on recent advances. Microchim Acta 186:1–29. https://doi.org/10.1007/s00604-019-3588-1

Shokuhi Rad A, Esfahanian M, Ganjian E, Tayebi H (2016) Ab-initio study of physisorption of hydrogen cyanide on 2PANI: a model for polyaniline gas sensor. Zeitschrift für Phys Chemie 230:1487–1498

Silva CHB, Iliut M, Muryn C, et al (2018) Ternary nanocomposites of reduced graphene oxide, polyaniline and hexaniobate: Hierarchical architecture and high polaron formation. Beilstein J Nanotechnol 9:2936–2946. https://doi.org/10.3762/bjnano.9.272

Singh P, Shukla SK (2020) Advances in polyaniline-based nanocomposites. J Mater Sci 55:1331–1365. https://doi.org/10.1007/s10853-019-04141-z

Singh WI, Sinha S, Devi NA, et al (2022) Fabrication and Characterization of Reduced Graphene Oxide/Polyaniline/Poly(Caprolactone) Electrospun Nanofiber. Arab J Sci Eng 47:925–934. https://doi.org/10.1007/s13369-021-05901-3

Skotheim TA (1997) Handbook of conducting polymers. CRC press

Skucha K, Fan Z, Jeon K, et al (2010) Palladium/silicon nanowire Schottky barrier-based hydrogen sensors. Sensors Actuators B Chem 145:232–238. https://doi.org/https://doi.org/10.1016/j.snb.2009.11.067

Słupek E, Makoś-Chełstowska P, Gębicki J (2021) Removal of siloxanes from model biogas by means of deep eutectic solvents in absorption process. Materials (Basel) 14:1–20. https://doi.org/10.3390/ma14020241

Smith KH, Tejeda-Montes E, Poch M, Mata A (2011) Integrating top-down and self-assembly in the fabrication of peptide and protein-based biomedical materials. Chem Soc Rev 40:4563–4577

Song Y, Liang J, Lu J, Zhao X (2017) An efficient instance selection algorithm for k nearest neighbor regression. Neurocomputing 251:26–34. https://doi.org/https://doi.org/10.1016/j.neucom.2017.04.018

Sonker RK, Yadav BC, Dzhardimalieva GI (2016) Preparation and properties of nanostructured PANI thin film and its application as low temperature NO2 sensor. J Inorg Organomet Polym Mater 26:1428–1433

Souza Jr FG, Sirelli L, Michel RC, et al (2006) In situ polymerization of aniline in the presence of carbon black. J Appl Polym Sci 102:535–541

Sreeja VG, Vinitha G, Reshmi R, et al (2019) Structural, spectral, electrical and nonlinear optical characterizations of RGO-PANI composites. Mater Today Proc 10:456–465. https://doi.org/10.1016/j.matpr.2019.03.010

Stockton WB, Rubner MF (1997) Molecular-level processing of conjugated polymers. 4. Layer-by-layer manipulation of polyaniline via hydrogen-bonding interactions. Macromolecules 30:2717–2725

Stoller MD, Park S, Zhu Y, et al (2008) Graphene-based ultracapacitors. Nano Lett 8:3498–3502

Stone M (1976) Cross-Validatory Choice and Assessment of Statistical Predictions (With Discussion). J R Stat Soc Ser B 38:102–102. https://doi.org/10.1111/j.2517-6161.1976.tb01573.x

Subramanian E, Santhanamari P, Murugan C (2018) Sensor functionality of conducting polyaniline-metal oxide (tio 2/sno 2) hybrid materials films toward benzene and toluene vapors at room temperature. J Electron Mater 47:4764–4771

Susaimanickam A, Manickam P, Joseph AA (2023) A Comprehensive Review on RSM-Coupled Optimization Techniques and Its Applications. Arch Comput Methods Eng 1–23

Syed AR (2011) A review of cross validation and adaptive model selection

Szabo A, Ostlund NS (2012) Modern quantum chemistry: introduction to advanced electronic structure theory. Courier Corporation

Tabari L, Farmanzadeh D (2020) Yttrium doped graphene oxide as a new adsorbent for H2O, CO, and ethylene molecules: Dispersion-corrected DFT calculations. Appl Surf Sci 500:144029. https://doi.org/https://doi.org/10.1016/j.apsusc.2019.144029

Tang T, Yuan R, Guo N, et al (2022) Improving the surface area of metal organic framework-derived porous carbon through constructing inner support by compatible graphene quantum dots. J Colloid Interface Sci 623:77–85. https://doi.org/https://doi.org/10.1016/j.jcis.2022.04.161

Tanguy NR, Arjmand M, Yan N (2019) Nanocomposite of Nitrogen-Doped Graphene/Polyaniline for Enhanced Ammonia Gas Detection. Adv Mater Interfaces 6:1900552. https://doi.org/https://doi.org/10.1002/admi.201900552

Tanguy NR, Khorsand Kazemi K, Hong J, et al (2022) Flexible, robust, and high-performance gas sensors based on lignocellulosic nanofibrils. Carbohydr Polym 278:118920. https://doi.org/https://doi.org/10.1016/j.carbpol.2021.118920

Tanguy NR, Thompson M, Yan N (2018) A review on advances in application of polyaniline for ammonia detection. Sensors Actuators, B Chem 257:1044–1064. https://doi.org/10.1016/j.snb.2017.11.008

Tanguy NR, Wiltshire B, Arjmand M, et al (2020) Highly sensitive and contactless ammonia detection based on nanocomposites of phosphate-functionalized reduced graphene oxide/polyaniline immobilized on microstrip resonators. ACS Appl Mater Interfaces 12:9746–9754

Terrones M, Martín O, González M, et al (2011) Interphases in graphene polymer-based nanocomposites: achievements and challenges

Tian H, Yang Y, Xie D, et al (2014a) Wafer-scale integration of graphene-based electronic, optoelectronic and electroacoustic devices. Sci Rep 4:1–9

Tian Z, Yu H, Wang L, et al (2014b) Recent progress in the preparation of polyaniline nanostructures and their applications in anticorrosive coatings. RSC Adv 4:28195–28208

Timmer B, Olthuis W, Van Den Berg A (2005) Ammonia sensors and their applications—a review. Sensors Actuators B Chem 107:666–677

Tiwari SK, Sahoo S, Wang N, Huczko A (2020) Graphene research and their outputs: Status and prospect. J Sci Adv Mater Devices 5:10–29. https://doi.org/https://doi.org/10.1016/j.jsamd.2020.01.006

Tomczykowa M, Plonska-Brzezinska ME (2019) Conducting polymers, hydrogels and their composites: Preparation, properties and bioapplications. Polymers (Basel) 11:350

Torrecilla JS, Palomar J, Lemus J, Rodríguez F (2010) A quantum-chemical-based guide to analyze/quantify the cytotoxicity of ionic liquids. Green Chem 12:123–13.

https://doi.org/10.1039/b919806g

Travis AS (1994) From Manchester to Massachusetts via Mulhouse: the transatlantic voyage of aniline black. Technol Cult 35:70–99

Tropsha A, Gramatica P, Gombar VK (2003) The importance of being earnest: Validation is the absolute essential for successful application and interpretation of QSPR models. QSAR Comb Sci 22:69–77. https://doi.org/10.1002/qsar.200390007

Tung NT, Van Khai T, Lee H, Sohn D (2011) The effects of dopant on morphology formation in polyaniline graphite nanoplatelet composite. Synth Met 161:177–182

Tung TT, Nine MJ, Krebsz M, et al (2017) Recent advances in sensing applications of graphene assemblies and their composites. Adv Funct Mater 27:1702891

Uka D, Blagojević B, Alioui O, et al (2023) An innovative and environmentally friendly approach for resveratrol solubilization and bioaccessibility enhancement by using natural deep eutectic solvents. J Mol Liq 123411. https://doi.org/https://doi.org/10.1016/j.molliq.2023.123411

Ullah H, Shah AUHA, Bilal S, Ayub K (2013) DFT study of polyaniline NH3, CO2, and CO gas sensors: Comparison with recent experimental data. J Phys Chem C 117:23701–23711. https://doi.org/10.1021/jp407132c

Umare SS, Shambharkar BH, Ningthoujam RS (2010) Synthesis and characterization of polyaniline–Fe3O4 nanocomposite: Electrical conductivity, magnetic, electrochemical studies. Synth Met 160:1815–1821. https://doi.org/https://doi.org/10.1016/j.synthmet.2010.06.015

Umehara M, Stein HS, Guevarra D, et al (2019) Analyzing machine learning models to accelerate generation of fundamental materials insights. npj Comput Mater 5:34

Usman F, Dennis JO, Seong KC, et al (2019) Synthesis and characterisation of a ternary composite of polyaniline, reduced graphene-oxide and chitosan with reduced optical band gap and stable aqueous dispersibility. Results Phys 15:102690. https://doi.org/10.1016/j.rinp.2019.102690

Vallés C, Jiménez P, Munoz E, et al (2011) Simultaneous reduction of graphene oxide and polyaniline: doping-assisted formation of a solid-state charge-transfer complex. J Phys Chem C 115:10468–10474

Veloso VA, Silva DL, Gastelois PL, et al (2022) Polyaniline/graphene nanocomposite: Effect of the graphene functionalization with a long-chain fatty acid. Mater Chem Phys 285:. https://doi.org/10.1016/j.matchemphys.2022.126162

Verdejo R, Tapiador FJ, Helfen L, et al (2009) Fluid dynamics of evolving foams. Phys Chem

Chem Phys 11:10860–10866

Vikrant K, Kumar V, Kim K-H (2018) Graphene materials as a superior platform for advanced sensing strategies against gaseous ammonia. J Mater Chem A 6:22391–22410

Vinet L, Zhedanov A (2011) A “missing” family of classical orthogonal polynomials. Springer Science & Business Media

Virji S, Huang J, Kaner RB, Weiller BH (2004) Polyaniline nanofiber gas sensors: examination of response mechanisms. Nano Lett 4:491–496

Visakh PM, Della Pina C, Falletta E (2017) Polyaniline blends, composites, and nanocomposites. Elsevier

Waite SR, Nazarpour S (2016) Graphene Technology: From Laboratory to Fabrication. John Wiley & Sons

Walczak S, Cerpa N (2019) Artificial Neural Networks In Advanced methodologies and technologies in artificial intelligence, computer simulation, and human-computer interaction. 40–53

Wang C, Wang L, Soo A, et al (2023) Machine learning based prediction and optimization of thin film nanocomposite membranes for organic solvent nanofiltration. Sep Purif Technol 304:122328

Wang H, Hao Q, Yang X, et al (2009) Graphene oxide doped polyaniline for supercapacitors. Electrochem commun 11:1158–1161

Wang H, Hao Q, Yang X, et al (2010) A nanostructured graphene/polyaniline hybrid material for supercapacitors. Nanoscale 2:2164–2170

Wang H, Nie S, Li H, et al (2019) 3D Hollow Quasi-Graphite Capsules/Polyaniline Hybrid with a High Performance for Room-Temperature Ammonia Gas Sensors. ACS Sensors 4:2343–2350. https://doi.org/10.1021/acssensors.9b00882

Wang L, Fu X (2005) Data mining with computational intelligence. Springer Science & Business Media

Wang L, Lu X, Lei S, Song Y (2014a) Graphene-based polyaniline nanocomposites: preparation, properties and applications. J Mater Chem A 2:4491–4509

Wang L, Ye Y, Lu X, et al (2013) Hierarchical nanocomposites of polyaniline nanowire arrays on reduced graphene oxide sheets for supercapacitors. Sci Rep 3:3568

Wang T, Huang D, Yang Z, et al (2016) A Review on Graphene-Based Gas/Vapor Sensors with Unique Properties and Potential Applications. Nano-Micro Lett 8:95–119. https://doi.org/10.1007/s40820-015-0073-1

Wang W, Hao Q, Lei W, et al (2014b) Ternary nitrogen-doped graphene/nickel ferrite/polyaniline nanocomposites for high-performance supercapacitors. J Power Sources 269:250–259. https://doi.org/https://doi.org/10.1016/j.jpowsour.2014.07.010

Wang Y, Liu A, Han Y, Li T (2020) Sensors based on conductive polymers and their composites: a review. Polym Int 69:7–17

Wei J, Liang B, Cao Q, et al (2017) Vertically aligned PANI nanorod arrays grown on graphene oxide nanosheets for a high-performance NH 3 gas sensor. RSC Adv 7:33510–33520

Wen L, Li K, Liu J, et al (2017) Graphene/polyaniline@carbon cloth composite as a high-performance flexible supercapacitor electrode prepared by a one-step electrochemical co-deposition method. RSC Adv 7:7688–7693. https://doi.org/10.1039/c6ra27545a

Williams T, Kelley C, Bröker HB, et al (2017) Gnuplot 4.5: an interactive plotting program. 2011. URL http//www gnuplot info 56:

Witek-Krowiak A, Chojnacka K, Podstawczyk D, et al (2014) Application of response surface methodology and artificial neural network methods in modelling and optimization of biosorption process. Bioresour Technol 160:150–160. https://doi.org/https://doi.org/10.1016/j.biortech.2014.01.021

Wnek GE (1986) A proposal for the mechanism of conduction in polyaniline. Synth Met 15:213–218. https://doi.org/10.1016/0379-6779(86)90026-3

Wu J-B, Lin M-L, Cong X, et al (2018a) Raman spectroscopy of graphene-based materials and its applications in related devices. Chem Soc Rev 47:1822–1873

Wu J, Wang J, Huang X, Bai H (2018b) A self-assembly route to porous polyaniline/reduced graphene oxide composite materials with molecular-level uniformity for high-performance supercapacitors. Energy Environ Sci 11:1280–1286

Wu Q, Shen W, Lv D, et al (2021) An enhanced flexible room temperature ammonia gas sensor based on GP-PANI/PVDF multi-hierarchical nanocomposite film. Sensors Actuators B Chem 334:129630. https://doi.org/https://doi.org/10.1016/j.snb.2021.129630

Wu S, Kondo Y, Kakimoto M aki, et al (2019) Machine-learning-assisted discovery of polymers with high thermal conductivity using a molecular design algorithm. npj Comput Mater 5:. https://doi.org/10.1038/s41524-019-0203-2

Wu Y, Wang S, Komvopoulos K (2020) A review of graphene synthesis by indirect and direct deposition methods. J Mater Res 35:76–89

Wu Z-S, Ren W, Gao L, et al (2009) Synthesis of graphene sheets with high electrical conductivity and good thermal stability by hydrogen arc discharge exfoliation. ACS Nano 3:411–417

Wu Z, Chen X, Zhu S, et al (2013a) Room temperature methane sensor based on graphene nanosheets/polyaniline nanocomposite thin film. IEEE Sens J 13:777–782. https://doi.org/10.1109/JSEN.2012.2227597

Wu Z, Chen X, Zhu S, et al (2013b) Enhanced sensitivity of ammonia sensor using graphene/polyaniline nanocomposite. Sensors Actuators, B Chem 178:485–493. https://doi.org/10.1016/j.snb.2013.01.014

Xavier PAF, Ajithkumar G, Varghese T (2019) Aldehyde functionalized multiwalled carbon nanotubes to synthesize highly conducting polyaniline-MWNT thin films. Mater Today Proc 25:129–133. https://doi.org/10.1016/j.matpr.2019.12.183

Xing X, Du L, Feng D, et al (2022) Twistable and tailorable V2O5/PANI/GO nanocomposites textile for wearable ammonia sensing. Sensors Actuators B Chem 351:130944. https://doi.org/https://doi.org/10.1016/j.snb.2021.130944

Xu F, Guo S, Luo Y-L (2014) Novel THTBN/MWNTs-OH polyurethane conducting composite thin films for applications in detection of volatile organic compounds. Mater Chem Phys 145:222–231

Xu J, Wang K, Zu S-Z, et al (2010) Hierarchical nanocomposites of polyaniline nanowire arrays on graphene oxide sheets with synergistic effect for energy storage. ACS Nano 4:5019–5026

Xu L-H, Wu T-M (2020) Synthesis of highly sensitive ammonia gas sensor of polyaniline/graphene nanoribbon/indium oxide composite at room temperature. J Mater Sci Mater Electron 31:7276–7283

Xu LQ, Liu YL, Neoh K, et al (2011) Reduction of graphene oxide by aniline with its concomitant oxidative polymerization. Macromol Rapid Commun 32:684–688

Xu P, Chen H, Li M, Lu W (2022) New opportunity: machine learning for polymer materials design and discovery. Adv Theory Simulations 5:2100565

Yan J, Wei T, Fan Z, et al (2010) Preparation of graphene nanosheet/carbon nanotube/polyaniline composite as electrode material for supercapacitors. J Power Sources 195:3041–3045

Yan Y, Chen J, Li N, et al (2018) Systematic bandgap engineering of graphene quantum dots and applications for photocatalytic water splitting and CO2 reduction. ACS Nano 12:3523–3532

Yan Y, Yang G, Xu J-L, et al (2020) Conducting polymer-inorganic nanocomposite-based gas sensors: a review. Sci Technol Adv Mater 21:768–786

Yang Y, Li S, Yang W, et al (2014) In situ polymerization deposition of porous conducting polymer on reduced graphene oxide for gas sensor. ACS Appl Mater Interfaces 6:13807–

13814

Yang Y, Zhang H, Chen J, et al (2013) Single-electrode-based sliding triboelectric nanogenerator for self-powered displacement vector sensor system. ACS Nano 7:7342–7351

Yang Z, Peng H, Wang W, Liu T (2010) Crystallization behavior of poly(ε-caprolactone)/layered double hydroxide nanocomposites. J Appl Polym Sci 116:2658–2667. https://doi.org/10.1002/app

Yap PL, Nine MJ, Hassan K, et al (2021) Graphene-based sorbents for multipollutants removal in water: a review of recent progress. Adv Funct Mater 31:2007356

Yasmin T, Mahmood A, Farooq M, et al (2023) Quince seed mucilage/β-cyclodextrin/Mmt-Na+-co-poly (methacrylate) based pH-sensitive polymeric carriers for controlled delivery of Capecitabine. Int J Biol Macromol 127032

Ye Z, Jiang Y, Tai H, et al (2015) The investigation of reduced graphene oxide@ SnO2–polyaniline composite thin films for ammonia detection at room temperature. J Mater Sci Mater Electron 26:833–841

Yi N, Abidian MR (2016) Conducting polymers and their biomedical applications. In: Biosynthetic polymers for medical applications. Elsevier, pp 243–276

Yin Q, Shu R, Xing H, et al (2016) Rheological behavior and electrical properties of graphene oxide/polyaniline nanocomposites. Nano 11:1650020

Young RJ, Kinloch IA, Gong L, Novoselov KS (2012) The mechanics of graphene nanocomposites: a review. Compos Sci Technol 72:1459–1476

Yu Y, Xu A, Zhang Y, et al (2023) Construction of hierarchical graphene/polyaniline@polyaniline electrodes by chemical and electrochemical polymerization for high-energy supercapacitors. Electrochim Acta 454:1–9. https://doi.org/10.1016/j.electacta.2023.142414

Zamiri G, Haseeb A (2020) Recent trends and developments in graphene/conducting polymer nanocomposites chemiresistive sensors. Materials (Basel) 13:3311

Zare EN, Makvandi P, Ashtari B, et al (2020) Progress in Conductive Polyaniline-Based Nanocomposites for Biomedical Applications: A Review. J Med Chem 63:1–22. https://doi.org/10.1021/acs.jmedchem.9b00803

Zegebreal LT, Tegegne NA, Hone FG (2023) Recent progress in hybrid conducting polymers and metal oxide nanocomposite for room-temperature gas sensor applications: A Review. Sensors Actuators A Phys 114472

Zengin H, Zhou W, Jin J, et al (2002) Carbon nanotube doped polyaniline. Adv Mater 14:1480–

1483

Zhan D, Yan J, Lai L, et al (2012) Engineering the electronic structure of graphene. Adv Mater 24:4055–4069

Zhang D (2007) On the conductivity measurement of polyaniline pellets. Polym Test 26:9–13. https://doi.org/https://doi.org/10.1016/j.polymertesting.2006.07.010

Zhang D, Wu Z, Zong X (2019a) Flexible and highly sensitive H2S gas sensor based on in-situ polymerized SnO2/rGO/PANI ternary nanocomposite with application in halitosis diagnosis. Sensors Actuators B Chem 289:32–41. https://doi.org/https://doi.org/10.1016/j.snb.2019.03.055

Zhang D, Xu Z, Yang Z, Song X (2020a) High-performance flexible self-powered tin disulfide nanoflowers/reduced graphene oxide nanohybrid-based humidity sensor driven by triboelectric nanogenerator. Nano Energy 67:104251. https://doi.org/10.1016/j.nanoen.2019.104251

Zhang D, Yang Y, Xu Z, et al (2022a) An eco-friendly gelatin based triboelectric nanogenerator for a self-powered PANI nanorod/NiCo2O4 nanosphere ammonia gas sensor. J Mater Chem A 10935–10949. https://doi.org/10.1039/d2ta01788a

Zhang F, Yang K, Liu G, et al (2022b) Recent Advances on Graphene: Synthesis, Properties, and Applications. Compos Part A Appl Sci Manuf 107051

Zhang L, Du W, Nautiyal A, et al (2018) Recent progress on nanostructured conducting polymers and composites: synthesis, application and future aspects. Sci China Mater 61:303–352

Zhang L, Tan Q, Kou H, et al (2019b) Highly sensitive NH3 wireless sensor based on Ag-RGO composite operated at room-temperature. Sci Rep 9:1–10

Zhang M, Li Y, Su Z, Wei G (2015) Recent advances in the synthesis and applications of graphene–polymer nanocomposites. Polym Chem 6:6107–6124

Zhang QH, Hou BS, Li YY, et al (2021) Two amino acid derivatives as high efficient green inhibitors for the corrosion of carbon steel in CO2-saturated formation water. Corros Sci 189:109596. https://doi.org/https://doi.org/10.1016/j.corsci.2021.109596

Zhang S, Wang H, Liu J, Bao C (2020b) Measuring the specific surface area of monolayer graphene oxide in water. Mater Lett 261:127098. https://doi.org/https://doi.org/10.1016/j.matlet.2019.127098

Zhang T, Qi H, Liao Z, et al (2019c) Engineering crystalline quasi-two-dimensional polyaniline thin film with enhanced electrical and chemiresistive sensing performances. Nat Commun 10:1–9

Zhang Y, Chen X, Chen H, et al (2023) Developing a highly-conductive and strength cotton yarn through dual shell architecture of graphene for smart wearable devices. Chem Eng J 470:143912. https://doi.org/https://doi.org/10.1016/j.cej.2023.143912

Zhang Y, Wan Q, Yang N (2019d) Recent advances of porous graphene: synthesis, functionalization, and electrochemical applications. Small 15:1903780

Zhao H-Y, Yu M-Y, Liu J, et al (2022) Efficient preconstruction of three-dimensional graphene networks for thermally conductive polymer composites. Nano-Micro Lett 14:129

Zhao N, Ma Z, Song H, et al (2018) Polyaniline/reduced graphene oxide-modified carbon fiber brush anode for high-performance microbial fuel cells. Int J Hydrogen Energy 43:17867–17872

Zhao Y, Mulder RJ, Houshyar S, Le TC (2023) A review on the application of molecular descriptors and machine learning in polymer design. Polym Chem 14:3325–3346

Zheng X, Ali Mohsin ME, Arsad A, Hassan A (2021) Polymerization of polyaniline under various concentrations of ammonium peroxydisulfate and hydrochloric acid by ultrasonic irradiation. J Appl Polym Sci 138:50637

Zhou T, Song Z, Sundmacher K (2019) Big Data Creates New Opportunities for Materials Research: A Review on Methods and Applications of Machine Learning for Materials Design. Engineering 5:1017–1026. https://doi.org/https://doi.org/10.1016/j.eng.2019.02.011

Zhou X, Wu T, Hu B, et al (2010) Synthesis of graphene/polyaniline composite nanosheets mediated by polymerized ionic liquid. Chem Commun 46:3663–3665

Zhou Y, Ding C, Qian X, An X (2015) Further improvement of flame retardancy of polyaniline-deposited paper composite through using phytic acid as dopant or co-dopant. Carbohydr Polym 115:670–676. https://doi.org/https://doi.org/10.1016/j.carbpol.2014.09.025

Zou Y, Zhang Z, Zhong W, Yang W (2018) Hydrothermal direct synthesis of polyaniline, graphene/polyaniline and N-doped graphene/polyaniline hydrogels for high performance flexible supercapacitors. J Mater Chem A 6:9245–9256

الملخص:

تقدم هذه الأطروحة استكشافًا شاملًا لتطوير وتحسين نانومركبات البولي أنيلين والغرافين المُعدّل، وهو تقدم محوري في علم وهندسة المواد. مع التركيز على المنهج الشمولي المتعدد التخصصات، يدمج هذا العمل استراتيجيات تجريبية مبتكرة ونمذجة حسابية وتقنيات تعلم الآلة المتقدمة لتحسين خصائص هذه النانومركبات. تتضمن البحوث طرق تصنيع مبتكرة وتستخدم نماذج التعلم الآلي الرائدة للتحليل التنبؤي، مما يعزز بشكل كبير الدقة في التنبؤ بالتوصيل الكهربائي واستجابات الكشف عن الغاز لنانومركبات بولي أنيلين/غرافين. تُعد هذه النماذج الأولى من نوعها في هذا المجال، تضع معايير جديدة في علم المواد المستدامة. علاوة على ذلك، تقدم الأطروحة طريقة تصنيع صديقة للبيئة لنانومركبات بولي أنيلين/أكسيد الجرافين المخفض باستخدام المذيبات المنصهرة بعمق، مما يمثل تطوراً مهماً نحو الاستدامة البيئية. هذا البحث المتكامل لا يثري فقط على إثراء فهم نانومركبات البولي أنيلين/الجرافين فحسب، بل يقدم أيضًا مساهمات جوهرية في تطوير المواد المستدامة. من المتوقع أن تكون النتائج والمنهجيات المقدمة في هذه الأطروحة ذات تأثيرات بعيدة المدى، فتفتح آفاقًا جديدة في التكنولوجيا والحفاظ على البيئة، خاصة في مجالات مثل المكثفات الفائقة وأجهزة استشعار الغازات وحلول تخزين الطاقة.

الكلمات المفتاحية : البولي أنيلين؛ نانومركبات الجرافين؛ التعلم الآلي في علم المواد؛ تحسين تصميم التجارب ؛ النمذجة الحسابية؛ نظرية الكثافة الوظيفية؛ التوصيل الكهربائي؛ الاستشعار للغاز؛ الاستدامة البيئية.

Résumé:

Cette thèse de doctorat offre une exploration complète du développement et de l'optimisation de nanocomposites de polyaniline (PANI) et de graphène fonctionnalisé, une avancée cruciale en science et ingénierie des matériaux. Mettant l'accent sur une approche multidisciplinaire, ce travail intègre des stratégies expérimentales innovantes, la modélisation informatique et des techniques avancées d'apprentissage automatique pour affiner les propriétés de ces nanocomposites. La recherche englobe des méthodes de synthèse novatrices et utilise des modèles révolutionnaires d'apprentissage automatique pour l'analyse prédictive, améliorant significativement la précision dans la prévision de la conductivité électrique et des réponses des capteurs de gaz des nanocomposites PANI/graphène. Ces modèles, une première dans le domaine, établissent de nouvelles normes en science des matériaux durables. De plus, la thèse présente un chemin de synthèse respectueux de l'environnement pour les nanocomposites PANI/oxide de graphène réduit en utilisant des solvants eutectiques profonds, marquant un pas vers la durabilité environnementale. Cette recherche intégrative enrichit non seulement la compréhension des nanocomposites PANI/graphène, mais contribue également de manière substantielle au développement de matériaux durables. Les découvertes et méthodologies présentées dans cette thèse devraient avoir un impact considérable, ouvrant de nouvelles voies dans la technologie et la conservation de l'environnement, notamment dans des domaines tels que les supercondensateurs, les capteurs de gaz et les solutions de stockage d'énergie.

Mots clés : Polyaniline (PANI) ; Nanocomposites de Graphène ; Machine Learning en Science des Matériaux ; Optimisation du Plan d'expérience ; Modélisation Moléculaire ; Théorie Fonctionnelle de la Densité (DFT) ; Conductivité Électrique ; Détection de Gaz ; Durabilité Environnementale.

Abstract:

This PhD thesis presents a comprehensive exploration of the development and optimization of polyaniline (PANI) and functionalized graphene nanocomposites, a pivotal advancement in materials science and engineering. Emphasizing a multidisciplinary approach, this work integrates innovative experimental strategies, computational modeling, and advanced machine learning techniques to refine the properties of these nanocomposites. The research encapsulates innovative synthesis methods and employs groundbreaking machine learning models for predictive analysis, significantly enhancing the accuracy in forecasting electrical conductivity and gas-sensing responses of PANI/graphene nanocomposites. These models, a first in the field, set new standards in sustainable material science. Furthermore, the thesis introduces an eco-friendly synthesis pathway for PANI/reduced graphene oxide nanocomposites using deep eutectic solvents, marking a leap towards environmental sustainability. This integrative research not only enriches the understanding of PANI/graphene nanocomposites but also makes substantial contributions to developing sustainable materials. The findings and methodologies presented in this thesis are anticipated to have far-reaching impacts, opening new avenues in technology and environmental conservation, particularly in areas such as supercapacitors, gas sensors, and energy storage solutions.

Keywords: Polyaniline (PANI); Graphene Nanocomposites; Machine Learning in Material Science; Experimental Design Optimization; Computational Modeling; Density Functional Theory (DFT); Electrical Conductivity; Gas Sensing; Environmental Sustainability.